Numerical Modelling of Sloshing Tanks and Their Application in Tuned Liquid Dampers

Mahdiyar Khanpour

Thesis submitted to the University of Ottawa
in partial Fulfillment of the requirements for the
Doctorate in Philosophy degree in Civil Engineering

Department of Civil Engineering
University of Ottawa

Abstract

In this study, we focus on sloshing tanks, particularly Tuned Liquid Dampers (TLDs). When a tank is excited, sloshing waves are generated and TLDs utilize these waves to mitigate the vibrations of the underlying structure. Due to their easy installation and cost-effective maintenance, TLDs are promising damping solutions for tall slender buildings subjected to wind or earthquake forces. Although extensive experimental research exists on TLD-coupled systems, further studies are needed to enhance the understanding of their dynamic characteristics. To address this, our research is divided into two main parts.

The first section of the first part focuses on the linear wave theory of shallow water equations and investigates how various widely used finite difference and finite volume methods introduce numerical diffusion errors in the simulation of sloshing waves from both initial perturbations and forced excitations. A model with low numerical diffusion, integrating physical diffusion, is then employed and coupled with a single degree of freedom (SDOF) system to develop a numerical model for TLD simulation. This facilitates a parametric study that includes the frequency ratio and damping ratio. The second section shifts to the nonlinear wave theory of shallow water equations. This model incorporates bottom topography and enables the simulation of high-gradient free surfaces. It employs the central upwind method and Minmod slope limiter function for flux approximation, along with the fourth-order Runge-Kutta method for time discretization. The model is verified for dam breaks on both horizontal and sloped beds, as well as for runup and rundown in a parabolic tank. Subsequently, the model integrates dissipation and dispersion terms to create asymmetric and steady waves. After verification with experimental box sloshing tanks, the model is coupled with an SDOF system to represent the TLD model. Finally, the TLD with a sloped bed demonstrates higher sloshing waves and greater suppression of the underlying structure vibrations compared to conventional box TLDs.

The last part includes an innovative analytical approach to model the dynamic behavior of a TLD-coupled system, bridging a significant gap in the literature. The separation of variables technique is employed to convert the linear shallow water equations, including the continuity and momentum equations, into a modal coordinate system. These equations are then strongly coupled with the dynamic equation of a single degree of freedom (SDOF) system under free vibration, resulting in a fourth-order characteristic equation. Using this equation, novel and significant concepts such as

the stability of the coupled system, natural frequencies of the coupled system, initial boundary conditions, and response of the coupled system are discussed. In the next stage, the model incorporates both structural and fluid dissipations, leading to a different characteristic equation. This allows for the study of new topics, including the influence of dissipations on the natural frequencies and stability of the coupled system. For the first time, an expression for the response of the coupled system, indicating an exponential reduction in vibration, is proposed. Additionally, the analytical model is modified to consider the effect of a sloshing tank equipped with screens on the coupled system response. Finally, contrary to previous cases focusing on free vibration, this stage examines the forced vibration of the coupled system. It presents a characteristic equation and describes the particular, complementary, and total responses in three scenarios: undamped coupled system, structurally damped coupled system, and fluid and structurally damped coupled system. Regarding the particular solution, the model introduces new concepts, including dynamic amplification and phase difference between the force and displacement of the coupled system. For the first time, closed-form analytical solutions for the response of the coupled system in all three scenarios are proposed. Notably, in each scenario, in addition to the general case, two special cases are analytically investigated: resonant excitation of the coupled system and when the excitation frequency approaches the water tank frequency.

I would like to dedicate this thesis to

My daughter, Viana. She is my greatest motivation in life and the primary reason for my progress. Her happiness is my deepest wish, and she serves as a constant source of encouragement and pure love.

Acknowledgments

I would like to express my deepest gratitude to Prof. Mohammadin for his incredible support, compassion, and guidance throughout my PhD journey. His unwavering encouragement, patience, understanding, and kindness have not only smoothed the path of my PhD research but also inspired me to grow both academically and personally. I am incredibly fortunate to have had the opportunity to work under such an exceptional and caring supervisor. I am deeply grateful to Dr. Shirkhani, whose expertise and invaluable comments have greatly enhanced my thesis. Furthermore, His financial support through two NRC projects helped me manage both my studies and family, and I cherish him not only as a mentor but as a dear and trusted friend. I sincerely thank Prof. Kinanoush for his thoughtful review of my papers and thesis, and for providing invaluable comments.

I express my heartfelt gratitude to my Ph.D. defense committee members, Prof. Samuel Li, Prof. Magdi Mohareb, Prof. Abhijit Sarkar, and Dr. Imanian for their dedication, valuable insights, and constructive feedback throughout this process.

I am profoundly grateful to my parents, Mansour and Sona, for their unwavering support and tireless efforts in nurturing my growth and education. Their dedication and sacrifices have been the foundation of all my achievements in life. I owe my success to their endless love and encouragement.

I am immensely thankful to my wife, Vida, for her steady support, patience, and kindness throughout this journey. Her encouragement and belief in me have been instrumental in ensuring a smooth and fulfilling experience. I am truly grateful for her presence in my life.

I would like to express my heartfelt gratitude to my sister, Motahareh, and my brother, Amirhossein, and for their unwavering support, energy, and positive feedback throughout this journey. Even from a distance, their encouragement has been a source of strength for me.

Journal Publications from this Thesis

[1] **Mahdiyar Khanpour** , Abdolmajid Mohammadian, Hamidreza Shirkhani, and Reza Kianoush" Numerical Simulation of Sloshing Tanks with Shallow Water Model Using Low Numerical Diffusion Schemes and its Application to Tuned Liquid Dampers", ***International Journal of Applied and Computational Mathematics***, Under Review.

[2] **Mahdiyar Khanpour**, Abdolmajid Mohammadian, Hamidreza Shirkhani, and Reza Kianoush (2024). "Simulation of Sloped-Bed Tuned Liquid Dampers Using a Nonlinear Shallow Water Model." ***Water***. *16*(10), 1394. https://doi.org/10.3390/w16101394

[3] **Mahdiyar Khanpour**, Abdolmajid Mohammadian, Hamidreza Shirkhani, and Reza Kianoush (2024). "Analytical solution to a coupled system including tuned liquid damper and single degree of freedom under free vibration with modal decomposition method". ***Physics of Fluids***, 36(5). https://doi.org/10.1063/5.0206390

[4] **Mahdiyar Khanpour** ," Analytical Solution to The Free Vibration of The Shallow Water Elevated Tank with Considering Dissipations- Case Study: Tuned Liquid Dampers", ***International Journal of Mechanical Sciences (IJMS)***, submitted.

[5] **Mahdiyar Khanpour**, Abdolmajid Mohammadian, Hamidreza Shirkhani, and Reza Kianoush "A novel analytical solution to a TLD coupled system under harmonic excitation". **Physics of Fluids**, Submitted.

Table of Contents

List of Figures

List of Tables

List of Acronyms

CEL	Coupled Eulerian Lagrangian
FDM	Finite Difference Method
FEM	Finite Element Method
FSI	Fluid Structure Interaction
FVM	Finite Volume Method
LCS	Liquid Containing Structure
LES	Large Eddy Simulation
RANS	Reynolds Averaged Navier Stokes
RTHS	Real Time Hybrid Simulation
SDOF	Single Degree of Freedom
SPH	Smoothed Particle Hydrodynamics
SWE	Shallow Water Equations
SWM	Shallow Water Models
TLD	Tuned Liquid Damper
TMD	Tuned Mass Damper
TVD	Total Variation Diminishing
VOF	Volume of FLUID

1. Introduction and Objectives

1.1. Background and introduction

Liquid storage tanks are crucial in various industries for storing liquids such as gas, petroleum, oil products, and other fluids. However, their safety and stability can be compromised by dynamic horizontal forces such as seismic excitation and strong winds. These forces can induce sloshing waves within the tanks, generating significant hydrodynamic forces capable of damaging the tanks. Such damage can range from localized issues, such as buckling or rupture, to catastrophic failures, such as overturning of elevated tanks. In cases where tanks contain hazardous materials, the damage can lead to leaks, potentially resulting in explosions, fires, or the release of toxic substances, posing severe health risks to people. Numerous instances of tank failures due to seismic excitation have been documented globally, highlighting the critical need for effective measures to mitigate these risks. Liquid storage tanks can be broadly categorized into two main types based on their support structure: grounded and elevated tanks. Elevated tanks are often employed in water supply systems to generate the pressure required for water distribution without relying on pumps. Typically, elevated tanks have lower capacities than ground tanks. References indicate that more than 200 significant earthquakes, with magnitudes greater than seven on the Richter scale, occur globally each year. Given the critical importance and widespread use of liquid storage tanks, along with the frequent occurrence of strong seismic events, an appropriate seismic design for these tanks is essential.

The initial step toward achieving an effective seismic design is to understand the dynamic behavior of these tanks. Consequently, researchers have explored the seismic performance of liquid storage tanks using experimental, analytical, and numerical methods. However, two key challenges arise in the modeling of sloshing tanks.

First, liquid storage tanks consist of two distinct materials: structure and liquid. The dynamic behaviors of these components are markedly different, with the natural frequency of sloshing waves generally being lower than that of the structure. Therefore, each component must be modeled using equations that accurately reflect its respective dynamic behavior.

Second, the sloshing problem falls under the category of fluid-structure interaction, where the displacement of the structure influences the sloshing waves; conversely, the sloshing waves impact the displacement of the structure. Therefore, a two-way coupling method is necessary to accurately model the interactions between these components.

As discussed previously, sloshing waves pose significant risks to the safety and stability of structures. However, a specific type of water tank has been designed to utilize sloshing waves to mitigate vibrations in high-rise buildings and tall towers. These tanks, known as Tuned Liquid Dampers (TLDs), are engineered such that the geometry of the tank and the depth of the water are optimized to ensure that the sloshing waves counterbalance the vibrations of tall structures.

With industrialization and land shortages in urban areas driving the trend toward tall and slender buildings, there is an increasing need to address the high and undesirable vibrations experienced by these structures during earthquakes and strong winds. Additionally, advancements in structural systems, materials, and design practices have led to taller, lighter, and more flexible buildings, further intensifying their dynamic responses. Consequently, reducing these dynamic responses is crucial not only for improving the serviceability of high buildings, but also for lowering the base shear and associated costs.

Engineers and researchers have explored various damping methods to mitigate these challenges. Among these, Tuned Liquid Dampers (TLDs) have attracted significant attention due to their advantages (Figure 1). TLDs, which are a type of passive damper, offer benefits such as low installation and maintenance costs, ease of application to both new and existing structures, and the added advantage of serving as water reservoirs for fire emergencies. Following the introduction of TLDs, researchers investigated their structural performance and sought to develop methods to enhance and optimize the damping efficiency of TLDs.

Fig. 1.1. Installation of a Tuned Liquid Damper (TLD) in Tall Buildings

1.2. Literature Review

As previously discussed, the effectiveness of a TLD largely depends on the sloshing behavior within the tank. Sloshing in tanks has been extensively investigated across multiple engineering disciplines, including civil, mechanical, ocean, aerospace, and nuclear engineering. Researchers have explored various aspects of sloshing waves to better understand their behavior and impact on tank dynamics. Notable studies include the influence of tank flexibility on sloshing forces, as examined by Veletsos (1992); the effects of vertical ground acceleration, tank aspect ratio, and base fixity, as studied by Moslemi and Kianoush (2012); the buckling behavior of steel tanks investigated by Sobhan et al. (2017); and the influence of various baffle configurations on sloshing waves by Panigrahy et al. (2009). Further research by Kianoush and Ghaemmaghami (2011) explored the impact of soil-structure interaction (SSI) on tank dynamics, while Bahreini et al. (2021) investigated the effects of bidirectional excitation on tank behavior.

However, this study focuses primarily on tuned liquid dampers (TLDs). Therefore, a detailed literature review was conducted specifically on TLDs to explore their role in mitigating structural vibrations and the corresponding advancements in their modeling and application.

As mentioned earlier, with the emergence of TLDs, extensive parametric studies have been conducted to optimize their design and performance. Regarding the design of TLDs, their natural frequency is typically tuned to match the dominant natural frequency of the underlying structure. Additionally, the mass of the TLD is kept much smaller than that of the underlying structure to avoid imposing a significant load on the ceiling or other structural elements, thereby ensuring efficient vibration mitigation without compromising the integrity of the building.

According to the literature, two key ratio parameters are essential in TLD design: the mass ratio, which is the ratio of the mass of the TLD to the mass of the underlying structure, and the frequency ratio, which refers to the ratio of the natural frequency of the TLD to the frequency of the excitation force. Ashasi-Sorkhabi et al. (2017) conducted extensive experimental studies on these two parameters. In addition, Fujino et al. (1992) investigated the response of structures to various frequency ratios.

Some researchers have devised additional dissipation devices to enhance the performance of the TLDs. This is where the installation of screens and other flow-damping devices (FDDs) comes into play (see Figure 1.2). For instance, Tait et al. (2005) modeled the behavior of sloshing waves and energy dissipation in a TLD equipped with multiple screens to study the response of the system across a wide range of excitation amplitudes. Their findings highlighted how screens significantly improved damping efficiency by increasing energy dissipation. Similarly, Konar and Ghosh (2021) explored various FDDs, including nets, screens, baffles, poles, and floating objects, to improve the damping effect of TLDs further. They analyzed the advantages and disadvantages of each type of FDD, providing valuable insights into the selection and application of these devices to optimize the TLD performance. These studies emphasize how adding flow-damping mechanisms can increase the effectiveness of TLDs, particularly in mitigating vibrations in tall, flexible structures. Marivani and Hamed (2017) investigated the pressure drop across slat screens in TLDs by considering both the screen solidity ratio and the screen pattern. They fully modeled the fluid flow around the screen using Computational Fluid Dynamics (CFD) software and verified their results with experimental data. Crowley and Porter (2012) investigated the optimal screen configurations within a Tuned Liquid Damper (TLD) tank, focusing on parameters such as the number and position of screens, as well as their porosity. Their analysis aimed to enhance the damping efficiency by determining the best arrangement of screens to maximize energy dissipation within the tank.

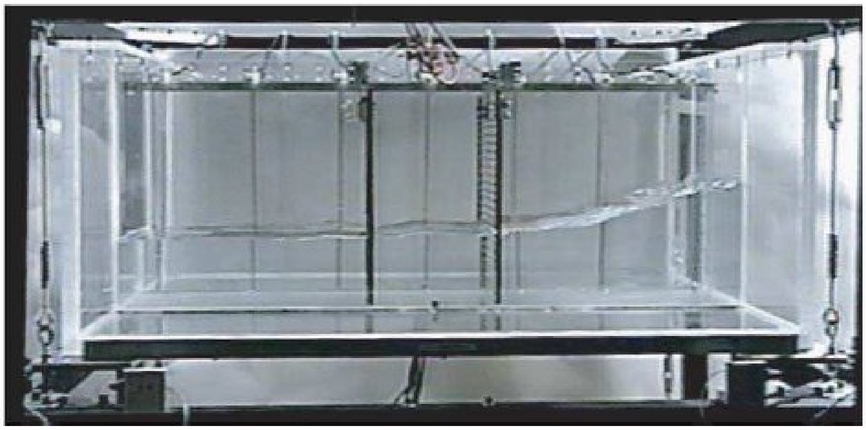

Fig. 1.2. Installation of Screens in a Tuned Liquid Damper (TLD) (Tait et al. 2005)

Only a few researchers have devised solutions for generating higher sloshing waves in TLDs. This led to the introduction of TLDs with sloped beds as an innovative approach (Figure 1.3). Pandit and Biswal (2020) investigated the efficiency of TLDs subjected to seismic excitations across a range of frequencies, including low-, intermediate-, and high-frequency content. Their research showed that sloped-bed TLDs can offer enhanced damping performance under various seismic conditions. Similarly, Zhang (2020) focused on the sloshing properties of sloped TLDs and studied the effects of several key parameters, such as the water level, slope angle, and ratio of the horizontal projection of the slope length to the total bottom length of the tank. Zhang highlighted how these variables influence sloshing dynamics, offering valuable insights into optimizing TLD performance through geometric adjustments, such as sloped beds.

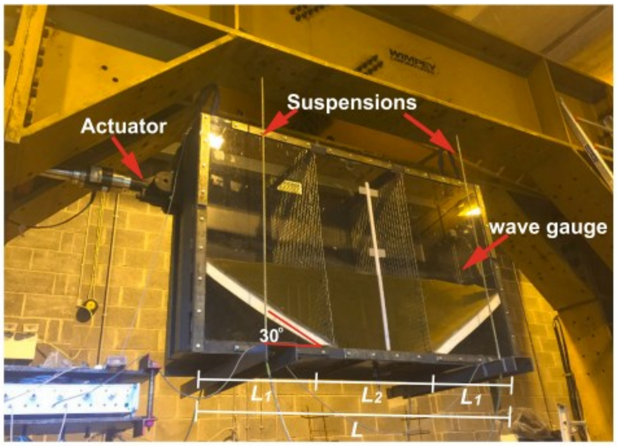

Fig. 1.3. Tuned Liquid Damper (TLD) Equipped with a Sloped Bed (Zhang 2020)

Most TLD modeling efforts focus on single-degree-of-freedom (SDOF) systems as simplified representations of the underlying structure. However, few researchers have explored how TLDs impact the vibration of multi-degree-of-freedom (MDOF) systems (Figure 1.4). In these cases, factors such as the number of TLDs and the location of the TLD installation across different floors can significantly influence the dynamic behavior of MDOF systems. With the advent of advanced experimental methods such as real-time hybrid simulations (RTHS), it has become more practical to investigate MDOF systems in experimental studies. The RTHS method allows for a more dynamic and interactive study of TLDs by experimentally deriving the TLD response, while the structure is modeled in a computer simulation. This method captures the interaction between the TLD and structure in real time, providing more accurate insights into how TLDs affect MDOF systems. Lee et al. (2007) applied the RTHS method to study the response of a three-story structure equipped with TLDs, providing valuable experimental data on the influence of TLDs on the vibration of MDOF systems in real-world scenarios. This type of study has expanded the understanding of TLD performance beyond SDOF systems, demonstrating the potential for optimized TLD placement and utilization in complex structures. Tang et al. (2023) used a frequency-domain transfer function to analyze the performance of Tuned Liquid Dampers (TLDs) in controlling multi-degree-of-freedom (MDOF) structures, considering higher modes of vibration. Hu et al. (2024) proposed the use of a pair of isolated Tuned Liquid Dampers (ITLDs) for vibration mitigation of MDOF structures. Their study showed that using a pair of ITLDs provides superior reduction in multi-response compared to single TLDs with the same parameters, effectively suppressing vibrations on different floors of a building. Pabarja et al. (2019) studied the efficiency of Tuned Liquid Dampers (TLDs) in reducing the dynamic responses of a three-story, one-bay scaled steel structure with vertical irregularities. To induce irregularities, additional mass was added to the first and third floors, increasing the contribution of the second mode. The tests evaluated the effectiveness of a single TLD and couple TLDs placed on different floors, tuned to both the first and second modes.

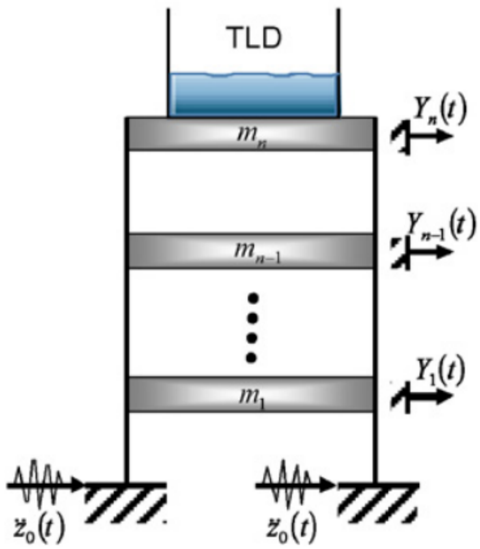

Fig. 1.4. Tuned Liquid Damper (TLD) Installed at the Top of a Multi-Degree-of-Freedom System (Lee et al. 2007)

Banerji et al. (2000) explored the dependence of the TLD performance on different ground motion characteristics. Their study demonstrated that the damping effect of TLDs is not significantly influenced by the bandwidth of the ground motion. Instead, it is primarily affected by the ratio of the significant frequencies of ground motion to the natural frequency of the structure. This finding suggests that the effectiveness of TLDs is highly dependent on how well the natural frequency of the TLD matches the dominant frequencies of the ground motion, reinforcing the importance of proper tuning in the TLD design.

Abd-Elhamed and Tolan (2022) examined the impact of soil-structure interaction on the performance of TLDs, focusing on how TLDs behave when the underlying structure is situated on soft soil. Their study involved a parametric investigation that considered various soil types, fundamental frequencies of structures, and different levels of earthquake peak ground accelerations (PGA). The findings highlighted the importance of accounting for the flexibility of the foundation, as the dynamic characteristics of the soil can significantly influence the effectiveness of TLDs in mitigating structural vibrations.

Murudi et al. (2012) found that TLDs are more effective in far-field ground motions, where a strong ground motion and the corresponding peak structural displacement occur after the initial cycles of vibration. This delayed peak response allows TLDs to dissipate energy more efficiently because they have more time to develop significant sloshing motions in response to the extended duration of the seismic event.

Saghi et al. (2024) demonstrated that TLDs are not only effective for tall buildings, but also show promising damping effects for offshore structures. Their study specifically highlights how TLDs can mitigate the pitch motion of floating offshore wind turbine substructures. This application extends the utility of TLDs to environments where they can help reduce the dynamic responses induced by waves and currents, showcasing their versatility in enhancing stability and performance in various engineering contexts. Sardar and Chakraborty (2022) investigated the effectiveness of Tuned Liquid Dampers (TLDs) in damping the wave-induced vibrations of offshore jacket platforms. Their study considered soil-pile interactions and modeled the TLD using a spring-mass system to account for the sloshing energy. They examined the performance of the TLDs under both regular and random wave loads.

Zhao et al. (2019) introduced a Tuned Liquid Inerter Damper (TLID) that integrates a traditional TLD with an inerter system. This combination includes a grounded inerter element, stiffness, and damping. Their research showed that TLID provides superior damping effects compared with conventional TLD systems. Sun et al. (2024) further advanced this concept by proposing a Damping Net and a Sloped-Bottom Tuned Liquid Inerter Damper (DNS-TLID). A schematic of the damper is shown in Figure (1.5). This innovative damper incorporates a damping net and sloped bottom, in addition to an inerter system. When applied to a single-story steel frame structure subjected to ground motion, the DNS-TLID demonstrated significant improvements, offering the highest displacement and acceleration damping effects while maintaining the same liquid mass ratio as the other systems.

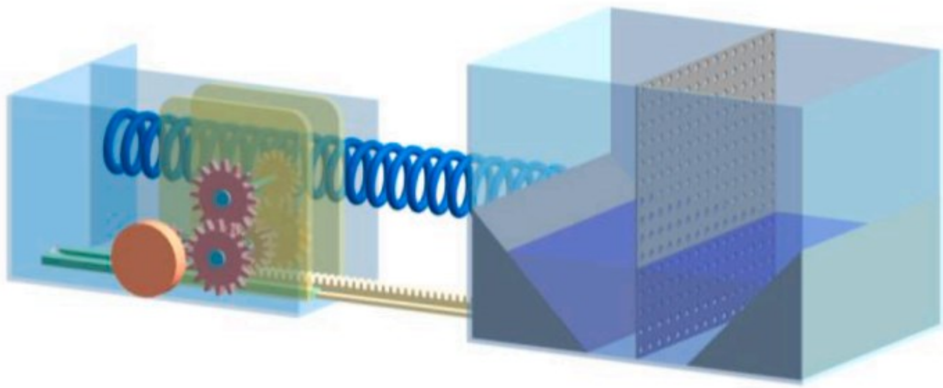

Fig. 1.5. Schematic of a DNS-TLID (Sun et al. 2024))

Domizio et al. (2024) introduced an innovative approach for designing Tuned Liquid Dampers (TLDs) that are suitable for high-frequency structures. Their design incorporated a series of spring cables that exert a force on the free surface of the liquid via a floating roof. This additional force enhances the gravitational restoring force, which in turn increases the natural frequency of the damper. Figure (1.6) reflect a schematic of this damper. This adaptation makes TLD more effective for structures experiencing higher frequency vibrations, addressing a gap in traditional TLD designs that typically target lower-frequency vibrations associated with tall buildings. Pandey et al. (2019) proposed a different approach to enhance the performance of TLDs for buildings with low natural period. They introduced a spring mechanism between the structure and TLD to make TLDs effective for structures with short periods. This approach involves using arrays of compliant elastic masses, functioning as springs, mounted on the underlying structure, and below the TLD. These mounting pads, similar to the elastomeric bearings used for isolation, are designed to be relatively stiffer to tune the system for low-period structures, typically between 0.2 and 0.6 seconds.

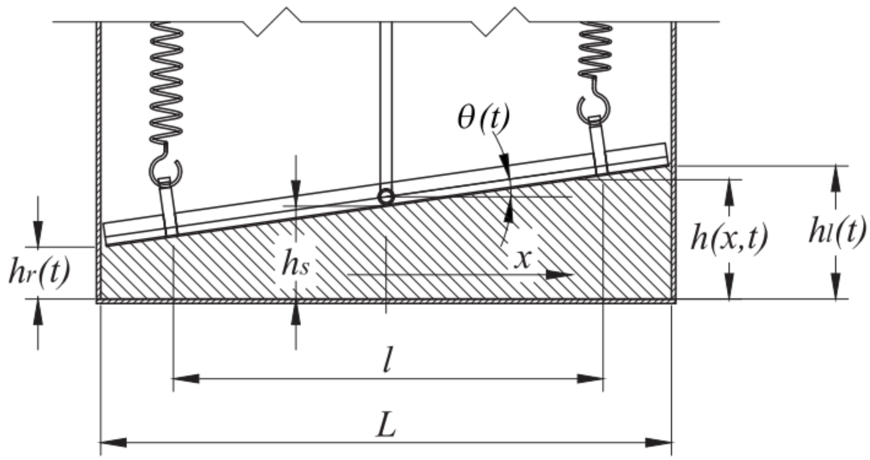

Fig. 1.6. Schematic of TLD Designed for a High-Frequency Structure (Domizio et al., 2024)

Awad et al. (2024) explored a novel dual-purpose water tank design that serves as both a vibration control system and a fire suppression system. Their approach integrates a perforated floor (a rigid floor with holes) within the tank, allowing water to pass between the two components. This design ensures that the water depth below the perforated floor meets the fire code requirements, while simultaneously tuning the water above the floor to the natural frequency of the building. This innovative solution combines structural damping with fire safety, optimizes the functionality of the water tank in meeting building codes, and enhances the overall performance. Similarly, Konar and Ghosh (2023) proposed an innovative solution for developing a tuned liquid damper (TLD) in deep-water storage tanks. They introduced a horizontal floating base (TLD-FB) system, in which the liquid above the floating base is tuned to the structural frequency (Figure 1.7). This design allows for the reduction of structural vibrations without compromising the primary function of the storage tank, making it an efficient approach for vibration control in large storage facilities.

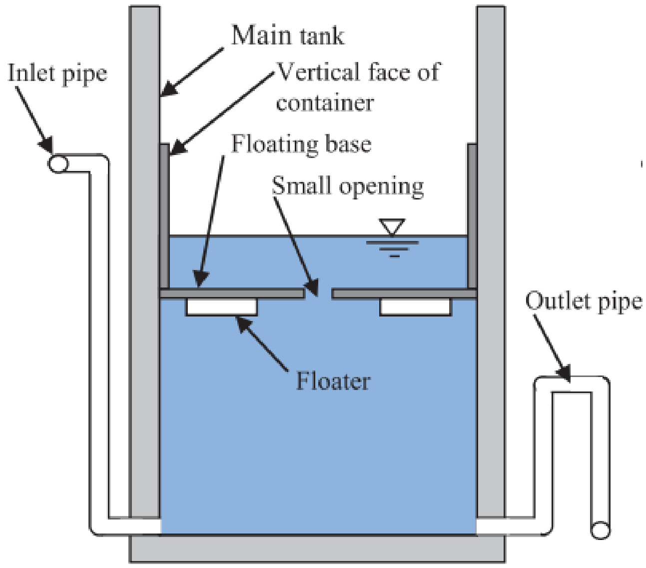

Fig. 1.7. Schematic of Storage Tank Equipped with a Tuned Liquid Damper (TLD) (Domizio et al., 2024)

Tang et al. (2023) investigated the performance of Tuned Liquid Dampers (TLDs) on nonlinear structural responses using Real-Time Hybrid Simulation (RTHS). Their study focused on the effect of the mass and frequency ratios on the efficiency of TLDs. The results indicated that while TLDs are effective in reducing structural vibrations, they can decrease hysteresis energy dissipation. Additionally, in the context of nonlinear responses, the damping frequency band of TLDs is relatively narrow, which can negatively affect their overall structural damping effectiveness.

McNamara et al. (2022) investigated how limited freeboards affect the efficiency of Tuned Liquid Dampers (TLDs) (Figure 1.8). They found that limiting the freeboard generally decreased TLD performance. To address this issue, they proposed an equivalent damping ratio that is proportional to the reduction in wave height and utilized a smoothed particle hydrodynamics (SPH) model to quantify this effect.

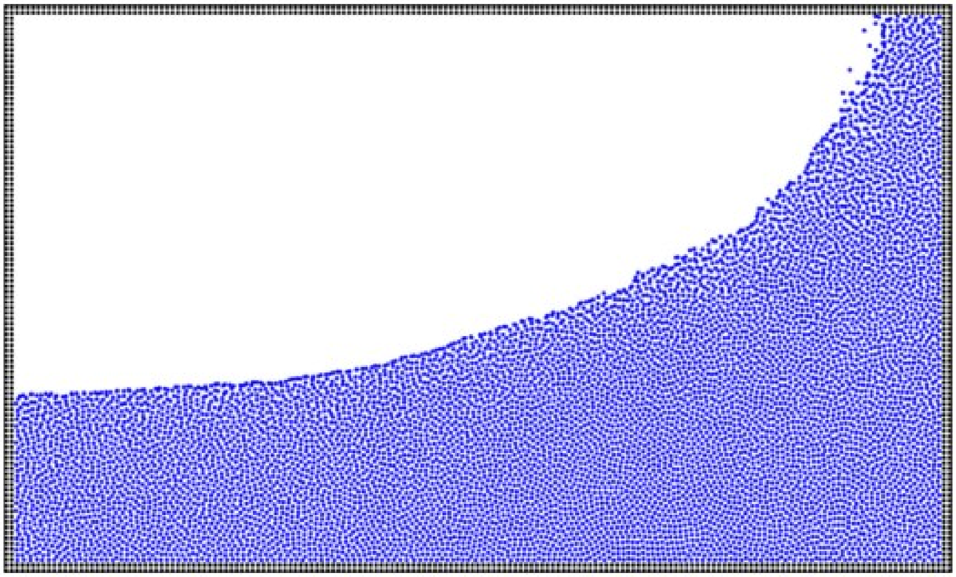

Fig. 1.8. Tuned Liquid Damper with Limited Freeboard (McNamara et al., 2022)

Tsao and Hwang (2018) explored the use of tuned liquid dampers filled with a porous medium. They introduced an equivalent system to account for the additional damping effects provided by porous media. This approach allows the incorporation of enhanced damping characteristics resulting from the interaction between the liquid and porous material.

Chang et al. (2018) conducted a parametric study on a modified tuned liquid damper (MTLD), which improves upon traditional TLDs by incorporating a rotational spring at the base (Figure 1.9). This design allows the MTLD to undergo both horizontal and rotational motions when the underlying structure sways, thereby increasing the sloshing effect and enhancing the counterbalancing force. Their study, performed using the real-time hybrid simulation (RTHS) method, examined the effects of several parameters, including dimensionless rotational stiffness, frequency ratio, and damping ratio.

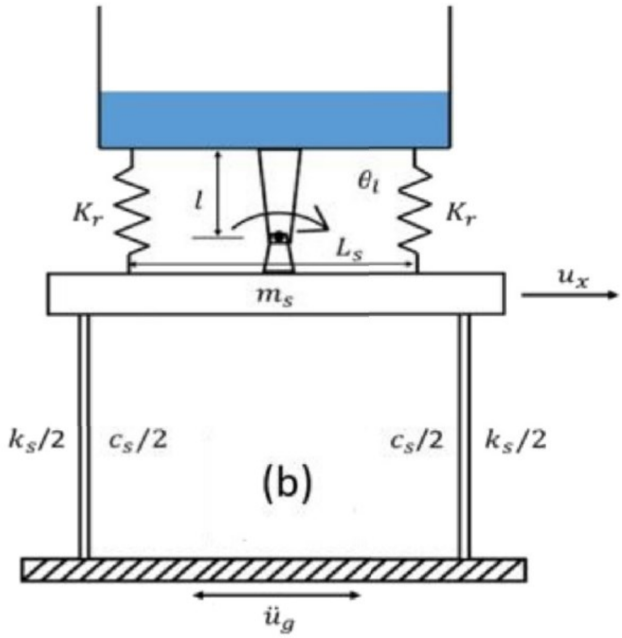

Fig. 1.9. Schematic of TLD with Modified Connection to the Roof (Chang et al., 2018)

1.3. Modelling of fluid sloshing in tuned liquid dampers (TLDs)

Although there are various methods for numerically modeling fluid sloshing in tanks, a review of the literature on Tuned Liquid Dampers (TLDs) reveals that these methods can be categorized into five distinct groups:

1.3.1. shallow-water equations (SWE)

These are hyperbolic partial differential equations (PDEs), derived by depth-integrating the Navier–Stokes equations under the assumption that the horizontal length scale is significantly greater than the vertical length scale. These equations inherently include both the bottom boundary and free surface boundary conditions. At the bottom, a nonpenetration boundary condition is applied, whereas at the free surface, both kinematic and dynamic boundary conditions are enforced. The governing continuity and momentum equations in the SWE directly generate the free surface, eliminating the need for additional equations to model the free surface. This approach substantially reduces the computational costs.

Given the geometric properties of TLDs, where the length of the tank is typically more than ten times the water depth, shallow water models (SWM) are well suited for modeling sloshing dynamics in these systems. As observed in the literature, researchers have often adopted this modeling approach for TLDs. Moreover, they introduced additional terms into the conventional SWM to capture the nonlinearities and asymmetries that arise when high-amplitude sloshing waves occur in the tank, further refining the accuracy of the simulations (Sun et al. 1992, Fujino et al. 1992, Banerji et al. 2000, Tait et al. 2005, Khanpour et al 2024a).

In this study, the primary focus of the modeling is based on the shallow water model (SWM) because of its computational efficiency, simplicity, and alignment with the physical properties of the problem. The SWM is particularly well-suited for modeling Tuned Liquid Dampers (TLDs) because it reduces the complexity of solving the full Navier-Stokes equations while accurately capturing the essential dynamics of sloshing. Chapter 2 emphasizes the application of linear shallow water equations, which are adequate for cases with relatively small wave amplitudes and where the nonlinear effects are negligible. These equations provide a foundational understanding of sloshing behavior under linear assumptions. Chapter 3 shifts focus to the nonlinear shallow water equations. The model incorporates conventional nonlinear terms to capture the behavior of sloshing waves at higher amplitudes, where the assumptions of linearity no longer hold. In addition to the standard nonlinear terms, new terms are integrated into the equations to enhance the precision of the model. In Chapters 4, 5, and 6, the focus shifts to an analytical approach for modeling Tuned Liquid Dampers (TLDs) in various scenarios. These chapters utilize linear wave theory as the foundation for understanding and analyzing the behavior of TLDs in different configurations and conditions.

The linear and nonlinear shallow water equations in a boxed tank subjected to horizontal excitation are expressed as equations (1-1, 1-2) and (1-3, 1-4), respectively. These equations are based on the conventional shallow water equations (Toro, 2001), with the addition of a tank acceleration term to account for the dynamic interaction between the fluid and the tank. As depicted in Figure (1.10), η represents wave height and u denotes velocity. The parameter H corresponds to the mean water level, and $h = H + \eta$, g represents gravitational acceleration, and a signifies tank acceleration.

Linear shallow water equations

$$\frac{\partial \eta}{\partial t} + H \frac{\partial u}{\partial x} = 0 \tag{1-1}$$

$$\frac{\partial u}{\partial t}+g\frac{\partial \eta}{\partial x}=-a \quad (1\text{-}2)$$

Nonlinear shallow water equations

$$\frac{\partial h}{\partial t}+\frac{\partial (uh)}{\partial x}=0 \quad (1\text{-}3)$$

$$\frac{\partial (uh)}{\partial t}+\frac{\partial (u^2h+0.5gh^2)}{\partial x}=-ah \quad (1\text{-}4)$$

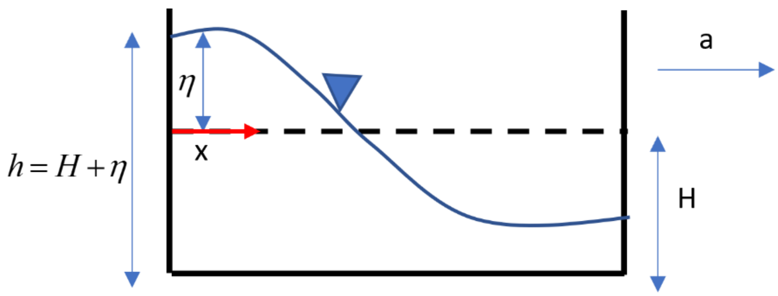

Fig. 1.10. Schematic of the parameter of a shallow water tanks

The aforementioned equations represent the classical nonlinear shallow-water equation. To improve the accuracy of this shallow-water model under large-amplitude excitation, additional terms have been introduced. These enhancements address the limitations of the classical model and provide a more accurate representation of the wave dynamics under extreme conditions. A detailed discussion of these terms and their implications is provided in Chapter 3.

1.3.2. potential flow theory

It assumes that the fluid is incompressible, inviscid, and irrotational. In such a framework, the flow can be described using a velocity potential function denoted by $\phi(t,x,y)$ for a two-dimensional problem, as illustrated in Figure (1.11).

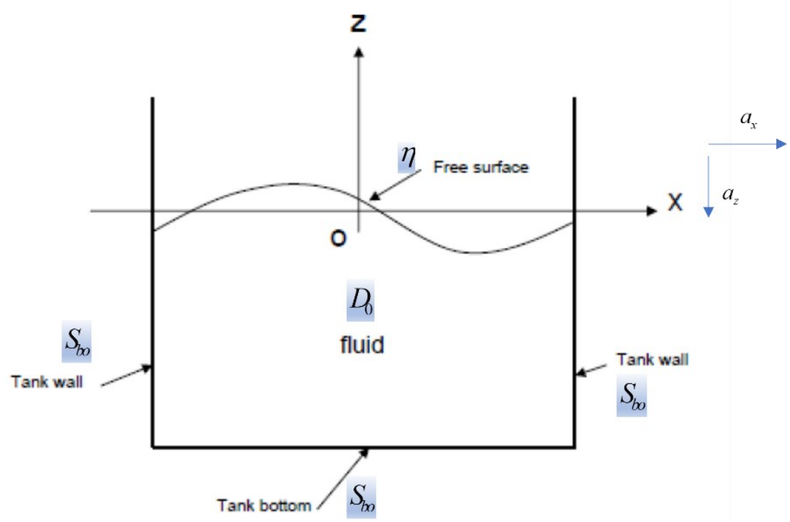

Fig. 1.11. Specifications of a sloshing tank in potential flow theory

The velocity v of the fluid is related to ϕ as

$$v = \nabla \phi(x,z,t) \tag{1-5}$$

Applying this to the continuity equation for incompressible flow, we arrive at the Laplace equation in the flow domain (D_0) (Cao et al. 2010):

$$\nabla^2 \phi(x,z,t) = 0 \quad \text{in the flow domain}\,(D_0) \tag{1-6}$$

This equation governs the fluid behavior in the potential flow model. The Laplace equation is a boundary value problem, meaning that the velocity potential ϕ or its gradient must be specified on the boundaries of the domain (such as the tank walls and free surface). Therefore, the core challenge is to satisfy the boundary conditions.

Boundary Conditions:

1. Solid Boundaries (Tank Walls): The non-penetration condition must hold on the rigid tank walls. This condition states that the fluid velocity component is normal to the wall boundary (S_{b0}) zero:

$$\vec{n}.\nabla \phi = 0 \quad \text{on the tank wall } (S_{b0}) \tag{1-7}$$

Where n is the direction normal to the wall.

2. Free Surface Boundary Conditions: The free surface, which is an unknown boundary, introduces two important boundary conditions (Wu et al. 1998):

   - Kinematic Boundary Condition: The velocity of the free surface must be equal to the velocity of the fluid at the surface. This condition ensures that the free surface moves with the fluid, given by

$$\frac{D\eta}{Dt}=\frac{\partial\phi}{\partial z} \quad or \quad \frac{\partial\eta}{\partial t}+\frac{\partial\phi}{\partial x}\frac{\partial\eta}{\partial x}-\frac{\partial\phi}{\partial z}=0 \qquad on\ \ z=\eta(x,\mathrm{z},t) \tag{1-8}$$

where η is the free surface displacement and z is the vertical coordinate.

   - Dynamic Boundary Condition: Derived from Bernoulli's equation, this condition requires the pressure at the free surface to be zero. The simplified Bernoulli equation for an incompressible inviscid fluid is as follows:

$$\frac{\partial\phi}{\partial t}=-(g+a_z)\eta-a_x x-\frac{1}{2}\nabla\phi.\nabla\phi \qquad on\ \ z=\eta(x,\mathrm{z},t) \tag{1-9}$$

where g is the gravitational acceleration, a_x and a_z are the instant acceleration of the tank in the horizontal and vertical directions, respectively.

linearization:

1- Using Taylor series expansion for small-amplitude waves, the boundary conditions at the free surface ($z=\eta$) can be approximated at $z=0$.

2- The last term of equation (1-9), which is a nonlinear term, can be disregarded.

Therefore, for the linear model, the following system of equations is established (Cao et al. 2010):

$$\left\{\begin{array}{ll}\nabla^2\phi=0 & (in\ D_0)\\ \phi=\phi_f & (\text{on } z=0)\\ \vec{n}.\nabla\phi=0 & (\text{on } S_{b0})\end{array}\right\}$$
$$\frac{\partial\eta(x,t)}{\partial t}=\frac{\partial\phi}{\partial z} \quad (on\ z=0)$$
$$\frac{\partial\phi}{\partial t}=-(g+a_z)\eta-a_x x \quad (on\ z=0)$$
$$\tag{1-10}$$

Pandit and Biswal (2020), Zhang (2020) utilized potential flow theory to model the behavior of sloshing waves in Tuned Liquid Dampers (TLDs).

1.3.3. Volume of Fluid (VOF) method

This is a numerical technique developed for modeling free surfaces, particularly for tracking and identifying the interface between different fluid phases. It is a part of the Eulerian method class, which employs a fixed computational mesh. The VOF approach was introduced by Nichols and Hirt in their 1975 paper "Methods for Calculating Multi-Dimensional, Transient Free Surface Flows Past Bodies." This method is particularly useful for handling complex free-surface flows, such as those found in fluid dynamics problems involving multiple phases or large interfacial movements.

The Volume of Fluid (VOF) method relies on a fraction function that quantifies the proportion of fluid within each computational cell relative to the total volume of the cell. This fluid fraction was updated using the advection equation as it moves through the grid cells. Although the VOF method is effective for capturing the shape and location of fluid interfaces, it does not solve fluid dynamics on its own; the Navier–Stokes equations, which govern fluid motion, must be solved separately. Lower-order schemes can lead to interface smearing or erratic behavior, particularly when the flow is not aligned with the grid. To address the inaccuracies and instability caused by lower-order schemes and avoid oscillations from higher-order schemes, it is important to use methods that preserve a sharp interface while ensuring monotonic volume fraction profiles. Various techniques, such as the donor-acceptor scheme, have been proposed to improve the accuracy and stability of the VOF method. Marivani and Hamed (2009, 2017) employed the Volume of Fluid (VOF) method to model the free-surface behavior of Tuned Liquid Dampers (TLDs). For a two-dimensional flow in a Cartesian coordinate system, the velocity vector V can be represented as

$$V = u(t,x,z)\hat{i} + w(t,x,z)\hat{k} \tag{1-11}$$

where u and w are the velocity components in the horizontal and vertical directions, respectively, and $\hat{i}$ and $\hat{k}$ are the unit vectors in the x- and z- directions, respectively.

The governing equations of incompressible flow in a Cartesian coordinate system consist of continuity and momentum equations in the x- and z-directions, forming the well-known system of equations referred to as the Navier–Stokes equations. These equations describe the motion of fluid particles and are fundamental to fluid dynamics.

- Continuity Equation (for incompressible flow):

$$\frac{\partial u}{\partial x}+\frac{\partial w}{\partial z}=0 \tag{1-12}$$

This ensures that the mass of fluid is conserved throughout the flow.

- Momentum Equation in the *x*-direction:

$$\frac{\partial u}{\partial t}+u\frac{\partial u}{\partial x}+w\frac{\partial u}{\partial y}=-\frac{1}{\rho}\frac{\partial p}{\partial x}+a+\upsilon(\frac{\partial^2 u}{\partial x^2}+\frac{\partial^2 u}{\partial z^2}) \tag{1-13}$$

- Momentum Equation in the *z*-direction:

$$\frac{\partial w}{\partial t}+u\frac{\partial w}{\partial x}+w\frac{\partial w}{\partial z}=-\frac{1}{\rho}\frac{\partial p}{\partial z}+g_z+\upsilon(\frac{\partial^2 w}{\partial x^2}+\frac{\partial^2 w}{\partial z^2}) \tag{1-14}$$

- u and w denote the velocity components in the horizontal (x) and vertical (z) directions, respectively.
- ρ is the fluid density.
- p is the pressure.
- υ is the kinematic viscosity of the fluid.
- a and g represents horizontal acceleration and gravitational acceleration, respectively.

The Volume of Fluid (VOF) equation is expressed as follows:

$$\frac{\partial F}{\partial t}+u\frac{\partial F}{\partial x}+w\frac{\partial F}{\partial z}=0 \tag{1-15}$$

Where F is the local volume fraction of the liquid phase within each computational cell.

- In cells fully occupied by the liquid phase, F=1.
- In cells entirely occupied by the gas phase, F=0.
- For cells containing an interface between the liquid and gas phases, F takes a value between 0 and 1, representing the free surface location.

The advection of F across the computational domain helps track the movement of the fluid interface.

1.3.4. Smoothed Particle Hydrodynamics (SPH)

It is a mesh-free Lagrangian method developed by Gingold and Monaghan (1977) and Lucy (1977) for astrophysical simulations. Over time, SPH has become a significant alternative to traditional Eulerian methods, particularly in cases involving large interfacial deformations and violent free surfaces (Violeau and Rogers 2016), hydraulic structures (Khanpour et al.2016a), multiphase flows (Pozorski and Olejnik 2024), and sediment transport (Khanpour et al. 2016b). Due to its ability to accurately model violent free surfaces and breaking waves, SPH is well suited for simulating sloshing, particularly under large excitations. One of the key advantages of SPH is its treatment of the convection term in its Lagrangian form, which eliminates the numerical diffusion errors. Consequently, SPH offers a robust approach for capturing the complex fluid behavior in free-surface problems, including dynamic sloshing in Tuned Liquid Dampers (TLDs) (English et al. 2022, McNamara et al. 2022).

The formulation of the Smoothed Particle Hydrodynamics (SPH) method is fundamentally based on the integral representation of functions. In SPH, a continuous function is approximated by its values for a set of discrete particles, using smoothing kernels. The basic idea is that any function can be expressed as an integral over the entire domain weighted by a smoothing kernel function. For particle *i*, the function $f(x_i)$ and its gradient are approximated as a summation over neighboring particles *j* as follows (Liu 2003).

$$f(x_i) = \sum_{j}^{N} m_j \frac{f(x_j)}{\rho_j} W(|r_i - r_j|, h) \tag{1-16}$$

$$\nabla f(x_i) = \sum_{j}^{N} m_j \left(\frac{f(x_j)}{\rho_j^2} + \frac{f(x_i)}{\rho_i^2}\right) \nabla W(|r_i - r_j|, h) \tag{1-17}$$

Where $f(x_j)$ is the quantity of interest, m_j is the particle mass, ρ_j is the particle density, W is the kernel function that depends on the distance between particles ($r_i - r_j$), and is the kernel function smoothing length, h. Kernel function must satisfy several important properties to ensure accurate and stable numerical approximations (Liu 2003):

1- Even Function Property 2- Compact Support Condition 3- Normalization Condition 4- Delta Function Property when h approaches zero (see Figure 1.12)

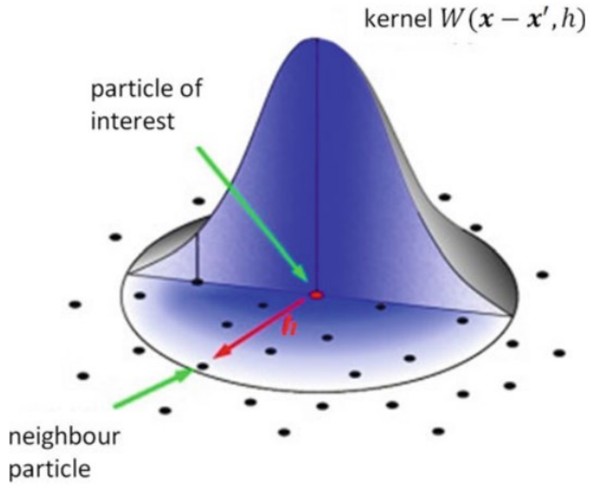

Fig. 1.12. Kernel function in SPH method (Ji and Liu 2020)

The continuity and momentum equations for an inviscid flow in the Lagrangian form are written as follows (English et al. 2022):

$$\frac{\partial \rho}{\partial t} + \rho \nabla \vec{V} = 0 \tag{1-18}$$

$$\frac{D\vec{V}}{Dt} = -\frac{1}{\rho}\nabla P + \vec{g} \tag{1-19}$$

Where $\vec{V}$ is the velocity vector, $\vec{g}$ is the horizontal acceleration in the *x*-direction and gravity acceleration in the *z*-direction (vertical direction), P is the pressure, and ρ is the fluid density.

The SPH approximation of the continuity and momentum equations leads to the following expression (English et al. 2022).

$$\frac{d\rho_i}{dt} = \sum_j^N m_j v_{ij} . \nabla W(\left|r_i - r_j\right|, h) + \delta h c_0 \sum_j^N \frac{m_j}{\rho_j} \psi_{ij} . \nabla W(\left|r_i - r_j\right|, h) \tag{1-20}$$

$$\frac{dv_i}{dt} = -\sum_{j}^{N} m_j \left(\frac{P_i + P_j}{\rho_i \rho_j} + \pi_{ij}\right) \nabla W(\left|r_i - r_j\right|, h) + g \tag{1-21}$$

Where ρ_j is the particle density, m_j its mass, c_0 is the speed of sound in the fluid, $v_{ij} = v_i - v_j$ is the velocity difference between particles *i* and *j* and ∇W is the kernel gradient and $\delta = 0.01$. ψ_{ij} is density diffusion function (Molteni and Colagrossi 2009) and π_{ij} is the artificial viscosity (Liu 2003). Finally, the pressure is derived from the Tait equation of state (Liu 2003).

$$P = \frac{c_0 \rho_0}{\gamma}\left[\left(\frac{\rho}{\rho_0}\right)^{\gamma} - 1\right] \tag{1-22}$$

where $\rho_0 = 1000 \frac{kg}{m^3}$ is the reference density of water and $\gamma = 7$.

This modeling approach relies on the weakly compressible Smoothed Particle Hydrodynamics (SPH) method, referred to as WSPH. In contrast, more advanced models consider the complete incompressibility of the fluid, which is denoted as ISPH. The ISPH method utilizes the Poisson equation to derive the pressure, as opposed to relying on the equation of state (McNamara and Tait 2021).

Boundary Condition:

Several algorithms have been designed to capture the behavior of rigid walls in SPH. One common approach is to define boundary particles along the rigid wall that impose an impulsive force on the inner particles as they approach, thereby satisfying the nonpenetration boundary condition. Additionally, by using ghost particles placed around and outside the boundary, which generate equal but opposite velocity vectors relative to the corresponding inner particles, a no-slip boundary condition can be achieved.

For the free surface, based on equation (1-20), the density of free surface particles is lower than that of inner particles due to the absence of particles above them. This allows the free surface to be identified solely from the density distribution, without the need for solving additional equations, offering a significant advantage. Figure (1.13) presents a schematic representation of the particle types used in modeling a weir in SPH (Khanpour et al. 2016a).

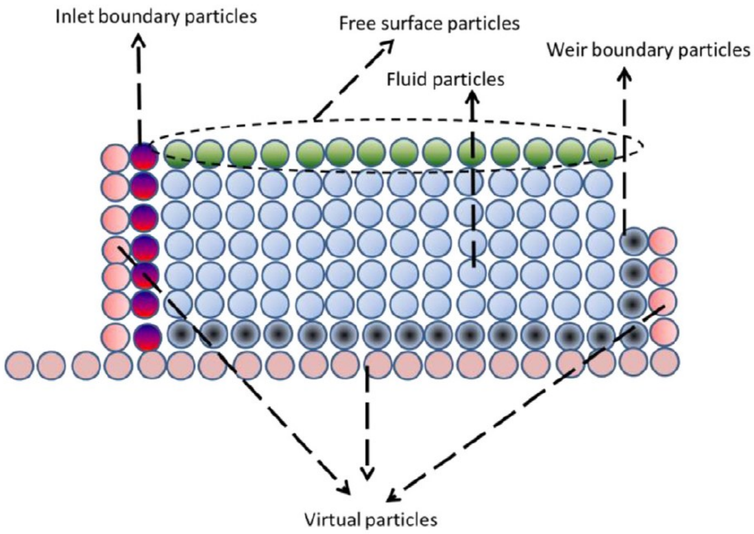

Fig. 1.13. Schematic of different type particles in SPH model (Khanpour et al. 2016b)

1.3.5. Housner Theory

Housner (1963) made a pivotal contribution to the modeling of sloshing tanks by conceptualizing the fluid dynamics within the tank as a two-degree-of-freedom system. This analytical theory characterizes the lower portion, termed the impulsive component, as moving in unison with the tank and being rigidly connected to the walls, while the upper portion, known as the convective component, corresponds to the sloshing waves (see Figure 1.14). Housner introduced the equivalent mass, stiffness, and natural frequencies for each degree of freedom.

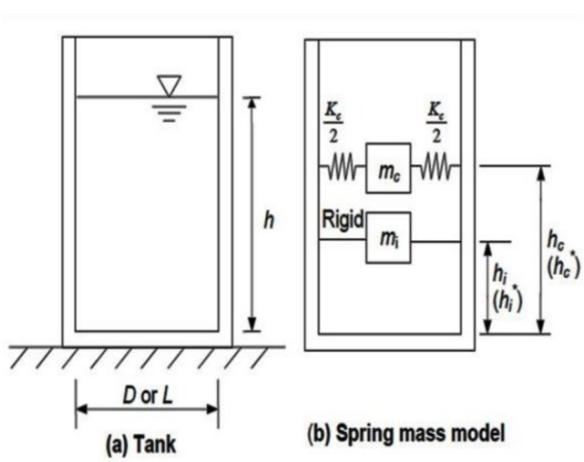

Fig. 1.14. Equivalent dynamic system of a water tank (Housner, 1963)

Upon the introduction of Housner's analytical formulation, it has been refined by various researchers. For instance, Veletsos (1974) posited that the flexibility of the tank influences the dynamic properties of the impulsive component, but does not affect the convective component. The impulsive component of the tank plays a significant role in the dynamic behavior of storage tanks. The impulsive component directly influences the overall stability and structural integrity of the tank. However, in the case of Tuned Liquid Dampers (TLDs), the mass of water in the tank is significantly smaller than that of the underlying structure. Consequently, the impulsive component of the water tank, which moves with the tank structure at a frequency different from the underlying structure, does not substantially affect the structure below. In contrast, the sloshing component, tuned to match the frequency of the underlying structure, has a significant effect on the structural response, despite its relatively small mass. Therefore, some researchers have modeled TLDs using equivalent mass, spring, and damping parameters based on the first mode of sloshing (Abd-Elhamed and Tolan 2022; Konar and Ghosh 2020).

The fundamental natural sloshing frequency for water inside a rectangular tank, based on the linear wave theory, can be determined using the following equation:

$$f_w = \frac{1}{2\pi}\sqrt{\frac{\pi g}{L}\tanh(\frac{\pi h}{L})} \tag{1-23}$$

where:

- f_w is the fundamental sloshing frequency,
- g is the gravitational acceleration,
- L is the length of the tank,
- h is the water depth, and
- tanh represents the hyperbolic tangent function.

This equation is derived from linear wave theory and is commonly used to estimate the natural sloshing frequency of rectangular tanks. The damping factor is linearly calculated using Abramson’s

Equation:

$$\xi_f = \sqrt{\frac{\upsilon_f}{L^{\frac{3}{2}}\sqrt{g}}} \tag{1-24}$$

Where υ_f is kinematic viscosity of the liquid. For the design of TLDs, the consideration of the first mode of sloshing is often sufficient. The equivalent mass, m_d, stiffness, k_d and damping, c_d for the first mode of sloshing of the conventional rectangular TLD are

$$m_d = \frac{8\rho L^2 b}{\pi^3} tanh(\frac{\pi h}{L}) \tag{1-25}$$

$$k_d = m_f \frac{\pi g}{L} tanh(\frac{\pi h}{L}) \tag{1-26}$$

$$c_d = \frac{m_f}{\sqrt{2}(h+\eta)} \sqrt{\omega_f \upsilon_f}[1+\frac{2h}{L}+S] \tag{1-27}$$

where m_f is the total mass of the contained water, ω_f is the damper sloshing frequency determined by the equation (1-23). the parameter η is free surface elevation and S is the surface contamination factor.

Modeling of a Single Degree of Freedom (SDOF) System

The dynamic equation of a Single Degree of Freedom (SDOF) system is given by

$$m\ddot{u}_s(t) + c\dot{u}_s(t) + ku_s(t) = p(t) = \bar{F}(t) + F_L(t) \tag{1-28}$$

In Equation (1-28), m represents the mass, k is the stiffness, and c is the viscous damping coefficient, which characterize the dynamic properties of the system. Here, $u_s(t)$ denotes the lateral displacement, whereas $\dot{u}_s(t)$ and $\ddot{u}_s(t)$ are the velocity and acceleration of the mass, respectively. The term $p(t)$ represents the total lateral excitation force, which in this study includes both seismic force excitation $\bar{F}(t)$ and water tank lateral dynamic force $F_L(t)$. A literature review indicates that structures are typically subjected to three types of seismic excitation: 1) harmonic excitation, 2) ground motion excitation, and 3) random excitation.

For the excitation of a Single Degree of Freedom (SDOF) system, there are four distinct solution methods (Humar 2012):

1. Classical Solution: This approach solves the dynamic equation, which is a second-order ordinary differential equation, using analytical methods.
2. Frequency-Domain Method: This method employs Fourier transforms to analyze the response of the system in the frequency domain, providing insights into how different frequencies affect the system.
3. Duhamel's Integrals: This technique uses the superposition principle to represent the applied force as a sequence of infinitesimally short impulses. The integral is evaluated to obtain the response of the system to harmonic excitation.
4. Numerical Methods: These methods are further divided into:
    - Central Difference Methods: This approach approximates the time derivatives of displacement (i.e., velocity and acceleration) using finite-difference approximations. It provides a numerical solution by discretizing the time domain.
    - Newmark's Method: This method involves acceleration interpolation to solve the dynamic equation. This includes the following two categories.
        - Constant Acceleration Interpolation: Assumes constant acceleration within each time step.
        - Linear Acceleration Interpolation: Assumes a linear variation of acceleration within each time step.

In the numerical modeling sections of this research, the central difference method with second-order accuracy was employed to model the Single Degree of Freedom (SDOF) system. The application of the central difference method to the dynamic equation of an SDOF system involves discretizing the time derivatives of the displacement (velocity and acceleration). By applying finite difference approximations to the expressions in equation (1-28), the following discretized equations are obtained (Chopra 2007):

$$\left[\frac{m}{(\Delta t)^2}+\frac{c}{2\Delta t}\right]u_s^{i+1}=p_s^i-\left[\frac{m}{(\Delta t)^2}-\frac{c}{2\Delta t}\right]u_s^{i-1}-\left[k-\frac{2m}{(\Delta t)^2}\right]u_s^i \tag{1-29}$$

Or

$$\widehat{k}\,u_s^{i+1}=\widehat{p}_s^i \quad \widehat{k}=\frac{m}{(\Delta t)^2}+\frac{c}{2\Delta t} \quad \widehat{p}_s=p_i-\left[\frac{m}{(\Delta t)^2}-\frac{c}{2\Delta t}\right]u_s^{i-1}-\left[k-\frac{2m}{(\Delta t)^2}\right]u_s^i \tag{1-30}$$

Based on the equation (1-29), u_s^{i+1} is derived from u_s^i and u_s^{i-1}. Thus the value of u_s^0 and u_s^{-1} are required to determine u_s^1, while the known initial values are initial displacement (u_s^0) and initial velocity ($\dot{u}_s^0$). The value of u_s^{-1} could be determined from the manipulation of dynamic equation (1-29) and central difference approximation.

To verify the model, a Single Degree of Freedom (SDOF) system with dynamic characteristics of *m*=4000 kg, *k*=631kN/m, and *c*=5kN/s is subjected to the El Centro earthquake. The El Centro ground acceleration is shown in Figure (1.15). Because an analytical solution is not available for this case, the results from the model are compared with those obtained using SeismoSignal software. The comparison demonstrates very good agreement, as illustrated in Figure (1.16).

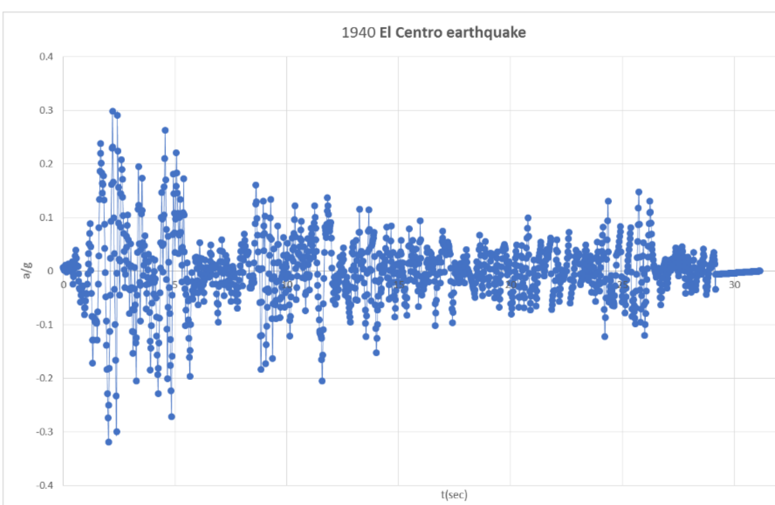

Fig. 1.15. El-Centro ground acceleration

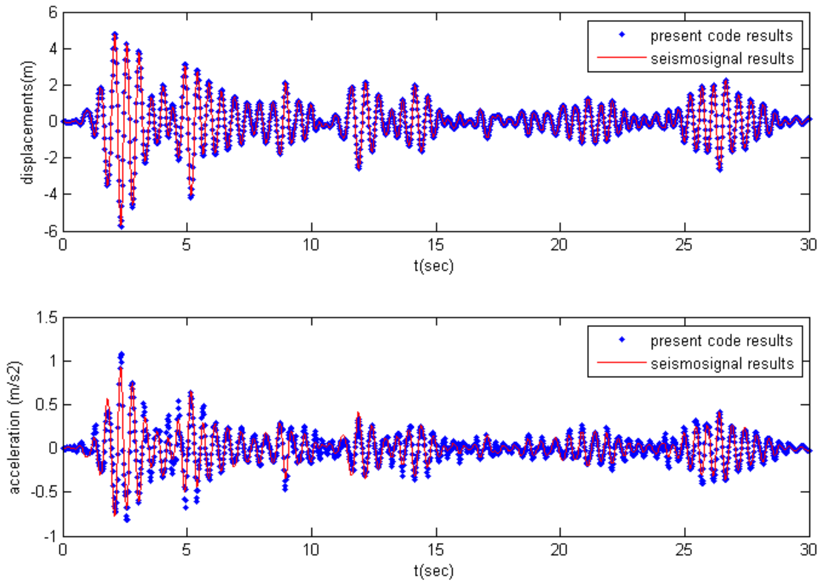

Fig. 1.16. Displacement and acceleration response of the SDOF under El-Centro earthquake acceleration

1.4. Modeling Fluid and structure Interaction in TLDs

In the simulation of TLDs, which account for both the fluid within the tank and the underlying structure, the coupling process is facilitated by two key parameters: sloshing force from the tank and acceleration of the structure. The sloshing force, generated by the fluid motion within the tank, acts on the underlying structure, whereas the structure's acceleration, resulting from its dynamic response, influences the fluid sloshing behavior. Consequently, the governing equation of the fluid incorporates the acceleration of the structure, whereas the dynamic equation of the structure integrates the sloshing force. This interdependency ensures that the interactions between the fluid and the structure are accurately captured in the coupled system simulation. An important consideration is that TLDs are generally defined as rigid shallow water tanks, meaning that their flexibility is negligible. Based on the literature, although the flexibility of a tank can have a significant impact on the impulsive component of the response, its influence on the convective component (i.e., sloshing waves) can be disregarded. Since TLDs primarily affect the underlying structure through sloshing waves, the flexibility of the tank itself does not significantly impact the dynamics of the coupled system. Therefore, in line with previous research, this study assumes the

TLD to be rigid, simplifying the modeling of fluid-structure interactions without compromising accuracy.

Numerical methods for fluid-structure interaction (FSI) simulations are traditionally categorized into two main approaches: the monolithic approach (strong coupling) and the partitioned technique (weak coupling). The monolithic approach addresses both the fluid and solid components, such as the single-degree-of-freedom (SDOF) system in this research, simultaneously through a unified set of algebraic equations encompassing all relevant unknown variables (Guruswamy, 2002). This method provides the advantage of simultaneously handling kinetic boundary conditions at the interface, which can result in a stable scheme. However, solving both fluid and solid equations simultaneously presents significant challenges for most FSI problems. Consequently, the partitioned technique is often preferred because it solves the fluid and solid domains sequentially. This approach is particularly advantageous because it permits the use of specialized software for each domain (Mehl et al., 2008). Iterative loops are required at each time step to achieve the convergence of the interaction forces. The principal benefit of the partitioned method is its flexibility, which allows for the application of optimal discretization techniques and procedures for each domain (Liao and Hu 2013). Interaction forces are computed iteratively in both the fluid and solid equations. In this research, Chapters 2 and 3 employ a weak coupling procedure for numerical modeling. In contrast, Chapters 4, 5, and 6 utilize a strong coupling method. Detailed explanations of both the coupling procedures are provided in the respective chapters.

1.5. Research Questions

With the emergence of Tuned Liquid Dampers (TLDs) for mitigating vibrations in tall, slender structures, a substantial body of research has developed. Nonetheless, significant gaps remain in the literature concerning TLDs. This research aims to address several key questions, with the objective of providing precise solutions through both numerical and analytical methodologies.

In relation to the numerical model, the following questions are examined in this study:

1. **What is the effect of different numerical models on the accuracy of sloshing simulations?**

The sloshing wave behavior plays a crucial role in determining the effectiveness of Tuned Liquid Dampers (TLDs). Thus, it is essential to develop accurate, stable, and computationally efficient models to simulate sloshing dynamics. A key inquiry in this context is the sensitivity of sloshing simulations to the choice of numerical methods. Specifically, how do different numerical schemes influence the accuracy of the results, particularly with regard to the introduction of numerical diffusion errors, which can significantly affect the performance of TLDs? Understanding the extent to which various numerical models impact these simulations is vital for optimizing the effectiveness of TLD systems.

2. **How does Tuned Liquid Damper (TLD) efficiency evolve with respect to the frequency ratio and damping ratio?**

Experimental studies indicate that TLD performance is highly sensitive to the frequency ratio, defined as the ratio between the excitation frequency and the natural frequency of the TLD. After developing a numerical method with minimal numerical diffusion and coupling it with a dynamic structural model, a critical question arises: Can the proposed numerical model accurately capture the sensitivity of TLD efficiency to the frequency ratio? Additionally, can it identify an optimal range for the frequency ratio to enhance performance? Furthermore, how does the structural damping ratio affect TLD efficiency, and how can this influence be incorporated into the model to provide deeper insights into the dynamic behavior of TLD systems? Addressing these questions is essential for optimizing TLD designs and their applications in mitigating structural vibrations.

3. **What are the necessary steps to develop a numerical model that accurately captures the behavior of a sloshing tank with a sloped bed under high excitation?**

In this regard, how should the topography term be effectively integrated into the model? Is it necessary to introduce additional terms alongside the standard nonlinear equations to account for the sloshing wave behavior induced by high excitation? Moreover, how can the model be designed to accurately simulate both wet and dry bed conditions that arise within a sloped tank during sloshing events? Another challenge lies in ensuring the model can precisely capture steep gradients in the free surface elevation, particularly under intense excitation, while preventing the occurrence of unphysical jumps or discontinuities in the representation of the free surface.

Finally, how can the model be developed to fulfill these requirements—ensuring accuracy, stability, and computational efficiency? Addressing these issues represents a significant aspect of the modeling challenge.

4. **Does the numerical model developed for Tuned Liquid Dampers (TLDs) with sloped beds predict superior vibration reduction compared to conventional TLDs?**

Specifically, does the inclusion of a sloped bed amplify sloshing waves in the numerical simulations? By coupling the nonlinear sloshing wave model with the underlying structure, how effectively does the model demonstrate a reduction in structural vibrations when sloped-bed TLDs are employed? Furthermore, can the model quantitatively compare the performance of conventional TLDs with sloped-bed TLDs? Does it reveal any significant advantages of sloped-bed designs in mitigating structural responses?

Following the development of an accurate, stable, and computationally efficient numerical model for TLD simulation, the focus of this research shifts toward the analytical modeling of the coupled system, encompassing the structure-TLD interaction. The remainder of this study addresses several critical questions by using analytical methods. It is important to note that the developed numerical model serves as a valuable tool for evaluating the accuracy of the proposed analytical approach.

5. **What are the dynamic properties of the coupled system composed of the structure and Tuned Liquid Damper (TLD)?**

One of the fundamental characteristics of each dynamic system is the natural frequency. This raises the question: What is the natural frequency of the coupled system? To address this, one approach is to perform a free vibration analysis of the coupled system. In this context, how stable is the coupled system? Specifically, how do the vibrations evolve over time—do they grow or diminish? Moreover, is it feasible to derive this response analytically for the coupled system undergoing free vibration? Providing an analytical solution to these questions is crucial, as it significantly enhances the understanding of the dynamic behavior of such systems.

6. **What is the influence of dissipation (damping) on the dynamic behavior of the coupled system?**

Damping in this context can arise from both the structure and the fluid. If both structural damping and fluid damping are incorporated into the modeling, what impact does this have on the natural period of the coupled system? Additionally, if the system experiences free vibration, how is its stability affected? Specifically, does the vibration decay over time, resulting in unconditional stability? In such a case, what is the decay function that governs this behavior? Furthermore, what is the response of the coupled system under free vibration when dissipation is considered? If the model includes dissipation from energy dissipation devices, such as screens, is it feasible to derive an analytical response for the coupled system? Providing an analytical solution to these questions would represent a significant breakthrough in the body of literature on TLD systems, enhancing our understanding of the role of damping in their dynamic behavior.

While the analytical approach has been applied to solve the preceding questions in the context of free vibration, the next phase of this thesis focuses on employing the analytical model for **forced excitation**. This shift aims to address the following key questions.

7. **What is the response of the coupled system when subjected to forced vibration?**

In this context, several important questions arise: What frequencies contribute to the system's response, and how does the amplitude of this response vary over time? In what ways can the dynamic force amplify or diminish the elastic response? What is the phase difference between the applied excitation force and the system's response? Finally, how does dissipation influence this response, including its effects on dynamic amplification and phase difference? Addressing these questions is crucial, as their solutions will significantly aid in the optimization of Tuned Liquid Dampers (TLDs).

9- What is the response of the coupled system under forced vibration in two specific but critical cases?

To gain a deeper understanding of Tuned Liquid Dampers (TLDs), it is essential to consider two significant scenarios. The first scenario involves the excitation force approaching the natural frequency of the coupled system. In this case, what is the resultant response of the coupled system? What are the dynamic amplification and phase difference under these conditions? The second scenario focuses on the excitation frequency nearing the natural frequency of the TLD tank itself. How does the coupled system respond in this instance? Additionally, how do the dissipation effects resulting from both the structure and the fluid influence the response in these two particular situations? Analyzing these cases is vital for comprehending the behavior of TLDs and optimizing their performance**.**

1.6. Research Objectives and Significance

Regarding the preceding questions, the research objectives and their significance are outlined as follows.

1. **Assessment of the influence of numerical diffusion on the accuracy of numerical models for simulation of sloshing waves**: In the initial phase of this study, a numerical model incorporating various schemes is developed to simulate sloshing waves. This model acts as a tool to assess the accuracy and degree of numerical diffusion inherent in each scheme. By evaluating the numerical diffusion generated by different approaches, this study facilitates the identification and selection of the most suitable numerical method for accurate and efficient simulations.
2. **Coupling procedure:** The subsequent objective of this study is to establish a robust coupling procedure. This involves integrating the sloshing numerical model with the dynamic structural model through an appropriate scheme that ensures both accuracy and stability. This step is essential for accurately capturing the fluid-structure interaction, which is a key aspect of the system behavior.
3. **Parametric study:** Another focus of this study is the introduction of additional terms to enhance the accuracy of the physical simulation of the TLD system. Moreover, this study aims at a comprehensive parametric analysis, with particular attention paid to the effects of the frequency and damping ratios. Investigating how these parameters affect the efficiency of TLD is fundamental for optimizing and improving the design of effective TLD systems.
4. **Modelling the sloped bed TLD**: In alignment with the central questions of this research, one of the primary objectives is to develop a numerical model capable of simulating the structure-TLD system where the TLD is equipped with a sloped bed. This study makes a significant contribution by providing a numerical tool to assess the suppression effects of this particular TLD configuration.
5. **Construction of an accurate Nonlinear numerical model with enhanced capabilities:** At this stage, the model must be designed to capture high-gradient free surfaces, simulate

both wet- and dry-bed conditions, and accurately reflect the asymmetric and stable sloshing wave patterns that emerge during high-amplitude excitations. To achieve this, the primary objective is to introduce additional terms, including nonlinear terms, to represent the physical phenomena within the system more effectively. Following this, the focus shifts to selecting and implementing numerical schemes that preserve the model's accuracy and stability while ensuring computational efficiency.

Upon the development of an accurate model for simulating the TLD, the focus of this research shifts towards creating analytical tools to analyze the coupled structure-TLD system. Furthermore, the numerical model developed in the preceding steps can be employed to evaluate and verify the accuracy of the proposed analytical approach.

6. **Analytical Approach to the Coupled System Undergoing Free Vibration:** At this stage, the research primarily focuses on analyzing the coupled system experiencing free vibration without considering the effects of damping. This part involves analytical coupling of the sloshing equation with the structural equation. The objectives are to investigate the stability of the coupled system, determine the natural frequencies, and introduce the response of the system under free vibration. Achieving these objectives is crucial for a deeper understanding of structure-TLD interactions. In addition, this stage assesses how the limitations of the model impact its accuracy and validity.
7. **Analyzing the impact of dissipations on the coupled system behavior**: The next objective is to examine the role of dissipation, both fluid and structural, on the dynamic behavior of the coupled system. By introducing dissipations and analytically coupling the sloshing and structural equations, the sub-objectives at this stage include evaluating the stability of the coupled system with dissipation, determining the natural frequencies of the coupled system that incorporates dissipations, assessing the decay of the system's displacement over time, and analyzing the system’s overall response under the influence of dissipation. These analytical insights are crucial for a deeper understanding of the coupled system and how the efficiency of TLD is affected by dissipation. Another key objective of this study is to assess the response of the coupled system when the TLD is equipped with screens, which is essential for recognizing how screens can enhance the damping effects of the TLD.

8. **Analytical Modeling of the Coupled System Subjected to Forced Excitation:** The final objective of this research is to analyze the behavior of a coupled system under forced vibration. The focus is on determining the total response, which combines complementary and particular responses, while identifying the contributing frequencies and assessing the decay due to dissipation. This study also investigates the feasibility of determining unknown response coefficients using a novel initial vector.

   Additionally, this research aims to analytically determine two critical dynamic parameters: the amplification of displacement from dynamic loading and the phase difference between the excitation force and displacement. Understanding these parameters is essential for evaluating the system's dynamic behavior and stability. A key aspect is to examine the coupled system's behavior as the excitation frequency approaches its natural frequencies, known as resonance excitation, which can lead to vey high dynamic amplification and instabilities. This study offers insights into the system's behavior when the excitation force frequency is close to the TLD's natural frequency. It also examines the impact of dissipation from both the structure and fluid on the dynamic characteristics. Overall, this research enhances the understanding of the coupled system's response to various excitation frequencies and the implications for TLD efficiency.

1.7. Novelty and Contribution of the Research

Although various shallow water models have been developed to simulate sloshing waves in tanks, there have been limited investigations into how the choice of numerical model affects the accuracy and reliability of these simulations. To address this gap in the literature, a comprehensive numerical study was conducted under both the initial perturbation and forced excitation conditions. The finite volume method was employed with both first-order and higher-order upwind schemes, whereas the finite difference method utilized two second-order schemes: McCormack and central methods. Additionally, both Preissmann and staggered schemes in fully implicit and semi-implicit forms were applied. The results indicate that the accuracy and stability of the shallow water model are significantly influenced by the choice of numerical method, with some methods exhibiting substantial numerical diffusion errors.

After utilizing a shallow water model equipped with a numerical method that minimizes numerical diffusion, the model was coupled with a single degree-of-freedom system to develop a structure-TLD (Tuned Liquid Damper) model. Upon verifying the model, two key parameters— the frequency ratio and damping ratio—were analyzed, representing a significant contribution to the existing literature.

As discussed in the preceding section, the implementation of sloped beds in TLDs appears to offer a greater damping effect on structures than conventional TLDs. However, a review of the literature reveals that very few studies have explored TLDs with sloped beds, and approximately all existing research is based on the linear potential flow theory, which assumes low sloshing waves. Therefore, developing a stable, reliable, and cost-effective numerical model that simulates TLD with a sloped bed and can handle high-amplitude sloshing waves would address a significant gap in the history of TLD research.

When the tank experiences high-amplitude excitation, a violent free surface with steep gradients is generated. Additionally, as the fluid sloshes over the sloped bed, wet-dry boundaries form within the model. Therefore, the model must first accurately capture the high-gradient free surface. To achieve this, a central upwind method with a slope limiter (Minmod function) is employed to approximate fluxes and interface variables. The bed topography term is integrated into the model and discretized using a second-order finite difference method.

The verification of the model in various case studies has demonstrated its reliability and accuracy in capturing high-gradient free surfaces and wet-dry-bed conditions. However, under high sloshing forces, the wave profile becomes asymmetric, characterized by sharp positive peaks and curved negative troughs, which classical nonlinear shallow water equations fail to accurately model. To improve the accuracy, the dispersion and dissipation terms are incorporated into the momentum equations of the classical nonlinear shallow water model. Although all the terms are treated explicitly, the dispersion term is implicitly discretized to ensure stability.

The accurate and stable model developed in the previous section was coupled with a single-degree-of-freedom (SDOF) system to create a structure-TLD model. A second-order midpoint method was introduced for the coupling process. The results reveal that the sloped-bed tank produces higher sloshing waves than the conventional designs. Moreover, the comparison between the sloped-bed

TLD and conventional TLD demonstrates a superior damping effect in the sloped-bed design, marking another significant contribution to the research on TLD systems.

Although the literature includes a few analytical approaches to sloshing waves, there is a lack of comprehensive analytical investigations of coupled systems, including both the structure and TLD. Key questions regarding the dynamic behavior of the coupled system, such as its natural frequency, damping, and analytical response to dynamic forces, remain insufficiently addressed. Chapters three, four, and five of this work focus on the analytical exploration of these dynamics, presenting novel solutions and proofs. These chapters provide a deeper understanding of how coupled systems behave under dynamic loading through analytical relationships, thereby contributing significantly to the field.

The first chapter of the analytical work focuses on the coupled system, neglecting damping and subjecting it to free vibrations. By applying the separation of variables technique, shallow water equations are decomposed into different modes, which are then strongly coupled with a single degree of freedom (SDOF) system. This coupling results in the derivation of the characteristic equation for each mode. Based on this characteristic equation, novel and important concepts are introduced. The stability of the coupled system is analyzed, and the natural frequencies—arguably the most important dynamic property—of each mode are derived through new analytical relationships. Additionally, with the introduction of new initial boundary value vectors, the undamped response of the coupled system is determined, making another significant contribution to the literature.

This study further investigates the response of the coupled system due to higher modes and examines the role of the initial perturbation in stimulating the natural frequencies of these modes. It is also demonstrated that the first mode primarily governs the behavior of the coupled system. The developed numerical model confirms the reliability of the analytical approach; however, it shows that the accuracy decreases for higher amplitude excitations because the model is based on linear theory for both sloshing waves and the structural response.

The incorporation of dissipation modifies the characteristic equation of the coupled system, which includes both the structure and tuned liquid damper (TLD), leading to an altered dynamic behavior. In this context, dissipation is categorized as structural, fluid, and local dissipation. An analysis of the characteristic equation for the coupled system with structural dissipation during free vibration reveals that it possesses two pairs of complex conjugate roots with negative real parts, ensuring the unconditional stability of the system. The analytical results indicated that the effect of dissipation on the natural frequency of the system is minimal. Furthermore, the response of the system decreases exponentially with the rate characterized by the dissipation factors (representing the damping of the coupled system). This study analytically introduces dissipation factors for two scenarios: (1) the inclusion of structural damping and (2) the integration of both structural and fluid damping, contributing novel and valuable insights to the existing literature.

In addition, by incorporating initial value vectors including initial displacement, initial velocity, initial wave height perturbation, and initial fluid velocity, the analytical response of the coupled system, incorporating dissipation and free vibration, is derived. This development addresses a significant gap in the literature. The analysis demonstrates the necessity of initial perturbations to stimulate higher frequency modes and reproduce the single-degree-of-freedom response in these modes. Lastly, the analytical model extends to consider local dissipation, potentially associated with the presence of a screen. A novel analytical solution based on the first modal analysis is presented, which introducing a modified dissipation approach to account for the effects of local dissipation. Hence, the comprehensive response of the coupled system, integrating structural, fluid, and screen dissipation, is derived, which is another significant contribution of this research.

The preceding chapters focused on free vibration to gain a deeper understanding of the dynamic behavior of the coupled system under both non-dissipative and dissipative conditions. This section shifts to the scenario of a coupled system subjected to forced excitation, specifically, harmonic excitation. This analysis is significant because any periodic dynamic force can be represented as a harmonic function via Fourier transformation. The response of the coupled system can be derived by employing the superposition technique. In addition, in the context of earthquake excitation, it is possible to determine the response of the system to the dominant earthquake frequency. Given that dissipation influences the response shape, this research is conducted in three stages: 1) an undamped coupled system, 2) a structurally damped coupled system, and 3) a structurally and fluid-damped coupled system. For each case, the separation of variables technique and strong coupling procedure are employed to derive a fourth-order ordinary differential equation that incorporates the continuity and momentum equations of the fluids along with a single degree of freedom subjected to harmonic excitation.

In a novel approach, a particular solution to this inhomogeneous ordinary differential equation is introduced for each scenario. The complementary solution, representing the response under free vibration, is derived from previous chapters: Chapter (4) for the undamped case and Chapter (5) for the structurally and fluid-damped case. Consequently, the total response composed of both complementary and particular solutions, is derived. The coefficients of the total response in each scenario are determined using a novel initial value vector. Thus, the total response of the coupled system under forced excitation in each scenario is derived, thereby making a significant contribution to the literature. Two critical dynamic parameters are analyzed: 1) the dynamic amplification factor, which amplifies the static displacement of the system due to the dynamic force, and 2) the phase difference between the displacement of the system and the excitation force. The behavior of these parameters depends on five frequencies: 1) and 2) the natural frequencies of the coupled system, 3) the excitation force frequency, 4) the water tank frequency, and 5) the SDOF frequency, as well as the damping effects in dissipative scenarios. Six diagrams illustrating the variation in these parameters with frequency ratios across all three scenarios are presented. It is demonstrated that in higher modes, both the particular and total responses of the coupled system replicate the SDOF response in both the undamped and damped scenarios. Finally, the total response in each scenario is further analyzed in two special cases: 1) resonance excitation, where the excitation frequency approaches the smaller or larger natural frequencies of the coupled system, and 2) when the excitation frequency approaches the natural frequency of the tank. These analytical findings represent new, innovative, and significant contributions to TLD research.

1.8. Thesis Structure

1. The first chapter introduces tuned liquid dampers (TLDs) and details their origins, operational principles, and development. This chapter includes a comprehensive literature review of TLDs, covering various modeling approaches for sloshing waves, such as shallow water models, potential flow theory, volume of fluid method, smoothed particle hydrodynamics, and Housner theory. Additionally, this chapter discusses the single-degree-of-freedom (SDOF) modeling approach employed in this research and presents its verification. This chapter provides a comprehensive summary of fluid-structure interactions in Tuned Liquid Dampers (TLDs). Following an extensive review of the literature, this chapter identifies several gaps and highlights how this study aims to address these deficiencies. The chapter concludes with an explanation of the structure of the thesis.

2. Chapter Two focuses primarily on the impact of numerical diffusion introduced by various numerical schemes on the accuracy of the sloshing models. To investigate this, several discretization methods for the linear shallow water equation are employed, including first-order upwind, higher-order upwind (classified as finite volume methods), McCormack, central methods, Preissmann (both full- and semi-implicit), staggered (both full-implicit and semi-implicit), and the separation of variables technique. Additionally, this chapter examines the use of ghost nodes in higher-order schemes and their effect on model accuracy. Both the initial perturbation and forced excitation scenarios are simulated using these models, and the resulting numerical diffusion is analyzed. A model exhibiting minimal numerical diffusion is then selected, and a physical diffusion term is incorporated into this model. This sloshing model is subsequently coupled with a single degree of freedom (SDOF) model using a partitioned method to establish a structure-TLD model. This chapter presents a flowchart of the coupling process. Following the verification of the TLD model against the experimental data, a parametric study is conducted to investigate the effects of frequency and damping ratios.
3. The goal of this chapter is to develop a stable and reliable numerical method for simulating a structure-TLD system equipped with a sloped bed. To achieve this, the nonlinear shallow water equation is utilized, with the central upwind method and the Minmod slope limiter function employed to accurately determine the flux and interface variables. The verification of the model through a case study involving high-gradient free surfaces (such as a dam-break scenario) demonstrates that this approach is both accurate and stable. The topography term is incorporated into the equation and discretized using a second-order finite difference method. The effectiveness of the model is further validated through two case studies: a dam break on a sloped bed and run-up and run-down over a parabolic bed. The inclusion of dispersion and dissipation terms in the nonlinear shallow water equation accounts for the asymmetric and steady patterns of sloshing waves. To maintain the model stability, the dispersion term is treated implicitly, requiring the solution of a matrix equation at each iteration. A comparison with experimental data from a sloshing tank shows excellent agreement. Additionally, simulations reveal that sloshing waves are more pronounced in a box tank with a sloped bed than in a rectangular box tank, suggesting a superior damping effect of the sloped bed TLDs. The model is coupled with a single-

degree-of-freedom system using a partitioned algorithm with a midpoint method, which is second-order accurate. The results indicate that the sloped-bed TLD significantly reduces structural vibrations compared with conventional box TLDs.

4. The fourth chapter is dedicated to the analytical investigation of the dynamic behavior of a single-degree-of-freedom (SDOF) system coupled with a tuned liquid damper (TLD), collectively referred to as the coupled system. This analysis focuses on the free vibration of the coupled system in the absence of dissipation, with the SDOF representing a structure such as a tall building. The analytical approach relies on the linear wave theory and the linear behavior of the structure, which limits the study to low-amplitude excitations. The partial differential equations governing the shallow water system are converted into ordinary differential equations through the separation of variables technique and subsequently decomposed into different modes. The sloshing forces transmitted from the TLD to the SDOF are expressed in a modal coordinate system. By coupling the continuity and momentum equations of the fluid with the SDOF equation, a fourth-order ordinary differential equation is derived. This characteristic equation is pivotal for research as it is used to analyze the stability of the coupled system. The natural frequency of the coupled system, a key dynamic characteristic, is determined, and the response coefficients of the coupled system are established using a novel initial value vector. This study further explores the dynamic properties of higher modes, including the influence of initial perturbations on stimulating higher natural frequencies. The dominance of the first mode in the response of the system is also demonstrated. This chapter employs a developed numerical model, as described in detail, and Fast Fourier Transform (FFT) to assess the accuracy of the analytical approach. Finally, the limitations of the proposed analytical method are discussed.
5. This chapter extends the analysis from the previous chapter, where the coupled system was subjected to free vibration by introducing dissipation into the equations. Dissipation arises from the structural damping, fluid damping, and screen presence. The integration of the fluid and structural dissipation results in a characteristic equation that is distinct from that of the undamped system discussed in the previous chapter. The methodology used to derive the modified characteristic equation was explained in detail. The roots of this characteristic equation were analyzed, showing that the coupled system remains unconditionally stable

during free vibration. This chapter provides an analytical proof that dissipation has a negligible impact on the natural frequency of the coupled system, allowing the natural frequencies to be derived from the equations of the undamped system. The response of the coupled system exhibits an exponential decay, with the power of this decay, known as the dissipation factor, being studied in detail. Analytical expressions for determining dissipation factors are presented. For higher modes, the analysis covers the natural frequencies, absence of a greater frequency in the response function, necessity of initial perturbation to trigger these frequencies, and replication of SDOF responses. This chapter further confirms that the system response is predominantly governed by the first mode. As in the preceding chapter, a developed numerical model and Fast Fourier Transform (FFT) are employed to validate the accuracy of the analytical results. The chapter concludes by incorporating the local dissipation stemming from screens into the analysis. A novel analytical solution based on first-mode dominance is proposed to determine the response of the coupled system. This solution introduces enhanced dissipation factors to account for the screen dissipation and natural frequencies of the undamped system. The validity and accuracy of this solution are confirmed through comparisons with the numerical models.

6. This chapter focuses on the investigation of the coupled system under forced excitation, building on the analytical approach developed in the previous chapters. Similar to earlier discussions, the governing equations of the coupled system include the fluid continuity and momentum equations as well as the SDOF equation, which are now subjected to harmonic forced excitation. Unlike the previous free vibration case, the coupled ordinary differential equation is now inhomogeneous; therefore, the total response comprises both a complementary response and a particular response. The complementary responses, which solve the homogeneous equation, represent the free vibration response of the coupled system and were derived in earlier chapters. Because dissipation impacts the particular response, the analysis is divided into three scenarios: undamped system, structurally damped system, and fluid and structurally damped systems. For each of these scenarios, the particular and total responses are derived. Initial value vectors are introduced to determine the coefficients of the total response. Two key dynamic parameters, namely the dynamic amplification factor and phase difference, are introduced, and their functions are analytically derived for all scenarios. In addition, variations in these parameters with

respect to the frequency ratio is investigated. It is shown that both the particular and total responses in higher modes, whether in the undamped or damped case, replicate the behavior of the SDOF system. In addition to the general response, two special cases of significant importance are examined separately for all the scenarios. The first special case deals with resonance excitation, in which the excitation frequency approaches either the smaller or greater natural frequency of the system. The second special case is considered when the excitation frequency approaches the natural frequency of the water tank, which is the most efficient scenario for TLD suppression. A Fast Fourier Transform (FFT) is utilized to extract the constitutive frequencies of the numerical response, and a numerical method is developed to verify the accuracy of the analytical responses for both the general and special cases across all scenarios.

7. Chapter 7 begins by summarizing the key findings from the preceding chapters, offering a detailed discussion on both the numerical modeling and analytical approaches. The research conclusions are thoroughly examined, highlighting the contribution in each area. Following this, the chapter turns its attention to potential future work, exploring how both numerical and analytical methodologies can be extended to address more practical and impactful topics. In terms of numerical modeling, this study presents an accurate, stable, and cost-effective model. This model has the potential to be further developed and applied to other related areas, thereby enhancing its practical utility. Regarding the analytical approaches, this study introduces a comprehensive understanding of the dynamic properties of a coupled system under both free and forced vibrations. The insights gained from this study can be refined and expanded to explore other complex scenarios within the field. These contributions open new avenues for advancing both theoretical and practical applications of TLDs.

At the end of this chapter, the structure of the thesis is illustrated in the following graph.

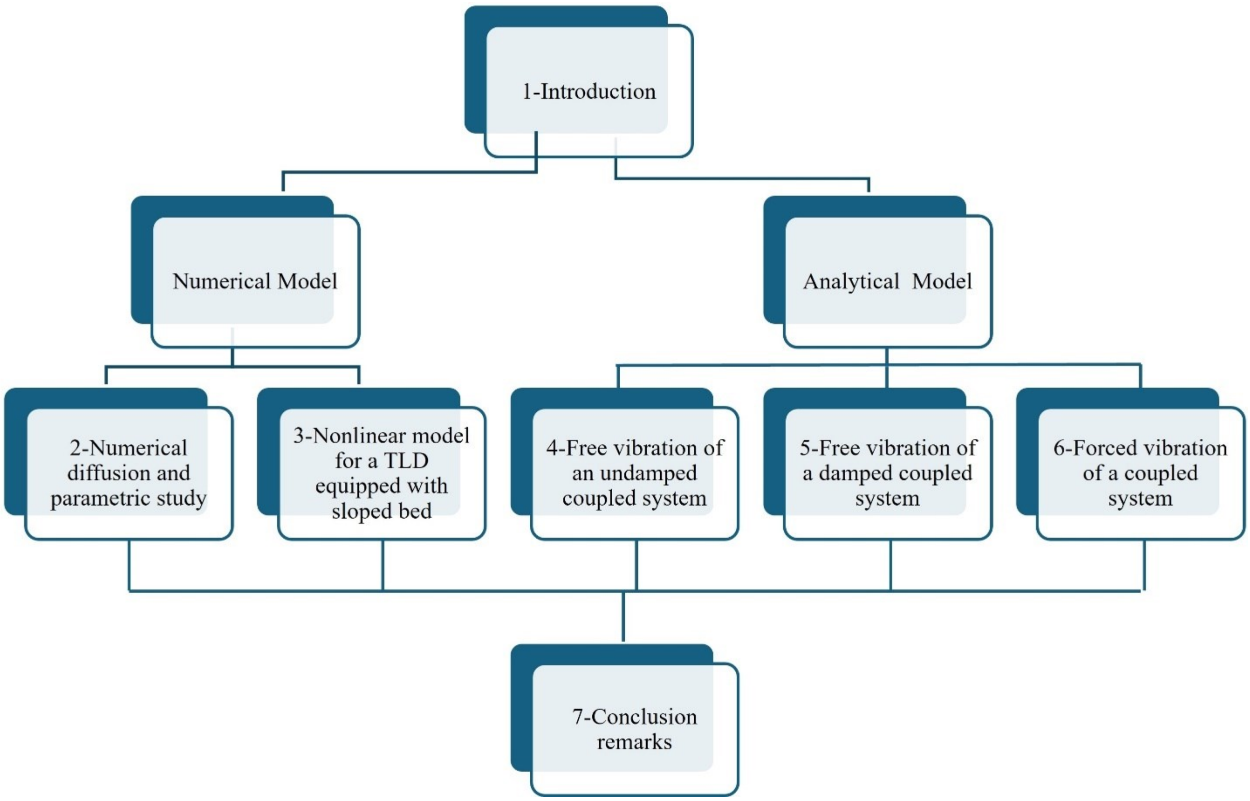

Fig. 1.17. Graph Illustrating the structure of chapters in this Thesis

References

1. Abd-Elhamed, A., & Tolan, M. (2022). Tuned liquid damper for vibration mitigation of seismic-excited structures on soft soil. Alexandria Engineering Journal, 61(12), 9583-9599.
2. Ashasi-Sorkhabi, A., Malekghasemi, H., Ghaemmaghami, A., & Mercan, O. (2017). Experimental investigations of tuned liquid damper-structure interactions in resonance considering multiple parameters. Journal of Sound and Vibration, 388, 141-153.

3. Awad, B. N., Tait, M. J., & Love, J. S. (2024). Numerical modelling of dual function tanks for fire suppression and tuned liquid damper applications. Engineering Structures, 299, 117080.
4. Bahreini Toussi, I., Kianoush, R. & Mohammadian, A. 2021.Numerical and Experimental Investigation of Rectangular Liquid-Containing Structures under Seismic Excitation. Infrastructures 6, 1.
5. Banerji, P., Murudi, M., Shah, A.H. & Popplewell, N. (2000). Tuned liquid dampers for controlling earthquake response of structures. Earthq Eng Struct Dyn, 29,587–602.
6. Cao, Y., Graczyk, M., Pakozdi, C., Lu, H., Huang, F., & Yang, C. (2010, June). Sloshing Load Due to Liquid Motion in a Tank Comparison of Potential Flow, CFD, and Experiment Solutions. In ISOPE International Ocean and Polar Engineering Conference (pp. ISOPE-I). ISOPE. Wu, G. X., Ma, Q. W., & Taylor, R. E. (1998). Numerical simulation of sloshing waves in a 3D tank based on a finite element method. Applied ocean research, 20(6), 337-355.
7. Chang, Y., Noormohamed, A., & Mercan, O. (2018). Analytical and experimental investigations of modified tuned liquid dampers (MTLDs). Journal of Sound and Vibration, 428, 179-194.
8. Chopra, A.K. (2007). Dynamic of Structures, Theory and Applications to Earthquake Engineering. 3rd Edition, Prentice Hall, Upper Saddle River.
9. Crowley, S., & Porter, R. (2012). An analysis of screen arrangements for a tuned liquid damper. Journal of Fluids and Structures, 34, 291-309.
10. Domizio, M., Ambrosini, D., & Campi, A. (2024). A novel tuned liquid damper for vibration control in high-frequency structures. Engineering Structures, 301, 117350.
11. English, A., Domínguez, J. M., Vacondio, R., Crespo, A. J. C., Stansby, P. K., Lind, S. J., & Gómez-Gesteira, M. (2022). Modified dynamic boundary conditions (mDBC) for general-purpose smoothed particle hydrodynamics (SPH): application to tank sloshing, dam break and fish pass problems. Computational Particle Mechanics, 9(5), 1-15.
12. Fujino, Y., Sun, L., Pacheco, B. M., & Chaiseri, P. (1992). Tuned liquid damper (TLD) for suppressing horizontal motion of structures. Journal of Engineering Mechanics, 118(10), 2017-2030.
13. Guruswamy, G. P. (2002). A review of numerical fluids/structures interface methods for computations using high-fidelity equations. Computers & structures, 80(1), 31-41.
14. Housner, G. W. (1963). The dynamic behavior of water tanks. Bulletin of the seismological society of America, 53(2), 381-387.
15. Hu, X., Zhao, Z., Weng, D., & Hu, D. (2022). Design of a pair of isolated tuned liquid dampers (ITLDs) and application in multi-degree-of-freedom structures. International Journal of Mechanical Sciences, 217, 107027.
16. Humar, J. (2012). Dynamics of structures. CRC press.
17. Ji, S., & Liu, L. (2020). Computational granular mechanics and its engineering applications. Singapore: Springer.

18. Khanpour, M., Mohammadian, A., Shirkhani, H., & Kianoush, R. (2024). Simulation of Sloped-Bed Tuned Liquid Dampers Using a Nonlinear Shallow Water Model. Water, 16(10), 1394.
19. Khanpour, M., Zarrati, A. R., Kolahdoozan, M., Shakibaeinia, A., & Jafarinik, S. (2016a). Numerical modeling of free surface flow in hydraulic structures using Smoothed Particle Hydrodynamics. Applied Mathematical Modelling, 40(23-24), 9821-9834.
20. Khanpour, M., Zarrati, A. R., Kolahdoozan, M., Shakibaeinia, A., & Amirshahi, S. M. (2016b). Mesh-free SPH modeling of sediment scouring and flushing. Computers & Fluids, 129, 67-78.
21. Kianoush, M. R., & Ghaemmaghami, A. R. (2011). The effect of earthquake frequency content on the seismic behavior of concrete rectangular liquid tanks using the finite element method incorporating soil–structure interaction. *Engineering structures*, *33*(7), 2186-2200.
22. Konar, T., & Ghosh, A. (2023). Development and design of a deep tank damper with submerged suspended plate. Advances in Structural Engineering, 26(5), 937-951.
23. Konar, T., & Ghosh, A. D. (2021). Flow damping devices in tuned liquid damper for structural vibration control: a review. Archives of Computational Methods in Engineering, 28, 2195-2207
24. Lee, S. K., Park, E. C., Min, K. W., Lee, S. H., Chung, L., & Park, J. H. (2007). Real-time hybrid shaking table testing method for the performance evaluation of a tuned liquid damper controlling seismic response of building structures. Journal of Sound and Vibration, 302(3), 596-612.
25. Liao, K., & Hu, C. (2013). A coupled FDM–FEM method for free surface flow interaction with thin elastic plate. Journal of marine science and technology, 18, 1-11.
26. Liu, G. R., & Liu, M. B. (2003). Smoothed particle hydrodynamics: a meshfree particle method. World scientific.
27. Marivani, M., & Hamed, M. S. (2017). Evaluate pressure drop of slat screen in an oscillating fluid in a tuned liquid damper. Computers & Fluids, 156, 384-401.
28. Marivani, M., & Hamed, M.S. (2009). Numerical simulation of structure response outfitted with a tuned liquid damper, Computers & Structures, 87, (17-18), 1154-1165.
29. McNamara, K. P., & Tait, M. J. (2022b). Modeling the Response of Structure–Tuned Liquid Damper Systems Under Large Amplitude Excitation Using Smoothed Particle Hydrodynamics. Journal of Vibration and Acoustics, 144(1), 011008.
30. McNamara, K. P., Love, J. S., & Tait, M. J. (2022a). Numerical investigation of the response of structures equipped with a limited freeboard tuned liquid damper. Journal of Fluids and Structures, 108, 103426.
31. Mehl, M., Brenk, M., Bungartz, H. J., Daubner, K., Muntean, I. L., & Neckel, T. (2008). An Eulerian approach for partitioned fluid–structure simulations on Cartesian grids. Computational Mechanics, 43, 115-124.
32. Molteni, D., & Colagrossi, A. (2009). A simple procedure to improve the pressure evaluation in hydrodynamic context using the SPH. Computer Physics Communications, 180(6), 861-872.

33. Moslemi, M. & Kianoush, M.R. 2012. Parametric study on dynamic behavior of cylindrical ground-supported tanks. Eng. Struct. 42, 214–230.
34. Murudi, M., & Banerji, P. (2012). Effective control of earthquake response using tuned liquid dampers. Journal of Earthquake Technology, 49(3-4), 53-71.
35. Pabarja, A., Vafaei, M., Alih, S. C., Yatim, M. Y. M., & Osman, S. A. (2019). Experimental study on the efficiency of tuned liquid dampers for vibration mitigation of a vertically irregular structure. Mechanical Systems and Signal Processing, 114, 84-105.
36. Pandey, D. K., Sharma, M. K., & Mishra, S. K. (2019). A compliant tuned liquid damper for controlling seismic vibration of short period structures. Mechanical Systems and Signal Processing, 132, 405-428.
37. Pandit, A. R., & Biswal, K.C. (2020). Seismic control of multi degree of freedom structure outfitted with sloped bottom tuned liquid damper. In Structures, 25: 229-240.
38. Panigrahy, P. K., Saha, U. K., & Maity, D. (2009). Experimental studies on sloshing behavior due to horizontal movement of liquids in baffled tanks. Ocean Eng. 36, 213–222.
39. Pozorski, J., & Olejnik, M. (2024). Smoothed particle hydrodynamics modelling of multiphase flows: an overview. Acta Mechanica, 235(4), 1685-1714.
40. Saghi, H., Ma, C., & Zi, G. (2024). Bidirectional tuned liquid dampers for stabilizing floating offshore wind turbine substructures. Ocean Engineering, 309, 118553.
41. Sardar, R., & Chakraborty, S. (2022). Wave vibration control of jacket platform by tuned liquid dampers. Ocean Engineering, 247, 110721.
42. Sobhan, M. S., Rofooei, F. R., & Attari, N. K. (2017). Buckling behavior of the anchored steel tanks under horizontal and vertical ground motions using static pushover and incremental dynamic analyses. Thin-Walled Structures, 112, 173-183
43. Sun, H. D., He, H. X., Cheng, Y., & Gao, X. J. (2024). Theoretical and experimental study on vibration control of a tuned liquid inerter damper with additional damping net and sloped-bottom. Mechanical Systems and Signal Processing, 213, 111356.
44. Sun, L. M., Fujino, Y., Pacheco, B. M., & Chaiseri, P. (1992). Modelling of tuned liquid damper (TLD). Journal of Wind Engineering and Industrial Aerodynamics, 43(1-3), 1883-1894.
45. Tait, M., El Damatty, A., Isyumov, N., & Siddique, R. (2005). Numerical flow models to simulate tuned liquid dampers (TLD) with slat screens. Journal of Fluids and Structures, 20, 1007-1023.
46. Tang, Z., Sheng, J., & Dong, Y. (2023). Effects of tuned liquid dampers on the nonlinear seismic responses of high-rise structures using real-time hybrid simulations. Journal of Building Engineering, 70, 106333.
47. Tsao, W. H., & Hwang, W. S. (2018). Tuned liquid dampers with porous media. Ocean Engineering, 167, 55-64.
48. Veletsos, A. S. (1974, June). Seismic effects in flexible liquid storage tanks. In Proceedings of the 5th world conference on earthquake engineering (Vol. 1, pp. 630-639). McLean, VA, USA: Bulletin of the Seismological Society of America.

49. Veletsos, A. S., Tang, Y., & Tang, H. T. (1992). Dynamic response of flexibly supported liquid storage tanks. Journal of Structural Engineering., 118, 264–283
50. Violeau, D., & Rogers, B. D. (2016). Smoothed particle hydrodynamics (SPH) for free-surface flows: past, present and future. Journal of Hydraulic Research, 54(1), 1-26.
51. Zhang, Z. (2020). Numerical and experimental investigations of the sloshing modal properties of sloped-bottom tuned liquid dampers for structural vibration control. Engineering Structures, 204, 110042.
52. Zhao, Z., Zhang, R., Jiang, Y., & Pan, C. (2019). A tuned liquid inerter system for vibration control. International Journal of Mechanical Sciences, 164, 105171.

List of Symbols

H	Mean water level
η	Wave height
U	Depth- average velocity
G	Gravity acceleration
H	Total water depth
A	Water tank acceleration
ϕ	Velocity potential function
V	Velocity function
W	Vertical velocity
a_x	Horizontal acceleration
a_z	Vertical acceleration
P	Pressure
υ	Kinematic viscosity of the fluid

F	Volume fraction
ρ_j	Particle density
m_j	Particle mass
W	Kernel function
c_0	Speed of sound in the fluid
ψ_{ij}	Density diffusion function
π_{ij}	Artificial viscosity
f_w	Fundamental sloshing frequency
L	Length of the water tank
m_f	TLD mass
S	surface contamination factor
M	Mass of the SDOF
K	Stiffness of the SDOF
C	Damping coefficient of the SDOF
$\bar{F}(t)$	seismic force excitation
$F_L(t)$	lateral dynamic force
u_s	Displacement of the SDOF
$\dot{u}_s$	Velocity of the SDOF
$\ddot{u}_s$	Acceleration y of the SDOF
Δt	Time step

2. Numerical Simulation of Sloshing Tanks with Shallow Water Model Using Low Numerical Diffusion Schemes and its Application to Tuned Liquid Dampers[1]

Abstract

The initial part of this study fills a notable research gap by investigating the substantial impact of numerical diffusion errors from different schemes on sloshing tank models. Multiple numerical models were developed: first and higher order upwind schemes equipped with precise wall treatment using ghost nodes, MacCormack and central methods that are explicit second-order finite difference methods, and Preissmann and staggered methods employed in full-implicit and semi-implicit modes. Furthermore, the separation of variables technique was proposed for simulating sloshing tanks and deriving an analytical equation for the tank's natural period. An analytical solution to the perturbation was employed to examine the numerical diffusion of the schemes. Subsequently, two sloshing tests, resonant and near-resonant excitations, were employed to determine the numerical diffusion and calibrate the physical diffusion coefficients, respectively. Finally, an efficient and accurate numerical scheme was applied to a linear shallow water model including physical diffusion and coupled with a single degree of freedom (SDOF), to simulate tuned liquid dampers (TLDs). It shows that the efficiency of TLD is associated with a compact domain around resonance excitation. Contrary to SDOF alone, when SDOF interacts with TLD the impact of structural damping on reducing the response is minimal in resonance excitation.

Keywords: Numerical diffusion, Shallow water model, Sloshing, Tuned Liquid Damper, Frequency ratio, Damping ratio

---

[1] Mahdiyar Khanpour , Abdolmajid Mohammadian, Hamidreza Shirkhani, and Reza Kianoush"*Numerical Simulation of Sloshing Tanks with Shallow Water Model Using Low Numerical Diffusion Schemes and its Application to Tuned Liquid Dampers*", **International Journal of Applied and Computational Mathematics**, Under Review.

2.1. Introduction

Liquid storage tanks have grown significantly over the past few decades and are considered vital component of industrial infrastructure. These structures are widely used for the storage of a variety of materials, such as oil and gas, liquefied natural gas, chemical fluids, waste in various forms, nuclear materials, and water supply facilities. Under seismic excitation, storage tanks experience fluid movement known as sloshing waves, which generates pressure within the tanks. While sloshing waves can potentially threaten the stability of tanks, they offer significant benefits when employed in tuned liquid dampers (TLDs).

TLDs are sloshing tanks mounted on the roof of structures to reduce vibrations when they undergo lateral dynamic movement. Typically, the natural frequency of a sloshing tank is tuned to match the natural frequency of the structure (Sun et al., 1992, Tait, 2005, and Bhattacharjee et al.2013, Malekghasemi et al., 2015). This alignment results in an amplified response of the sloshing tank, which in turn influences the behavior of the structure. Experimental and numerical studies have shown that when seismic loading closely approaches the structural frequency, known as near-resonance excitation, the sloshing waves significantly reduce the structural vibration (Sun et al., 1992, Tait, 2005). This indicates that the tuned liquid damper (TLD) performs optimally under near-resonance excitation, whereas it represents the worst-case scenario for the stability of the structure in the absence of a TLD. Certainly, researchers have explored various aspects of tuned liquid dampers (TLDs) in their studies. For example, Sun and Fujino (1994) conducted research into the impact of wave breaking on TLD modeling. Marivani and Hamed (2017) and Love and Tait (2013) separately investigated the influence of screens and depth ratio on the performance of TLDs. Pandit and Biswal (2020) investigate numerically how the sloped bottom changes the damping effect of TLDs. The primary part of the TLDs are sloshing tanks and researchers have made significant efforts to model them by applying certain simplifying assumptions. So, the first section of this research focuses on the numerical molding of sloshing tanks.

Former methods rely on Hounser's (1963) analytical approach, which divides the fluid in moving tanks into convective and impulsive parts. Although this method has many applications in engineering because of its simplicity, it should be acknowledged that this method provides a quite rudimentary approximation of fluid sloshing.

Later, potential flow theory (Faltinsen, 1974; Solaas and Faltinsen, 1997; Wu et al., 1998) was applied to sloshing tank to provide a more accurate picture of fluid movement. However, most of these models assume linear and small-amplitude waves.

Other researchers have employed more advanced methods, such as volume of fluid (VOF) (Bahraini et al., 2021; Marivani and Hamed, 2009; Liu and Lin, 2008) and smoothed particle hydrodynamics (SPH) (Cao et al., 2014; and Moslemi et al., 2019) to model sloshing tanks. Although these models are capable of generating more accurate and detailed results, they suffer from high computational costs and noisy solutions (Sun et al., 2021).

Shallow water models are hyperbolic equations based on depth-averaged Euler equations (Abbott and Minns 2017) that can be used for modelling sloshing tanks. The literature review indicates that a few studies used shallow water models for sloshing tanks simulations (Saburin, 2015), and most of them were applied to simulate sloshing tanks in TLDs (Sun et al., 1992; Sun and Fujino, 1994; Tait, 2005; Banerji et al., 2000). Each of these models has merits and disadvantages. Shallow water models that benefit from low-cost calculations and decent accuracy, appear to be an appropriate tool for modeling TLDs.

Although some studies have focused on the application of shallow water models to sloshing tanks, there is a gap in how the temporal and spatial discretization schemes using numerical models influence the accuracy of the modeling of sloshing tanks. One of the primary objectives of this study is to evaluate the performance of various schemes utilized in simulation of sloshing tanks, and to propose efficient and accurate numerical methods for such applications. The focus of this study will be on linear shallow water equations, which is an extremely fast system with a low computational cost. Such a low-cost numerical solution is particularly useful for tank optimization purposes where many simulations are demanded. First, upwind schemes (Mohammadian and Le Roux, 2008; Kurganov, 2018), that approximate the advection term with respect to the flow direction was investigated. The simplest upwind scheme is the first-order scheme, which can be enhanced by higher-order upwind methods, such as κ schemes, that rely on more data points for flux approximation. In addition, a solution is proposed in this study to model wall boundaries with less numerical diffusion error. Subsequently, the MacCormack method and the central scheme, which are second-order explicit finite-difference schemes, were studied. MacCormack, a type of finite difference scheme introduced by MacCormack (1971), was first used as a solution to compressible Navier-Stokes equations. Then, it was applied by Chaudhry and Hussaini (1985) and subsequently developed by Amara et al. (2013) for water hammer analysis. Furthermore, Fennema and Chaudhry (1986) and Garcia and Kahawita (1986) utilized this method for unsteady free-surface flows. The MacCormack scheme includes predictor and corrector procedures, whereas the central method utilizes the central finite-difference method for spatial discretization and relies on the midpoint scheme for time discretization (Abbott, M., & Minns 2017).

For implicit and semi-implicit methods, two efficient second-order schemes of: (i) Preissmann (Wang, 2019) and (ii) Staggered methods (Abbot and Minns 1998) were discussed. In open-channel hydraulics, the Preissmann scheme (developed by Preissmann in 1961) has been extensively employed (Wu, 2008, Popescu, 2014). Abbott and Basco (1989) stated that the scheme is flexible and appropriate for hyperbolic equations. The Preissmann scheme has also been applied to simulate flood wave propagation and unsteady flows in channel networks (Liu et al., 1992, Venutelli, 2002). Guo and Yu (2016) used this scheme to solve the Hairsine-Rose erosion equations**.** This scheme solves both the continuity and momentum equations at the control volume of each node. Although the early use of staggered implicit and semi-implicit schemes was relevant to viscous compressible flows (Gallouët et. al., 2007), Herbin (2014) proposed a scheme for shallow-water equations. A staggered method, unlike the Preissman scheme, provides a continuity control volume at one node and a momentum control volume at a subsequent node. This results in the velocity grid being non-overlapping downstream of the wave height grid. Furthermore, a separation of variables approach was proposed in this study to model the sloshing process. Different disciplines have used this technique to solve partial differential equations, such as the dynamics of continuous systems (Humar 2012) and wave modeling (Wazwaz 2009). This technique relies on the assumption that the solution to the partial differential equation can be separated into the product of several functions. Each function depends only on a single independent variable. In current research, the separation variable technique was not only applied to model sloshing tanks but was also utilized within linear shallow water equations to derive an analytical expression for the natural period of the tank. When comparing this expression with another commonly used and reliable formula found in the literature, it revealed a range of water depth to tank length ratios that yield accurate results for the natural period of the tank.

To verify the accuracy and evaluate numerical diffusion error associated with above-mentioned schemes in the present research, an analytical solution to a perturbation test and experimental data associated with resonant sloshing were employed. After verification, more accurate numerical schemes with reduced numerical diffusion errors were identified. Following that, a method benefits from a cost-effective computation and negligible numerical diffusion errors was incorporated with a physical diffusion term, whose coefficient was calibrated with experimental data. In the next step, this developed model was coupled with a dynamic equation of a single degree of freedom to model the TLDs. Subsequently, the influence of two parameters, 1-frequency ratio (excitation force frequency / natural TLD frequency) and 2-damping ratio (damping constant / critical damping constant, Humar 2012) on TLD performance were investigated.

The remainder of this paper is organized as follows. Section 2 outlines the methodology, including the governing equations. Additionally, it elaborates on the process of coupling these equations to create a TLD model. Section 3 describes several numerical methods for solving the governing equations, and most of the equations are presented in the Appendix. Section 4 addresses four test cases where the impact of numerical methods is compared to analytical solutions or experimental data. In addition, a parametric study of TLD is done in this part. The concluding remarks complete the study in Section 5.

2.2. Methodology

The linear shallow water equations for a one-dimensional rectangular tank with length L and averaged depth H (see Figure 2.1) subjected to acceleration a_x can be written as follows:

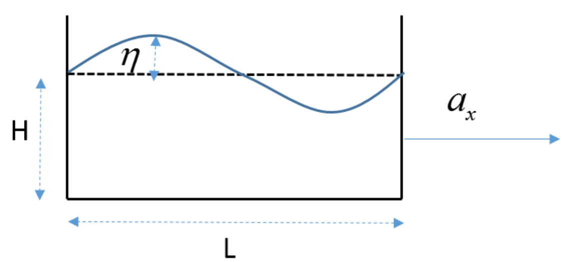

Fig. 2.1. Rectangular tank parameters

$$\frac{\partial \vec{U}}{\partial t} + \frac{\partial \vec{F}}{\partial x} = \vec{R} \tag{2-1}$$

with

$$\vec{U}=\begin{bmatrix}\eta\\u\end{bmatrix}\qquad \vec{F}=\begin{bmatrix}Hu\\g\eta\end{bmatrix}\qquad \vec{R}=\begin{bmatrix}0\\a_x+\alpha D\dfrac{\partial^2 u}{\partial x^2}\end{bmatrix}$$

In this equation $\vec{U}$ is variable vector, and $\vec{F}$ is flux vector as well as $\vec{R}$ is source vector. Also, u is the depth-averaged velocity, g is the gravitational acceleration. H refer to averaged depth and η is the wave height relative to averaged depth. In the source term, a_x refers to the tank acceleration and D is the coefficient of physical diffusion. Also, α is the contribution coefficient of physical diffusion. Sections (2.4.1) and (2.4.2) focus on the numerical diffusion associated with the above-mentioned numerical schemes in the case of both initial perturbation and sloshing, respectively. As a result, to identify numerical diffusion error, the physical diffusion was not contributed so $\alpha=0$. However, following that, in the section (2.4.3), physical diffusion is incorporated into the model to capture more accurate and realistic solution, i.e., $\alpha=1$. Note that for a stagnant tank the vector R is zero.

Two wall boundary conditions were applied: zero velocity and zero wave height gradient.

A non-conservative form of Equations (2-1) utilized in upwind schemes is expressed in Equations (2-2).

$$\frac{\partial U}{\partial t}+A\frac{\partial U}{\partial x}=R \tag{2-2}$$

with

$$\vec{U}=\begin{bmatrix}\eta\\u\end{bmatrix}\qquad A=\begin{bmatrix}0&H\\g&0\end{bmatrix}\qquad \vec{R}=\begin{bmatrix}0\\a_x+\alpha D\dfrac{\partial^2 u}{\partial x^2}\end{bmatrix}$$

Section (2.4.4) combines the shallow water model defined by equations (2-1) with the dynamic equation of a single degree of freedom (SDOF) system to create a model for a Tuned Liquid Damper (TLD). This portion of the study utilizes a single degree of freedom (SDOF) characterized by dynamic attributes like mass (m), stiffness (k), and damping coefficient (c), situated beneath the sloshing tank as illustrated in Figure (2.2).

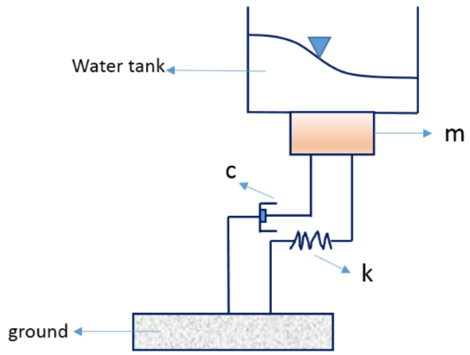

Fig. 2.2. Schematic of a SDOF equipped with sloshing water tank

The dynamic response of a SDOF is obtained from equation (2-3), in which $u_s(t)$ is the displacement, $\dot{u}_s(t)$ is the velocity, and $\ddot{u}_s(t)$ refers to the acceleration of the SDOF. In addition, *F(t) is* seismic force excitation and $G(t)$ denotes the water tank sloshing force. Here, the finite difference model is applied to discretize dynamic equation (2-3) (Chopra, 2007).

$$m\ddot{u}_s(t) + c\dot{u}_s(t) + ku_s(t) = F(t) + G(t) \tag{2-3}$$

To couple the system of equations (2-1 and 2-3), the acceleration of sloshing tank, a_x in equation (2-1), is set equal to the acceleration of the SDOF, $\ddot{u}_s$ in equation (2-3). In addition, besides the seismic excitation force, $F(t)$, the SDOF is influenced by sloshing force, $G(t)$. The sloshing force is determined from the difference in hydrostatic force on the tank walls at *x=0* and *x=L* in the shallow-water model. This coupled model involves an iterative procedure in each time step to reach convergence for sloshing force. Figure (2.3) illustrates the flowchart of the developed numerical model for coupling a SDOF to a sloshing tank. Under the shallow water modeling (SWM) module, all of the discussed numerical schemes can be implemented, including upwind methods, the MacCormack method, semi-implicit methods, and separation of variables.

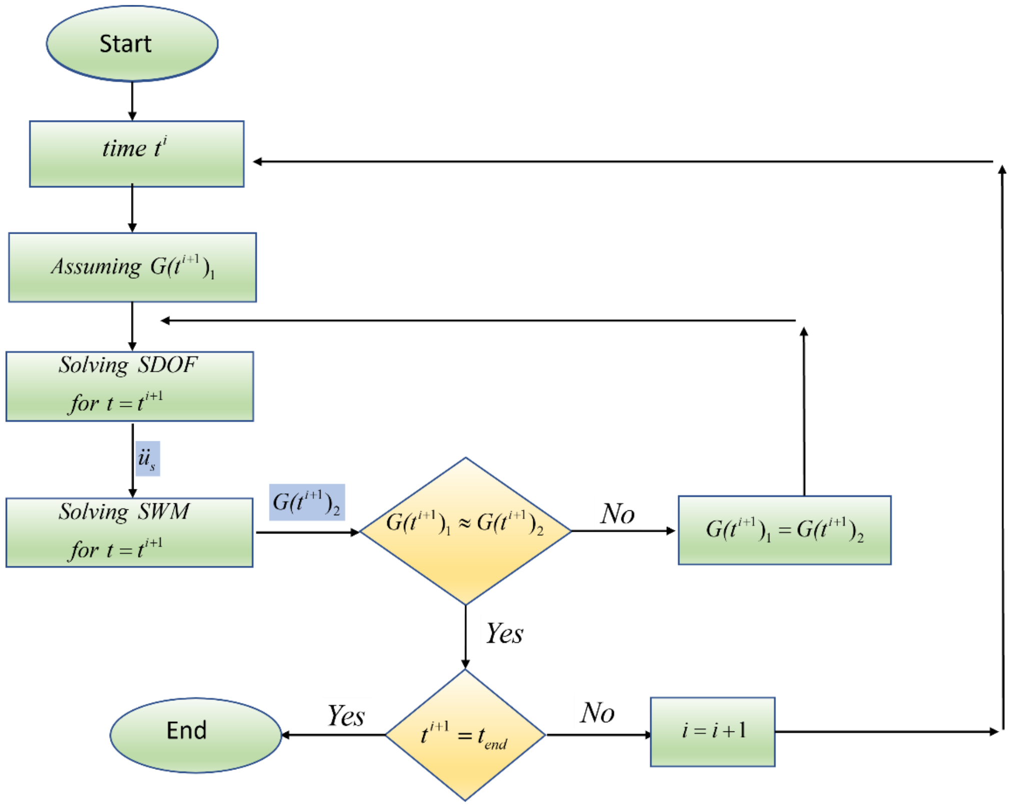

Fig. 2.3. Flowchart used in the present model to couple SDOF dynamic with sloshing tank

2.3. Numerical Methods

2.3.1 Upwind schemes

A numerical solution to the system of partial differential equations (2.1) necessitates both a spatial and a temporal discretization described subsequently.

2.3.1.1 Temporal discretization

Four methods for discretizing temporal terms $\frac{\partial \vec{U}}{\partial t}$ were examined :1-first order Euler, 2-midpoint, 3-third order Total Variation Diminishing (TVD), and 4-fourth order Runge Kutta methods. The third and fourth schemes yielded approximately the same and more accurate results. Here, the third scheme (TVD), Equation (2-A1), proposed by Gottlieb and Shu (1998), was used because of its lower computational cost than the fourth-order Runge–Kutta.

2.3.1.2 Spatial discretization

With respect to the control volume of node j shown in Figure (2.4), the term $\frac{\partial \vec{F}}{\partial x}$ can be determined using Equation (2-4).

$$\frac{\partial F}{\partial x} = \frac{F_{j+1/2} - F_{j-1/2}}{\Delta x} \tag{2-4}$$

There are a variety of approaches for obtaining $F_{j+1/2}$ and $F_{j-1/2}$ at the control surface, which is called flux approximation.

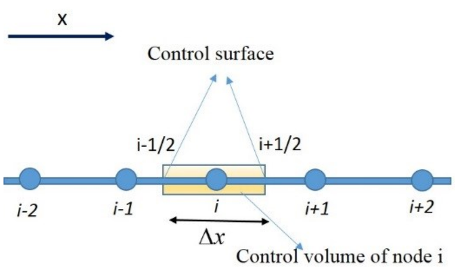

Fig. 2.4. Schematic of control volume of node i

To evaluate the flux at the interface in upwind schemes, matrix $|A|$ should be determined. This matrix relies upon the eigenvalues and eigenvectors of matrix A in the nonconservative form of the shallow water equation (2-2). Appendix A provides the equations (2-A 2) and (2-A 3) for calculating matrix $|A|$.

First Order upwind

According to the first-order upwind scheme, the flux is calculated using equation (2-A 4) in the Appendix. This scheme approximates the flux using two nodes near the control surface, with a high contribution from an upstream node. The first-order upwind scheme is stable but leads to a high level of numerical diffusion.

Higher Order upwind

In this method, which includes a family of schemes known as the κ method, the numerical flux is calculated using the relations (2-A 5), (2-A 6), and (2-A 7) in the appendix. In this study, the choice of κ is 1/3, which is equivalent to third-order upwind. In addition, a slope limiter, S, was employed to reduce oscillations (see Mohammadian and Roux 2008). In this scheme, the flux approximation at each control surface was determined from the values of the two nearest upstream and downstream nodes.

To remedy the lack of neighborhood nodes near the boundary (nodes 2 and n-1 in Figure 2.5), two strategies can be implemented. The first approach uses a first-order upwind scheme for nodes 2 and N-1. In the second solution, ghost nodes (nodes 0 and n+1 in fig 5) are provided outside the domain near the boundary nodes (1 and N), whose specifications are derived from a zero-gradient condition.

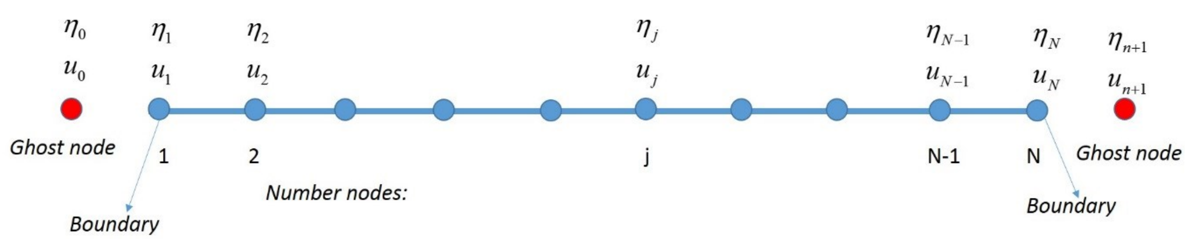

Fig. 2.5. Schematic of main and ghost nodes in flow domain in higher order method

2.3.2. MacCormack method

This scheme is a predictor-corrector method in which backward differences are employed in the predictor step, and forward differences are used in the corrector step (Amara et al. 2013). In the second alternative, forward and backward differences can be applied to predictors and correctors, respectively. Equation (2-A 8) in the appendix illustrates the application of this scheme to the discretization of a non-conservative shallow water equation (2-2).

2.3. 3 Central difference in time and space

In this method for discretization in space and time, the central difference and midpoint are utilized, respectively, to reach second-order approaches. When this scheme is utilized for the non-conservative shallow water equation (2-2), equation (2-A 9) is provided in the Appendix.

2.3.4. Implicit and semi-implicit method

The main difference between implicit and explicit schemes for Equation (2-1), the pure advection equation, is that implicit schemes evaluate the term $\frac{\partial F}{\partial x}$ at time n+1, which is unknown. Therefore, this approach yields coupled equations.

2.3.4.1. Preissmann method

This scheme proposes the second-order approximation presented in Equation (2-A 10) to discretize the temporal and spatial derivatives (Wang, 2019). Expression (2-A 11) is developed when this scheme is employed to discretize the shallow water equation. Both the fully implicit and semi-implicit schemes can be obtained using this numerical method.

Considering the velocity and wave height as unknown parameters, *2N* unknowns exist for *N* nodes in the flow domain (see Figure 2.6). This scheme establishes 2*N*-2 equations using discretized equations. Regarding two extra zero velocity equations at the wall boundaries, a matrix equation (Equation 2-5) is derived in which *A* is the coefficient matrix, *X* is the unknown vector, and *B* is the known vector updated in each time step. *A* is a band matrix with four non-zero elements in each row.

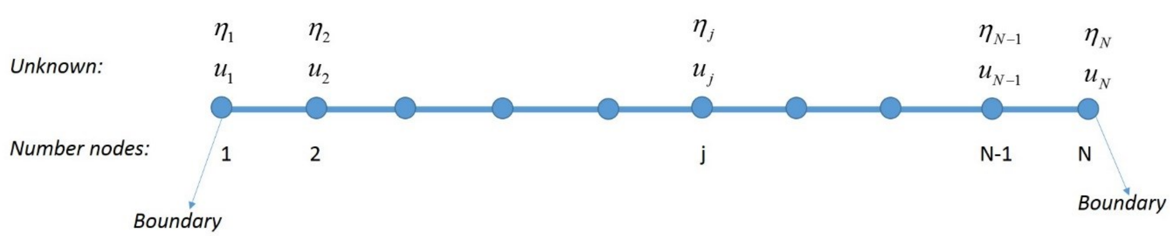

Fig. 2.6. Schematic of nodes and unknowns in Preissmann method

$$[A]_{2N*2N} * [X]_{2N*1} = [B]_{2N*1} \tag{2-5}$$

As an illustration, this matrix equation for *N*=4 is shown in equation (2-A 12) in the Appendix.

2.3.4.2. Staggered method

The main difference between this scheme and the Priessmann method is that the unknown parameters u and η are not stored on the same node in this scheme (see Figure 2.7). The staggered scheme employs two different control volumes for the continuity (mass cell) and momentum (momentum cell) equations. A benefit of this method is that the flux values are derived directly from the variables stored on the surface of the control volume. Therefore, flux approximation methods are not required. This method defines the time and space derivative operations based on Equation (2-A 13) in the Appendix. In the Appendix, expression (2-A 14) demonstrates how Equation (2-1) can be discretized using this scheme.

Consider $2N$-1 nodes in the flow domain, as shown in Figure (2.7). In this case, the number of unknowns is $2N$-1. Meanwhile, the number of equations based on expression (2-A 14) in the appendix is equal to $2N$-3. Introducing zero velocity as the wall boundary condition results in the same number of unknowns and equations. Hence, matrix Equation (2-6) is developed, in which A is the coefficient matrix, X is the unknown vector, and B is the known vector. Although the coefficient matrix was constant, the known vector was updated at each time step.

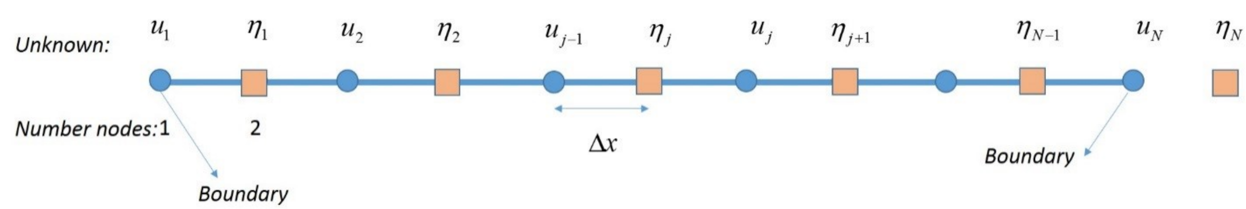

Fig. 2.7. Schematic of nodes and unknowns in staggered method

$$[A]_{(2N-1)*(2N-1)} * [X]_{(2N-1)*1} = [B]_{(2N-1)*1} \tag{2-6}$$

Equation (2-A 15) in the Appendix shows the matrix equation for N=4. Matrix A is a band matrix with three nonzero elements; therefore, this method requires fewer computations than the Preissmann method.

2.3.5. Separation of variables scheme

In this step, a technique known as the separation of variables method is proposed and will be applied to obtain a solution to the sloshing problem. In this method, it is assumed that unknown variables, velocity and wave height here, depending on space and time can be expressed as the product of a function of spatial coordinates and a function of time (Equation 2-7). The assumed space function should satisfy the boundary condition of zero velocities at x=0 and x=L as well as the zero-wave height gradient at x=0 and x=L. If n, which is known as the number of mode shapes, is greater, a more precise solution is provided.

$$\eta = \sum a_n(t)\cos(\frac{n\pi x}{l}) \quad u = \sum b_n(t)\sin(\frac{n\pi x}{l}) \tag{2-7}$$

Replacing these variables in Equation (2-2), Equation (2-8) is derived.

$$\begin{aligned} &\sum \dot{a}_n(t)\cos(\frac{n\pi x}{l}) + H\sum b_n(t) * \frac{n\pi}{l}\cos(\frac{n\pi x}{l}) = 0 \\ &\sum \dot{b}_n(t) * \sin(\frac{n\pi x}{l}) - \mathrm{g}\sum a_n(t)\frac{n\pi}{l}\sin(\frac{n\pi x}{l}) = -\sum M_n \sin(\frac{n\pi x}{l}) * \mathrm{a} \\ &M_n = -2 * \left[\frac{(-1)^n - 1}{n\pi}\right] \end{aligned} \tag{2-8}$$

Because Equation (2-8) should be satisfied for each x, the following expression is derived for each mode, n.

$$\begin{aligned} &\dot{a}_n(t) + H * b_n(t)\frac{n\pi}{l} = 0 \\ &\dot{b}_n(\mathrm{t}) - \mathrm{g}\, a_n(t)\frac{n\pi}{l} = -M_n * \mathrm{a} \\ &M_n = -2 * \left[\frac{(-1)^n - 1}{n\pi}\right] \end{aligned} \tag{2-9}$$

Consequently, with the aid of the separation of variables method, partial differential equations are transformed into ordinary differential equations.

Prior to delving into the numerical modeling, the separation of variables method is manipulated to derive an analytical expression for the natural period of tanks, which holds a significant role in sloshing dynamics. This analytical approach establishes a parameter range for $\frac{H}{L}$ within which the linear shallow water equations provide accurate predictions for the natural period of tanks. For this purpose, let's examine a stationary tank subjected to a standing wave as an initial perturbation. Using the separation of variables method, the wave height and velocity can be determined based on Equation (2-10) (Liu et al., 2015). This solution satisfies the boundary conditions of zero velocity and zero wave height gradient at the walls located at x=0 and x=L.

$$\begin{aligned} \eta &= \sum_{n=1}^{N} a_n \cos(\frac{n\pi x}{L})\cos(\omega_n t) \\ u &= \sum_{n=1}^{N} b_n \sin(\frac{n\pi x}{L})\sin(\omega_n t) \end{aligned} \tag{2-10}$$

The proposed analytical solution for the wave height and velocity in Equation (2-10) for n=1 is converted to Equation (2-11).

$$\begin{aligned} \eta &= a\cos(\frac{\pi x}{L})\cos(\omega t) \\ u &= b\sin(\frac{\pi x}{L})\sin(\omega t) \end{aligned} \tag{2-11}$$

By replacing u and η , which satisfy the boundary condition, in the linear shallow water equation for a stagnant tank (Equation 2-1 with vector R=0), the following expressions can be established:

$$\begin{bmatrix} -\omega\cos(\frac{\pi x}{L})\sin(\omega t) & H\frac{\pi}{L}\cos(\frac{\pi x}{L})\sin(\omega t) \\ -g\frac{\pi}{L}\sin(\frac{\pi x}{L})\cos(\omega t) & \omega\sin(\frac{\pi x}{L})\cos(\omega t) \end{bmatrix}\begin{bmatrix} a \\ b \end{bmatrix} = \begin{bmatrix} 0 \\ 0 \end{bmatrix} \tag{2-12}$$

The left matrix should be singular to obtain a nontrivial solution. With the determinant of the left matrix, the coefficient matrix, equal to zero, Equation (2-13) can be derived.

$$\omega = \frac{\pi}{L}\sqrt{gH} \rightarrow f = \frac{\sqrt{gH}}{2L} \tag{2-13}$$

On the other hand, in literature, many researchers have used the analytical equation (2-14) to determine the natural frequency of the water tank.

$$f=\frac{1}{2\pi}\sqrt{(\frac{n\pi g}{L})tanh(\frac{n\pi H}{L})} \tag{2-14}$$

The analytical natural frequency for n=1 is converted to the following expression

$$f=\frac{1}{2\pi}\sqrt{(\frac{\pi g}{L})tanh(\frac{\pi H}{L})} \tag{2-15}$$

With the assumption of $tanh(\frac{\pi H}{L})=(\frac{\pi H}{L})$ in Equation (2-15), the following expression is developed for the natural frequency of the shallow water tank:

$$f=\frac{\sqrt{gH}}{2L} \tag{2-16}$$

Consequently, when $tanh(\frac{\pi H}{L})$ approaches $\frac{\pi H}{L}$, the analytical formula provides the same results as the linear shallow water equations (see equations 2-13 and 2-16). The Tylor series for $tanh(x)$ is developed in Equation (2-17), revealing that it can be approximated by x with a second-order truncation error for small values of x.

$$tanh(x)=x+O(x^3) \tag{2-17}$$

In Figure (2.8) diagrams of both $y=x$ and $y=tanh(x)$ are presented. From this graph, it can be deduced that $tanh(x)=x$ is a good approximation up to about $x\approx 0.7$. Consequently, for $\frac{\pi H}{L}<=0.7$ or $\frac{H}{L}<=0.23$, linear shallow-water equations provide an approximately accurate natural period, which is crucial for the design of sloshing tanks.

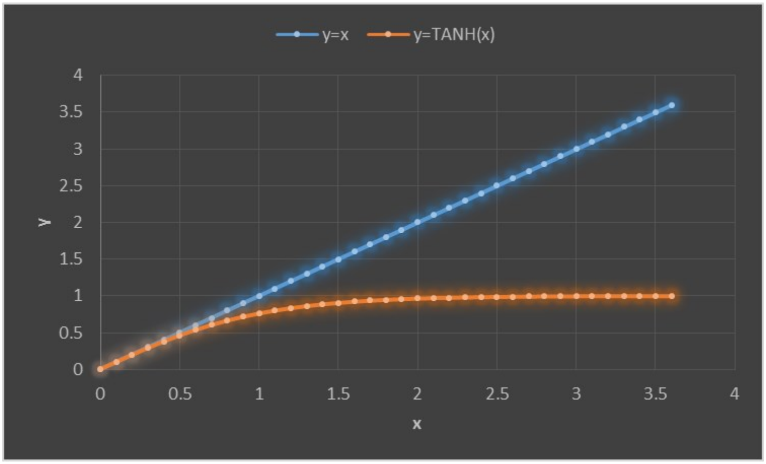

Fig. 2.8. $y = x$ and $y = tanh(x)$ diagrams

2.4. Test cases and Results

2.4.1. Perturbation test

This test pertains to a stationary tank subjected to a standing wave as the initial condition. In this scenario, as mentioned earlier, the analytical solution is provided by Equation (2-10) (Liu et al., 2015).

For the case where n=1, the analytical solution was employed as the initial condition (t=0) in the shallow water model, as depicted in Equation (2-18). This initial condition corresponds to a half-cosine wave height, as illustrated in Figure (2.9).

$$\begin{aligned} &\eta = a\cos(\frac{\pi x}{L}) \\ &u = 0 \end{aligned} \tag{2-18}$$

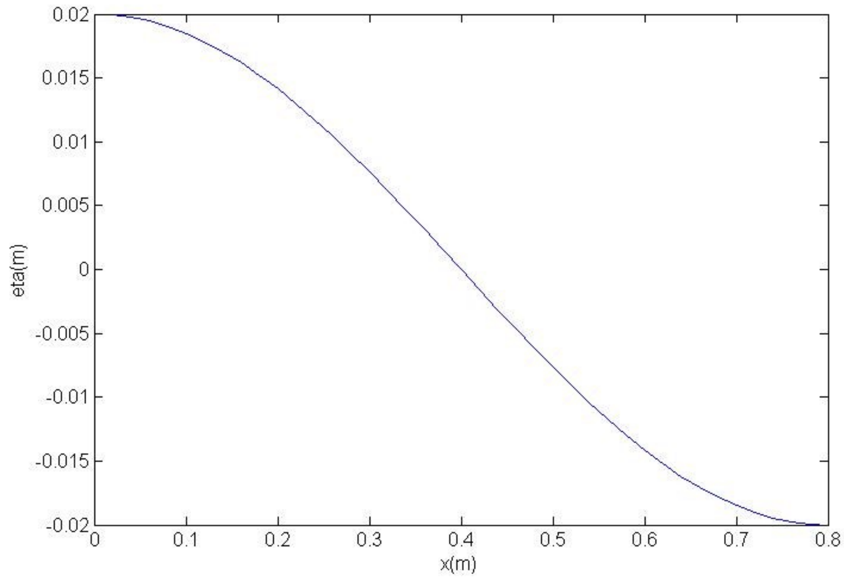

Fig. 2.9. A half-cosine wave imposed in the model as an initial condition

According to the analytical solution for n=1, equation (2-11), and initial condition, the numerical model should generate expression (2-19) for the free surface at $x=L$. In this equation ω is the wave frequency.

$$\eta = -a\cos(\omega t) \tag{2-19}$$

In this scenario, where physical diffusion is absent in the shallow water equation, the difference between the numerical model outcomes and the analytical solution is attributed to numerical diffusion errors. The numerical diffusion resulting from the truncation error caused smaller waves in the numerical model. Due to the accumulated error at each time step, this difference grows over time.

As shown in Figure (2.10a), the amplitude of the initial perturbation decreased significantly over time predicted by first order upwind. Thus, the first-order upwind method is associated with high numerical diffusion errors and the results are inaccurate.

Figures (2.10b and 2.10c) show the results of higher order upwind scheme, indicating low numerical diffusion compared to Figure (2.10a). As mentioned previously, two alternatives can be employed for the treatment of the wall boundary condition in this scheme. Figure (2.10b) presents the results when the first-order upwind is applied to two nodes near the boundary nodes, and Figure

(2.10c) is associated with the application of ghost nodes, as discussed in higher upwind schemes section. Evidently, the use of ghost particles results in less numerical diffusion and a higher level of accuracy.

Figures (2.10d and 2.10e) reflect the results of the central method and MacCormack scheme, respectively. Although both schemes are explicit and second-order in time and space discretization, MacCormack's method produces accurate and stable results with negligible numerical diffusion errors. A central method solution, on the other hand, is subject to numerical diffusion and instability. In addition to high accuracy, the MacCormack scheme has lower computational costs than the central method.

The Preissmann method could provide two alternative results 1-fully implicit and 2-semi-implicit. Figure (2.10f) indicates that the fully implicit method, which is first-order accurate, is accompanied by more numerical diffusion. Conversely, the semi-implicit scheme depicted in Figure (2.10g), which boasts second-order accuracy, produces highly accurate outcomes while maintaining minimal numerical diffusion errors. Although the semi-implicit method necessitates the solution of matrix equations in each time step, leading to elevated computational expenses, its precision and stability are notably significant.

Figures (2.10h and 2.10i) reveal that the staggered method, similar to the Preissmann method, is associated with high-level accuracy for the semi-implicit scheme, whereas it suffers from numerical diffusion error for the fully implicit scheme.

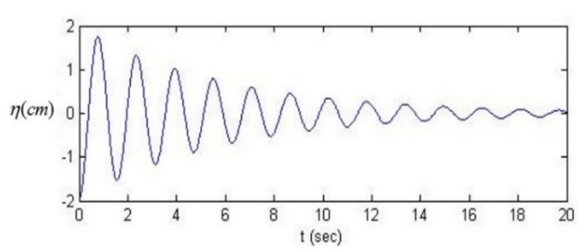

a: First order upwind method

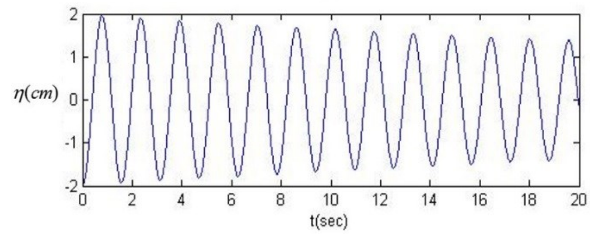

b: Higher order upwind method

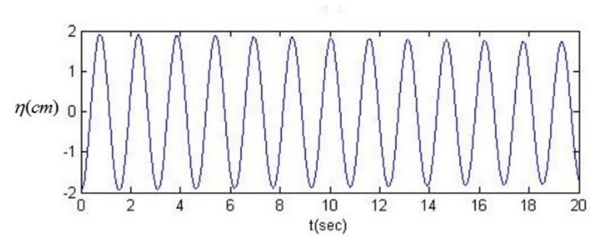

c: Higher order upwind method equipped with ghost nodes

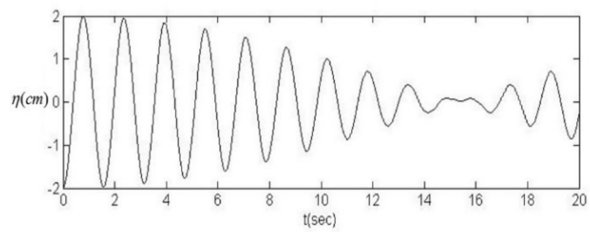

d: Central method

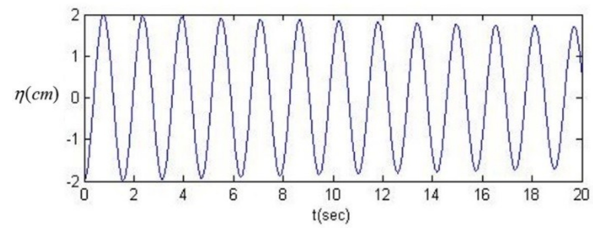

e: McCormack method

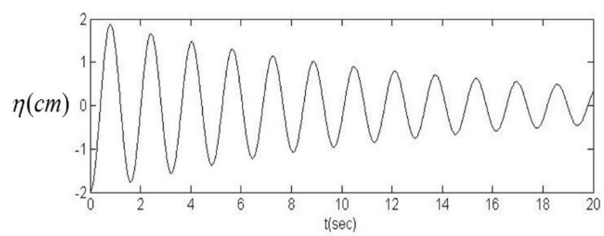

f: Full-implicit Preissmann method

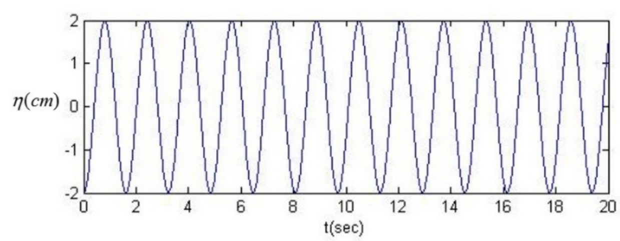

g: Semi-implicit Preissmann method

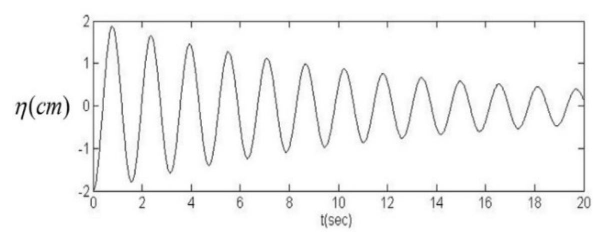

h: Full-implicit Staggered method

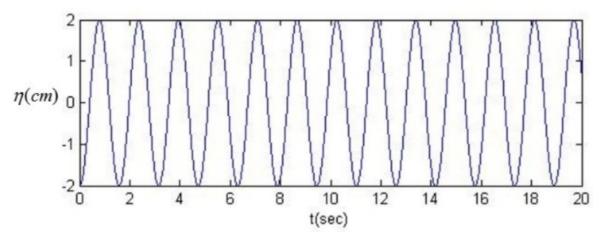

i: Semi-implicit Staggered method

Fig. 2.10. Different numerical schemes result for wave height at the wall in the perturbation test

2.4.2. Sloshing test

This test was applied to a rectangular tank with a length of L=0.8m and an initial water depth of H=0.1 (see Figure 2.1), which was subjected to resonant harmonic excitation. The natural frequency of the tank is $f = 0.603Hz$, with respect to Equation (2-15). Equation (2-20) provides the displacement of the excitation, *x*, with respect to time, *t*. In this equation *a*=0.05 cm is the amplitude of the excitation, and $\bar{f}$ is the frequency of the excitation taken to be the same as the natural frequency of the tank to generate resonant harmonic excitation (Chen et al. 2007).

$$x = a\,sin(2\pi \bar{f} t) \tag{2-20}$$

The results of the upwind schemes for this test are presented and compared with the experimental data in Figures (2.11a and 2.11b). The use of first order upwind causes the prediction of considerably smaller sloshing waves resulting from numerical diffusion, while higher order upwind provides accurate results.

Figures (2.11c and 2.11d) reveal the results of both the Central Methods and MacCormack, accompanied by experimental data. Although both schemes benefit from second-order accuracy, the MacCormack method has a slightly lower computational cost and provides slightly more accurate results. The free-surface profile predicted by MacCormack is smooth, whereas the central method estimates the free surface with a stepped and rough shape (see Figures 2.12). Hence, as discussed in the previous test, the central scheme tended to be unstable.

In this stage, two implicit schemes (Preissmann and Staggered) were applied to the resonant harmonic excitation. Both schemes experienced slightly smaller sloshing waves when they were adjusted to the full implicit methods (Figures 2.11e and 2.11f). This underestimated prediction of wave height is largely due to the numerical diffusion associated with these schemes, as in previous test. However, for the semi-implicit scheme, as shown in figures (2.11g and 2.11h), both models overestimated the wave height. Because numerical models are devoid of physical diffusion, which is inherent to the nature of the flow, they predict higher wave sloshing.

The last part of this simulation is dedicated to the numerical solution of the system of ordinary Equations (2-9) that arises from the separation of variable methods. The present study employed the midpoint method to solve the system of ordinary differential equations. The results indicate that the solution converges at n=9 and does not change as n increases. The numerical results obtained from this method in the resonance excitation test are compared with the experimental data in Figure (2.11i). Evidently, this numerical scheme can yield accurate results.

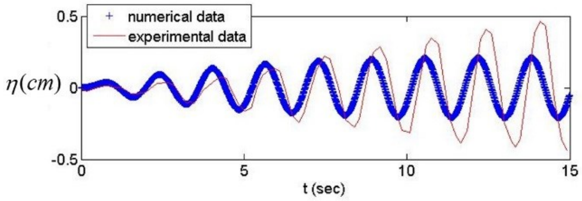

a: First order upwind method

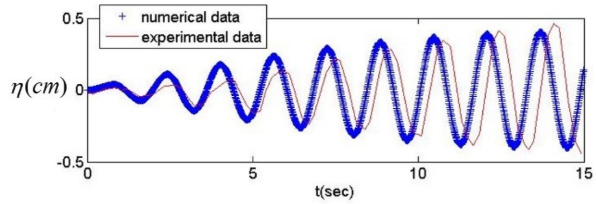

b: Higher order upwind method

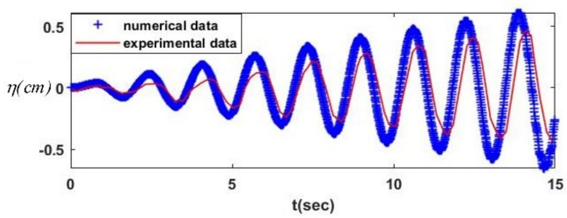

c: Central method

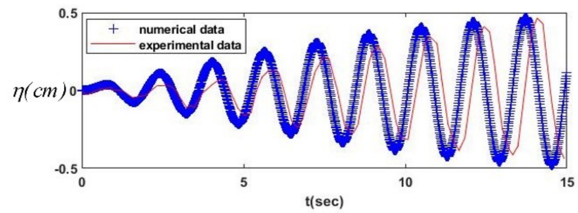

d: McCormack method

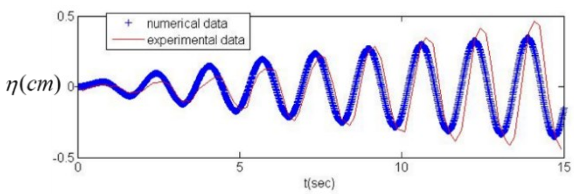

e: Full-implicit Preissmann method

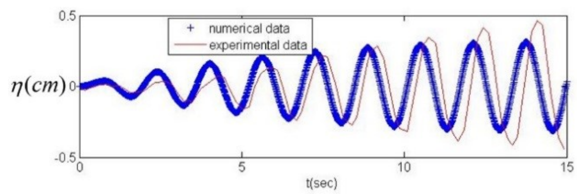

f: Full-implicit Staggered method

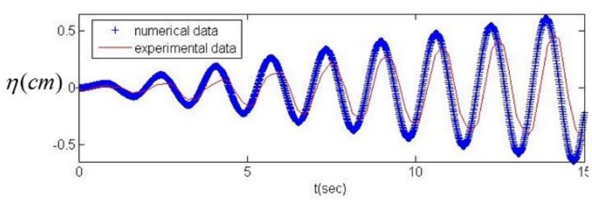

g: Semi-implicit Preissmann method

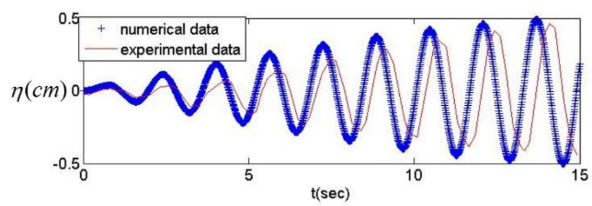

h: Semi-implicit Staggered method

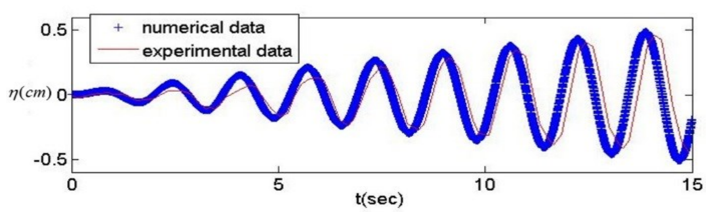

i: Separation of variables method

Fig. 2.11. Different numerical schemes results for wave height at the wall in the resonance sloshing

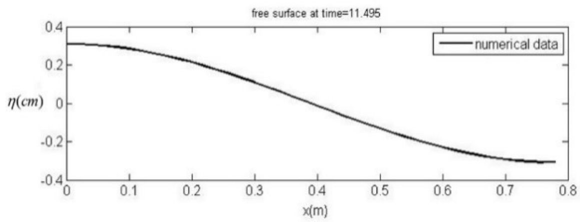

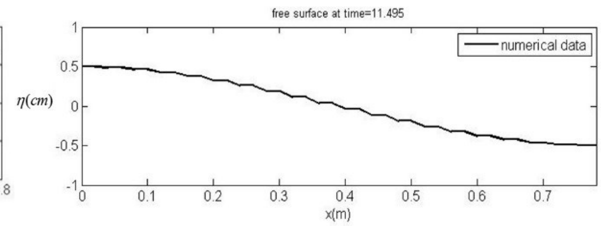

a: MacCormack method

b: Central method

Fig. 2.12. Free surface predicted by numerical models

Note that all of the developed codes associated with various numerical schemes are provided in MATLAB. Regarding the comparison of time calculations among the second-order accuracy methods for modeling the preceding case study, the McCormack method benefits from faster computation, taking around 5 minutes. However, the semi-implicit Prissmann method, which requires solving matrix equations, is the most time-consuming, taking approximately 10 minutes, which is about twice as long. The laptop used for the simulations is equipped with a 12th Gen Intel Core i7-1255U processor (1.70 GHz base clock), 16 GB of RAM, and a 64-bit operating system.

2.4.3 Physical diffusion

This verification test used rectangular water tanks with geometric specifications L= 0.966 m and H=0.119m. Therefore, with respect to Equation (2-15), the natural frequency is *f=0.545 Hz*. The tank experiences a harmonic near-resonance excitation obtained from formula (2-21), in which *a=0.259 cm* $\bar{f} = 0.594\,Hz$ and ϕ, the phase angle, is equal to 4 degrees (Marivani and Hamed 2009).

$$x = a * \sin(2\pi \bar{f} * t + \phi) \tag{2-21}$$

The semi-implicit numerical scheme predicts a higher sloshing wave in Figure (2.13a) due to the lack of physical diffusion. A fully implicit scheme, because of the numerical diffusion error, provides a smaller wave and shows better agreement with the experimental data (Figure 2.13b). To enhance the accuracy of the model, the physical diffusion term $D\frac{\partial^2 u}{\partial x^2}$ was introduced into the momentum equation of a linear shallow water system (1), $\alpha = 1$. D is the physical diffusion coefficient.

The equation was solved using numerical schemes with negligible numerical diffusion errors, such as the Preissmann semi-implicit and MacCormack methods. The diffusion coefficient was derived by calibrating the numerical model with experimental data. Figure (2.13c) illustrates the outcome of using a precise scheme when the physical diffusion term is included in the flow equations. With all the assumptions of the linear shallow water equation, this numerical model can predict the trend, period, and peak of sloshing waves in good agreement with the experimental data. On the other hand, the first-order upwind provides a considerably smaller wave high with an approximately uniform pattern, showing a significant deviation from the experimental data (Figure 2.13d).

In addition to the acceptable accuracy of shallow water models when using negligible numerical diffusion schemes, their computational cost is extremely low compared with advanced models such as VOF and SPH. Hence, the model is well suited to the simulation of fluid-structure interactions, which are computationally intensive. In the final step of the present research, a tuned liquid damper (TLD), an example of fluid-structure interaction, was simulated using the proposed model.

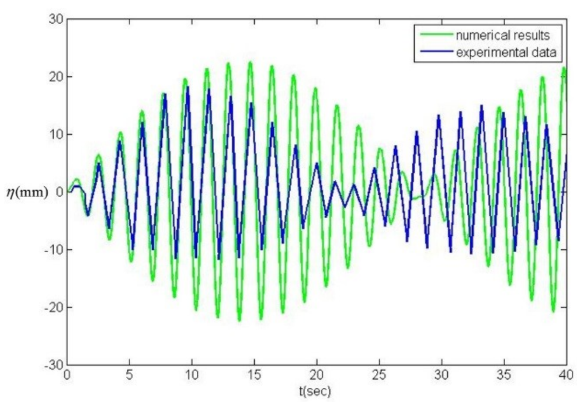

a: Semi-implicit method without physical diffusion

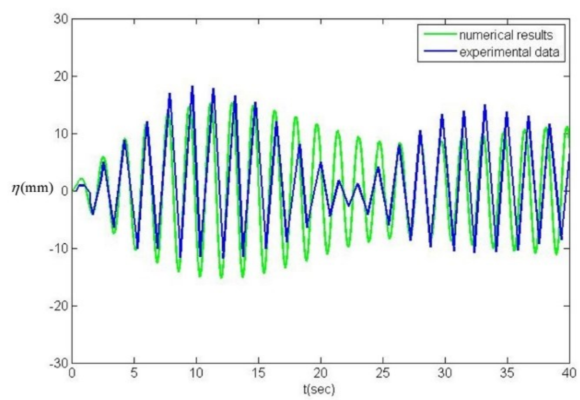

b: Fully implicit method

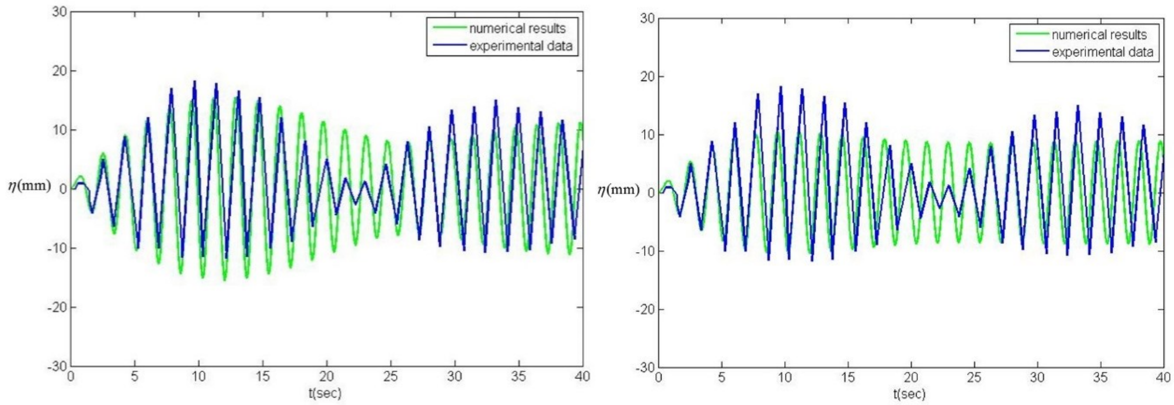

c: Semi-implicit method with physical diffusion   d: First-order upwind method

Fig. 2.13. Numerical schemes result for wave height at the wall in the physical diffusion test

2.4.4. Tuned Liquid damper Test

In this test, a Single Degree of Freedom (SDOF) system is connected to a sloshing tank, referred to as a Tuned Liquid Damper (TLD), utilizing the partitioned method as elucidated in the methodology section. The coupled system undergoes harmonic excitation force. The dynamic properties of the SDOF and water tank dimensions used in this test are presented in Table (2.1) (Sorkhabi et al. 2017). The natural frequency of the SDOF derived from Equation (2-22) (Chopra, 2007) is $f_s = 0.67\,Hz$, which is equal to the natural frequency of the water tank determined from Equation (2-15).

Table 2.1. Dynamic properties of the structure and dimension of the water tank

structure			water tank	
Mass (kg)	Stiffness(KN/m)	Damping Cofficient (KN.s/m)	Length (m)	Water depth (m)
282	4997.5	4.75	0.46	0.04

$$f_s = \frac{1}{2\pi}\sqrt{\frac{k}{m}} \tag{2-22}$$

Sinusoidal excitation at the same frequency as the SDOF was applied to the structure. Therefore, in this test, the SDOF experienced a harmonic resonance excitation. The response of the SDOF with and without TLD was derived and compared to the experimental results in Figure (2.14). In this simulation, the MacCormack method, which takes advantage of less numerical diffusion and computational cost, was used to solve the shallow water equations provided by physical diffusion. Despite the limitations and assumptions of shallow water models and the complexity of TLD simulations, the model equipped with an accurate numerical scheme could generate reasonably accurate results.

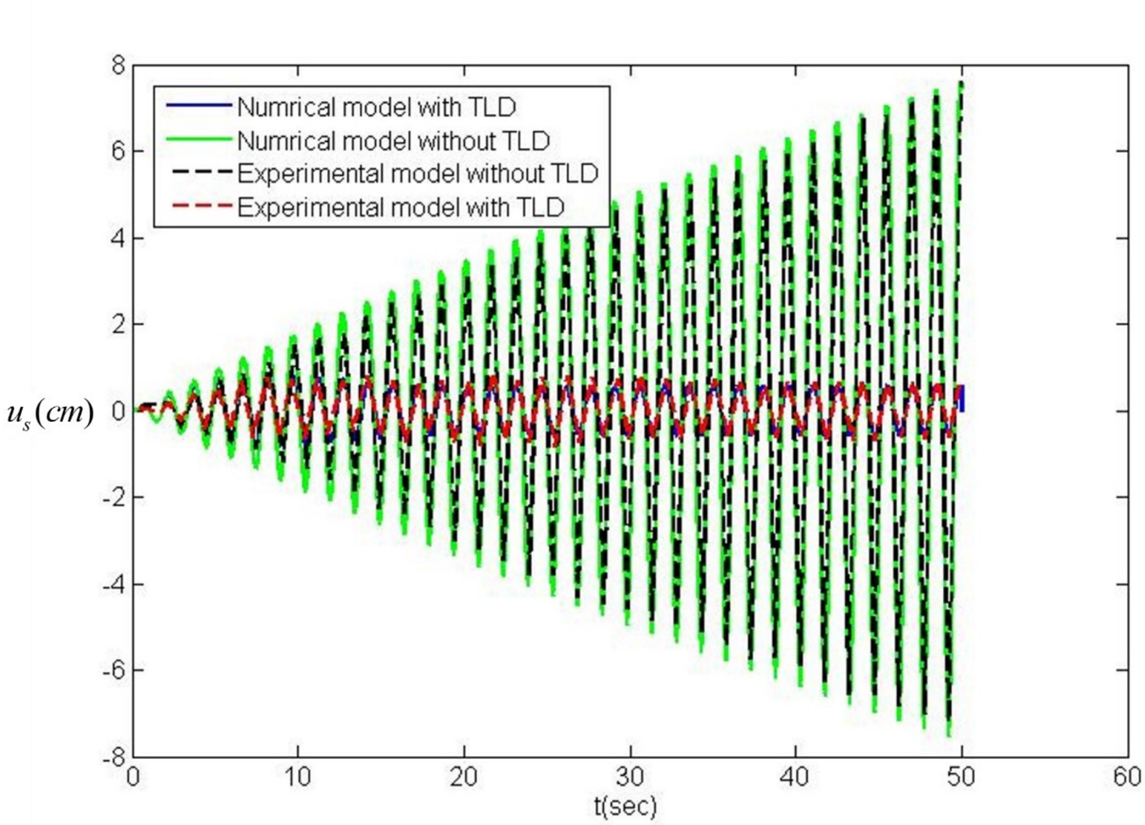

Fig. 2.14. Numerical and experimental results for structure response with and without TLD

2.4.4.1. The influence of frequency ratio on the response of the TLD

In this section, the focus is on conducting a parametric study of a Tuned Liquid Damper (TLD) using two key parameters: frequency ratio and damping ratio. The TLD and SDOF systems being studied are described in Table (2.1). To carry out the study, a harmonic sinusoidal excitation force described in Equation (2-23) is applied to the SDOF. The force amplitude, A_0, is tuned to achieve a 1cm displacement under resonance excitation in the absence of TLD.

$$F(t) = A_0 \sin(2\pi \bar{f}\, t) \tag{2-23}$$

The frequency of the excitation force, $\bar{f}$, is adjusted in such a manner that the frequency ratio (β), defined as the excitation force frequency divided by the natural frequency of the SDOF system, falls within the range of 0.9 to 1.1. The simulation results are presented in Figure (2.15), where the vertical axis represents the amplitude of the SDOF displacement when it reaches a steady-state response. The figure reveals that the TLD has a considerable impact on the response of the SDOF within a narrow range around a frequency ratio of one, referred to as the impact range in this context. In this case study, the impact range is approximately between 0.97 and 1.05. The effect of the SDOF response diminishes significantly as the frequency ratio moves away from one within this impact range. Additionally, it should be noted that the impact range is not entirely symmetric and exhibits a slightly greater extension for frequency ratios greater than one.

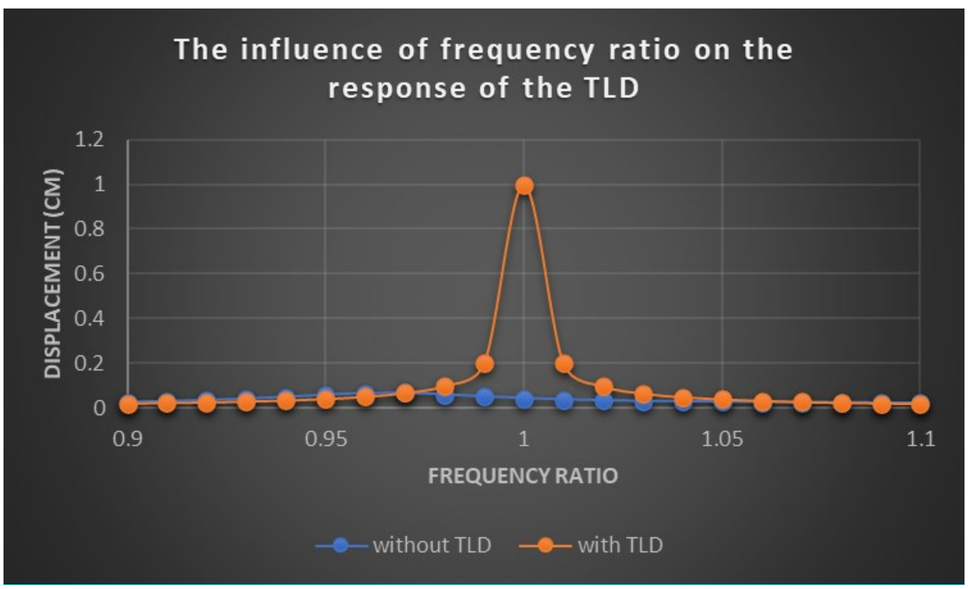

Fig. 2.15. Displacement of the SDOF versus frequency ratios

2.4.4.2. The influence of damping on the response of TLD

This section focuses on examining the effect of structural damping on Tuned Liquid Damper performance. The investigation specifically considers resonance excitation, which yields optimal performance of TLDs regarding the impact range discussed in the previous section. The TLD system described in Table (2.1) is subjected to various damping ratios. Damping ratio, ζ, is determined from Equation (2-24). In this equation c_c is critical damping and equals to $4\pi mf$.

$$\zeta = \frac{c}{c_c} \tag{2-24}$$

Although critical damping is constant for all simulations, the model utilizes a distinct damping coefficient, c, in each simulation. The damping coefficient varies to generate damping ratios ranging from 0.1% to 1%. For each damping ratio, the SDOF displacement in steady state condition was derived within simulation.

Based on the results presented in Figure (2.16), it can be observed that in resonance excitation the damping ratio has a significant impact on the Single Degree of Freedom (SDOF) system in the absence of TLD. The data points exhibit a strong correlation, indicated by a high regression coefficient, and can be fitted with a curve described by the $u_s \propto \frac{1}{\zeta^{0.99}} \simeq \frac{1}{\zeta}$. On the other hand, the influence of the damping on the response of the SDOF provided with TLD is not considerable. In this test, as the damping ratio increases, the steady state displacement of the SDOF in resonance excitation reduces with a small slope equal to 0.76. This reduction is insignificant compared to the decrease observed in the SDOF response when the sloshing tank is not present.

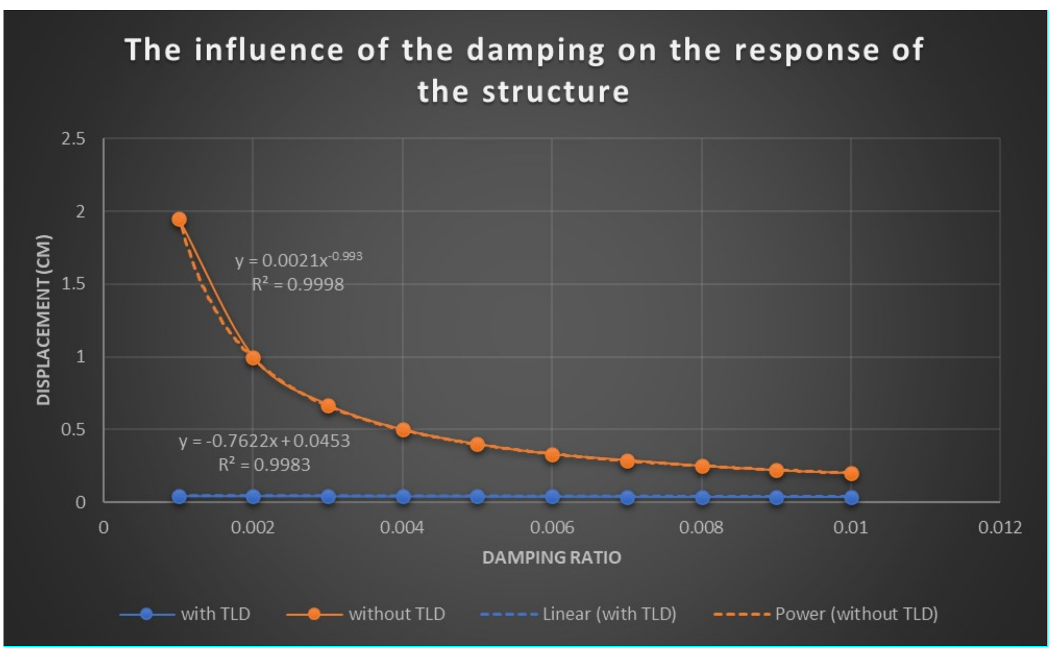

Fig. 2.16. Displacement of the SDOF versus damping ratios

2.5. Discussion and conclusion

The first part of the research addressed the impact of numerical modeling on sloshing tank simulations, which is a significant gap in the literature. Various efficient numerical models were examined to simulate initial perturbation and resonant sloshing tanks, revealing a high sensitivity of results to the chosen numerical schemes. To assess numerical diffusion errors, physical diffusion was deliberately omitted from the linear shallow water equation. The first-order upwind scheme displayed considerable numerical diffusion errors, while higher-order upwind schemes yielded more accurate wave predictions compared to analytical solutions and experimental data. The use of ghost nodes at wall boundaries significantly reduced numerical diffusion errors. Although both the McCormack and the central methods are second-order accurate finite difference methods, the McCormack method produced more accurate and stable results with a smoother free surface. Employing the Preissmann and Staggered methods, leading to a matrix equation, showed that semi-implicit solutions had significantly lower numerical diffusion errors than fully implicit schemes.

In addition to the above-mentioned schemes, separation of variables technique was manipulated to linear shallow water for the simulation of the sloshing tanks, revealing high level of accuracy. Furthermore, when this scheme was applied to a stagnant tank undergoing a standing wave, an analytical expression for the period of the tank, which is a key factor in seismic response, was derived. Besides, the current research introduced a range for water depth to tank length, where linear shallow water theory predicts precise natural period.

During this stage, the current model incorporated physical diffusion into the equations and adjusted its coefficient using experimental data. Additionally, the McCormack method, recognized for its accuracy and cost-effectiveness as discussed in the previous section, was combined with the dynamics of a Single Degree of Freedom (SDOF) to formulate the Tuned Liquid Damper (TLD) model. The dynamic equation was solved using the finite difference method, and the coupled system employed the partition method through an iterative approach. Despite the constraints of shallow water theory, the TLD model offered accurate and rational predictions.

In the final section of this research, a parametric study of Tuned Liquid Dampers (TLDs) was conducted, focusing on two key parameters: frequency ratios and damping ratios. The current model indicates a compact asymmetry range ratio around one for the frequency ratios within which TLD performance affects the SDOF response, considerably. The optimal efficiency of TLD is achieved when the frequency ratio equals one, during resonance excitation, and this proficiency reduces exponentially when the frequency ratio gets far from one. Moreover, the steady state displacement of the SDOF under resonance excitation with different damping ratios shows that although damping plays an important role in the SDOF response in the absence of a sloshing tank, its contribution to the reduction of the SDOF provided with TLD is insignificant.

2. Appendix A

Total Variation Diminishing (TVD) temporal integration schemes:

$$
\begin{aligned}
U_j^{(1)} &= U_j + \frac{\partial(U_j^n)}{\partial t} \times \Delta t \\
U_j^{(2)} &= \frac{3}{4}U_j + \frac{1}{4}U_j^{(1)} + \frac{1}{4} \times \frac{\partial(U_j^{(1)})}{\partial t} \times \Delta t \\
U_j^{(n+1)} &= \frac{1}{3}U_j + \frac{2}{3}U_j^{(2)} + \frac{2}{3} \times \frac{\partial(U_j^{(2)})}{\partial t} \times \Delta t
\end{aligned}
\qquad \text{(2-A 1)}
$$

The subscripts indicate the node number, and the superscripts denote the time step in this equation. The unknown parameters at time step *n+1* can be derived from the parameters at time *n* which are known.

Evaluation of matrix $|A|$

Matrix *A* in Equation (2-1) has two real eigenvalues with the corresponding eigenvalues and eigenvectors presented in Equation (2-A 2).

$$a_1 = \sqrt{gH} \qquad a_2 = -\sqrt{gH} \qquad \text{(2-A 2)}$$

$$\vec{e}_1 = \begin{bmatrix} 1 \\ +\sqrt{\dfrac{g}{H}} \end{bmatrix} \qquad \vec{e}_2 = \begin{bmatrix} 1 \\ -\sqrt{\dfrac{g}{H}} \end{bmatrix}$$

The matrix $|A|$ required for flux approximation in upwind schemes is obtained from Equation (2-A 3) (Mohammadian and Roux 2008)

$$|A| = P|D|P^{-1} \tag{2-A 3}$$

Where

$$|D| = \begin{bmatrix} |a_1| & 0 \\ 0 & |a_2| \end{bmatrix} \qquad P = [\vec{e}_1, \vec{e}_2]$$

First order upwind

$$\vec{F}_{j+1/2} = 0.5(\vec{F}^L_{j+1} + \vec{F}^R_j) - 0.5|A|(\vec{U}^L_{j+1} - \vec{U}^R_j) \tag{2-A 4}$$

Higher order upwind

$$\vec{F}_{j+1/2} = 0.5(\vec{F}^L_{j+1/2} + \vec{F}^R_{j+1/2}) - 0.5|A|(\vec{U}^L_{j+1/2} - \vec{U}^R_{j+1/2}) \tag{2-A 5}$$

Where R and L represent the evaluations of the right and left sides of the interfaces, respectively, with

$$\vec{F}^L_{j+1/2} = F(\vec{U}^L_{j+1/2}) \qquad F^R{}_{j+1/2} = F(\vec{U}^R_{j+1/2}) \tag{2-A 6}$$

The interface values in the κ method are calculated as (Mohammadian and Roux 2008):

$$\begin{aligned} \vec{U}^L_{j+1/2} &= \vec{U}_j + \frac{1}{4}((1-\kappa * s)(\vec{U}_j - \vec{U}_{j-1}) + (1+\kappa * s)(\vec{U}_{j+1} - \vec{U}_j)) \\ \vec{U}^R_{j+1/2} &= \vec{U}_{j+1} - \frac{1}{4}((1-\kappa * s)(\vec{U}_{j+2} - \vec{U}_{j+1}) + (1+\kappa * s)(\vec{U}_{j+1} - \vec{U}_j)) \end{aligned} \tag{2-A 7}$$

MacCormack method

$$\widehat{U}_i = U_i^n - A\times(\frac{U_i^n - U_{i-1}^n}{\Delta x})\times\Delta\,\mathrm{t} + \mathrm{R}\times\Delta\,\mathrm{t}$$
$$\bar{U}_i = U_i^n - A\times(\frac{\widehat{U}_{i+1}^n - \widehat{U}_i^n}{\Delta x})\times\Delta\,\mathrm{t} + \mathrm{R}\times\Delta\,\mathrm{t} \tag{2-A 8}$$
$$U_i^{n+1} = \frac{1}{2}\times(\widehat{U}_i + \bar{U}_i)$$

Central method

$$U_i^m = U_i^n - A\times(\frac{U_{i+1}^n - U_{i-1}^n}{2*\Delta x})\times\Delta\,\mathrm{t}/2 + \mathrm{R}\times\Delta\,\mathrm{t}/2$$
$$U_i^{n+1} = U_i^n - A\times(\frac{U_{i+1}^m - U_{i-1}^m}{2*\Delta x})\times\Delta\,\mathrm{t} + \mathrm{R}\times\Delta\,\mathrm{t} \tag{2-A 9}$$

Preissmann method:

$$\frac{\partial U_j}{\partial t} = \frac{1}{2}[\frac{U_j^{n+1} - U_j^n}{\Delta t} + \frac{U_{j+1}^{n+1} - U_{j+1}^n}{\Delta t}]$$
$$\frac{\partial F_j}{\partial t} = [\alpha\frac{F_{j+1}^{n+1} - F_j^{n+1}}{\Delta x} + (1-\alpha)\frac{F_{j+1}^n - F_j^n}{\Delta x}] \tag{2-A 10}$$

In Equation (2-A 10), $\alpha = 1$ and $\alpha = 0.5$ correspond to the implicit and semi-implicit methods, respectively.

$$\frac{1}{2}\left[\frac{\eta_j^{n+1} - \eta_j^n}{\Delta t} + \frac{\eta_{j+1}^{n+1} - \eta_{j+1}^n}{\Delta t}\right] + H\times\left[\alpha\frac{u_{j+1}^{n+1} - u_j^{n+1}}{\Delta x} + (1-\alpha)\frac{u_{j+1}^n - u_j^n}{\Delta x}\right] = 0$$
$$\frac{1}{2}\left[\frac{u_j^{n+1} - u_j^n}{\Delta t} + \frac{u_{j+1}^{n+1} - u_{j+1}^n}{\Delta t}\right] + g\times\left[\alpha\frac{\eta_{j+1}^{n+1} - \eta_j^{n+1}}{\Delta x} + (1-\alpha)\frac{\eta_{j+1}^n - \eta_j^n}{\Delta x}\right] = a \tag{2-A 11}$$

The matrix equation obtained from the Preissmann scheme for *N=4* is given by Equation (2-A 12): In this matrix, *dx* and *dt* are space and time steps, respectively. The second and last rows are zero-velocity conditions at the walls, and *LL* refers to a large number.

(2-A 12)

$1/(2\Delta t)$	$-\alpha H/\Delta x$	$1/(2\Delta t)$	$\alpha H/\Delta x$	0	0	0	0
0	LL	0		0	0	0	0
$-\alpha g/(2*\Delta x)$	$1/(2\Delta t)$	$\alpha g/(2*\Delta x)$	$1/(2\Delta t)$			0	0
0	0	$1/(2\Delta t)$	$-\alpha H/\Delta x$	$1/(2\Delta t)$	$\alpha H/\Delta x$	0	0
0	0	$-\alpha g/(2*\Delta x)$	$1/(2\Delta t)$	$\alpha g/(2*\Delta x)$	$1/(2\Delta t)$	0	0
0	0	0	0	$1/(2\Delta t)$	$-\alpha H/\Delta x$	$1/(2\Delta t)$	$\alpha H/\Delta x$
0	0	0	0	$-\alpha g/(2*\Delta x)$	$1/(2\Delta t)$	$\alpha g/(2*\Delta x)$	$1/(2\Delta t)$
0	0	0	0	0	0		LL

8*8

*

η_1
u_1
η_2
u_2
η_3
u_3
η_4
u_4

8*1

=

$\frac{1}{2\Delta t}(\eta_1^n)+\frac{H(1-\alpha)}{\Delta x}(u_1^n)+\frac{1}{2\Delta t}(\eta_2^n)-\frac{H(1-\alpha)}{\Delta x}(u_2^n)$
0
$\frac{g(1-\alpha)}{2\Delta x}(\eta_1^n)+\frac{1}{2\Delta t}(u_1^n)-\frac{g(1-\alpha)}{2\Delta x}(\eta_2^n)+\frac{1}{2\Delta t}(u_2^n)+a$
$\frac{1}{2\Delta t}(\eta_2^n)+\frac{H(1-\alpha)}{\Delta x}(u_2^n)+\frac{1}{2\Delta t}(\eta_3^n)-\frac{H(1-\alpha)}{\Delta x}(u_3^n)$
$\frac{g(1-\alpha)}{\Delta x}(\eta_2^n)+\frac{1}{2\Delta t}(u_2^n)-\frac{g(1-\alpha)}{\Delta x}(\eta_3^n)+\frac{1}{2\Delta t}(u_3^n)+a$
$\frac{1}{2\Delta t}(\eta_3^n)+\frac{H(1-\alpha)}{\Delta x}(u_3^n)+\frac{1}{2\Delta t}(\eta_4^n)-\frac{H(1-\alpha)}{\Delta x}(u_4^n)$
$\frac{g(1-\alpha)}{\Delta x}(\eta_3^n)+\frac{1}{2\Delta t}(u_3^n)-\frac{g(1-\alpha)}{\Delta x}(\eta_4^n)+\frac{1}{2\Delta t}(u_4^n)+a$
0

8*1

Staggered method:

$$\frac{\partial U_j}{\partial t}=\frac{U_j^{n+1}-U_j^n}{\Delta t}$$

$$\frac{\partial F_j}{\partial t}=[\alpha\frac{F_j^{n+1}-F_{j-1}^{n+1}}{2*\Delta x}+(1-\alpha)\frac{F_j^n-F_{j-1}^n}{2*\Delta x}] \tag{2-A 13}$$

$$\frac{\eta_j^{n+1}-\eta_j^n}{\Delta t}+H\times\left[\alpha\frac{u_j^{n+1}-u_{j-1}^{n+1}}{2*\Delta x}+(1-\alpha)\frac{u_j^n-u_{j-1}^n}{2*\Delta x}\right]=0$$

$$\frac{u_j^{n+1}-u_j^n}{\Delta t}+g\times\left[\alpha\frac{\eta_{j+1}^{n+1}-\eta_j^{n+1}}{2*\Delta x}+(1-\alpha)\frac{\eta_{j+1}^n-\eta_j^n}{2*\Delta x}\right]=a \tag{2-A 14}$$

(2-A 15)

LL	0	0	0	0	0	
$-\alpha H/(2*\Delta x)$	$1/\Delta t$	$\alpha H/(2*\Delta x)$	0	0	0	0
0	$-\alpha g/(2*\Delta x)$	$1/\Delta t$	$\alpha g/(2*\Delta x)$	0	0	0
0	0	$-\alpha H/(2*\Delta x)$	$1/\Delta t$	$\alpha g/(2*\Delta x)$	0	0
0	0	0	$-\alpha g/(2*\Delta x)$	$1/\Delta t$	$\alpha g/(2*\Delta x)$	
0	0	0	0	$-\alpha H/(2*\Delta x)$	$1/\Delta t$	$\alpha g/(2*\Delta x)$
0	0	0	0	0	0	LL

7*7

*

u_1
η_1
u_2
η_2
u_3
η_3
u_4

7*1

=

0
$\frac{1}{\Delta t}(\eta_1^n)+\frac{H(1-\alpha)}{2\Delta x}(u_1^n)-\frac{H(1-\alpha)}{2\Delta x}(u_2^n)$
$\frac{g(1-\alpha)}{2*\Delta x}(\eta_1^n)+\frac{1}{\Delta t}(u_2^n)-\frac{g(1-\alpha)}{\Delta x}(\eta_2^n)$
$\frac{1}{\Delta t}(\eta_2^n)+\frac{H(1-\alpha)}{2\Delta x}(u_2^n)-\frac{H(1-\alpha)}{2\Delta x}(u_3^n)$
$\frac{g(1-\alpha)}{2*\Delta x}(\eta_2^n)+\frac{1}{\Delta t}(u_3^n)-\frac{g(1-\alpha)}{\Delta x}(\eta_3^n)$
$\frac{1}{\Delta t}(\eta_3^n)+\frac{H(1-\alpha)}{2\Delta x}(u_3^n)-\frac{H(1-\alpha)}{2\Delta x}(u_4^n)$
0

7*1

References

1. Abbott, M., & Minns, A. 2017. Computational Hydraulics (2nd Ed.). Taylor and Francis
2. Abbott, M.B., Basco, D. R. 1989. Computational Fluid Dynamics. Longman Scientific and Technical, New York.
3. AMARA, L., Berreksi, A., & Achour, B. 2013. Adapted MacCormack Finite-Differences Scheme for Water Hammer Simulation. Journal of Civil Engineering and Science. 2. 226-233.
4. Bahreini Toussi, I., Kianoush, R. & Mohammadian, A. 2021.Numerical and Experimental Investigation of Rectangular Liquid-Containing Structures under Seismic Excitation. Infrastructures 6, 1.
5. Banerji, P., Murudi, M., Shah, A.H. & Popplewell, N. 2000. Tuned liquid dampers for controlling earthquake response of structures. Earthq Eng Struct Dyn, 29,587–602.
6. Cao, X., Ming, F. & Zhang, A.M. 2014. Sloshing in a rectangular tank based on SPH simulation. Applied Ocean Research, 47, 241–254.
7. Chaudhry, M. H., & Hussaini, M. Y .1985. Second-Order Accurate Explicit Finite-Difference Schemes for Water Hammer Analysis. ASME J. Fluids Eng. 107. 523–529.
8. Chen, Y. H., Hwang, W. S., & Ko, C. H. (2007). Sloshing behaviors of rectangular and cylindrical liquid tanks subjected to harmonic and seismic excitations. Earthquake Engineering & Structural Dynamics. 36. 1701 – 1717.
9. Chopra, A.K. 2007. Dynamic of Structures, Theory and Applications to Earthquake Engineering. 3rd Edition, Prentice Hall, Upper Saddle River.
10. Faltinsen, 0. M. 1974. A Nonlinear Theory of Sloshing in Rectangular Tanks', Journal of Ship Research, 18(4), 224-241
11. Fennema. R. J., & Chaudhry, M. H. 1986. Explicit Numerical Schemes for Unsteady Free-Surface Flows with Shocks", Water Resources Research, 22(13), 923-1930.
12. Gallouët, T., Gastaldo, L., Herbin, R., & Latché, J. 2007. An unconditionally stable pressure correction scheme for compressible barotropic Navier–Stokes equations. ESAIM Mathematical Modelling and Numerical Analysis. 42(2). 303-331.
13. Garcia. R., & Khahawita. R. A. 1986. Numerical solution of the St Venant equations with the MacCormack finite-differences scheme. International Journal for Numerical Methods in Fluids, 6, 259-274.
14. Gottlieb, S., Shu, C. W. 1996. Total Variation Diminishing Runge-Kutta Schemes. Mathematics of Computation. 67 (221). 73–85.
15. Guo, D., Yu, B. 2016. Implementation of the Preissmann scheme to solve the Hairsine-Rose erosion equations: Verification and evaluation. 541. 988-1002
16. Housner,W.G. 1963 .The dynamic behavior of water Tanks. Bulletin of the Seismological Society of America, 53(2), 381–387
17. Humar, J. 2012. Dynamics of Structures (3rd Ed.). CRC Press.
18. Kheriji, W., Herbin, R., & Latché, J. 2014. On some implicit and semi-implicit staggered schemes for the shallow water and Euler equations. ESAIM Mathematical Modelling and Numerical Analysis. 48. 1807 - 1857.
19. Kurganov, A. 2018. Finite-volume schemes for shallow-water equations. Acta Numerica, 27, 289-351.

20. Liu, D. & Lin, P. A. 2008. Numerical Study of Three-Dimensional Liquid Sloshing In Tanks. J. Comput. Phys., 227, 3921–3939
21. Liu, F., Feyen, J., & Berlamont, J. 1992. Computation method for regulating unsteady flow in open channels. J. Irrig. Drain Eng. 118 (5), 674–689.
22. Liu, X., Mohammadian, A., & Sedano, J. 2016. Three-dimensional modeling of non-hydrostatic free-surface flows on unstructured grids. International Journal for Numerical Methods in Fluids. 82. 130-147.
23. Love, J. S., & Tait, M. J. 2013. Parametric depth ratio study on tuned liquid dampers: Fluid modelling and experimental work. Computers & fluids, 79, 13-26.
24. MacCormack, R. W.1971. Numerical solution of the interaction of a shock wave with a laminar boundary layer. Lectures notes in physics, Springer-Verlag, 8, 151-163.
25. Marivani, M., & Hamed, M.S. 2009. Numerical simulation of structure response outfitted with a tuned liquid damper, Computers & Structures, 87, (17-18), 1154-1165.
26. Marivani, M., & Hamed, M. S. 2017. Evaluate pressure drop of slat screen in an oscillating fluid in a tuned liquid damper. Computers & Fluids, 156, 384-401.
27. Mohammadian, A., Le Roux, D. 2008. Fourier analysis of a class of upwind schemes in shallow water systems for gravity and Rossby waves. International Journal for Numerical Methods in Fluids. 57, 389 - 416.
28. Moslemi, M. & Kianoush, M.R. 2012. Parametric study on dynamic behavior of cylindrical ground-supported tanks. Eng. Struct. 42, 214–230.
29. Pandit, A. R., & Biswal, K.C., 2020. Seismic control of multi degree of freedom structure outfitted with sloped bottom tuned liquid damper. In Structures, 25: 229-240.
30. Popescu, I., 2014. Computational Hydraulics: Numerical Methods and Modeling. IWA Publishing, London.
31. Preissmann, A., 1961. Propagation des intumescences dans les canaux et Les Rivieres. In: 1 Congres de l'Association Francaise de Calcule, Grenoble, France (in French).
32. Saburin, D.S. 2015. Tank sloshing simulations in shallow-water approximation. Proceedings of the VI International Conference on Computational Methods in Marine Engineering, 1039-1050.
33. Solaas, F. & Faltinsen, 0. M. 1997. Combined Numerical and Analytical Solution for Sloshing in Two-dimensional Tanks of General Shape. Journal of Ship Research, 41(2).
34. Sorkhabi, A. A., Malekghasemi, H., Ghaemmaghami, A., & Mercan, O. 2017. Experimental investigations of tuned liquid damper-structure interactions in resonance considering multiple parameters. Journal of Sound and Vibration. 388, 141-153.
35. Sun, L. M., Fujino, Y., Pacheco, B. M., & Chaiseri, P. 1992. Modelling of tuned liquid damper (TLD). Journal of Wind Engineering and Industrial Aerodynamics, 43(1-3), 1883-1894.
36. Sun, L.M. and Fujino, Y. 1994.A semi-analytical model for tuned liquid damper (TLD) with wave breaking. Journal of Fluids and Structures, 8, 471 - 488.
37. Sun, P., Colagrossi, A., Marrone, S., Antuono, M. & Zhang, A. 2018. Multi-resolution Delta-plus-SPH with tensile instability control: towards high Reynolds number flows. Comput. Phys. Commun. 224, 63–80.
38. Tait, M., El Damatty, A., Isyumov, N., & Siddique, R. 2005. Numerical flow models to simulate tuned liquid dampers (TLD) with slat screens. Journal of Fluids and Structures, 20, 1007-1023.

39. Venutelli, M., 2002. Stability and accuracy of weighted four-point implicit finite difference schemes for open channel flow. J. Hydraul. Eng. 128 (3), 281–288.
40. Wang, Y., Zhang, C., Li, Z., Sun, B. & Zhou, H. (2019). Applicability of Preissmann box scheme for calculation of transcritical flow in pipes. Water Science and Technology: Water Supply. 19. 10.2166/ws.2019.010.
41. Wang, Yanmei & Zhang, Chengcai & Li, Zhansong & Sun, Bin & Zhou, Haolan. (2019). Applicability of Preissmann box scheme for calculation of transcritical flow in pipes. Water Science and Technology: Water Supply. 19 (5): 1429–1437.
42. Wazwaz, A.M. 2009. Partial Differential Equations and Solitary Waves Theory. Higher Education Press, Beijing and Springer-Verlag, Berlin Heidelberg.
43. Wu, G. X., Ma, Q. W. & Taylor, R. 1998. Numerical simulation of sloshing waves in a 3-D tank based on a finite element method. Applied Ocean Res., 20(6), 337-355.
44. Wu, W., 2008. Computational River Dynamics. Taylor & Francis, London.

List of Symbols

$\vec{U}$	Variable vector
$\vec{F}$	Flux vector
$\vec{R}$	Source vector
u	Depth-averaged velocity
H	Averaged depth
L	Water tank length
η	Wave height relative to averaged depth
L	Water tank length
a_x	Tank acceleration
g	Gravity acceleration
D	Physical diffusion
α	Contribution coefficient of physical diffusion
m	Mass of SDOF

k	Stiffness of SDOF
c	Damping coefficient of SDOF
$u_s(t)$	Displacement of SDOF
$\dot{u}_s(t)$	Velocity of SDOF
$\ddot{u}_s(t)$	Acceleration of SDOF
$F(t)$	Excitation force on SDOF
$G(t)$	Sloshing Force on SDOF
f	Natural frequency of the water tank
$\bar{f}$	Frequency of excitation force
f_s	Natural frequency of SDOF
A	Amplitude of harmonic excitation displacement
ϕ	phase angle of excitation displacement
β	Frequency ratio
ζ	Damping ratio
c_c	Critical damping

3. Simulation of Sloped Bed Tuned Liquid Dampers Using Nonlinear Shallow Water Model[2]

Abstract:

This research aims to develop an efficient and accurate model for simulating Tuned Liquid Dampers (TLDs) with sloped beds. The model, based on nonlinear shallow water equations, is enhanced by introducing new terms tailored to each specific case. It employs the central upwind method and Minmod limiter functions for flux and interface variable assessment, ensuring both high accuracy and reasonable computational cost. While acceleration, slope, and dissipation are treated as explicit sources, an implicit scheme is utilized for dispersion discretization to enhances the model stability, resulting in matrix equations. Time discretization uses the fourth-order Runge-Kutta scheme for precision. The performance of the model has been evaluated using several test cases including dam-breaks on flat and inclined beds, run-up, and run-down simulations over parabolic beds, relevant to sloshing in tanks with sloped beds. It accurately predicts phenomena such as asymmetric sloshing waves, especially in sloped beds, where pronounced waves occur. Dispersion and dissipation terms are crucial for capturing these effects and maintaining stable wave patterns. An initial perturbation method assesses the tank's natural period and numerical diffusion. Furthermore, the model integrates with a Single Degree of Freedom (SDOF) system to create a TLD model, demonstrating enhanced damping effects with sloped beds.

Keywords: nonlinear shallow water models; central upwind; sloshing; sloped TLD

---

[2] This chapter has been **published** as Mahdiyar Khanpour, Abdolmajid Mohammadian, Hamidreza Shirkhani, and Reza Kianoush (2024). "*Simulation of Sloped-Bed Tuned Liquid Dampers Using a Nonlinear Shallow Water Model*." ***Water***. *16*(10), 1394. https://doi.org/10.3390/w16101394

3.1. Introduction

Liquid storage tanks are crucial structures with significant importance in various industrial sectors, including water supply facilities and oil refineries that play a fundamental role in public services. However, these tanks are vulnerable to seismic hazards, and their failure can result in severe damages. Numerous studies were conducted to model the sloshing phenomenon in tanks given their widespread use and criticality.

Bahreini et al. (2021) and Liu and Lin (2008) employed the Volume of Fluid (VOF) method to accurately represent the free surface in sloshing simulations of rectangular tanks supported on the ground and Vîlceanu et al., (2023) utilized this approach for the simulation of tuned liquid dampers. The VOF equation, originally introduced by Hirt and Nichols (1981), is coupled with the Navier-Stokes equations and turbulence models to track the dynamic behavior of the free surface. Although the VOF method offers high accuracy in modelling violent free-surface flow and wave breaking, it is associated with computationally expensive calculations.

Some studies focused on different aspects of sloshing tank behavior. Researchers such as Veletsos et al. (1992) and Ghaemmaghami and Kianoush (2010) focused on the influence of wall tank flexibility on the structural response. Their findings suggest that while flexibility may have a minimal effect on sloshing waves, it leads to an increased base shear of the tank owing to an amplified impulsive response. Panigrahy et al. (2009) examined the impact of baffles on the pattern of sloshing waves. They explored various types of baffles, such as horizontal, vertical, and inclined baffles, and investigated how different baffle arrangements can influence and control the behavior of sloshing waves. Virella et al. (2008) and Sobhan et al. (2017) examined the damage modes and buckling of the sloshing tanks. Hashemi et al. (2022) investigated the effects of soil-structure interaction on sloshing. The impact of excitation forces on the sloshing process was also explored. For instance, Sriram et al. (2006) investigated the sloshing waves resulting from random horizontal and vertical excitations. Ghaemmaghami and Kianoush (2010) studied the influence of vertical acceleration during earthquakes on the responses of rectangular grounded tanks. Additionally, researchers examined the contribution of oblique excitation to sloshing phenomena. Bahreini et al. (2021) investigated the bidirectional effect of excitation on closed rectangular tanks, whereas Ikeda et al. (2012) studied the effect of nonlinear sloshing in rigid tanks with square plan shapes excited by harmonic and oblique loads.

When the water depth in the tank is significantly smaller than tank length, shallow water tank, it exhibits more pronounced nonlinearity in sloshing waves compared to deep water tanks, making potential flow theory less suitable for modelling. So Special treatment is required to accurately model the asymmetric pattern of sloshing waves in shallow tanks. In this context, shallow water models (SWM) that enables the consider of nonlinearity come into play.

Although various methods exist for modelling fluid sloshing in tanks, those based on shallow water models are uncommon in the literature. Antuono (2012) employed a shallow water model and incorporated a decomposition technique to simulate sloshing in a shallow-water tank subjected to near-resonance excitation. Saburin (2015) utilized a specific form of averaging, known as Regularized Shallow Water Equations (RSWE), to simulate sloshing in a fuel tank.

One of the interesting and positive applications of sloshing tanks is tuned liquid dampers (TLDs). TLDs are sloshing tanks installed at the top of structures. These tanks were tuned to suppress the vibration of the structures with their sloshing waves. As mentioned, because shallow-water tanks produce higher sloshing waves and pronounce more nonlinear waves, they are primarily used as TLDs. Therefore, some previous studies adopted shallow water models to investigate the performance of TLDs. Sun (1992) used shallow water models to model TLD with the introduction of breaking wave terms. Koh et al. (1994), Tait et al. (2005), Murudi (2012), and Banerji et al. (2010) applied a shallow-water model to conduct parametric studies on TLDs.

In the literature, researchers used approaches other than (SWM) to simulate TLDs. An alternative approach involves employing equivalent mechanical models, which consist of an impulsive mass that moves rigidly with the tank container along with a series of masses representing convection or sloshing (Konar and Ghosh, 2020; Abd-Elhamed and Tolan, 2022). Some studies utilized potential flow theory to simulate the performance of TLDs. For instance, Pandit and Biswal (2019) and Chaiviriyawong et al. (2007) employed a velocity potential solved using a finite element model (FEM) to model fluid sloshing in a tuned liquid column damper (TLCD).

Several parametric studies were conducted on TLDs. For example, some studies investigated TLD/structure mass ratio (Banerji et al., 2000) and TLD/structure frequency ratio (Fujino et al., 1992). Tait et al. (2005) and Marivani and Hamed (2017) examined the motion of the free surface, resulting in base shear forces and energy dissipation by a TLD equipped with slat screens. Zhao et al. (2019) conducted research utilizing a unique method known as the liquid inerter system (TLIS).

This system incorporates a tuned liquid element and an inerter-based subsystem, amalgamating damping, stiffness, and inerter elements to enhance its efficiency. Wang et al. (2019) further integrated this approach into a tuned liquid column damper and examined its effectiveness in single-degree-of-freedom vibration.

Sorkhabi et al. (2016) and Saha and Debbarma (2017) conducted experimental studies to assess the efficiency of multiple TLDs compared to a single TLD. Hu et al. (2022) investigated the utilization of a pair of isolated TLDs (ITLDs) for the multi-performance vibration modification of multi-degree-of-freedom (MDOF) structures. Banerji et al. (2000, 2010) and Murudi et al. (2012) investigated the influence of ground-motion specifications, including excitation amplitude and bandwidth excitation frequency. Banerji et al. (2000) explored the impact of structural damping on the efficiency of TLDs.

Bhattacharjee (2013) conducted experimental studies to examine the influence of two parameters, namely the dimensions of the rectangular tank and water depth, on TLD performance. Samanta and Banerji (2010) and Chang et al. (2018) proposed a modified TLD design that incorporates an appropriate torsional spring connection to the floor instead of a rigid connection. They suggested that this modified TLD design is more effective than conventional designs. Abd-elhamed and Tolan (2022) developed a numerical model to investigate the impact of soil-structure interactions on TLD performance. Their study explored how different soil types could influence the performance of the TLDs. Murudi and Banerji (2012) found that TLDs are more efficient in far-field ground motions because the peak structural response occurs after a few cycles of vibration, when the TLD starts to influence the structural response. In addition, some researchers have applied TLDs to systems with multiple degrees of freedom. Ocak et al. (2022) utilized a two-degree-of-freedom system as a TLD and coupled it with single-story, 10-story, and 40-story buildings.

Few studies investigated the geometric shape of the TLD and its influence on the structural response. Most of these studies utilized potential flow theory to model TLD behavior. Pandit and Biswal (2019, 2020) developed a finite element model based on potential flow theory to simulate sloshing in a sloped bottom-tuned liquid damper. In their research TLD was connected to both single-degree-of-freedom (SDOF) and multi-degree-of-freedom (MDOF) systems subjected to different types of excitations with varying frequencies (references). Gardarsson et al. (2000) conducted experimental investigations of sloshing in a sloped-bottom TLD directly attached to a shaking table (referred to as a grounded sloshing tank). They found that the sloped tank exhibited a different nonlinear behavior compared to a box tank because of the amplitude of the dispersion effects and run-up onto the sloped walls.

The main focus of this investigation was on SWM for the simulation. Shallow water equations are derived by integrating Navier-Stokes equations over the depth of water when the horizontal length scale is much larger than the vertical length scale. In this situation, the conservation equations for mass and momentum lead to a small-scale vertical velocity and a nearly hydrostatic pressure distribution throughout the depth. However, the key difference from potential flow models is that the nonlinear kinematic boundary condition is directly incorporated into the depth-integrated mass and momentum equations, allowing for an exact representation of the nonlinear free surface without the need for special treatment. Consequently, the modelling process becomes straightforward and more cost-effective because only the equations for mass and momentum need to be solved.

The aim of this study was to develop an efficient and accurate model capable of simulating Tuned Liquid Dampers (TLDs) featuring both horizontal and sloped beds. To achieve this objective, a series of innovative steps and systematic approaches were employed. Firstly, an efficient model was devised to simulate free surface flow with high gradients, such as dam breaks. Numerical investigations demonstrated that the central upwind method proved effective in accurately simulating free surface behavior without the need for entropy correction or kinematic boundary conditions. This capability to handle high gradient depths is particularly relevant to sloshing waves, especially during resonance excitation. Subsequently, the model was enhanced with a bed topography term discretized using a second-order method. The model exhibited excellent agreement when applied to simulate the first dam break over a dry-sloped bed, followed by perturbed flow over a parabolic bed. Subsequently, the validated current model was further enhanced by incorporating new terms: dissipation and dispersion terms, and applied to simulate the sloshing behavior of both a box tank and a box tank with a sloped bed. To ensure the stability and efficiency of the model, an innovative approach was employed: the dissipation term was treated explicitly, while an implicit scheme was applied to the dispersion term, resulting in a matrix equation. Utilizing an innovative technique known as initial perturbation, the numerical diffusion of the developed method, which relies on the central upwind scheme and Minmode slope limiter function for flux and variable interface approximation, respectively, was assessed. The sloshing model exhibited excellent agreement with experimental data. Additionally, another noteworthy contribution of the study was the investigation into how the dissipation and dispersion terms affect the numerical simulation of the sloshing tank. Moreover, utilizing the novel and efficient current model, it was demonstrated how a sloped bed induces asymmetrical sloshing waves with significantly higher heights at the walls. Following that, an innovative partitioned method, based on prediction and correction, was introduced to couple the developed fluid model with a single degree of freedom representing the underlying structure. In conclusion, this research culminated in the development of a novel and efficient model capable of simulating both conventional Tuned Liquid Dampers (TLDs) and those incorporating the bed slope. With this efficient model, it is predicted that TLDs equipped with sloped beds exhibit more pronounced damping effects during resonance excitation, although further investigation is required to assess their promising impact in other scenarios.

3.2. Governing Equations

The equations for modelling fluid motion here rely on depth-averaged Navier–Stokes equations, called shallow-water equations. These equations, including the continuity and momentum equations, are expressed in Equation (3-1). Contrary to the conventional nonlinear shallow water equations (Toro 2001), the momentum equation's right-hand side incorporates four terms: the slope term (Benkhaldoun and Seaïd, 2010), acceleration term (Ardakani & Bridges, 2011), and the dissipation and dispersion terms (Tait et al., 2005).

$$
\begin{aligned}
&\frac{\partial h}{\partial t}+\frac{\partial (uh)}{\partial x}=0\\
&\frac{\partial (uh)}{\partial t}+\frac{\partial (u^2h+0.5gh^2)}{\partial x}=-\alpha_1 h\frac{\partial z}{\partial x}-\alpha_2 ah-\alpha_3 c_d uh+\alpha_4\frac{1}{3}h^3\frac{\partial^3 u}{\partial t\partial^2 x}
\end{aligned}
\qquad (3\text{-}1)
$$

In equation (3-1), *h (x, t)* and *u (x, t)* are the water depth and velocity (Figure 3.1), respectively. *z* is the bottom elevation, *x* and *t* represent the position, and time. In addition, the parameter η , called wave height, is the water free surface elevation with respect to the mean water level. In the momentum equation, *a(t)* is the tank acceleration, *g* is the gravitational acceleration, and c_d is the damping coefficient. In this equation $\alpha_1,\alpha_2,\alpha_3,\alpha_4$ denotes the participation factors for the sloped bed, acceleration, dissipation (damping), and dispersion terms. Depending on the case study test, if these terms are introduced into the modelling the corresponding coefficients of α are equal to one; otherwise, they are zero.

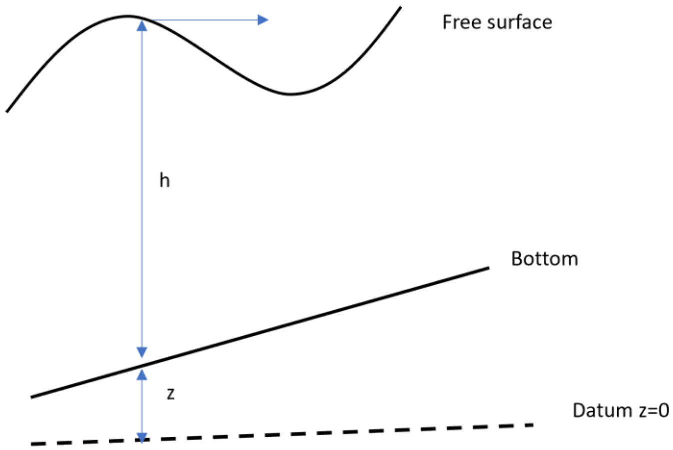

Fig. 3.1. Schematic of shallow water equation parameters.

3.3. Numerical Model

Equation (3-2) reflects equation (3-1) for a point j and time n and superscript $n+1$ is associated with $t+\Delta t$, where Δt is a time step. As shown in this equation most of the terms including convection, dissipation, acceleration, pressure gradient, and bed slope, are evaluated using explicit schemes, whereas the dispersion term is solved implicitly. Put simply, due to the significant magnitude of the dispersion term, handling this term explicitly requires a very small time step. Therefore, an implicit method was employed to discretize the dispersion term and enhance the stability of the model.

$$\begin{aligned}
&\frac{\partial h}{\partial t}=-\frac{\partial (uh)_j^n}{\partial x} \\
&\frac{\partial (uh)}{\partial t}=-\frac{\partial (u^2h+0.5gh^2)_j^n}{\partial x}-\alpha_1(h\frac{\partial z}{\partial x})_j^n-\alpha_2(ah)_j^n-\alpha_3(c_d uh)_j^n+\alpha_4\frac{1}{3}(h^3\frac{\partial^3 u}{\partial t\partial^2 x})_j^{n+1}
\end{aligned} \tag{3-2}$$

Equation (3-2) could be written in the following conservative vector form.

$$
\frac{\partial \vec{U}}{\partial t} + \frac{\partial \vec{F}}{\partial x} = \vec{R}
$$

$$
\vec{U} = \begin{bmatrix} h \\ uh \end{bmatrix} \quad \vec{F} = \begin{bmatrix} uh \\ u^2 h + 0.5 g h^2 \end{bmatrix} \quad \vec{R} = \begin{bmatrix} 0 \\ -\alpha_1 h \dfrac{\partial z}{\partial x} - \alpha_2 a h - \alpha_3 c_d u h + \alpha_4 \dfrac{1}{3} h^3 \dfrac{\partial^3 u}{\partial t \partial^2 x} \end{bmatrix} \tag{3-3}
$$

The flux gradient ($\frac{\partial \vec{F}}{\partial x}$) in Equation (3-3) can be represented by Equation (3-4) for the control volume of node *j* depicted in Figure (3.2).

$$
(\frac{\partial F}{\partial x})_j = (\frac{F_{j+1/2} - F_{j-1/2}}{dx}) \tag{3-4}
$$

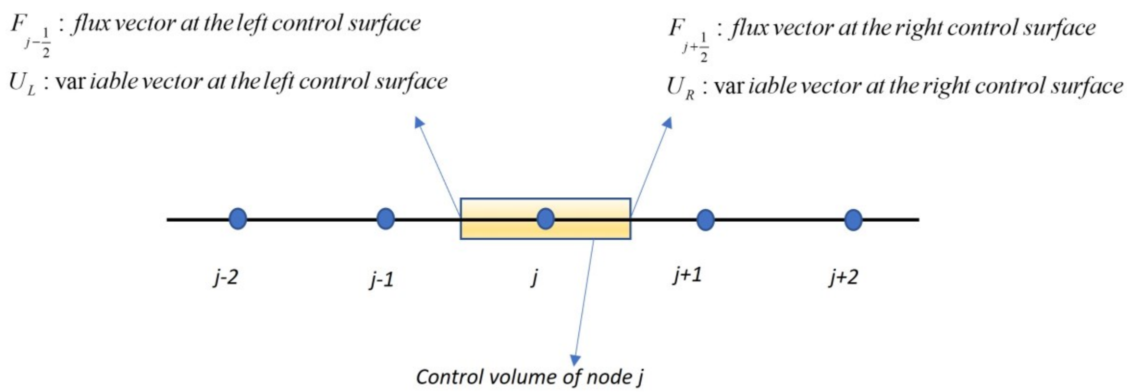

Fig. 3.2. Schematic of control volume and control surfaces of node *j*

The main difference between various numerical models is in the approximation of the flux vector ($\vec{F}$) and the variable vector ($\vec{U}$) at the surfaces of the control volume.

The nonconservative form of equation (3-3) is expressed as

$$
\frac{\partial \vec{U}}{\partial t} + A \frac{\partial \vec{U}}{\partial x} = \vec{R}
$$

$$
A = \begin{bmatrix} 0 & 1 \\ C^2 - u^2 & 2u \end{bmatrix} \tag{3-5}
$$

Matrix *A* has two eigen values (λ_1, λ_2) and two corresponding eigen vectors $(\vec{e}_1, \vec{e}_2)$

$$\lambda_1 = u + C \quad \lambda_2 = u - C \quad C = \sqrt{gh}$$
$$e_1 = \begin{bmatrix} 1 \\ u + C \end{bmatrix} \quad e_2 = \begin{bmatrix} 1 \\ u - C \end{bmatrix} \tag{3-6}$$

3.3.1. Flux Approximation

Several flux approximation schemes have been proposed in the literature. Here, the Roe and central upwind approaches are selected and described in subsequent sections.

3.3.1.1. Roe Method

In this approach, the convective flux $\vec{F}$ is calculated using the following expression (Mohammadian and Le Roux, 2006).

$$\vec{F}_{j+1/2} = 0.5 * (\vec{F}^{L}_{j+1/2} + \vec{F}^{R}_{j+1/2} - \Delta\vec{F})$$
$$\vec{F}^{L}_{j+1/2} = \vec{F}_j \quad \vec{F}^{R}_{j+1/2} = \vec{F}_{j+1} \tag{3-7}$$

where $\Delta\vec{F}$, flux differences relying on the eigenvalues and eigenvectors of matrix A, is obtained from the following procedure (Equations 3-8 and 3-9). In the equation (3-8), $\tilde{u}$ and $\tilde{C}$ are the Roe-averaged values obtained from the right-hand side of the vector variables (h_R, u_R) and the left-hand side of the vector variables (h_L, u_L) at the control surfaces. These vector variables, right and left, can be evaluated using the different order numerical schemes discussed in section (3.3.2).

$$\tilde{u} = \frac{u_R\sqrt{h_R} + u_L\sqrt{h_L}}{\sqrt{h_R} + \sqrt{h_L}} \quad \tilde{C} = \sqrt{g(h_R + h_L)/2} \tag{3-8}$$

$$\Delta\vec{F} = \sum_{k=1}^{2} \tilde{\alpha}_k \left|\tilde{\lambda}_k\right| \tilde{e}_k$$
with
$$\tilde{\lambda}_1 = \tilde{u} + \tilde{C} \quad \tilde{\lambda}_2 = \tilde{u} - \tilde{C} \quad e_1 = \begin{bmatrix} 1 \\ \tilde{u} + \tilde{C} \end{bmatrix} \quad e_2 = \begin{bmatrix} 1 \\ \tilde{u} - \tilde{C} \end{bmatrix} \tag{3-9}$$
$$\tilde{\alpha}_1 = \frac{\Delta h}{2} + \frac{1}{2\tilde{C}}\left[\Delta(hu) - \tilde{u}\Delta h\right]$$
$$\tilde{\alpha}_2 = \frac{\Delta h}{2} - \frac{1}{2\tilde{C}}\left[\Delta(hu) - \tilde{u}\Delta h\right]$$

3.3.1.2. Central Upwind Method

In the scheme proposed by (Kurganov and Levy, 2002) the interface flux is approximated using the following expression:

$$\vec{F} = \frac{S_R \vec{F}(\vec{U}_L) - S_L \vec{F}(\vec{U}_R) + S_R S_R (\vec{U}_R - \vec{U}_L)}{S_R - S_L} \tag{3-10}$$

S_R and S_L , depending on the eigenvalues and eigenvectors of A, are approximated by the procedure presented in Equation (3-11).

$$\begin{aligned} &a_{L,\min} = \min(u_L - C_L, u_L + C_L) \quad a_{L,\max} = \max(u_L - C_L, u_L + C_L) \\ &a_{R,\min} = \min(u_R - C_R, u_R + C_R) \quad a_{R,\max} = \max(u_R - C_R, u_R + C_R) \\ &S_L = \min(a_{L,\min}, a_{R,\min}, 0) \qquad S_R = \max(a_{L,\max}, a_{R,\max}, 0) \end{aligned} \tag{3-11}$$

3.3.2. Variable Vector Approximation

Several methods can be used to evaluate the variable vector at the interfaces, including the first-order upwind, higher-order upwind, Minmod, and WENO methods. This study primarily focuses on the Minmod scheme. Generally, employing a higher-order method to evaluate the vector variable at the interface leads to reduced numerical diffusion but may result in more oscillatory solutions. In the Minmod scheme, the interface variables for node j (Figure 3.2) are determined using the following expression (Mohammadian et al.2007):

$$\begin{aligned} &S_{R1} = U_j - U_{j+1} \quad S_{R2} = U_{j-1} - U_j \\ &U_R = U_j + 0.5\,minmod(S_{R1}, S_{R2}) \\ &S_{L1} = U_{j-1} - U_{j-2} \quad S_{L2} = U_j - U_{j-1} \\ &U_L = U_{j-1} + 0.5\,minmod(S_{L1}, S_{L2}) \end{aligned} \tag{3-12}$$

where Minmod function is defined based on the following expression for scalers S1 and S2 (Mohammadian et al.2007).

$$\begin{aligned} &minmod(S1, S2) = \begin{Bmatrix} m(S1, S2), & if\ (S1 * S2) > 0 \\ 0, & if\ (S1 * S2) < 0 \end{Bmatrix} \\ &m(S1, S2) = \begin{Bmatrix} S1, & if\ |S1| < |S2| \\ 0, & otherwise \end{Bmatrix} \end{aligned} \tag{3-13}$$

3.3.3. Source Terms

3.3.3.1. Explicit Terms

In the current model, the sloped bed, acceleration, and dissipation terms are treated as source terms. They were evaluated explicitly using the following expression. The second-order finite difference method was employed to approximate the slope bed term.

$$
\begin{aligned}
&(-gh\frac{\partial z}{\partial x})_j^n = -gh_j^n \frac{z_{j+1}^n - z_{j-1}^n}{2\Delta x} \\
&(-ah)_j^n = -a(h)_j^n \\
&(-c_d uh)_j^n = -c_d (uh)_j^n
\end{aligned}
\tag{3-14}
$$

3.3.3.2. Implicit Term

As mentioned earlier, the dispersion term was evaluated using an implicit approach in the model. Accordingly, the discretized form of this term is given by Equation (3-15):

$$
\left[\frac{1}{3}h^3(\frac{\partial^3 u}{\partial^2 x \partial t})\right]_j^{n+1} = \frac{1}{3}(h^{n+1})^3 \left[\frac{u_{i+1}^{n+1} - 2u_i^{n+1} + u_{i-1}^{n+1}}{\Delta x^2} - \frac{u_{i+1}^n - 2u_i^n + u_{i-1}^n}{\Delta x^2}\right] \tag{3-15}
$$

In this context, the matrix equation presented below was established: The coefficient matrix, A, is a banded matrix with a bandwidth of one. The values in the first and last rows of matrix A, denoted LL, represent large numbers. Essentially, the first and last equations signify zero velocity at the walls, specifically at nodes 1 and NI, where NI is the last point. The unknown variable vector X represents the nodal velocities. The known vector B contains various components, including the known term from Equation (3-15) at time n, as well as nodal velocities obtained from the momentum equation (Equation 3-2), with the dispersion term neglected. The parameter u^* denotes these nodal velocities.

$$[A]_{NI*NI}[X]_{NI*1}=[B]_{NI*1}$$

$$A=\frac{\frac{1}{3}(h^{n+1})^3}{\Delta x^2}\begin{bmatrix} LL & 0 & 0 & 0 & 0 & 0 & 0 \\ 1 & -2 & 1 & 0 & 0 & 0 & 0 \\ . & . & . & . & . & . & . \\ . & . & . & . & . & . & . \\ . & . & . & . & . & . & . \\ 0 & 0 & 0 & 0 & 1 & -2 & 1 \\ 0 & 0 & 0 & 0 & 0 & 0 & LL \end{bmatrix}_{NI*NI} \qquad X=\begin{bmatrix} u_1 \\ u_1 \\ . \\ . \\ . \\ u_{NI-1} \\ u_{Ni} \end{bmatrix}_{NI*1}$$

$$B=\begin{bmatrix} 0 \\ \frac{\frac{1}{3}(h^{n+1})^3}{\Delta x^2}(\frac{u_3^n-2u_2^n+u_1^n}{\Delta x^2})+u_2^* \\ . \\ . \\ . \\ \frac{\frac{1}{3}(h^{n+1})^3}{\Delta x^2}(\frac{u_{NI-2}^n-2u_{NI-1}^n+u_{NI}^n}{\Delta x^2})+u_2^* \\ 0 \end{bmatrix}_{NI*1} \qquad (3\text{-}16)$$

3.3.4. Time Integration

The analysis of time integration methods indicates that the first-order Euler method is unstable. However, both the midpoint method which is a second-order Runge-Kutta method, as well as the fourth-order Runge-Kutta method provide stable solutions. Further information about the numerical schemes mentioned can be found in Durran (2010). Given that the fourth-order method yields slightly more accurate results and the computational cost of these two methods does not differ considerably, the fourth-order method was employed in this study. In this scheme, the discretization of the temporal derivative, $\frac{\partial \vec{U}}{\partial t}$ in Equation (3- 17), is derived by Equations (3-18) (Durran 2010):

$$\frac{\partial \vec{U}}{\partial t} = \frac{\partial}{\partial t}\begin{bmatrix} h \\ uh \end{bmatrix} = \begin{bmatrix} -\dfrac{\partial}{\partial x}(uh) \\ -\dfrac{\partial}{\partial x}(u^2 h + 0.5 * gh^2) - \alpha_1 h \dfrac{\partial z}{\partial x} - \alpha_2 ah - \alpha_3 c_d uh \end{bmatrix} \tag{3-17}$$

$$\begin{aligned} & k_1 = \frac{\partial}{\partial t}(U^n) \\ & U^{(1)} = U^n + k_1 \frac{\Delta t}{2} \quad k_2 = \frac{\partial}{\partial t}(U^1) \\ & U^{(2)} = U^n + k_2 \frac{\Delta t}{2} \quad k_3 = \frac{\partial}{\partial t}(U^2) \\ & U^{(3)} = U^n + k_3 \Delta t \quad k_4 = \frac{\partial}{\partial t}(U^3) \\ & U^{n+1} = U^n + \frac{1}{6}(k_1 + 2k_2 + 2k_3 + k_4)\Delta t \end{aligned} \tag{3-18}$$

3.3.5. Boundary conditions and Courant Number

The boundary conditions employed in the current research are the wall boundary condition, which implies zero velocity at both the right and left walls (Mohammadian et al.2007). Additionally, this boundary condition incorporates zero gradient for flow depth, indicating that the flow depth at wall nodes is adjusted to match the depth of the nearest inner nodes. Additionally, in all case studies, the sizes of the time steps and mesh were adjusted to ensure that the Courant number remains below 0.6. Courant Number expresses the distance that any information travels during the timestep length within the mesh over the distance between mesh elements (Durran 2010).

3.3.6. Dynamic Equation of SDOF

The dynamic equation of a single degree of freedom, which is a second-order ordinary differential equation, is expressed in Equation (3-19) (Humar, 2012).

$$m\ddot{x} + c\dot{x} + kx = F_{exc} + F_{slo} \tag{3-19}$$

In this equation m is the mass of the SDOF, c is the damping coefficient, and k denotes the SDOF stiffness $\ddot{x}, \dot{x}, x$ are acceleration, velocity and displacement of the SDOF, respectively. In other words, $m\ddot{x}$ is the inertial force, $c\dot{x}$ represents the damping force, and kx refers to the elastic force. The first term on the right-hand side of this equation, F_{exc}, is the excitation force, which was assumed to be a sinusoidal harmonic excitation force in the current study. The second term on the right-hand side, F_{slo}, represents the sloshing force. The excitation force and sloshing force communicate from below the SDOF, ground, and top of the SDOF, water tank, respectively (Figure 3.3). A second-order finite-difference method was used to solve this equation. For more information, the reader is referred to (Humar, 2012). The discretized form of Equation (3-19) using this scheme leads to the following expression:

$$[\frac{m}{\Delta t^2}+\frac{c}{2\Delta t}]x^{n+1}=F_{exc}^{n}+F_{slo}^{n}-[\frac{m}{\Delta t^2}-\frac{c}{2\Delta t}]x^{n-1}-[k-\frac{2m}{\Delta t^2}]x^{n} \tag{3-20}$$

As observed in Equation (3-20), the values of x^{-1} and x^{0} are necessary to derive x^{1}. The initial displacement x^0 and initial velocity $\dot{x}^0$ are physical parameters that can be measured. However, to obtain x^{-1}, the following procedure has been introduced (Chopra ,2007). Using second-order finite difference, the initial velocity, $\dot{x}^0$, and initial acceleration $\ddot{x}^0$ can be expressed as:

$$\dot{x}^0=\frac{x^1-x^{-1}}{2\Delta t} \quad \& \quad \ddot{x}^0=\frac{x^1-2x^0+x^{-1}}{2\Delta t} \tag{3-21}$$

Obtaining x^1 from the first expression of equations (3-21) and substituting it into the second one yields:

$$x^{-1}=x^0-\Delta t\,\dot{x}^0+\frac{(\Delta t)^2}{2}\ddot{x}^0 \tag{3-22}$$

Manipulating the single degree of freedom equation, equation (3-19), for the initial time leads to:

$$m\ddot{x}^0+c\dot{x}^0+kx^0=F^0{}_{exc}+F^0{}_{slo} \tag{3-23}$$

Thus, the initial acceleration can be determined from the above equation as:

$$\ddot{x}^0=\frac{F^0{}_{exc}+F^0{}_{slo}}{m}-\frac{c}{m}\dot{x}^0-\frac{k}{m}x^0 \tag{3-24}$$

Substituting this expression into the equation (3-22) leads to Equation (3-25) to derive x^{-1}. Based on this expression, the value of x^{-1} can be obtained from physical parameters such as initial displacement, initial velocity, time step, initial excitation, and initial sloshing force, as well as single degree of freedom specifications including mass, stiffness, and damping.

$$x^{-1} = x^0\left(1 - \frac{(\Delta t)^2}{2}\frac{k}{m}\right) + \dot{x}^0\left(-\Delta t - \frac{(\Delta t)^2}{2}\frac{c}{m}\right) + \frac{(\Delta t)^2}{2}\frac{F^0{}_{exc} + F^0{}_{slo}}{m} \tag{3-25}$$

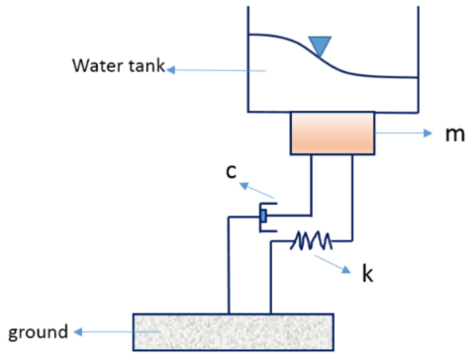

Fig. 3.3. Schematic of SDOF subjected to the ground excitation form bottom and water tank sloshing from top

3.3.7. Coupling Schemes

The system of equations presented in Equation (3-26) includes four equations:1) mass continuity of the fluid, 2) momentum continuity of the fluid, 3) dynamic equation of the SDOF, and 4) interaction or sloshing force, here, is the pressure force acting on the right wall (F_{PR}) minus the pressure force on the left wall (F_{PL}). These four equations were coupled to simulate the SDOF attached to a water tank (TLD) and subjected to an excitation force. In the specific case of sloshing occurring in a box-shaped tank with a sloped bed, special consideration must be given to the treatment of the interaction forces. This issue is addressed in section (4.6). The coupling scheme, which is a partitioned method (Liao et al. 2013), relies on an iterative interaction force. Additionally, the midpoint method (Durran,2010) was adopted to enhance the accuracy of the coupling scheme. In this scheme, the prediction value for F_{slo} and the known parameters *h, u*, and x at the beginning of the time step were employed to evaluate the SDOF acceleration, $\ddot{x}$, and sloshing force, F_{slo}, at the middle of the time step. Subsequently, using these middle-step values, the acceleration of the SDOF and sloshing force at the end of the time step were derived. This scheme involved a two-step prediction and correction process for the sloshing force, which was iterated until convergence was achieved. A flowchart depicting this coupling system is shown in Figure (3.4). In this flow chart, ε is used as the convergence criterion of F_{slo} is a small number of order of magnitude 10^{-3} and t^{End} is the time associated with the end of the simulation.

$$
\begin{aligned}
&\frac{\partial h}{\partial t}+\frac{\partial (uh)}{\partial x}=0\\
&\frac{\partial (uh)}{\partial t}+\frac{\partial (u^2h+0.5gh^2)}{\partial x}=-\alpha_1 h\frac{\partial z}{\partial x}-\alpha_2\ddot{x}h-\alpha_3 c_d uh+\alpha_4\frac{1}{3}h^3\frac{\partial^3 u}{\partial t\partial^2 x}\\
&m\ddot{x}+c\dot{x}+kx=F_{exc}+F_{slo}\\
&F_{slo}=F_{PR}-F_{PL}
\end{aligned}
\tag{3-26}
$$

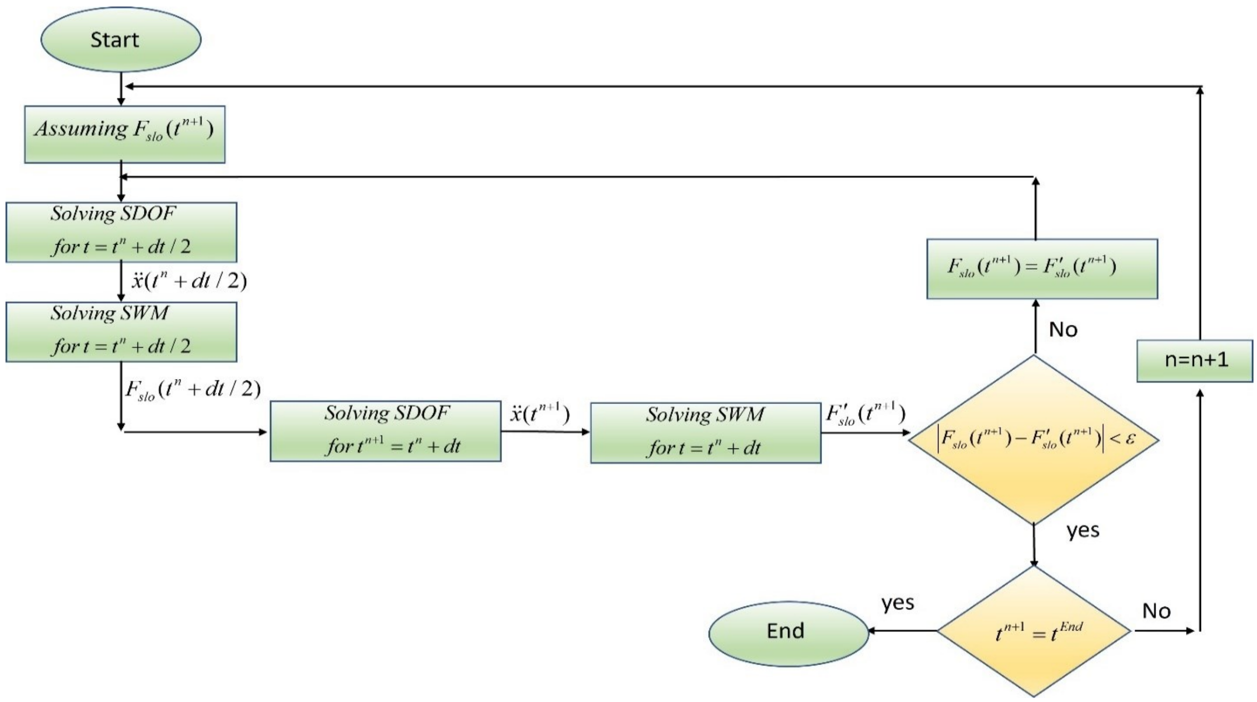

Fig. 3.4. Flowchart of coupling system for TLD simulation

3.4. Results

In this section, the accuracy and stability of the numerical model are examined using a series of diverse test cases. These carefully chosen tests aim to demonstrate the capability of the proposed model to simulate various scenarios that could arise during the sloshing phenomenon in tanks with sloped beds.

3.4.1. Test Case 1: Dam Break on the Dry Bed

This test was selected from Mohammadian et al.' work (2007) to examine the ability of the proposed model to simulate a high-gradient flow. In addition, it shows how the model simulates flow over a dry bed. Both scenarios can occur in the sloshing of a shallow water tank.

The water depths at the left and right sides of the dam were 1 m and 0.01 m, respectively. The dam was instantaneously removed, and the simulation was performed up to time $t = 4$ s. The system of Equation (3-1) with $\alpha_1 = \alpha_2 = \alpha_3 = \alpha_4 = 0$ was used to simulate this test case. In other words, the bed slope, dispersion, acceleration, and dissipation terms did not contribute to the modelling of this test.

A wall boundary condition (zero velocity) was employed at the inlet (x=0) and the outlet (x=50). In addition, this simulation included the sonic point at which the flow regime changed from supercritical to subcritical. Most numerical models generate non-physical jumps and fluctuations at the sonic point (Mohammadian et al. 2007). The results of the proposed model equipped with different schemes are derived and compared with the analytical solution. In this test, the efficiency and accuracy of three schemes were investigated:1) Central upwind method, 2) Roe method, and 3) McCormack method. MacCormack's pioneering work in 1971 initially introduced the MacCormack scheme as a solution to compressible Navier-Stokes equations. Subsequently, Chaudhry and Hussaini in 1985 adopted this scheme and further advancements were made by Amara et al. in 2013, specifically for water hammer analysis. Additionally, Fennema and Chaudhry in 1986, along with Garcia and Kahawita in the same year, employed the McCormack method to study unsteady free-surface flows. The traditional McCormack scheme, which is classified as a second-order finite-difference scheme, is discussed in Appendix A for this case study. Figure (3.5a) reveals that the central upwind method produces accurate results. However, the McCormack method produces a nonphysical jump at the free surface, although it has the advantage of second-order accuracy. Figure (3.5b) indicates that the conventional Roe method provides a jump in the middle of the solution, which does not agree with a physically free surface.

Some approaches have been introduced to enhance the efficiency of the Roe scheme in the case of problems with discontinuity such as dam breaks. In this regard, an approach introduced by van Leer et al. (1979) and used by Bradford and Sanders (2002), called entropy correction, was utilized. This includes modification of the eigenvalues when they are in the range of Equation (3-27). k is the number of eigenvalues, which is two here. The correction was performed based on Equation (3-28).

$$-\frac{\Delta\lambda^k}{2} < \tilde{\lambda}^k < \frac{\Delta\lambda^k}{2} \quad where \quad \Delta\lambda^k = 4(\lambda_R^k - \lambda_L^k) \tag{3-27}$$

$$\left|\tilde{\lambda}^{k}\right| = \frac{(\tilde{\lambda}^{k})^{2}}{\Delta\lambda^{k}} + \frac{\Delta\lambda^{k}}{4} \tag{3-28}$$

Figure (3.5b) indicates that when the Roe method is improved by this treatment, the unphysical jump is removed and a smooth, accurate free surface is produced. In relation to this validation process, it is worth noting that both central upwind method and Roe method with entropy correction yield accurate solutions. However, in this context, the central upwind scheme was chosen because of its significantly lower computational costs.

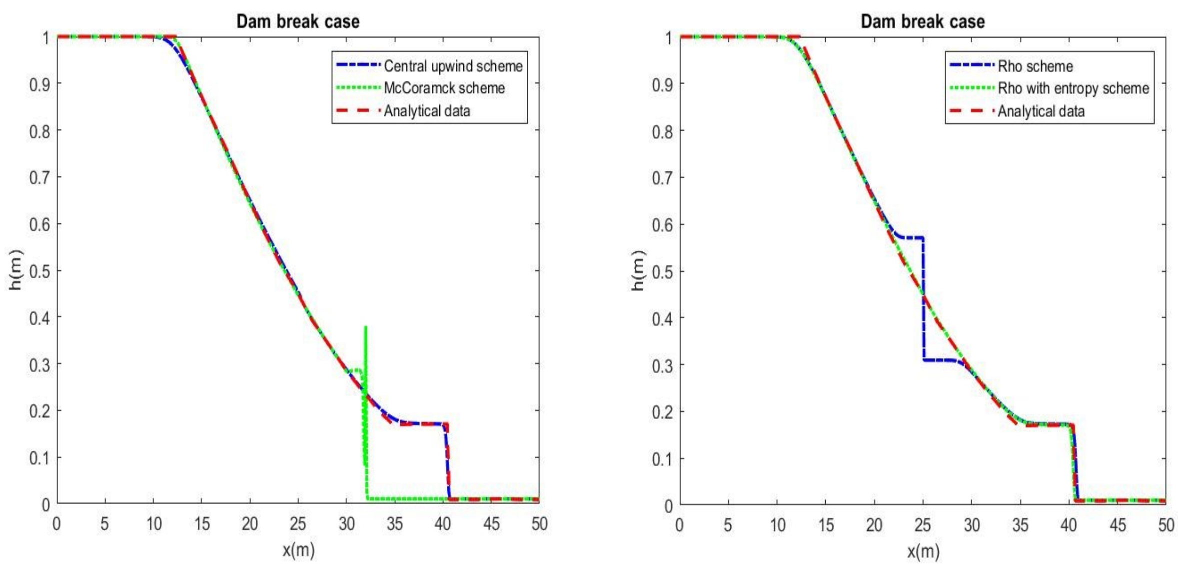

A B

Fig. 3.5. Comparison of analytical solution of dam break on the horizontal dry bed with those obtained using (a) central upwind method and McCormack method and (b) Roe scheme with and without entropy correction

3.4.2. Test Case 2: Dam Break on the Sloped Bed

Following the dam break on the horizontal bed, this case investigates the present model in the simulation of a dam break over a sloped bed (Xing et al. 2010). This test measures the accuracy of the numerical model when bed topography plays an important role. The governing equation for this case includes Equation (3-1) regarding $\alpha_1 = 1$ *and* $\alpha_2 = \alpha_3 = \alpha_4 = 0$, which means that the dispersion, acceleration, and dissipation terms are neglected in the model. However, unlike in the previous case, the slope-bed term was introduced into the model.

In this case, the computational domain is defined based on Equation (3-29), where α is the bed slope and is defined as $-\frac{\pi}{60}$ and $\frac{\pi}{60}$ in this study.

$$z(x) = -x\tan(\alpha) \qquad -15 \le x \le 15 \tag{3-29}$$

The initial condition of this case is presented in Equation (3-30)

$$h_0(x) = \begin{Bmatrix} 1 - z(x) & x \le 0 \\ z(x) & x > 0 \end{Bmatrix} \tag{3-30}$$

In this problem, the analytical solution for the wet/dry front is given by the following expression (Xing et al. 2010): h_0 in this equation is 1m.

$$x_f = 2t\sqrt{gh_0\cos(\alpha)} - \frac{1}{2}gt^2\tan(\alpha) \tag{3-31}$$

The results of the present model when $\alpha = -\frac{\pi}{60}$ was compared with Zhu's results (2018) for two different times (t=2 s and t=2.5 s). Figure (3.6) shows an excellent agreement between the present model and the Zhu model. Furthermore, wet/dry front positions were obtained from the present numerical model and then compared with the analytical expression and Zhu model for two cases of $\alpha = \frac{\pi}{60}$ *and* $\alpha = -\frac{\pi}{60}$. The comparison presented in Figure (3.7) for both cases demonstrate the high accuracy of the proposed model.

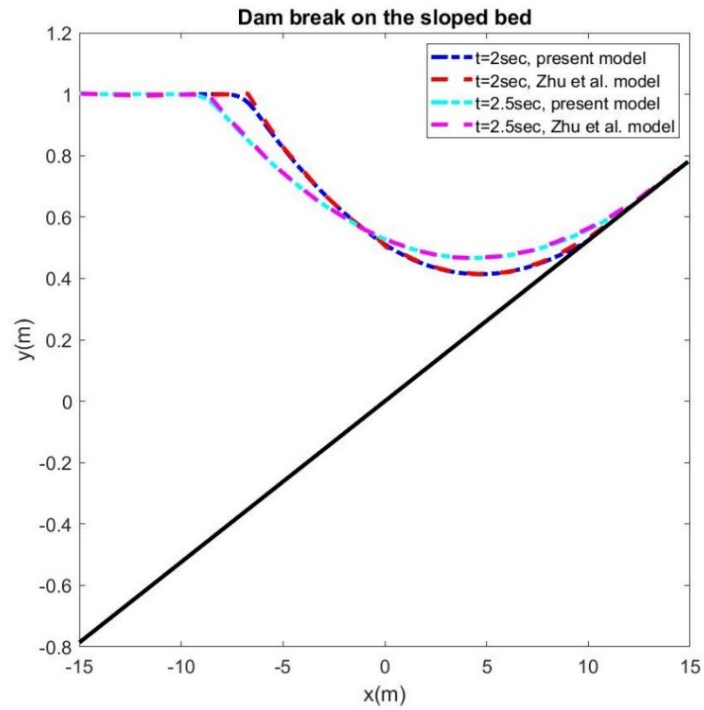

Fig. 3.6. Free surface obtained from the present numerical model and Zhu et al. model 2018 for dam break over sloped bed ($\alpha = -\frac{\pi}{60}$).

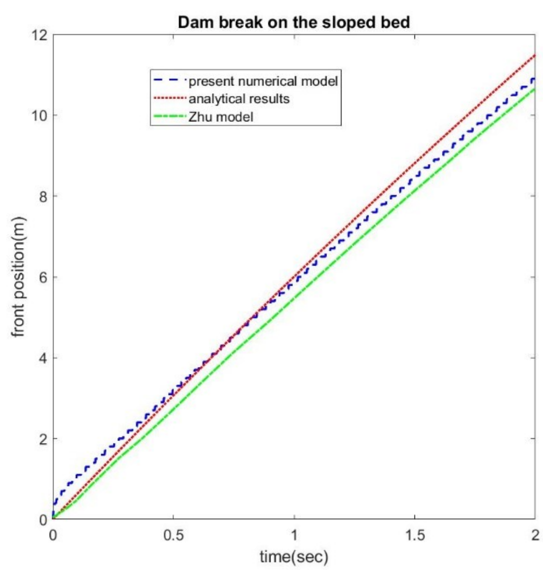

a

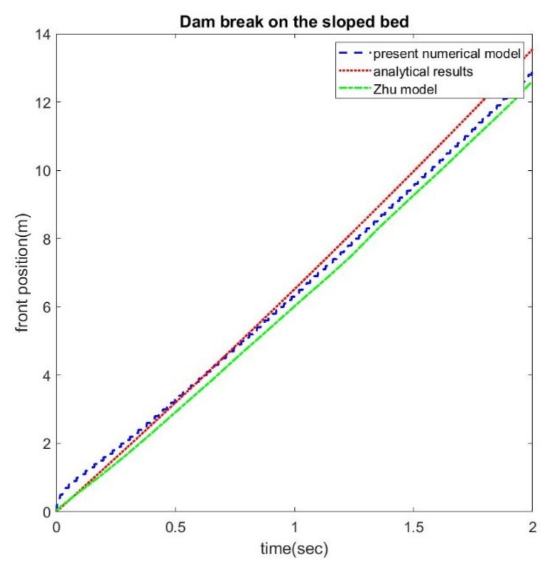

B

Fig. 3.7. Wet/dry front position obtained from present numerical model, Zhu model 2018 as well as analytical solution for (a) $\alpha = -\frac{\pi}{60}$ and (b) $\alpha = \frac{\pi}{60}$.

3.4.3. Test Case 3: Perturbated Flow Over a Parabolic Topography

In this test case, an initial perturbation was introduced into the shallow water over a parabolic tank. To address this intricate problem, Sampson et al. (2006) proposed an analytical solution for a one-dimensional shallow water equation. The present model includes central upwind and minmod functions for flux approximation and interface vector evaluation, respectively. It applies the fourth order Runge-Kutta scheme for time discretization, treats the topography (bed slope) term as a source, and excludes dissipation, dispersion, and acceleration terms. The verification of this test reflects how the proposed model can process shallow water movement on a smoothed curved bed topography. The parabolic shape of the bottom is calculated using Equation (3-32).

$$z(x) = h_0 (\frac{x}{a})^2 \tag{3-32}$$

Where h_0 and a are constants. The computational domain used was $-5000(m) \le x \le 5000(m)$. Assuming negligible friction, the analytical water level can be obtained using the following equation:

$$h(x,t) + z(x,t) = \max(h_0 - \frac{b^2}{4g}\cos(2\omega t) - \frac{b^2}{4g} - \frac{bx}{2a}\sqrt{\frac{8h_0}{g}}\cos(\omega t), z(x)) \tag{3-33}$$

Where $\omega = \sqrt{\frac{2gh_0}{a}}$ and b are constants. The constant values were a=3000, b=5, and $h_0 = 10$.

The initial perturbation is imposed using equation (3-33) for t=0. The evaluation of the water level over a parabolic tank owing to this perturbation was simulated using the proposed model. The results of the model for times t = 1000 s, t = 2000 s, t = 3000 s, t = 4000 s, t = 5000 s, and t = 6000 s are derived and compared with the analytical expression in Figure (3.8). As seen in the figure the numerical model results agree very well with the analytical solution.

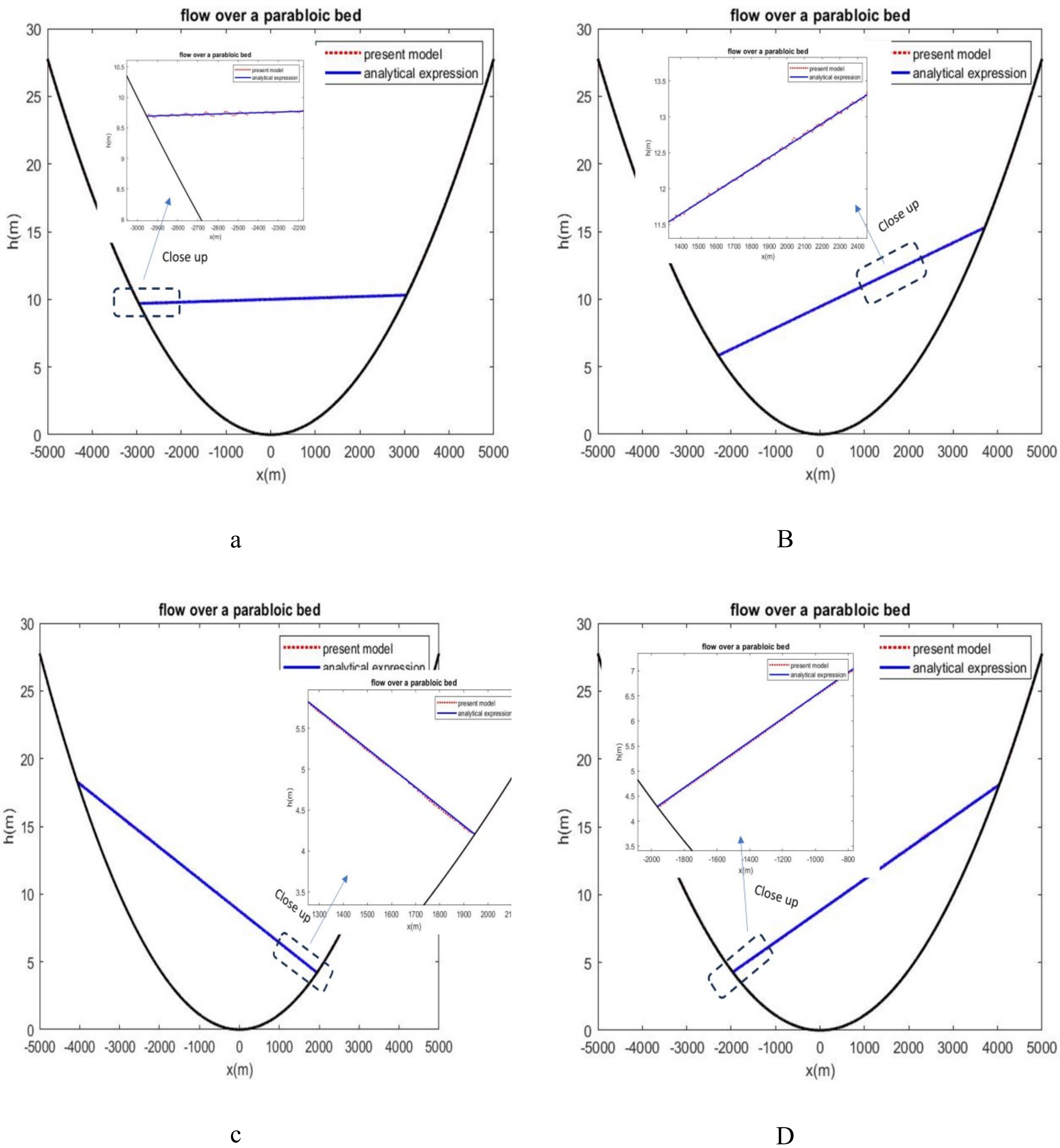

Fig. 3.8. Comparison of the present numerical model results with analytical expression for different time (a) t=1000s, (b) t=2000s, (c) t=4000s, and (d) t=6000s

3.4.4. Test Case 4: Sloshing Simulation of Box Tank

This section focuses on the analysis of the fluid movement within a rectangular tank subjected to oscillatory and transient translational motions. The water depth within the tank was significantly smaller than the length of the enclosed rectangular tank, aligning with the assumptions of shallow water models. In this simulation, the length of the box tank was $L=0.6095$ m, and the water depth was $H= 0.06\ m$. These dimensions were the same as those used in the experimental work conducted by Lepelletier et al. (1988).

The test case consists of two stages. The first stage involves modelling and comparing the natural period of a box tank with an analytical solution. The subsequent stage focused on simulating the sinusoidal excitation of the box tank. Furthermore, the influence of dispersion and dissipation terms on the sloshing wave pattern was investigated in this study. The results obtained from the current model demonstrate that, unlike in previous cases, both dissipation and dispersion terms play a significant role in achieving accurate results.

3.4.4.1. Natural Period Evaluation

In this study, an innovative approach was used to determine the natural period of a tank. This approach is similar to free vibration analysis used in dynamic structures to capture the natural period of a structure. To this end, a consistent form perturbation, such as a cosine form with a small amplitude, is imposed on the free surface as the initial condition. Then, the evaluation of the free surface due to this initial perturbation was modelled using the present nonlinear shallow water model, and the temporal free surface elevation at a point was derived (Figure 3.9). The time distance of the consecutive peaks reflects the natural period of the tank, which is T=1.598 s. Therefore, the natural frequency of the tank is $f = \frac{1}{T} = 0.625Hz$.

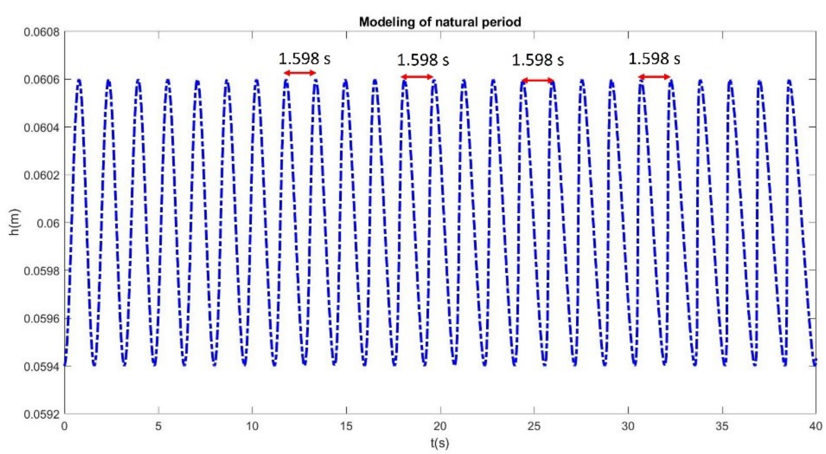

Fig. 3.9. Time history of free surface at the right wall of the tank subjected to initial perturbation

Numerous studies in the existing literature have utilized the analytical formula (3-34) to calculate the fundamental frequency of sloshing waves. According to this equation, the natural frequency of the tank was determined as $f_w = 0.619Hz$. Hence, the natural frequency predicted by the proposed model demonstrates a deviation of less than 1 percent when compared to the analytical value.

$$f_w = \frac{1}{2\pi}\sqrt{\frac{\pi g}{L}\tanh(\frac{\pi H}{L})} \tag{3-34}$$

Furthermore, the perturbation test can be utilized to assess not only the natural period but also the numerical diffusion error. Because this test excludes the friction and dissipation effects, the decrease in the amplitude of the time history of the free surface at a specific point is attributed to numerical diffusion error. Numerical diffusion errors accumulated over the course of the simulation, resulting in a more pronounced reduction in the peak response as time progressed. Figure (3.10) illustrates that the first-order upwind method employed to evaluate the interface vector introduces greater numerical diffusion and necessitates a more refined mesh to achieve lower numerical diffusion results. Conversely, the Minmod scheme offers the advantage of reduced numerical diffusion errors even with a coarser mesh, albeit at the cost of higher computational calculations.

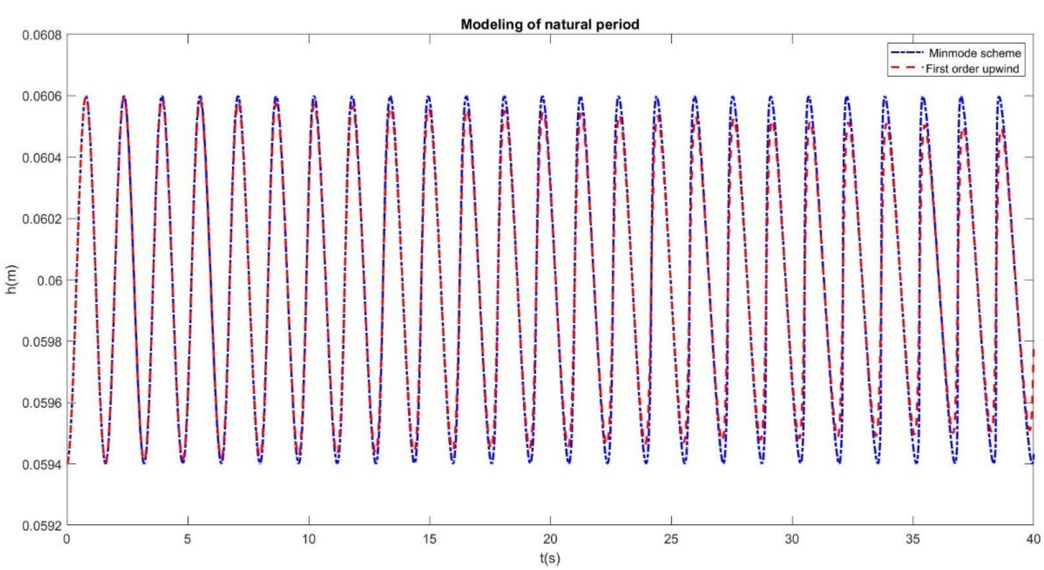

Fig. 3.10. Numerical diffusion errors in perturbation test associated to first order upwind and Minmod schemes

3.4.4.2. Harmonic Excitation of Box Tank

The present numerical model for the simulation of a rectangular water tank subjected to seismic excitation force relies on Equation (3-1) for $\alpha_1 = 0$ *and* $\alpha_2 = \alpha_3 = \alpha_4 = 1$. Because the bed is horizontal, the contribution of the sloped bed is cancelled. In the present model, the dissipation term is considered an explicit source term. Conversely, to preserve the stability of the model, the dispersion term was discretized implicitly, leading to a matrix equation at each time step.

The sloshing wave was considerably higher when the force excitation frequency approached the natural frequency of the tank. The frequency ratio parameter $\alpha = \dfrac{f_e}{f_w}$, which is the ratio of the excitation frequency to the natural tank frequency, has been applied in several studies in this context. The simulation was carried out for different α near resonance excitations, and the results of the model showed very good agreement with the experimental data presented by Lepelletier et al. (1988) (Figures 3.11a and 3.11b). Despite the complexity and nonlinearity of the sloshing waves, the present model provides highly accurate results for both the pattern and magnitude of the sloshing waves.

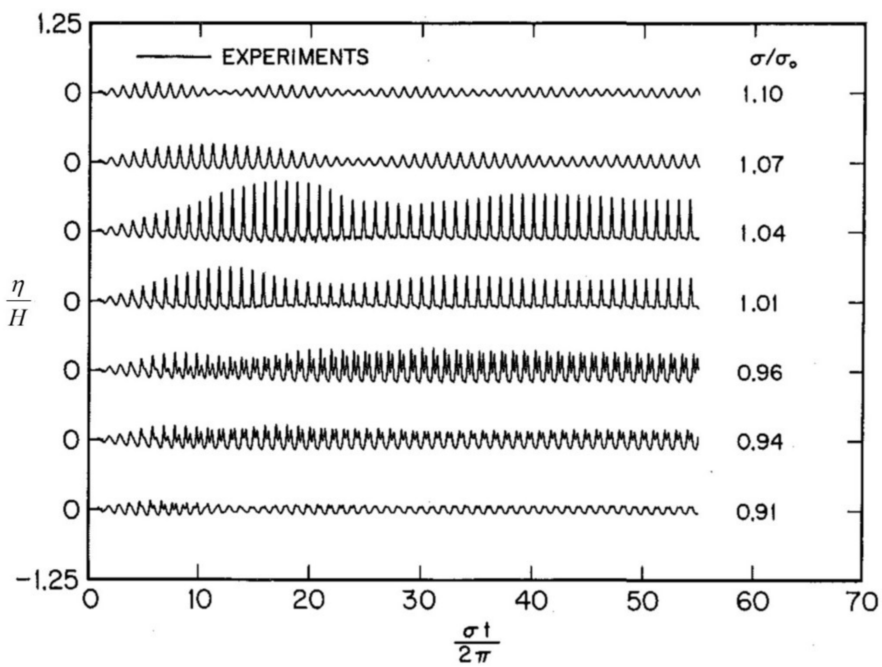

a

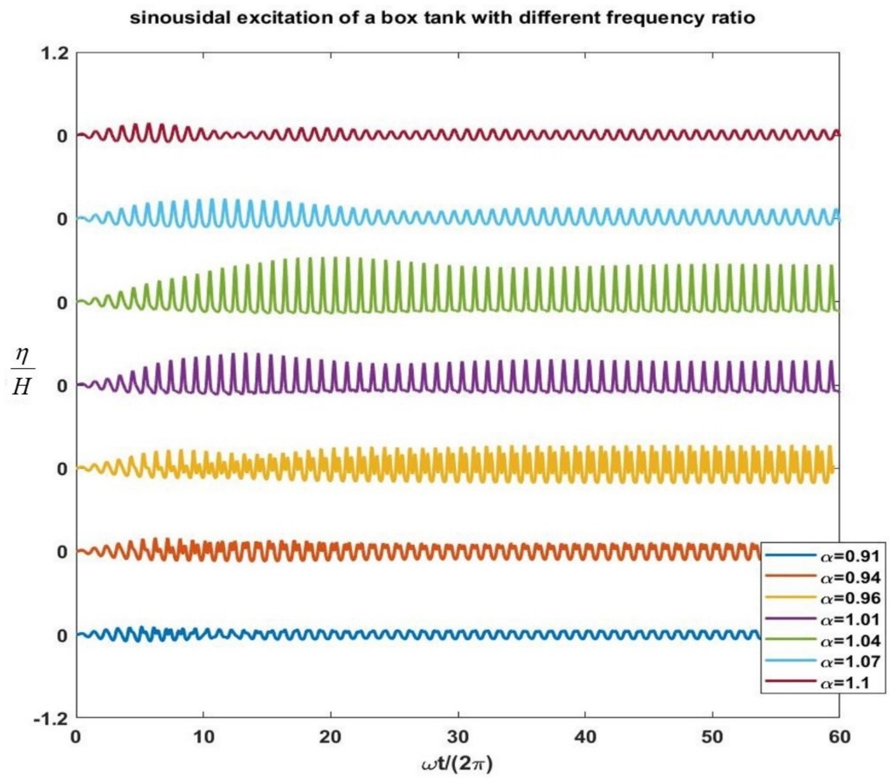

b

Fig. 3.11. Time history of wave height at the right wall of the tank subjected to near resonance excitations derived from (a) experimental results of Lepelletier et al. (1988) and (b) present numerical model.

The present model developed for simulating sloshing tanks appears to be more efficient compared to other models in the literature. A variety of models based on potential flow have been adapted for sloshing simulations. Typically, these models, in addition to the continuity and momentum equations, necessitate the inclusion of kinematic boundary conditions for the free surface. This addition, within the context of nonlinear partial differential equations, results in an increase in computational cost. In the context of shallow water models, the current model relies on the central upwind and Minmod function for flux and variable approximation at the control surfaces, respectively. This enables the prediction of a free surface with high gradients without the need for additional equations. On the other hand, models such as Roe method, as demonstrated, should incorporate an entropy correction equation to prevent unphysical jumps. If advanced methods such as SPH and VOF are considered for the sloshing model, they typically solve the momentum equation in two directions. Furthermore, SPH method requires very small-time steps (Cao et al.

2014), and the VOF method incorporates an additional equation (Bahreini et al. 2021), resulting in significantly higher computational costs compared to the current model. In conclusion, the verification of the current model's efficiency against those commonly found in the literature indicates its high efficiency. The verification process detailed in the preceding section not only confirms its efficiency but also demonstrates its ability to generate accurate results.

3.4.4.3. The Role of Dispersion Term

To examine the significance of the dissipation term in sloshing dynamics, the outcomes of the present model are depicted in Figure (3.12) for the resonance excitation scenario, both with and without the inclusion of the dispersion term. As shown in this figure, the lack of a dissipation term results in an approximately symmetric sloshing wave, which is generally generated and travels as shock waves and short-length waves with a high gradient depth. However, when the dissipation term is introduced in Equation (3-1), the free-surface evolution is in the form of long-length wave propagation with a smooth curve. In this case, the waves are higher and asymmetrical with respect to the mean water level. This asymmetry is characterized by two points. First, the wave amplitude above the mean water level is significantly greater than that below the mean water level. Second, the wave crest was sharp, and the wave trough was smooth.

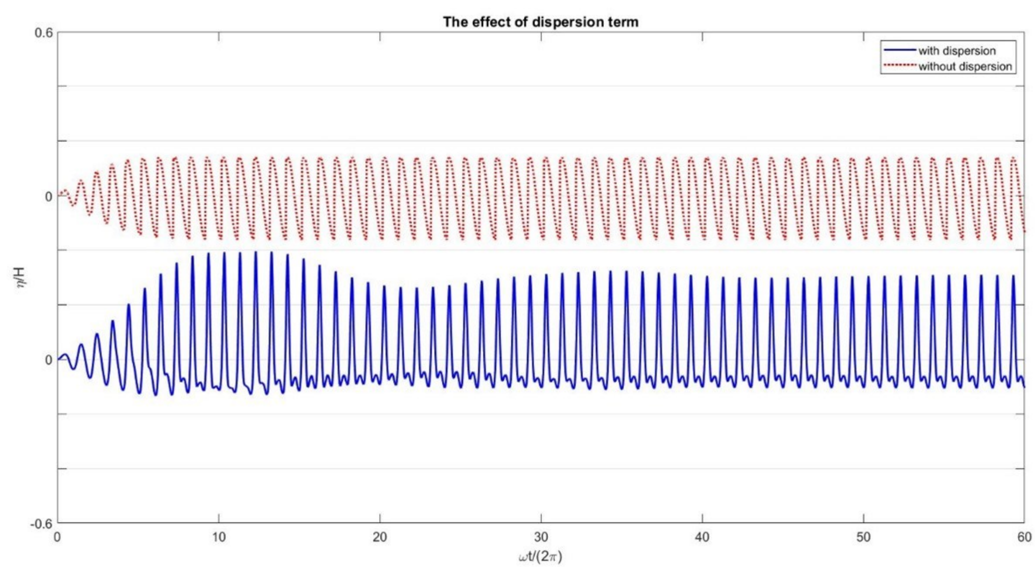

Fig. 3.12. Time history of wave height with and without dispersion term

3.4.4.4. The Role of Dissipation Term

Lepelletier et al. (1988) conducted an experimental study on the sinusoidal excitation of a shallow water tank, which revealed two types of waves during the sloshing process: 1) transient waves $(\frac{\eta}{h})_T$ and 2) steady-state waves $(\frac{\eta}{h})_S$ in Figure (3.13). Initially, during excitation, transient waves develop, typically resulting in a maximum sloshing wave. As time progressed, because of the presence of friction, the system reached a steady-state condition in which steady-state waves were established. However, in the absence of dissipation or damping terms, there is no force to counterbalance the sloshing force and establish equilibrium. Consequently, in such cases, as shown in Figure (3.14), the system does not reach a steady-state condition, leading to higher maximum wave amplitudes. The damping coefficient, $c_d = 0.1$, in Equation (3-1) was determined by calibrating the model using one set of experimental data conducted by Lepelletier et al. (1988) and verified with six other sets of experimental data.

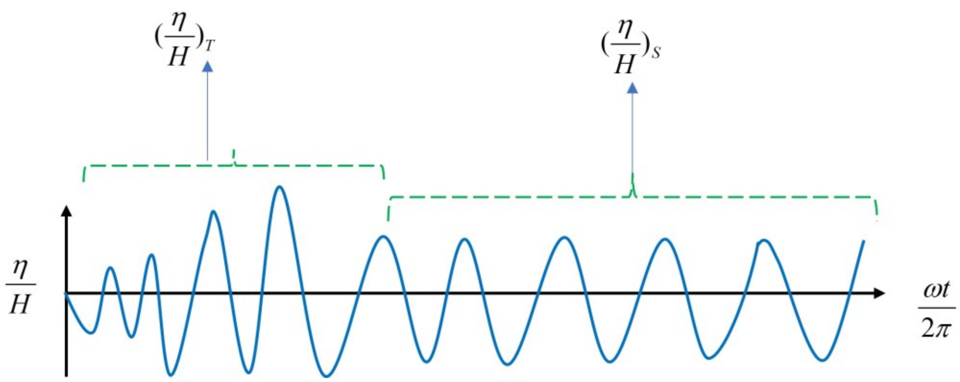

Fig. 3.13. Transient and steady waves formed in sloshing experimental test (based on Lepelletier et al. 1988)

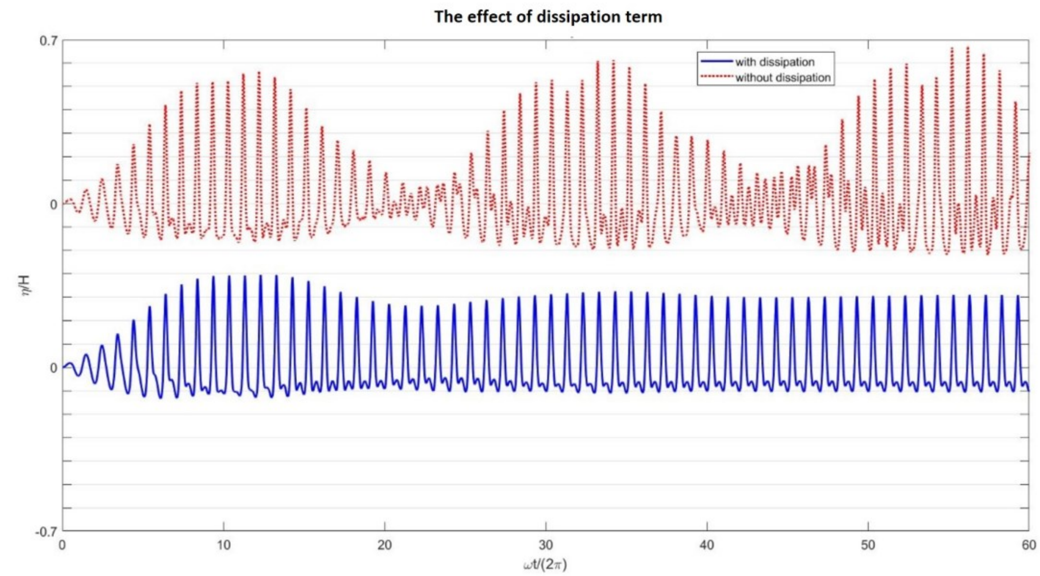

Fig. 3.14. Time history of wave height with and without dissipation term

3.4.5. Test Case 5: Sloshing of Box Tank with Sloped Bed

After successfully validating the present model through various test cases, it was applied to simulate the sloshing behavior of a shallow box tank with a sloped bed. For this purpose, all terms in Equation (3-1) were considered in the simulation. The flux approximation term was discretized using the central upwind scheme, and the interface vector was approximated using the Minmod technique. The time discretization was based on the fourth-order Runge-Kutta method, and the sloped bed, acceleration, and dissipation terms were treated as source terms. As explained in section (3.3.5), to improve the stability of the model and allow for larger time steps, the dispersion term is discretized implicitly in the present model. This results in a matrix equation with dimensions equal to the number of nodes, which must be solved at each time step.

The tank configuration used in this study is shown in Figure (3.15). The sloped section has a ratio of 2 (horizontal) to 1 (vertical). The initial water depth, H, is set at 0.06 m, and the length of the free surface, L, is 0.6095 m. These values were intentionally chosen to match those of the box tank in the previous case study, thereby enabling direct comparison between the two cases. Consequently, the water mass in this scenario accounts for 80 percent of the water mass in the box tank case.

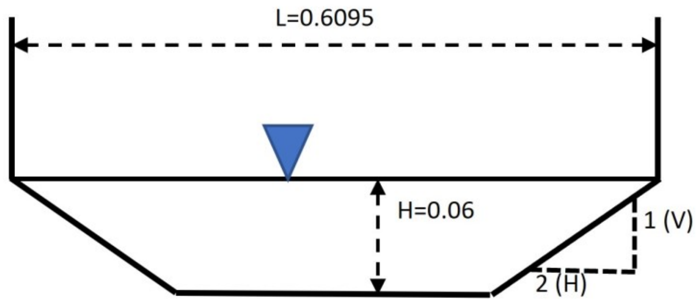

Fig. 3.15. The geometry of the box tank with sloped bed

It was anticipated that the inclusion of an inclined bed in the tank would result in a reduction in the velocity within the inclined bed area, leading to higher sloshing waves. Previous research conducted in this area has confirmed the generation of larger sloshing waves in tanks with sloped beds. The results obtained from the current numerical model for both the box tank and the box tank with a sloped bed under resonance excitation are presented in Figure (3.16). Figure (3.16) shows the time history of the wave height near the end node of the box tank and the box tank with a sloped bed. Both tanks exhibited similar sloshing wave patterns with transient waves followed by steady sloshing waves. However, the presence of the sloped bed prevented the free surface from traveling below the mean water level at the wall point (Figure 3.15). Therefore, in this case, there was no development of negative wave height at this particular point.

Moreover, the box-sloped bed tank demonstrated higher amplitude waves in both the transient and steady states. Specifically, the box-sloped bed tank produced approximately 25 percent larger waves. Consequently, despite the smaller water mass, the box-sloped bed tank generated more pronounced sloshing waves. Another subtle distinction was observed in the timing of the peak sloshing waves, which were slightly delayed in the case of the box-sloped bed tank.

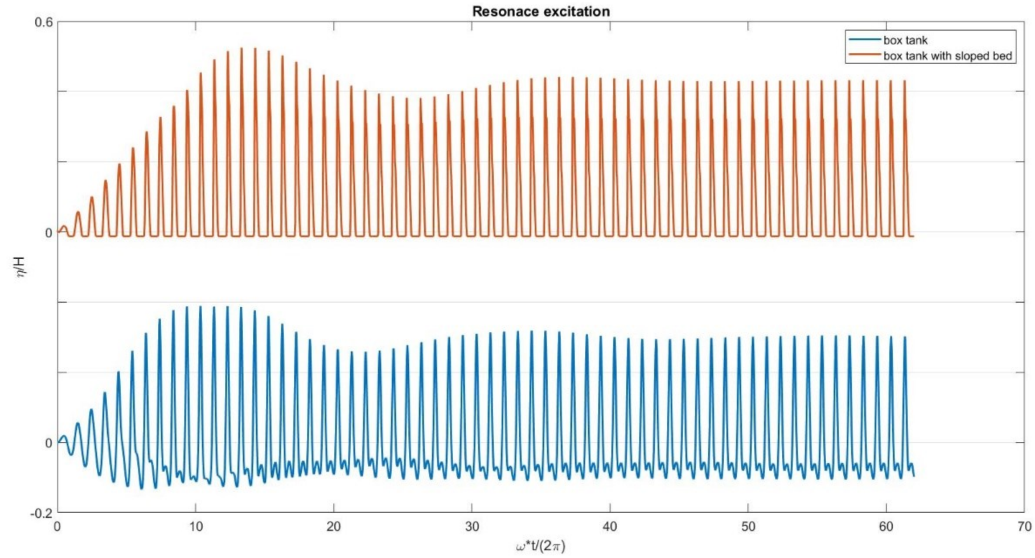

Fig. 3.16. Time history of wave heigh at the right wall of the box tank (bottom) and box tank with sloped bed (top) subjected to resonance excitation

3.4.6. Test Case 6: TLD Simulation

Based on the findings of the previous test case, it was observed that despite having less mass, the box-sloped bed tank generated larger sloshing waves than the box tank. This suggests that the box-sloped bed tank sounds to be more suitable than the conventional Tuned Liquid Damper (TLD) for attenuating structural vibrations. To verify this hypothesis, both the box tank and box sloped bed tank were separately coupled with the dynamic equation of a single-degree-of-freedom (SDOF) system and subjected to seismic excitation. The dynamic equation of the SDOF system is solved using the finite difference method (FDM) described in section (3.3.6). The coupling between the shallow water model and the SDOF equation was established through the iterative partition procedure discussed in section (3.3.7). A two-step coupling scheme, consisting of prediction and correction steps, was employed to enhance the accuracy and stability of the proposed model.

In this particular case, the geometries of both tanks were consistent with the previous sloshing test case. The widths of both the tanks were assumed to be unity. The dynamic properties of a single-degree-of-freedom (SDOF) system are evaluated based on the characteristics of the box tank. According to the literature, the mass ratio, which is the ratio of the water mass to the SDOF mass, typically ranges from one to two percent. In this study, a mass ratio of one percent was assumed. The stiffness of the SDOF system was determined from Equation (3-35) (Humar 2012), and considering the frequency of the SDOF system, f_s, was equal to the natural frequency of the box tank, f_w. The damping ratio of the SDOF system was selected to be 1.2 percent. Further details on the damping ratio can be found in Humar (2012).

$$f_s = \frac{\sqrt{k}}{2\pi\sqrt{m}} \tag{3-35}$$

Subsequently, the interconnected system comprising the water tank and SDOF system (described in Equation 3-26) was subjected to a sinusoidal excitation force, as shown in Equation (3-36), originating from the ground. The frequency of the excitation force, f_e, matches that of the SDOF system, resulting in resonance excitation. In other words, the frequency ratio, which is the ratio of the force frequency to the SDOF frequency, is set to unity. The amplitude of the excitation force, A_0, was adjusted to ensure that the maximum amplitude of the SDOF vibration in the absence of a Tuned Liquid Damper (TLD) under steady-state condition (A) was 1 cm.

$$F_{exc} = A_0 \sin(2\pi f_e t) \tag{3-36}$$

As previously mentioned, the interaction force was determined by subtracting the pressure force on the left wall from that on the right wall. However, there were slight differences in the evaluation of hydrostatic pressure forces between the two boxes. In the rectangular box (Figure 3.17a), the hydrostatic force on the right wall is equal to $F_{PR} = \frac{1}{2}\gamma h_{ni}^2$, where γ refers to the unit weight of water, and it is assumed to be $9810\frac{N}{m^3}$. However, in the box with a sloped bed TLD, if the water level at point *ni* exceeds the mean water level (Figure 3.17b), the magnitude of the hydrostatic force on the right wall is determined using $F_{PR} = \frac{1}{2}\gamma(h_{ni} + z_{ni})^2$. However, when the water level at point *ni* fell below the mean water level, a search algorithm was implemented in the model to locate the wet/dry interface point, as represented by node *k* in Figure (3.17c). In this case, the hydrostatic force was calculated based on $F_{PR} = \frac{1}{2}\gamma z_k^2$. The pressure force on the left wall, F_{PL}, was evaluated using the same procedure.

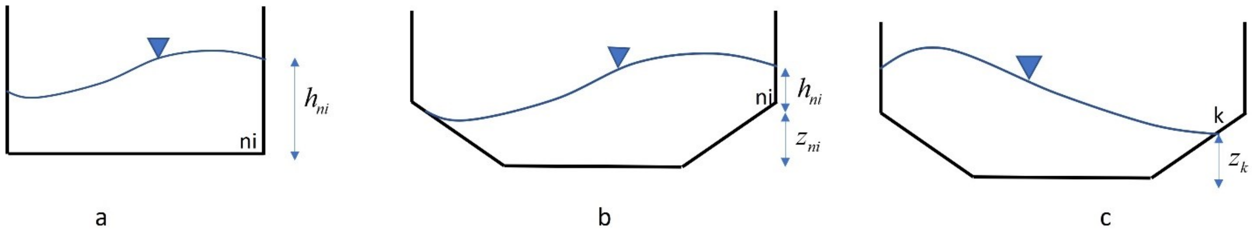

Fig. 3.17. Different scenarios for the evaluation of the pressure force acting on right wall.

The results of the model for both cases with and without TLDs are shown in Figure (3.18). Initially, both tanks exhibited minimal influence on the vibration of the structure for a short duration of approximately 1 s after excitation. However, after this initial period, both tanks exhibited significantly reduced structural vibration. Consequently, they are more efficient for far-fault earthquakes than for near faults. Figure (3.19) presents a close-up view of the SDOF response when equipped with a box TLD or a box-sloped bed TLD. In the steady state, the box-sloped bed TLD exhibited a more profound reduction in structural vibration than the box TLD. In steady state conditions, the amplitude of vibration of the SDOF equipped with a box-sloped bed TLD is approximately 75% of that of the case where the SDOF is equipped with the box TLD. This indicates that the box-sloped bed TLD takes advantage of its smaller water mass and demonstrates a more pronounced suppressing effect on structural vibration in resonance excitation. However, its potentially superior damping effect compared to conventional TLDs in other scenarios requires further investigation.

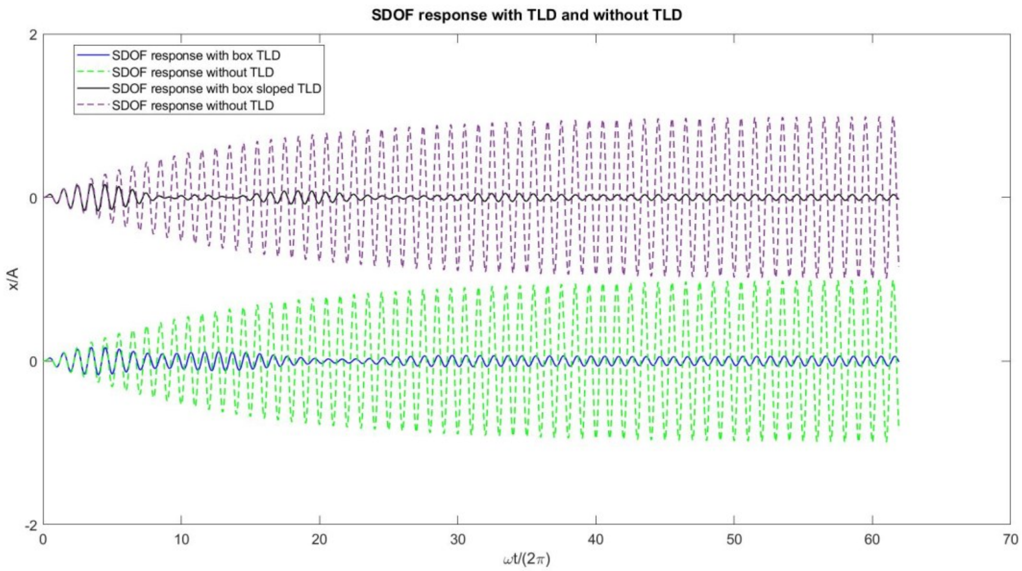

Fig. 3.18. The response of SOF equipped with and without TLD for two cases: box TLD (bottom) and box TLD with sloped bed (top)

-

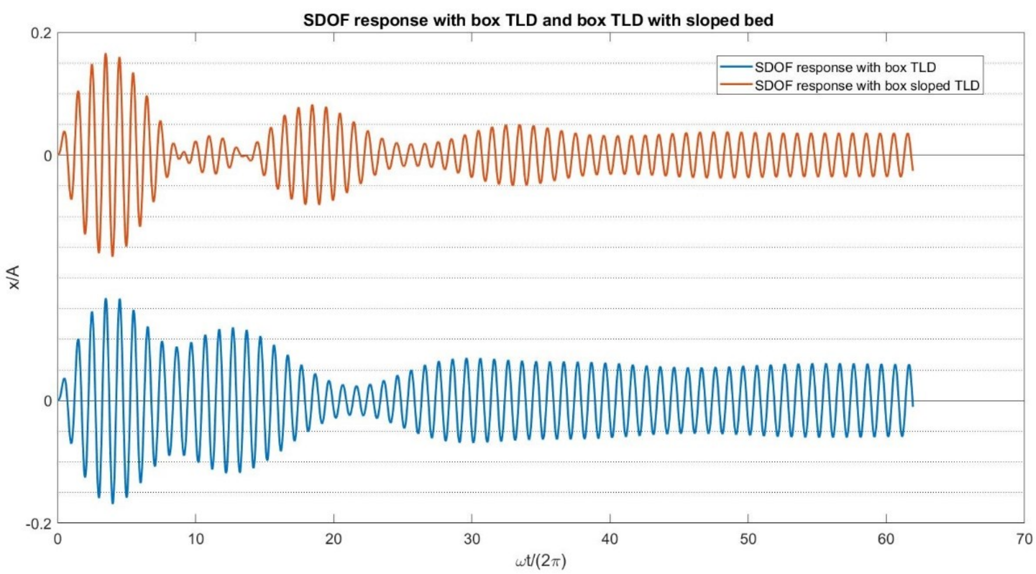

Fig. 3.19. Close up view of the SDOF response when it is equipped with TLD for two cases: box TLD (bottom) and box TLD with sloped bed (top)

3.5. Discussion and Conclusions

This study focuses on developing a numerical model capable of simulating sloshing waves in tanks with both horizontal and sloped beds, which is then coupled with a Single Degree of Freedom (SDOF) system to establish a Tuned Liquid Damper (TLD) model. The model is based on the nonlinear shallow water equations and includes additional terms such as the acceleration term, bed slope term, dissipation term, and dispersion term, depending on the specific case study. To balance accuracy and computational cost, the current model employs the central upwind method for approximating flux and the Minmod function for evaluating interface variables. While the slope bed, dissipation, and acceleration terms are treated as explicit source terms in the model, an implicit scheme is utilized for the discretization of the dispersion term to improve model stability, resulting in a matrix equation. Additionally, temporal discretization is achieved using the fourth-order Runge-Kutta method.

The dynamic equation of a single-degree-of-freedom (SDOF) system is numerically solved using a second-order finite difference method. The system of equations, including SDOF dynamics and fluid movement, was coupled with an iterative procedure composed of prediction and correction steps.

The application of the model for simulation of dam break over a dry bed that includes high gradient depth, indicates that both the McCormack scheme, which is a second-order finite difference method, and the Roe scheme produce a nonphysical jump in the free surface profile, while the central upwind and Roe methods, when equipped with entropy correction, are accurate for modelling this rapid varied flow. Because of the lower computational cost, we adopted the central upwind method for subsequent modelling.

When the current model is applied to a dam break on a sloped bed, it provides accurate results compared to both another numerical model outcome and analytical data. Furthermore, the simulation of perturbed flow over a parabolic bed using the current mode produced a free surface that agreed well with the analytical solutions.

The perturbation of the free-surface test in the box tank indicates that the current model can accurately predict the natural frequency of the tank. In addition, this test was used to measure the numerical diffusion errors of the proposed schemes.

The current model was applied to simulate a box-grounded tank that was subjected to near-resonance excitation. Despite the complexity and asymmetry of the sloshing wave, the present model takes advantage of precise results compared with the experimental data. Neglecting the dispersion term results in nonphysical approximately symmetric shock waves, whereas ignoring the dissipation term prevents the system from reaching steady sloshing waves.

The application of the current model for the sloshing of a box tank with a sloped bed, which requires the contribution of all terms in Equation 1, resulted in more pronounced and stronger sloshing waves compared to the box tank.

In the systematic approach employed in this study, the existing model based on nonlinear shallow water equations was expanded by introducing new terms, the specific selection of which depended on the characteristics of each test case. The accuracy and efficiency of this model were rigorously assessed in the preceding test cases. In the final stage of this research, the model, now encompassing all the pertinent terms, was integrated with a Single Degree of Freedom (SDOF) system to emulate a Tuned Liquid Damper (TLD) featuring a sloped bed. The outcomes derived from this model demonstrate that when the SDOF system undergoes harmonic resonance excitation, a TLD equipped with a sloped bed yields a substantially more pronounced reduction in the SDOF response in comparison to a conventional box TLD. Despite the intricate nature of the simulation, this current model, characterized by its superior accuracy and reasonable computational efficiency, emerges as a suitable tool for TLD modeling, even in cases involving sloped beds.

3. Appendix A McCormack scheme

First, the nonlinear shallow water equations used for the dam-break case are expressed as (Toro 2001)

$$\begin{aligned} &\frac{\partial h}{\partial t}+\frac{\partial (uh)}{\partial x}=0 \\ &\frac{\partial (uh)}{\partial t}+\frac{\partial (u^2 h+0.5gh^2)}{\partial x}=0 \end{aligned} \tag{3-A-1}$$

The equation could be converted to the following equation.

$$\frac{\partial h}{\partial t}+u\frac{\partial(h)}{\partial x}+h\frac{\partial(u)}{\partial x}=0$$
$$\frac{\partial(u)}{\partial t}+u\frac{\partial(u)}{\partial x}+g\frac{\partial(h)}{\partial x}=0 \quad (3\text{-A-2})$$

The McCormack scheme, which is a second-order accurate finite-difference method, utilizes averaged forward and backward differences for discretization in space (Amara et al. 2013). Therefore, the discretized form of Equation (3-A-2) is expressed as follows: Equations (3-A-3) and (3-A-4) correspond to the forward and backward approaches, respectively, and Equation (3-A-5) is the averaged variable determined from previous schemes.

$$h_j^*=h_j^n+u_j^n(\frac{h_{j+1}^n-h_j^n}{\Delta x}+h_j^*\frac{u_{j+1}^n-u_j^n}{\Delta x})\Delta t$$
$$u_j^*=u_j^n+u_j^n(\frac{u_{j+1}^n-u_j^n}{\Delta x}+g\frac{h_{j+1}^n-h_j^n}{\Delta x})\Delta t \quad (3\text{-A-3})$$

$$h_j^{**}=h_j^n+u_j^*(\frac{h_j^n-h_{j-1}^n}{\Delta x}+h_j^*\frac{u_j^n-u_{j-1}^n}{\Delta x})\Delta t$$
$$u_j^{**}=u_j^n+u_j^*(\frac{u_j^n-u_{j-1}^n}{\Delta x}+g\frac{h_j^n-h_{j-1}^n}{\Delta x})\Delta t \quad (3\text{-A-4})$$

$$h_j^{n+1}=\frac{h_j^*+h_j^{**}}{2}$$
$$h_j^{n+1}=\frac{h_j^*+h_j^{**}}{2} \quad (3\text{-A-5})$$

References

1. Abd-Elhamed, A., & Tolan, M. 2022. Tuned liquid damper for vibration mitigation of seismic-excited structures on soft soil. Alexandria Engineering Journal, 61(12), 9583-9599.

2. Amara, L., Berreksi, A., & Achour, B. 2013. Adapted MacCormack Finite-Differences Scheme for Water Hammer Simulation. Journal of Civil Engineering and Science. 2. 226-233.

3. Antuono, M., Bouscasse, B., Colagrossi, A., & Lugni, C. 2012. Two-dimensional modal method for shallow-water sloshing in rectangular basins. Journal of Fluid Mechanics, 700, 419-440.

4. Ashasi-Sorkhabi, A., Malekghasemi, H., Ghaemmaghami, A., & Mercan, O. 2017. Experimental investigations of tuned liquid damper-structure interactions in resonance considering multiple parameters. Journal of Sound and Vibration, 388, 141-153.

5. Bahreini Toussi, I., Kianoush, R. & Mohammadian, A. 2021. Numerical and experimental investigation of rectangular liquid-containing structures under seismic excitation. Infrastructures 6, 1.

6. Banerji, P., Murudi, M., Shah, A. H., & Popplewell, N. 2000. Tuned liquid dampers for controlling earthquake response of structures. Earthquake engineering & structural dynamics, 29(5), 587-602.

7. Bhattacharjee, E., Halder, L., & Sharma, R. P. (2013). An experimental study on tuned liquid damper for mitigation of structural response. International Journal of Advanced Structural Engineering, 5, 1-8.

8. Bradford SF, Sandres BF. 2002. Finite-volume model for shallow-water fooding of arbitrary topography. Journal of Hydraulic Engineering (ASCE) 2002; 128:289–298.

9. Chaiviriyawong, P., Webster, W. C., Pinkaew, T., & Lukkunaprasit, P. 2007. Simulation of characteristics of tuned liquid column damper using a potential-flow method. Engineering Structures, 29(1), 132-144.

10. Chang, Y., Noormohamed, A., & Mercan, O. 2018. Analytical and experimental investigations of modified tuned liquid dampers (MTLDs). Journal of Sound and Vibration, 428, 179-194.

11. Durran, D. R. 2010. Numerical methods for fluid dynamics: With applications to geophysics (Vol. 32). Springer Science & Business Media.

12. Fujino, Y., Sun, L., Pacheco, B. M., & Chaiseri, P. 1992. Tuned liquid damper (TLD) for suppressing horizontal motion of structures. Journal of Engineering Mechanics, 118(10), 2017-2030.

13. Gardarsson, S., Yeh, H., & Reed, D. (2001). Behavior of sloped-bottom tuned liquid dampers. *Journal of engineering mechanics*, *127*(3), 266-271.

14. Ghaemmaghami, A.R. & Kianoush, M. R. 2010. Rectangular liquid storage tanks under horizontal and vertical ground motions. Journal of Structural Engineering. 136, 441-451.

15. Hashemi, S., Kianoush, R., & Khoubani, M., 2022. A mechanical model for soil-rectangular tank interaction effects under seismic loading. Journal of Soil Dynamics and Earthquake Engineering.153. 107092.

16. Hirt, C.W. & Nichols, B. D. 1981. Volume of fluid (VOF) method for the dynamics of free boundaries. J. Comput. Phys. 39, 201–225.

17. Hu, X., Zhao, Z., Weng, D., & Hu, D. (2022). Design of a pair of isolated tuned liquid dampers (ITLDs) and application in multi-degree-of-freedom structures. International Journal of Mechanical Sciences, 217, 107027.

18. Humar, J. 2012. Dynamics of structures. CRC press.

19. Ikeda,T., Ibrahim, R., A., Harata, Y., & Kuriyama, T., 2012. Nonlinear liquid sloshing in a square tank subjected to obliquely horizontal excitation. J. Fluid Mech. 700, 304.

20. Koh, C. G., Mahatma, S., & Wang, C. M. 1994. Theoretical and experimental studies on rectangular liquid dampers under arbitrary excitations. earthquake engineering and structural dynamics, 23, 17–31.

21. Konar, T., & Ghosh, A. D. (2021). Flow damping devices in tuned liquid damper for structural vibration control: a review. Archives of Computational Methods in Engineering, 28, 2195-2207.

22. Kurganov, A., & Levy, D. 2002. Central-upwind schemes for the Saint-Venant system. ESAIM: Mathematical Modelling and Numerical Analysis, 36(3), 397-425.

23. Lepelletier, T. G., & Raichlen, F. (1988). Nonlinear oscillations in rectangular tanks. Journal of Engineering Mechanics, 114(1), 1-23.

24. Liao, K., & Hu, C. 2013. A coupled FDM–FEM method for free surface flow interaction with thin elastic plate. Journal of marine science and technology, 18, 1-11.

25. Liu, D. & Lin, P. A. 2008. Numerical study of three-dimensional liquid sloshing in tanks. J. Comput. Phys., 227, 3921–3939

26. Marivani, M., & Hamed, M. S. 2017. Evaluate pressure drop of slat screen in an oscillating fluid in a tuned liquid damper. Computers & Fluids, 156, 384-401.

27. Mohammadian, A., & Le Roux, D. Y. (2006). Simulation of shallow flows over variable topographies using unstructured grids. International journal for numerical methods in fluids, 52(5), 473-498.

28. Mohammadian, A., Le Roux, D. Y., & Tajrishi, M. 2007. A conservative extension of the method of characteristics for 1-D shallow flows. Applied Mathematical Modelling, 31(2), 332-348.

29. Murudi, M., & Banerji, P. 2012. Effective control of earthquake response using tuned liquid dampers. Journal of Earthquake Technology, 49(3-4), 53-71.

30. Ocak, A., Bekdaş, G., Nigdeli, S. M., Kim, S., & Geem, Z. W. (2022). Optimization of tuned liquid damper including different liquids for lateral displacement control of single and multi-story structures. Buildings, 12(3), 377.

31. Pandit, A. R., & Biswal, K. C. (2019). Seismic control of structures using sloped bottom tuned liquid damper. International Journal of Structural Stability and Dynamics, 19(09), 1950096.

32. Pandit, A. R., & Biswal, K. C. 2019. Seismic control of structures using sloped bottom tuned liquid damper. International Journal of Structural Stability and Dynamics, 19(09), 1950096.

33. Pandit, A. R., & Biswal, K. C. 2020. Seismic control of multi degree of freedom structure outfitted with sloped bottom tuned liquid damper. *Structures*, 25. 229-240.

34. Panigrahy, P. K., Saha, U. K., & Maity, D. 2009. Experimental studies on sloshing behavior due to horizontal movement of liquids in baffled tanks. Ocean Eng. 36, 213–222.

35. Saburin, D., S. 2015. Tank sloshing simulations in shallow-water approximation. In MARINE VI: proceedings of the VI International Conference on Computational Methods in Marine Engineering (pp. 1039-1050). CIMNE.

36. Saha, S., & Debbarma, R. 2017. An experimental study on response control of structures using multiple tuned liquid dampers under dynamic loading. *International Journal of Advanced Structural Engineering*, *9*, 27-35.

37. Sampson, J., Easton, A., Singh, M. 2006. Moving boundary shallow water flow above parabolic bottom topography. Anziam J., 47, C373–C387.

38. Sobhan, M. S., Rofooei, F. R., & Attari, N. K. 2017. Buckling behavior of the anchored steel tanks under horizontal and vertical ground motions using static pushover and incremental dynamic analyses. Thin-Walled Structures, 112, 173-183.

39. Sun, L. M., Fujino, Y., Pacheco, B. M., & Chaiseri, P. 1992. Modelling of tuned liquid damper (TLD). Journal of Wind Engineering and Industrial Aerodynamics, 43(1-3), 1883-1894.

40. Tait, M., El Damatty, A., Isyumov, N., & Siddique, R. 2005. Numerical flow models to simulate tuned liquid dampers (TLD) with slat screens. Journal of Fluids and Structures, 20, 1007-1023.

41. van Leer B, Lee WT, Powell KG. Sonic point capturing. 9th CFD Conference, American Institute of Aeronautic and Astronautics, Buffalo, NY.

42. Veletsos, A. S., Tang, Y., & Tang, H. T. 1992. Dynamic response of flexibly supported liquid storage tanks. Journal of Structural Engineering., 118, 264–283.

43. Vîlceanu, V., Kavrakov, I., & Morgenthal, G. 2023. Coupled numerical simulation of liquid sloshing dampers and wind–structure simulation model. Journal of Wind Engineering and Industrial Aerodynamics, 240, 105505.

44. Virella, J. C., Suárez, L. E., & Godoy., L. A. 2008. A static nonlinear procedure for the evaluation of the elastic buckling of anchored steel tanks due to earthquakes, J. Earthq. Eng. 12, 999–1022.

45. Wang, Q., Tiwari, N. D., Qiao, H., & Wang, Q. (2020). Inerter-based tuned liquid column damper for seismic vibration control of a single-degree-of-freedom structure. International Journal of Mechanical Sciences, 184, 105840.

46. Xing, Y.L.; Zhang, X.X.; Shu, C.W. 2010. Positivity-preserving high order well-balanced discontinuous Galerkin methods for the shallow water equations. Adv. Water Resour. 33, 1476–1493.

47. Zhao, Z., Zhang, R., Jiang, Y., & Pan, C. 2019. A tuned liquid inerter system for vibration control. International Journal of Mechanical Sciences, 164, 105171.

48. Zhu, Z., Yang, Z., Bai, F., & An, R. 2018. A new well-balanced reconstruction technique for the numerical simulation of shallow water flows with wet/dry fronts and complex topography. Water, 10(11), 1661.

List of Symbols

H	Mean Water depth
u	Depth- averaged velocity
h	Total water depth in tank
z	Bottom elevation
η	Wave height
$a(t)$	Tank acceleration
g	Gravity acceleration
α_1	Slope contribution factor
α_2	Acceleration contribution factor
α_3	Dispersion contribution factor

α_4	Dissipation contribution factor
Δt	Time step
$\vec{F}$	Flux vector
C	Wave celerity
m	Mass of SDOF
k	Stiffness of SDOF
c	Damping coefficient of SDOF
x	Displacement of SDOF
$\dot{x}$	Velocity of SDOF
$\ddot{x}$	Acceleration of SDOF
F_{exc}	Excitation force on SDOF
F_{slo}	Sloshing Force on SDOF
ε	Convergence criteria number
L	Water tank length
f_w	Natural frequency of the water tank
f_e	Frequency of excitation force
α	Frequency ratio
f_s	Natural frequency of SDOF
A_0	Amplitude of harmonic excitation displacement
$V: H$	representation of the bed slope
γ	Unit weight of water

F_{PR} Hydrostatic force on the right wall

F_{PL} Hydrostatic force on the left wall

4. Analytical solution to a coupled system including Tuned Liquid Damper and Single Degree of Freedom under free vibration with modal decomposition method[3]

Abstract

This research focuses on employing a linear analytical approach to transform free surface waves and velocities into mode coordinates, with the aim of investigating the free vibration behavior of a coupled system consisting of a Single Degree of Freedom (SDOF) and a sloshing tank. Through a series of manipulations and simplifications of the coupled equations, a fourth-order ordinary differential equation is derived to showcase the overall response of the system, highlighting the contribution of each odd mode. Key concepts explored include system stability, mode-specific natural periods, establishment of initial boundary conditions, and formulation of the complete system response. The analytical method applied to study Tuned Liquid Dampers (TLDs), a type of elevated sloshing tank, reveals that in higher modes, the lower frequency aligns with the structural natural frequency, while the higher frequency is approximately n times the structural natural frequency (where n is the odd mode number). This approach also elucidates why the system's response does not exhibit a higher-frequency component in higher modes. The study further investigates concepts such as employing an initial perturbation to excite higher frequencies and the potential for approximating the system through the first mode. Additionally, a numerical model was developed using variable separation and modal decomposition methods to complement and validate the analytical approach. Finally, further verification of the model was performed using the Preismann scheme applied to the relevant equations and the central upwind applied to nonlinear equations.

[3] This chapter has been **published** as Mahdiyar Khanpour, Abdolmajid Mohammadian, Hamidreza Shirkhani, and Reza Kianoush (2024). "*Analytical solution to a coupled system including tuned liquid damper and single degree of freedom under free vibration with modal decomposition method*". **Physics of Fluids**, 36(5). https://doi.org/10.1063/5.0206390

Keywords: Coupled system, Shallow Sloshing Tanks, Modal Coordinate System, Stability, Natural Frequencies, Initial Perturbation, First Mode Dominant, Tuned Liquid Damper.

4.1. Introduction

Storage tanks serve a crucial purpose in various industries and are essential components of structures that affect public service and safety. However, these tanks are susceptible to instability and collapse during seismic events. Seismic excitation, combined with fluid movement known as sloshing, can lead to huge dynamic forces exerted on water tanks. Numerous instances of water tank failure have been documented, underscoring the importance of seismic design. Given the global frequency of substantial earthquakes and the critical role of storage tanks, extensive research has been conducted using numerical, analytical, and experimental methods. Storage tanks can be categorized into two main types based on their support :1) grounded tanks, supported directly by the ground, and 2) elevated tanks, which are supported by the structures below them. Elevated tanks play a crucial role in providing the head for the water supply system, and their response is influenced not only by their own characteristics and fluid sloshing, but also by the dynamic behavior of the underlying supporting structure.

Because of the intricate interplay between the dynamic characteristics of the fluid and the structural elements of storage tanks, as well as the inherent complexity of two-way coupling in the sloshing process, researchers have sought simplified models to effectively capture the seismic response of these tanks. Housner (1963) introduced a conceptual division of sloshing fluid into two distinct single degree of freedom components. The lower portion, referred to as the "impulsive" component, exhibits behavior akin to that of solid materials, responding similarly to dynamic forces. In contrast, the upper layer, known as the "convective" component, engages in sloshing with distinct dynamics characterized by longer vibration periods. This division helps to simplify the analysis of the complex behavior of the tank during seismic events. Software tools such as Ansys and Abaqus have incorporated specialized techniques to model fluid-structure interaction, including the sloshing of fluids within structures. These methods often involve the use of specialized structural elements that incorporate stress-strain tensor manipulation to approximate the behavior of the sloshing fluid (Moslemi et al., 2011 and Elkholy et al., 2014). Some methods employ potential flow to capture sloshing (Wu et al., 1998 and Faltinsen et al., 2000 and Rawata et al., 2019). In this approach, the velocity potential function is utilized to satisfy both the continuity and momentum equations of fluid motion, resulting in a Laplace equation. In addition, it introduces a kinematic boundary condition for the free surface, which can increase the computational complexity of the simulations.

In contrast, certain computational approaches have embraced sophisticated methodologies to simulate sloshing dynamics. A notable example is the volume-of-fluid (VOF) technique employed to monitor fluid surfaces in numerical simulations. This method entails an equation referred to as the VOF equation, which governs a fraction function across each cell within the computational grid (as discussed in studies by Bahreini et al., 2021, and Liu and Lin, 2008). By integrating the VOF equation with the Reynolds Average Navier Stokes (RANS) equations, the movement of the fluid can be comprehensively represented. An additional advanced approach to simulating sloshing is the employment of Smoothed Particle Hydrodynamics (SPH), as observed in studies by Moslemi et al. (2019), Cao et al. (2014), and Sun et al. (2021). This method delineates the fluid motion by tracing the Lagrangian motion of individual particles. These particles engage in interactions based on a kernel function that adheres to specific conditions. Although both of these cutting-edge models capture fluid behavior, even in scenarios involving violent free surfaces and wave breaks, they are hindered by the drawbacks of remarkably high computational demands and the generation of noisy outcomes.

Given the computationally intensive nature of simulating sloshing tanks involving structural-water interactions, opting for a method that strikes a balance between computational efficiency and reasonable accuracy is a pragmatic choice. In this context, the utilization of shallow water models, characterized by hyperbolic equations grounded in depth-averaged Navier-Stokes equations, has been considered (Antuono et al., 2012, Saburin, 2015, Ardakani and Bridges 2012). Notably, contrary to potential flow theory, the inclusion of kinematic boundary conditions directly into the depth-integrated mass and momentum equations enables a low-computational cost approach to the representation of the free surface, bypassing the need for specialized treatment. It is important to note that this approach is primarily applicable to shallow water tanks. In scenarios where the pressure distribution significantly deviates from hydrostatic conditions, conventional shallow-water equations may fall short in precision and necessitate the incorporation of novel terms.

In coupling fluids with Lagrangian solids, two main strategies are commonly employed in the literature. The first strategy involves one-way coupling from fluid to solid and solid to fluid, known as weak-way coupling or the partitioned method (Lia et al. 2013, Fuchs et al. 2021, Zhang et al., 2024). This method treats each domain separately, allowing for diverse discretization schemes and solution methods, with interactions managed by exchanging interface conditions. Conversely, some researchers advocate a two-way coupling approach that simultaneously considers both fluid and deformable solid dynamics, termed strong two-way coupling, or the monolithic method (Robinson-Mosher et al. 2008, Takahashi and Lin 2019 and Xie et al. 2023). This method concurrently addresses the kinetic boundary conditions at the interface, resulting in a stable scheme. The analytical model used in this study adopted a monolithic approach.

The literature extensively explores parametric investigations of tank sloshing encompassing a broad spectrum of themes. Given the intricate nature of the sloshing phenomenon entailing fluid-structure interplay, a substantial portion of numerical modeling has been conducted using commercially available software such as ABAQUS and ANSYS. The impact of tank flexibility on sloshing dynamics has been explored by researchers, such as Ghaemmaghami and Kianoush (2010) and Veletsos et al. (1992). Kamarroudi et al. (2021) examined the influence of the P–Δ effect using finite element methods (FEM) in ABAQUS, addressing vertical acceleration and additional base moment in elevated tanks. Moslemi and Kianoush (2016) investigated the implications of seismic isolation using FEM and potential flow theory within ABAQUS. The effects of foundation embedment were studied by Livaoglua and Dogangun (2007) by employing ANSYS for Finite Element modeling and Lagrangian fluid approximation. Baghban et al. (2022) numerically explored the roles of annular and horizontal baffles in base shear reduction using ABAQUS for the FEM. Mishra (2023) investigated the impact of different vertical bracing systems on elevated tank dynamics using software, and comprehensively assessed the time period, base shear, base moment, top displacement, and sloshing wave height. The STAAD-Pro software package was used to incorporate both uncoupled and coupled idealizations of impulsive and convective masses.

Tuned Liquid Dampers are a specific type of sloshing tank strategically positioned atop structures to mitigate vibrations during seismic events such as earthquakes and wind-induced motion. The key strategy involves aligning the natural frequency of the TLD with that of the structure. The mass of a TLD is typically restricted to less than 5 percent of the structural mass. TLDs are typically shallow water tanks whose responses are mainly influenced by the sloshing wave (convective part). Consequently, the assumption of a rigid shallow-water tank model is suitable for these physical characteristics. This is due to the fact that, in contrast to the impulsive component, the convective forces are largely independent of the tank's flexibility.

Similar to the approaches adopted for sloshing tanks, researchers have employed a diverse array of techniques to simulate fluid sloshing. For instance, studies such as (Sun et al., 1992, Koh et al., 1994, Sun and Fujino 1994, Fujino et al., 1992) have employed shallow water models, while others like (Pandit and Biswal, 2020 and Chaiviriyawonga et al., 2007) have led to potential flow theory. Marivani and Hamed (2009) incorporated the Volume of Fluid (VOF) method, and Awad and Tait (2022) applied Smoothed Particle Hydrodynamics (SPH) to model Tuned Liquid Dampers. Analogous to the Housner theory, certain models, such as the one proposed by Abd-Elhamed and Tolan (2021), have introduced mechanical springs to represent the convective component, with the impulsive part moving in tandem with the tank structure.

A literature review indicates that extensive endeavours have been undertaken to examine the effectiveness of Tuned Liquid Dampers in various scenarios and to evaluate their optimization. Some research investigations have focused on aspects such as TLD geometry. For example, Bhattacharjee et al., (2013) conducted experimental research to examine how the performance of TLDs is influenced by the water-depth-to-tank length ratio. Another focal point is the impact of the wall slope on intensifying sloshing waves, as explored in the studies by Olson and Reed (2001) and Pandit and Biswal (2020). In terms of energy-dissipation devices, Tait et al. (2005) and Crowley et al. (2012) conducted both experimental and numerical analyses, focusing on the application of mechanisms such as screens to exert greater control over the sloshing waves generated by TLDs. The influence of two important parameters, namely the mass ratio (TLD mass/structural mass) and the frequency ratio (TLD natural frequency/structural natural frequency), on the efficiency of Tuned Liquid Dampers have been extensively explored in the literature (Banerji et al., 2000; Banerji et al., 2010). Studies, such as that by Banerji et al. (2010), determined the performance of TLDs concerning the amplitude, duration, and frequency content of the excitation force across narrow and wide ranges. Additionally, Murudi and Banerji (2012) investigated the efficiency of TLDs at varying distances from the earthquake center, both in the near field and far field. Furthermore, Sorkhabi et al. (2017) experimentally examined the response of structures equipped with multiple TLDs compared to a single TLD. While most research employed a single degree of freedom for structures beneath TLDs, Pandit and Biswal (2020) studied a three-story structure, and Ocak et al. (2022) analyzed a 40-story building with multiple degrees of freedom attached to TLDs. Other topics, such as the influence of soil type on TLD performance (Abd-Elhamed and Tolan, 2021), and state-of-the-art experimental techniques like real-time hybrid simulation (RTHS) (Malekghasemi et al., 2015), are also discussed in the literature.

Despite significant research efforts focused on evaluating the performance and optimization of Tuned Liquid Dampers, the literature review reveals a substantial gap in terms of conducting a free vibration analysis of TLDs. The examination of free vibration behavior serves to enhance comprehension of TLDs by offering insights into the natural periods of the system.

4.2. Methodology

As discussed earlier, the primary focus of this study is the analysis of a shallow elevated water tank using a modal coordinate system. In this study, the term 'coupled system' refers to the combination of a single degree of freedom system coupled with a shallow sloshing tank at the top. This paper presents a comprehensive analytical solution for the natural frequency of this coupled system and outlines the procedure for analyzing its response. Furthermore, the study introduces an innovative analytical approximation for a coupled system consisting of Tuned Liquid Dampers. The results obtained from this research regarding stability, mode-specific natural periods, boundary conditions, and the response of the coupled system are significant and contribute to a better understanding of TLD seismic behavior.

4.2.1. Governing Equations

In this study, fluid movement is modeled using the linear shallow water approach. The governing equations of the coupled system, which include the shallow water tank and SDOF, are presented in Equations (4-1).

$$\frac{\partial \eta}{\partial t} + H\frac{\partial u}{\partial x} = 0 \tag{4-1-1}$$

$$\frac{\partial u}{\partial t} + g\frac{\partial \eta}{\partial x} = -\ddot{X} \tag{4-1-2}$$

$$m\ddot{X} + c\dot{X} + kX = F_{exc} + F_{slo} \tag{4-1-3}$$

Equations (4-1-1) and (4-1-2) represent the continuity and momentum equations in linear shallow water models (Toro 2001), while the last equation pertains to the dynamic equation of the SDOF (Humar 2012). In Figure (4.1), H denotes the mean water level, η represents the wave height relative to the mean water level, and u signifies the depth-averaged velocity. Additionally, x indicates position, and t denotes time. The parameters associated with the SDOF include m for mass, k for stiffness, and c for damping coefficient. In Equation (4-1-3), X, $\dot{X}$, and $\ddot{X}$ represent displacement, velocity, and acceleration, respectively. Thus, $m\ddot{X}$, $c\dot{X}$, and kX denote the inertia force, damping force, and elastic force, respectively. On the right-hand side, the equation includes the excitation force (F_{exc}) and the sloshing force (F_{slo}). This research primarily focuses on determining the natural period of a coupled system comprising a single degree of freedom structure and a sloshing tank. Consequently, the study primarily concentrates on free vibration analysis, disregarding external excitation forces. However, it incorporates the sloshing force or fluid-structure interaction force in forming a coupled system.

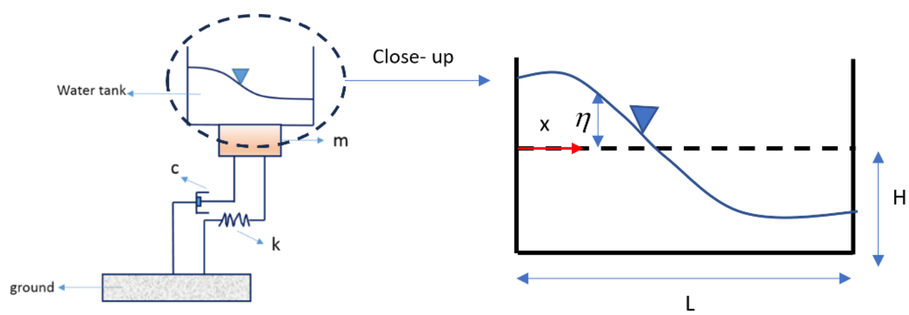

Fig. 4.1. Schematic of the system including SDOF and sloshing tank

4.2.2. Transforming Shallow water equations into modal coordinate system

Using this innovative approach, the separation of variables technique is utilized to determine the wave height and velocity parameters. The separation of variables is a mathematical technique commonly used to solve partial differential equations (PDEs) with multiple variables. The idea is to assume that the PDE solution can be written as a product of functions, each depending on only one variable. This allowed us to transform the original PDE into a set of ordinary differential equations (ODEs) that are easier to solve. Using this approach, the wave height and velocity, which are functions of x and t can be converted to Equations (4.2). Regarding equation (4-2-2), both velocities at $x=0$ and $x=L$ are equal to zero, which satisfies the wall boundary condition at these nodes. Similarly, equation (4-2-1) expresses that the gradient of the wave height at these two nodes is equal to zero, which is equivalent to the zero-gradient boundary condition. In other words, regarding equations (4-2-1 and 4-2-2), the wave height and velocity are expressed in the modal coordinate system in the shape of $cos(\frac{n\pi x}{L})$ and $sin(\frac{n\pi x}{L})$, respectively, and each mode meets the prescribed boundary conditions.

$$\eta(x,t)=\sum_{i=1}^{N} A_i(t)cos(\frac{i\pi x}{L})=A_1(t)cos(\frac{i\pi x}{L})+...+A_n(t)cos(\frac{n\pi x}{L})+...A_N(t)cos(\frac{N\pi x}{L}) \tag{4-2-1}$$

$$u(x,t)=\sum_{i=1}^{N} B_i(t)sin(\frac{i\pi x}{L})=A_1(t)sin(\frac{i\pi x}{L})+...+A_n(t)sin(\frac{n\pi x}{L})+...A_N(t)sin(\frac{N\pi x}{L}) \tag{4-2-2}$$

Replacing equations (4-2-1 and 4-2-2) in Equations (4-1-1), the continuity of linear shallow water, yields the following expressions:

$$\sum_{i=1}^{N} \dot{A}_i \cos(\frac{i\pi x}{L}) + \sum_{i=1}^{N} HB_i \cos(\frac{i\pi x}{L}) = 0 \tag{4-3}$$

Because equation (4-3) should be valid for each x, the following expression is established for each mode, such as n.

$$\dot{A}_n = -HB_n(\frac{n\pi}{L}) \tag{4-4}$$

Using the Fourier transformation, the constant 1 could be expresses as

$$1 = (-2)\sum_{i=1}^{N} \left[\frac{(-1)^i - 1^i}{i\pi} \right] \sin(\frac{i\pi x}{L}) \tag{4-5}$$

Similarly, by substituting equations (4-2-1 and 4-2-2) and equation (4-5) into equation (4-1-2), the momentum equation of the shallow water model, results in the following relation for each mode:

$$\sum_{i=1}^{N} \dot{B}_i \sin(\frac{i\pi x}{L}) + \sum_{i=1}^{N} gA_i(-\frac{i\pi}{L})\sin(\frac{i\pi x}{L}) = \sum_{i=1}^{N} -\ddot{X}(-2)\left[\frac{(-1)^n - 1^n}{n\pi} \right] \sin(\frac{n\pi x}{L}) \tag{4-6}$$

Hence, for each mode, the subsequent expression is derived, which is referred to as the momentum equation in the modal coordinate system.

$$\dot{B}_n + gA_n(-\frac{n\pi}{L}) = -\ddot{X}M_n$$
$$where \qquad (4\text{-}7)$$
$$M_n = -2\left[\frac{(-1)^n - 1^n}{n\pi}\right] \rightarrow \begin{Bmatrix} M_n = 0 \quad for \ n = 2K \\ M_n = \dfrac{4}{n\pi} \quad for \ n = 2K+1 \end{Bmatrix}$$

According to Equation (4-7), the acceleration of the SDOF can impact the momentum of the fluid in odd modes. On the other hand, there is no interaction between the SDOF response and fluid movement in even modes.

Taking the derivative of Equation (4-4) with respect to time yields Equation (4-8)

$$\ddot{A}_n = -\dot{B}_n(\frac{Hn\pi}{L}) \qquad (4\text{-}8)$$

When the first derivative of B with respect to time, $\dot{B}_n$, is substituted from Equation (4-7) to Equation (4-8), the following expression is established. This equation includes both continuity and momentum equations for the fluid in the modal coordinate system.

$$\ddot{A}_n = -A_n(\frac{Hgn^2\pi^2}{L^2}) + \ddot{X}(\frac{Hn\pi}{L})M_n \qquad (4\text{-}9)$$

Equation (4-9) can be reformulated as follows: This expression is a second-order differential equation in which k_{1n} is a positive coefficient, and k_{2n} is zero for even modes and positive for odd modes. In addition to the mode numbers, these coefficients are functions of tank length and water depth.

$$\ddot{A}_n + A_nk_{1n} - \ddot{X}k_{2n} = 0$$
$$where \qquad (4\text{-}10)$$
$$k_{1n} = (\frac{Hgn^2\pi^2}{L^2}) > 0 \quad k_{2n} = (\frac{Hn\pi}{L})M_n = \begin{Bmatrix} 0 \quad for\, n = 2K \\ \dfrac{4H}{L} \quad for\, n = 2K+1 \end{Bmatrix} \geq 0$$

Before analyzing the third equation in the coupled system of equations (referring to the dynamic behavior of the SDOF), the sloshing force is analytically determined in the following section.

4.2.3. The evaluation of Sloshing force in the modal coordinate system

For the element shown in Figure (4.2), the sloshing force communicated from the water tank to the lower SDOF is equal to expression (4-11), where m_d and a_d are the mass and acceleration of the element, respectively.

$$F_{slo} = -\int_{x=0}^{x=L} m_d a_d dx \tag{4-11}$$

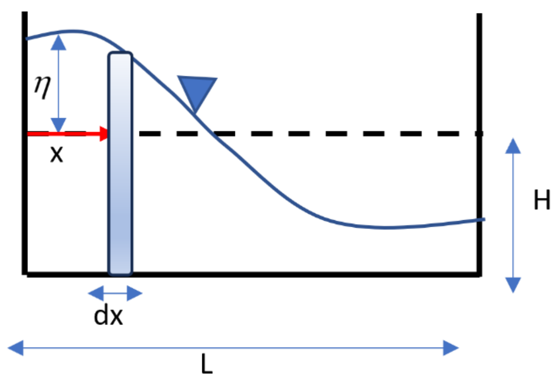

Fig. 4.2. Schematic of an element in the sloshing tank

According to Figure (4.2), $m_d = \rho(H+\eta)bdx$ where ρ refers to water density. In accordance with the principles of fluid mechanics, the acceleration experienced by each individual element is directly proportional to the slope of the free surface and is represented as $-g\dfrac{\partial \eta}{\partial x}$. Consequently, the sloshing force of an element can be evaluated using the following expression.

$$F_{slo} = \int_{x=0}^{x=L} \rho(H+\eta)bdx(g\frac{\partial \eta}{\partial x}) \tag{4-12}$$

The abovementioned equation can be written as

$$F_{slo} = \rho g H b\int_{x=0}^{x=L} (\frac{\partial \eta}{\partial x})dx + \rho g b\int_{x=0}^{x=L} \eta(\frac{\partial \eta}{\partial x})dx \tag{4-13}$$

The term $\eta(\frac{\partial\eta}{\partial x})$ is equivalent to $\frac{\partial}{\partial x}(\frac{\eta^2}{2})$, leading to Equation (4-14) for the sloshing force.

$$F_{slo} = \rho gHb\int_{x=0}^{x=L}(\frac{\partial\eta}{\partial x})dx + \rho gb\int_{x=0}^{x=L}\frac{\partial}{\partial x}(\frac{\eta^2}{2})dx \tag{4-14}$$

If *f(x)* is a function, according to the Leibnitz Integral rule $\int_{x=a}^{x=b}\frac{\partial}{\partial x}f(x)dx = f(b) - f(a)$, the following expression can be derived for the sloshing force:

$$F_{slo} = \underbrace{\rho gHb\left(\eta\right]_{x=0}^{x=L}}_{term1} + \underbrace{\rho gb\left(\frac{\eta^2}{2}\right]_{x=0}^{x=L}}_{term2} \tag{4-15}$$

Hence the subsequent relation is obtained for evaluated sloshing force.

$$\begin{aligned}
term1 &= \rho gHb\left(\eta\right]_{x=0}^{x=L} = \rho gHb\left[\left(\eta\right]_{x=L} - \left(\eta\right]_{x=0}\right] \\
term2 &= \rho gb\left(\frac{\eta^2}{2}\right]_{x=0}^{x=L} = \frac{\rho gb}{2}\left[\left(\eta^2\right]_{x=L} - \left(\eta^2\right]_{x=0}\right]
\end{aligned} \tag{4-16}$$

The approach adopted here involves investigating the contribution of each mode to the response of the SDOF. Consequently, the sloshing force is derived for each mode (e.g., *n*), and the response of the structure, characterized by the vibration frequency and vibration amplitude resulting from this mode, is determined analytically. To accomplish this, consider mode *n* of the free surface, $\eta(for\, mode\, n) = A_n\cos(\frac{n\pi}{L}x)$ .The sloshing force for mode *n* is evaluated from:

$$\begin{aligned}
term1 &= \rho gHb\left(\eta\right]_{x=0}^{x=L} = \rho gHbA_n(\cos(n\pi) - 1) \\
term2 &= \frac{\rho gb}{2}\left(\eta^2\right]_{x=0}^{x=L} = \frac{\rho gb}{2}A_n^2(\cos^2(n\pi) - 1) = 0
\end{aligned} \tag{4-17}$$

Evidently, in each mode, the contribution of the nonlinear term in determining the sloshing force disappears, leaving only the linear term. Hence, the sloshing force from the contribution of mode *n* was calculated using Equation (4-18). In this equation, the coefficient k_{3n} plays a crucial role: zero for even modes and positive for odd modes. This coefficient value is influenced by factors such as tank width and water depth. Similarly, the sloshing force only impacts the single degree of freedom response in the case of odd modes, whereas no interaction force emerges for even modes.

$$F_{slo} = -k_{3n} A_n$$
$$where \tag{4-18}$$
$$k_{3n} = \begin{Bmatrix} 0 & for\ n = 2i \\ 2\rho g H b & for\ n = 2i+1 \end{Bmatrix} \quad k_{3n} \geq 0$$

4.2.4. Coupling dynamic shallow water equation and dynamic of SDOF in mode coordinate system

The dynamic equation of the single degree of freedom system, represented by equations (4-1-3), can be expressed as Equation (4-19) in the free vibration case.

$$m\ddot{X} + c\dot{X} + kX = 0 + F_{slo} \tag{4-19}$$

The dynamic response of the SDOF due to mode n's contribution to the sloshing force, as given by Equation (4-18), is determined by Equation (4-20)

$$m\ddot{X} + c\dot{X} + kX = -k_{3n} A_n \tag{4-20}$$

Thus, A_n could be determined from the following expression.

$$A_n = (-\frac{m}{k_{3n}})\ddot{X} + (-\frac{c}{k_{3n}})\dot{X} + (-\frac{k}{k_{3n}})X \tag{4-21}$$

If the second derivative operator with respect to time is applied to both sides of Equation (4-21), the following expression is derived.

$$\ddot{A}_n = (-\frac{m}{k_{3n}})\ddot{\ddot{X}} + (-\frac{c}{k_{3n}})\dddot{X} + (-\frac{k}{k_{3n}})\ddot{X} \tag{4-22}$$

The substitution of $\ddot{A}_n$ from Equation (4-22) and A_n from Equation (4-21) into Equation (4-10), which is a second-order linear ordinary differential equation including both the continuity and momentum equations of mode n, results in Equation (4-23). Note that certain simplification steps were performed to arrive at this equation.

$$(m)\ddot{\ddot{X}} + (c)\dddot{X} + (k + mk_{1n} + k_{2n}k_{3n})\ddot{X} + (ck_{1n})\dot{X} + (kk_{1n})X = 0 \tag{4-23}$$

This derived equation, which is a fourth-order linear ordinary differential equation including continuity, momentum, and dynamic equations of SDOF, plays an important role in this research. As mentioned earlier, this study disregards the contribution of damping. However, it is anticipated that damping has a negligible impact on the natural period of the system, although it substantially affects the amplitude of the vibration. The influence of structure dissipation and fluid dissipation on the response of the structure will be investigated in future studies. By excluding the damping terms from equation (4-23), equation (4-24) is developed.

$$(m)\ddot{\ddot{X}} + (k + mk_{1n} + k_{2n}k_{3n})\ddot{X} + (kk_{1n})X = 0 \tag{4-24}$$

The solution to this differential equation with a constant coefficient takes the form of $e^{\lambda t}$. To determine λ, this solution is substituted into the differential equation, resulting in the following equation. In this context, this equation is referred to as the characteristic equation.

$$(m)\lambda^4 + (k + mk_{1n} + k_{2n}k_{3n})\lambda^2 + (kk_{1n}) = 0 \tag{4-25}$$

The characteristic equation is a fourth-order polynomial. Assuming $y = \lambda^2$, the characteristic equation is then converted to a second-order polynomial, as presented in Equation (4-26).

As demonstrated in the preceding sections, all $k_{1n},\ k_{2n},\ k_{3n} > 0$ are positive constants. Therefore, the coefficients and constant values of this polynomial, as indicated in Equation (4-26), are also constant and positive.

$$\begin{aligned}
&(m)y^2 + (k + mk_{1n} + k_{2n}k_{3n})y + (kk_{1n}) = 0 \\
&\text{where} \quad y = \lambda^2 \\
&\left\{\begin{matrix} m > 0 \ k > 0 \\ k_{1n} > 0 \ \ k_{2n} > 0 \ \ k_{3n} > 0 \end{matrix}\right\} \rightarrow m > 0, \quad p = k + mk_{1n} + k_{2n}k_{3n} > 0, \quad q = kk_{1n} > 0
\end{aligned} \tag{4-26}$$

The roots of this equation, y_1 and y_2, are derived from the following relationship.

$$\begin{aligned}
&y_1 = \lambda_1^2 = \frac{-p + \sqrt{\Delta}}{2m} \quad \text{and} \quad y_2 = \lambda_2^2 = \frac{-p - \sqrt{\Delta}}{2m} \\
&\text{where} \\
&\Delta = p^2 - 4mq \quad p = k + mk_{1n} + k_{2n}k_{3n} > 0, \quad q = kk_{1n} > 0
\end{aligned} \tag{4-27}$$

4.2.5. Analysing the stability of the free vibration analysis of the coupled system

According to Equation (4-27), two scenarios could lead to instability of the coupled system under free vibration. In the first case, the parameter under the square root, Δ, is negative.

Remark: if the value of Δ in Equation (4-27) is negative, the free vibration of the coupled system is not stable.

Proof:

In this case, with respect to Equation (4-27), the roots of the equation are two complex numbers that take the form of $y = \lambda^2 = -A + Bi$, where A>0. λ, the square root of λ^2, is assumed to be $C + Di$, so its square is $\lambda^2 = C^2 - D^2 + 2CDi$. Therefore, the following system of equations is established:

$$\begin{Bmatrix} C^2 - D^2 = -A \\ 2CD = B \end{Bmatrix} \tag{4-28}$$

By eliminating *D* from the system of equations (4-28) and applying simplification steps, Equation (4-29) is derived.

$$4C^4 + 4AC^2 - B^2 = 0 \tag{4-29}$$

If C_1 and C_2 are the roots of this equation, the following relationship can be formulated:

$$\begin{gathered} C_1^2 = \frac{-4A + \sqrt{\Delta_1}}{8} \quad C_2^2 = \frac{-4A - \sqrt{\Delta_1}}{8} \\ where \\ \Delta_1 = \sqrt{16A^2 + 16B^2} > 0 \end{gathered} \tag{4-30}$$

Because Δ_1 in Equation (4-30) is positive, C_1^2 and C_2^2 are real numbers. According to Equation (4-29), the product of the two roots is $C_1^2 \times C_2^2 = -\frac{B^2}{4} < 0$. Therefore, C_1^2 and C_2^2 have opposite signs; for instance $C_1^2 > 0$ and $C_2^2 < 0$. Hence, the square root of the positive ones (C_1^2) results in a positive real number. Therefore, in this case, $\lambda = C_1 + Di$ has a positive real value, and the solution of the characteristic equation is in the form of $e^{(C_1+Di)t} = e^{C_1 t} \times e^{iDt}$, where $C_1 > 0$. Consequently, in this scenario, attributed to $\Delta < 0$ in the characteristic equation, the displacement grows exponentially in time, so the coupled system is not stable.

The second scenario which leads to instability of the model develops when $y_1 > 0$ or $y_2 > 0$

Remark: if $y_1 \, or \, y_2 > 0$, the free vibration of the coupled system is unstable

In this scenario, if either $\lambda_1^2 = y_1 > 0$ or $\lambda_2^2 = y_2 > 0$, the solution of the characteristic equation for a positive one (e.g., λ_1) takes the form of $e^{\lambda_1 t}$, where $\lambda_1 > 0$. In this case, the solution is unstable.

Regarding the prescribed remark and proof discussion, two conditions are required for the stability of the coupled model subjected to free vibration analysis 1- $\Delta > 0$ 2- $y_1 \,\&\, y_2 < 0$.

Remark: The value of Δ in the characteristic equation is always positive

Proof: Regarding equation (4-27), $\Delta = (k + mk_{1n} + k_{2n}k_{3n})^2 - 4mkk_{1n}$. Thus, it can be written as

$$\Delta = (k + mk_{1n} + k_{2n}k_{3n})^2 - 4mkk_{1n} = (k + mk_{1n})^2 + (k_{2n}k_{3n})^2 + 2(k + mk_{1n})k_{2n}k_{3n} - 4mkk_{1n} \tag{4-31}$$

After simplifying the first and last terms on the right-hand side of Equation (4-31), the following equation is obtained.

$$\Delta = (k - mk_{1n})^2 + (k_{2n}k_{3n})^2 + 2(k + mk_{1n})k_{2n}k_{3n} \tag{4-32}$$

since $\left\{ \begin{matrix} m > 0 \;\; k > 0 \\ k_{1n} > 0 \;\; k_{2n} > 0 \;\; k_{3n} > 0 \end{matrix} \right\}$, the parameter Δ is the sum of three positive terms and is always positive.

Remark: the square of characteristic equation' roots, $y_1 = \lambda_1^2$ and $y_2 = \lambda_2^2$, are always negative:

Proof: According to the previous statement, which establishes $\Delta > 0$, the characteristic equation (4-27) yields two real roots, y_1 and y_2. The product of the two roots is denoted as $y_1 y_2 = \dfrac{q}{m} > 0$, and their sum is evaluated as $y_1 + y_2 = -\frac{p}{m} < 0$. Since the product of the two roots is positive while their sum equals a negative value, both roots, $y_1 = \lambda_1^2$, $y_2 = \lambda_2^2$, are negative.

According to this discussion, because the characteristic equation satisfies both required conditions for stability, namely $\Delta > 0$ and $y_1 \,\&\, y_2 < 0$, the free vibration of the coupled system, including the SDOF and sloshing tank, is unconditionally stable.

4.2.6. The evaluation of the natural frequency of the coupled system

Regarding the discussion above, the characteristic equation, a fourth order polynomial equation (Equation 4-27), demonstrates stability. The square power of these roots, $y_1 = \lambda_1^2$, $y_2 = \lambda_2^2$, based on the previous proof, are two real negative values. As a result, the roots of the characteristic equation are four complex numbers with no real parts, $\pm\lambda_1 i$ and $\pm\lambda_2 i$ where $\lambda_1 \; and \; \lambda_2 > 0$ and $i = \sqrt{-1}$. All in all, according to equation (4-27), the parameters λ_1 and λ_2 are derived from the following expression.

$$\lambda_1 = \sqrt{(\frac{p+\sqrt{\Delta}}{2m})} \quad and \quad \lambda_2 = \sqrt{(\frac{p-\sqrt{\Delta}}{2m})}$$
$$where \tag{4-33}$$
$$p = k + mk_{1n} + k_{2n}k_{3n} \quad and \quad q = kk_{1n} \; and \quad \Delta = p^2 - 4mq$$

Therefore, the solution of the fourth-order differential equation presented in (4-24) takes the form of (4-34). In this equation, λ_1 and λ_2 are determined from Equation (4-33), and *A, B, C, D* are evaluated from the initial boundary conditions discussed in the subsequent sections.

$$X = Ae^{i\lambda_1 t} + Be^{-i\lambda_1 t} + Ce^{i\lambda_2 t} + De^{-i\lambda_2 t} \tag{4-34}$$

Using de Moivre's theorem, Equation (4-35) can be expressed as follows:

$$X = A\sin(\lambda_1 t) + B\cos(\lambda_1 t) + C\sin(\lambda_2 t) + D\cos(\lambda_2 t) \tag{4-35}$$

Equation (4-35) demonstrates that the response of the coupled system has two natural frequencies, ω_1 and ω_2, for mode *n* where $\omega_1 = \lambda_1$ and $\omega_2 = \lambda_2$. In summary, for each fluid mode, a fourth-order ordinary differential equation is derived. This leads to a fourth-order characteristic equation that provides the two natural frequencies obtained from Equation (4-33). In conclusion, this analytical approach provides an evaluation of the natural frequency of a coupled system, which is a crucial factor for seismic design considerations in elevated tanks.

4.2.7. Initial conditions for the evaluation of the unknown coefficients in the response

Generally, in dynamic structures, there are two initial conditions for the free vibration analysis of an SDOF: initial displacement and initial velocity. However, in this coupled system, four initial conditions are required to evaluate the four constants. Regarding Equation (4-35) and considering ω_1 and ω_1 as the natural frequencies resulting from mode *n*, the displacement and its first, second, and third derivatives of the coupled system are expressed in Equation (4-36).

$$\begin{aligned}
X &= A\sin(\omega_1 t) + B\cos(\omega_1 t) + C\sin(\omega_2 t) + D\cos(\omega_2 t) \\
\dot{X} &= A\omega_1\cos(\omega_1 t) - B\omega_1\sin(\omega_1 t) + C\omega_2\cos(\omega_2 t) - D\omega_2\sin(\omega_2 t) \\
\ddot{X} &= -A\omega_1^2\sin(\omega_1 t) - B\omega_1^2\cos(\omega_1 t) - C\omega_2^2\sin(\omega_2 t) - D\omega_2^2\cos(\omega_2 t) \\
\dddot{X} &= -A\omega_1^3\cos(\omega_1 t) + B\omega_1^3\sin(\omega_1 t) - C\omega_2^3\cos(\omega_2 t) + D\omega_2^3\sin(\omega_2 t)
\end{aligned} \tag{4-36}$$

These four equations at *t=0*, which represent the initial conditions, result in the following system of equations:

$$\begin{aligned}
X_{0n} &= B + D \\
\dot{X}_{0n} &= A\omega_1 + C\omega_2 \\
\ddot{X}_{0n} &= -B\omega_1^2 - D\omega_2^2 \\
\dddot{X}_{0n} &= -A\omega_1^3 - C\omega_2^3
\end{aligned} \tag{4-37}$$

The left-hand side of these two equations has a physical concept. They are X_{0n} and $\dot{X}_{0n}$ which represent the initial displacement and initial velocity resulting from mode *n*. On the other hand, an innovative analytical approach is used here to determine the values of the remaining terms, $\ddot{X}_{0n}$ and $\dddot{X}_{0n}$.

Equation (4-20), $m\ddot{X} + c\dot{X} + kX = -k_{3n}A_n$, is employed to determine the value of $\ddot{X}_{0n}$. When this equation is applied to the initial time, Equation (4-38) is obtained for mode *n*. Here, A_{0n} is the initial amplitude of the wave height from the contribution of mode *n*.

$$m\ddot{X}_{0n} + c\dot{X}_{0n} + kX_{on} = -k_{3n}A_{0n} \tag{4-38}$$

Since the damping of the structure, c, is neglected in this study, the initial acceleration due to the contribution of mode *n* is obtained from the following expression:

$$\ddot{X}_{0n} = -(k_{3n}A_{0n} + kX_{on})/m \tag{4-39}$$

In addition, the time derivative of Equation (4-20) results in the following expression:

$$m\dddot{X} + c\ddot{X} + k\dot{X} = -k_{3n}\dot{A}_n \tag{4-40}$$

Regarding Equation (4-4), $\dot{A}_n = -HB_n(\frac{n\pi}{L})$, the equation (4-40) can be converted into the following expression.

$$m\dddot{X} + c\ddot{X} + k\dot{X} = k_{3n}H(\frac{n\pi}{L})B_{0n} \tag{4-41}$$

Applying this equation to the initial time *(t=0)* and disregarding the damping force, the value of $\dddot{X}_{0n}$ can be derived from the following expression, where B_{0n} refers to the initial amplitude of wave velocity resulting from the mode *n* contribution.

$$\dddot{X}_{0n} = [k_{3n}H(\frac{n\pi}{L})B_{0n} - k\dot{X}_{0n}]/m \tag{4-42}$$

Therefore, $\ddot{X}_{0n}$ and $\dddot{X}_{0n}$ depend not only on the measurable and physical parameters, initial displacement, and initial velocity, but also on the functions of A_{0n} and B_{0n}, respectively.

In summary, the following matrix equation is derived for the evaluation of unknown constants: In this matrix equation, $\ddot{X}_{0n}$ and $\dddot{X}_{0n}$ are determined from Equations (4-39) and (4-42). Therefore, in a novel solution, all the initial value parameters X_{0n}, $\dot{X}_{0n}$, A_{0n}, and B_{0n} participate in the evaluation of unknown constants.

$$\begin{bmatrix} 0 & 1 & 0 & 1 \\ \omega_1 & 0 & \omega_2 & 0 \\ 0 & -\omega_1^2 & 0 & -\omega_2^2 \\ -\omega_1^3 & 0 & -\omega_2^3 & 0 \end{bmatrix} \begin{bmatrix} A \\ B \\ C \\ D \end{bmatrix} = \begin{bmatrix} X_{0n} \\ \dot{X}_{0n} \\ \ddot{X}_{0n} \\ \dddot{X}_{on} \end{bmatrix} \tag{4-43}$$

Noted that the physical free vibration of the coupled system includes the initial displacement or initial velocity. Because the water is stagnant at the initial time, the amplitude of wave height and velocity is attributed to $A_{0n}=0$ and $B_{0n}=0$. However, non-zero values for A_{0n} or B_{0n} can be applied analytically in the current model to stimulate a particular response of the coupled system. This technique, called initial perturbation, will be used in this study.

The current concern pertains to the determination of the initial displacement and velocity derived from the contribution of mode *n*.

4.2.8. The evaluation of initial displacement velocity from the contribution of mode n

In the current analytical approach, Equation (4-44) is proposed to evaluate the contribution of mode *n* from the initial displacement and velocity, where X_{on} and $\dot{X}_{on}$ are the initial displacement and velocity from the mode *n* contribution, respectively. As proved, the sloshing tank only influences the response of the SDOF in odd modes, whereas the interaction force for even numbers disappears. In this equation, *n* and *N* are odd numbers.

$$\begin{Bmatrix} X_0 \\ \dot{X}_0 \end{Bmatrix} = \sum_{i=1}^{N} \begin{Bmatrix} X_{oi} \\ \dot{X}_{0i} \end{Bmatrix} \sin[\frac{(2i+1)\pi x}{L}] = \begin{Bmatrix} X_{o1} \\ \dot{X}_{01} \end{Bmatrix} \sin[\frac{1\pi x}{L}] + \ldots + \begin{Bmatrix} X_{on} \\ \dot{X}_{0n} \end{Bmatrix} \sin[\frac{n\pi x}{L}] + \ldots . \begin{Bmatrix} X_{oN} \\ \dot{X}_{0N} \end{Bmatrix} \sin[\frac{N\pi x}{L}]$$

(4-44)

According to the following expression, the mode shapes of *m* and *n* are orthogonal to each other:

$$\int_{x=0}^{L} \sin(\frac{n\pi x}{L}) \sin(\frac{m\pi x}{L})\, dx = \begin{Bmatrix} 0 & m \neq n \\ \frac{L}{2} & m = n \end{Bmatrix} \qquad (4\text{-}45)$$

Consequently, due to the orthogonality of the mode shapes, the participation of each mode (e.g., *n*) in the initial displacement and velocity is determined from the following expression:

$$\begin{Bmatrix} X_{on} \\ \dot{X}_{0n} \end{Bmatrix} = \frac{\int_{x=0}^{L} \sin(\frac{n\pi x}{L})\,\mathrm{dx}}{\int_{x=0}^{L} \sin^2(\frac{n\pi x}{L})\,\mathrm{dx}} \begin{Bmatrix} X_o \\ \dot{X}_0 \end{Bmatrix} = \frac{4}{n\pi} \begin{Bmatrix} X_o \\ \dot{X}_0 \end{Bmatrix} \qquad (4\text{-}46)$$

4.3. Numerical models:

To investigate the accuracy of the current analytical approach, the analytical results are compared with those of the numerical method developed in this study. The numerical method utilized to model the coupled system relies on the separation of variables in the modal coordinate system. The numerical model is based on the system of ordinary differential equations presented in (4-47). It includes the continuity equation for mode *n* (equation 4-47-1), momentum equation for mode *n* (equation 4-47-2), modal superposition for the evaluation of the wave height (equation 4-47-3), sloshing force (equation 4-47-4) and dynamic equation of SDOF (equation 4-47-5). Thus, the system of equations used in the numerical method is the same as that used in the current analytical model.

$$\dot{A}_n = -HB_n(\frac{n\pi}{L}) \tag{4-47-1}$$

$$\dot{B}_n + gA_n(-\frac{n\pi}{L}) = -\ddot{X}M_n \tag{4-47-2}$$

$$\eta(x,t)=\sum_{n=1}^{N} A_n(t)cos(\frac{n\pi x}{L}) \tag{4-47-3}$$

$$F_{slo}(x,t)=2\rho gH\,[\eta(x=0)+\eta(x=L)] \tag{4-47-4}$$

$$m\ddot{X} + c\dot{X} + kX = 0 + F_{slo} \tag{4-47-5}$$

By employing the finite difference method to the dynamic equation of a single degree of freedom system, the following equation is derived: For more details, refer to (Humar, 2012)

$$[\frac{m}{\Delta t^2} + \frac{c}{2\Delta t}]x^{n+1} = F_{slo}^n - [\frac{m}{\Delta t^2} - \frac{c}{2\Delta t}]x^{n-1} - [k - \frac{2m}{\Delta t^2}]x^n \tag{4-48}$$

Equations (4-47-1 and 4-47-2) within this system of equations are solved using the midpoint method, specifically the Runge-Kutta second-order method. This method, categorized as a prediction and correction technique, involves evaluating the slope at the midpoint of a time step. The value of *N*, which represents the number of modes, is chosen to ensure convergence. Once the model achieves convergence in terms of the mode numbers, further increases in *N* no longer affect the shape of the free surface. This numerical approach, which is based on modal decomposition, presents a significant advantage over other numerical methods. It not only allows the generation of the total structural response but also enables the extraction of the response associated with a specific mode's contribution (e.g., *m*). To achieve this, in Equation 45-3, the lower and upper limits of summation are set to be the same $\sum_{n=m}^{m}$ to accommodate the desired mode.

The partition method is employed to couple the system of equations, and the sloshing force is used as an iterative parameter. To combine the system of equations, an assumed value was attributed to the sloshing force at the beginning of each time step. Then, the dynamic equation of the single degree of freedom, equation (4-47-5), is solved with respect to the initial condition for the free vibration test, and the acceleration of the SDOF ($\ddot{X}$) is the outcome of this equation. Subsequently, the first and second equations of system 4-47 were solved for odd modes from 1 to N to extract both $A(1,t),...,A(N,t)$ and $B(1,t),..,B(N,t)$. Then, the free surface is evaluated by Equation (4-47-3) of the system of equations. This step also ensures that N is sufficiently large to reach convergence for the free-surface wave. Using equation (4-47-4), the sloshing force is computed. If the calculated sloshing force closely matches the assumed value, the iteration converges and coupling is established for that specific time step. This process continues for the subsequent time steps. A flowchart illustrating the coupling process of this system of equations is shown in Figure (4.3).

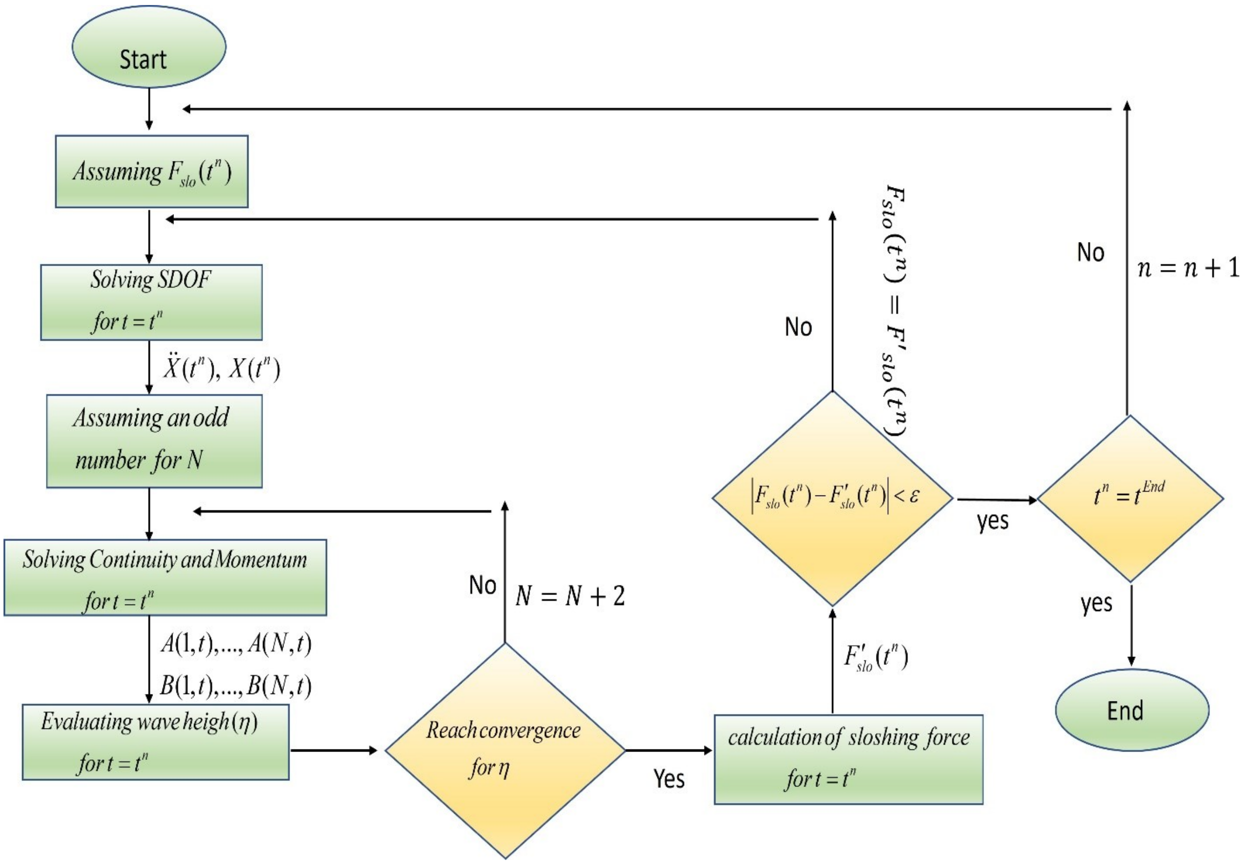

Fig. 4.3. Flowchart of the numerical model relying on the separation of variables

Concerning the structural response, elevated tanks can be divided into two categories:1) massive, elevated tanks, and 2) small-scale elevated tanks. In the case of massive tanks, the fluid significantly influences the structure response due to the considerable inertial force exerted by the fluid. However, for small-scale tanks where the fluid mass is much smaller than the structure mass (less than five percent), the interaction is virtually negligible, unless the natural frequency of the tank closely matches that of the structure, as in the case of tuned liquid dampers.

4.4. Application of the current model for TLDs

The proposed method has some limitations as mentioned in the following. The fluid governing equations are designed for shallow tanks, which have numerous industrial applications, including the use of tuned liquid dampers. Additionally, the current analytical model is reliable for small wave amplitudes. However, in cases of high-amplitude waves, the prominence of the nonlinear term increases, and there is a potential for the occurrence of breaking waves, necessitating the consideration of additional terms. In this analytical approach, the sloshing tank is on top of a single degree of freedom, which represents the structure. Dynamic structural analysis employs methods such as the generalized coordinate system and energy method (Humar, 2012) to simplify complex systems into single degree of freedom systems.

Contrary to these limitations, this section elaborates on how this analytical model can effectively predict the response of the coupled system, encompassing tuned liquid dampers and single degree of freedom structures. The TLDs characterized by shallow water tanks exhibit two significant dynamic characteristics:1) the mass of the TLD is considerably smaller than that of the Single Degree of Freedom (SDOF) system, and 2) the natural frequency of the TLD matches the natural frequency of the SDOF system. Through an illustrative example centered on TLD, the remainder of the study is dedicated to examining the analytical derivation of both the natural frequencies and structural responses. For clarity and comparison, the analytical results were cross-validated against the numerical model data developed in Section 4.3. Additionally, the current analytical approach introduces an approximation to the natural frequency and the coupled system response for higher, offering a more profound understanding of TLD performance. A Fast Fourier Transformation technique is also used here to drive the fundamental frequencies of the numerical results in order to compare the analytical and numerical results. Section 4 validates the current model using a second-order finite difference method and discusses the impact of nonlinear terms.

Examples

This example is associated with a coupled system including the SDOF and TLD derived from experimental research conducted by Sorkhabi et al. (2017). The dynamic properties of the SDOF, mass, and stiffness were equal to those of $m = 282(Kg)$ and $K = 4997.5\,(N/m)$. As a result, the angular and natural frequencies of the SDOF determined from equation (4-49) (Humar 2012) are $\omega_s = 4.21(Rad/s)$ and $f_s = 0.67(Hz)$, respectively.

$$\omega_s = \sqrt{\frac{k}{m}} \quad , f_s = \frac{\omega}{2\pi} \tag{4-49}$$

Accordingly, the length of the sloshing tank (TLD) and water depth are L=0.46(m) and H=0.04(m), respectively. By employing equation (4-50), which has been frequently cited in various publications (Ghaemmaghami and Kianoush, 2010), it was established that the natural frequency of the tank is equivalent to $f_L = 0.67(Hz)$. Therefore, the natural frequency of the structure aligns with that of the tank, confirming their equality.

Additionally, in this particular instance, the tank's width is set at 0.31m. Consequently, the calculated mass ratio, defined as the TLD's mass divided by the structure's mass, results in 2%. Generally, the mass ratio of a TLD is < 5%.

$$f_L = \frac{1}{2\pi}\sqrt{\frac{\pi g}{L} tanh(\frac{\pi H}{L})} \tag{4-50}$$

4.4.1. Natural frequency of the coupled system

Employing the present analytical method, the natural frequencies of the coupled system are calculated for modes 1, 3, 5, 7, and 9 using Equation (4-33), as summarized in Table (4.1). As previously mentioned, each odd mode leads to two natural frequencies, whereas the even modes do not influence the response of the system. Examination of these natural frequencies highlights that for higher modes (n>1), the smaller frequencies are approximately equivalent and closely align with the natural frequency of the structure, ω_s (compare columns 4 and 6 for n>1), while the larger frequency is in close proximity to $n\omega_s$ (refer to columns 5 and 7).

Table 4.1. Analytical natural frequencies of the coupled system associated with different modes.

Mode Number (n)	*Lower Agular Frequency*	*Higher Agular Frequency*	*Lower Frequency*	*Higher Frequency*	*SDOF Frequency*	*n*SDOF Frequency*
1	3.9758	4.5276	0.6331	0.721	0.67	0.67
3	4.2054	12.8411	0.6697	2.0448	0.67	2.01
5	4.2083	21.3872	0.6701	3.4056	0.67	3.35
7	4.209	29.937	0.6702	4.767	0.67	4.69
9	4.2093	38.4878	0.6703	6.1286	0.67	6.03

Remark: For higher modes (n>1), the lower natural frequency is close to the natural frequency of SDOF ω_s, and the higher frequency is approximately equal to $n\omega_s$.

Proof:

In shallow tanks, where $\frac{H}{L} << 1$, $tanh\frac{\pi H}{L} \approx \frac{\pi H}{L}$. Replacing this value in Equation (4-50) results in $f_L = \frac{\sqrt{gH}}{2L}$. Recall that $k_{1n} = (\frac{Hgn^2\pi^2}{L^2})$, so this coefficient can be converted to $k_{1n} = 4f_L^2 n^2 \pi^2$. Because the $\omega_L = 2\pi f_L$ and TLDs frequency of the sloshing tank equals the frequency of the SDOF $\omega_L = \omega_s$, the coefficient k_{1n} can be written as $k_{1n} = n^2\omega_s^2$. Recall that for odd modes, the coefficients are $k_{2n} = 4\frac{H}{L}$ and $k_{3n} = 2\rho gHb$, while for the even modes, both coefficients are inactive; thus, the product of these two coefficients is $k_{2n}k_{3n} = 4\frac{H}{L}2\rho gHb$ for odd modes and zero for even mode. Because $\rho gHLb$ is equal to the weight of TLD (*W*), $k_2k_3 = 8\frac{WH}{L^2}$. Replacing the values of k_{1n} and $k_{2n}k_{3n}$ in the characteristic equation, $(m)\lambda^4 + (k + mk_{1n} + k_{2n}k_{3n})\lambda^2 + (kk_{1n}) = 0$, yields the following equation:

$$(m)\lambda^4 + (k + mn^2\omega_s^2 + \frac{8WH}{L^2})\lambda^2 + (kn^2\omega_s^2) = 0 \tag{4-51}$$

Regarding the natural frequency of the SDOF, $\omega_s^2 = \frac{k}{m}$, the characteristic equation leads to:

$$(m)\lambda^4 + (k + kn^2 + \frac{8WH}{L^2})\lambda^2 + (\frac{k^2}{m}n^2) = 0 \tag{4-52}$$

Let us examine the coefficient of λ^2, denoted by $[k(1+n^2) + \frac{8WH}{L^2}]$, in terms of its order of magnitude. For higher modes with increasing values of *n*, the $k(1+n^2)$ coefficient experiences substantial growth, reaching magnitudes that become quite large. Conversely, considering that the mass of the water sloshing tank in TLD is typically small and in shallow tanks $\frac{H}{L} << 1$, the term

$\frac{8WH}{L^2}$ tends to be a small number. Consequently, for higher modes, the $\frac{8WH}{L^2}$ term can be considered negligible in comparison with the order of magnitude of $k(1+n^2)$. Therefore, with a high level of accuracy, the characteristic equation of the TLD for higher modes can be approximated using the following equation:

$$(m)\lambda^4 + [k(1+n^2)]\lambda^2 + (\frac{k^2}{m}n^2) = 0 \tag{4-53}$$

If the two sides of equation (4-53) are divided by m and the value of $\frac{k}{m}$ is substituted with $\omega_s{}^2$, the subsequent equation is derived for higher modes (n>1).

$$\lambda^4 + [\omega_s^2(1+n^2)]\lambda^2 + (\omega_s^4 n^2) = 0 \tag{4-54}$$

Assuming $y = \lambda^2$, the solution to the roots of this equation results in:

$$y_1, y_2 = \frac{-\omega_s^2(1+n^2) \pm \sqrt{[\omega_s^2(1+n^2)]^2 - 4\omega_s^4 n^2}}{2} \tag{4-55}$$

Applying some simplification leads to

$$y_1, y_2 = \frac{-\omega_s^2(1+n^2) \pm \sqrt{[\omega_s^4(n^2-1)^2]}}{2} = \frac{-\omega_s^2(1+n^2) \pm [\omega_s^2(n^2-1)]}{2} \tag{4-56}$$

Therefore, the two roots derived for y are $y_1 = -\omega_s^2$ and $y_2 = -n^2\omega_s^2$ which lead to $\lambda_1 = \pm\omega_s i$ and $\lambda_2 = \pm n\omega_s i$. As a result, it is proven that for higher modes, the lower natural frequency of the coupled system is equal to the frequency of the structure ($\omega_1 = \omega_s$), and a higher natural frequency is n times the natural frequency of the structure ($\omega_2 = n\omega_s$) with a precise approximation method.

4.4.2. Comparison of the analytical frequencies with numerical ones

4.4.2.1 non-perturbed free vibration

The coupled system described in Section 4.4 is numerically subjected to an initial displacement ($X_0 = -0.01m$) without fluid perturbation. In the first step, the numerical approach focuses solely on the first mode (n=1), that is, the wave height and velocity are developed exclusively by this first mode. The time history of the displacement of the coupled system and sloshing force is depicted in Figure (4.4) for two cases: 1) with TLD and without TLD (just SDOF). It is worth noting that in this study, the damping effects in both the fluid and the structure are neglected.

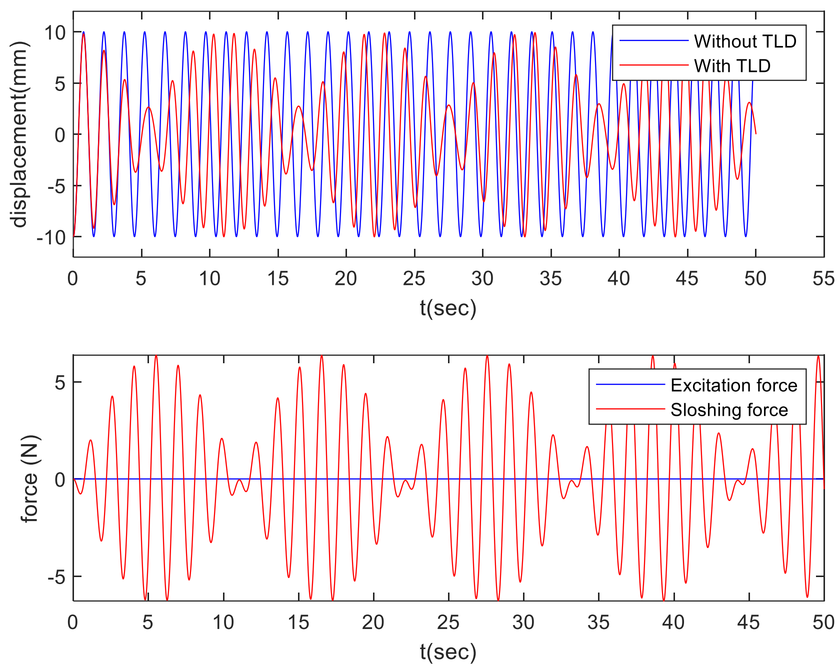

Fig. 4.4. Time history of numerical displacement and sloshing force with TLD and without TLD for the mode n=1

To gain a clearer insight into the inherent patterns and characteristics of the outcomes, Fast Fourier Transformation (FFT) was employed on the data. The FFT is a mathematical transformation that converts a signal from its time-domain representation to its frequency-domain representation. In simple terms, it dissects a signal into its individual frequency components.

As indicated in Figure (4.5), the numerical model generates two fundamental modes that closely align with the natural frequencies of mode 1 predicted by the analytical approach in Table (4.1) (0.63 Hz and 0.72 Hz).

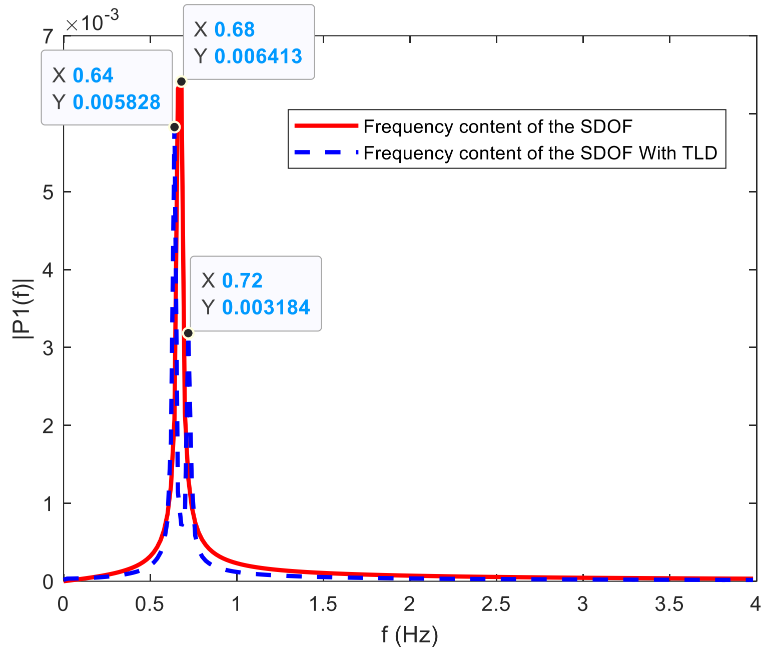

Fig. 4.5. FFT transformation of numerical displacement of mode *n*=1 related to the coupled system subjected to free vibration

This numerical process is replicated for modes 3, 5 and 7. The data shown in Figures (4.6) illustrate that, for higher modes, only one natural frequency appears in the frequency domain. In essence, for higher modes (more than one), the lower natural frequency agrees well with the analytical predictions, whereas a higher natural frequency does not contribute to the response.

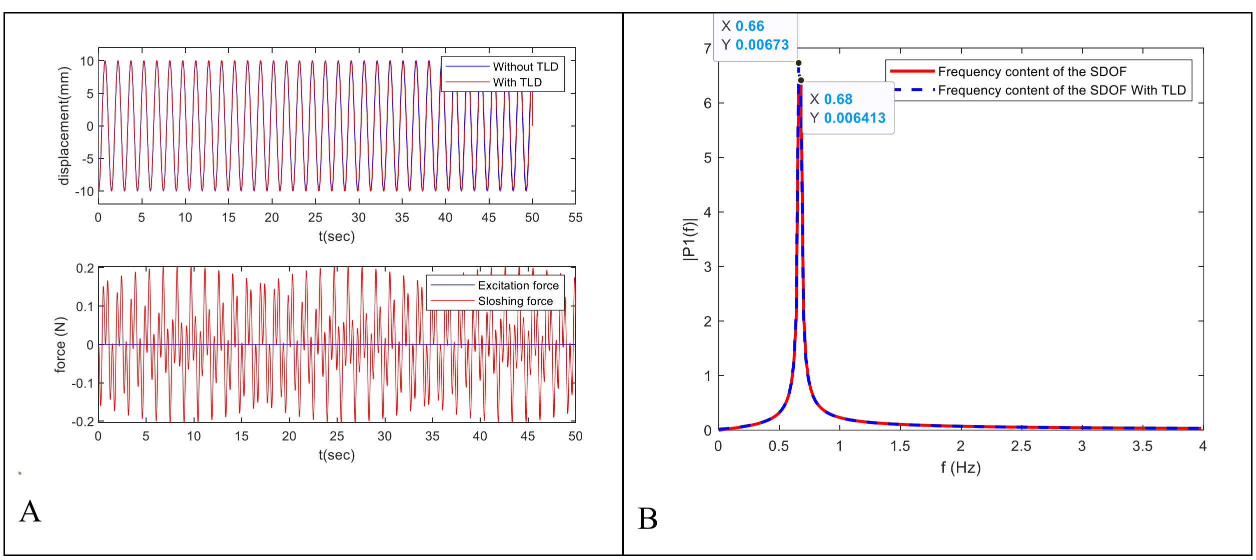

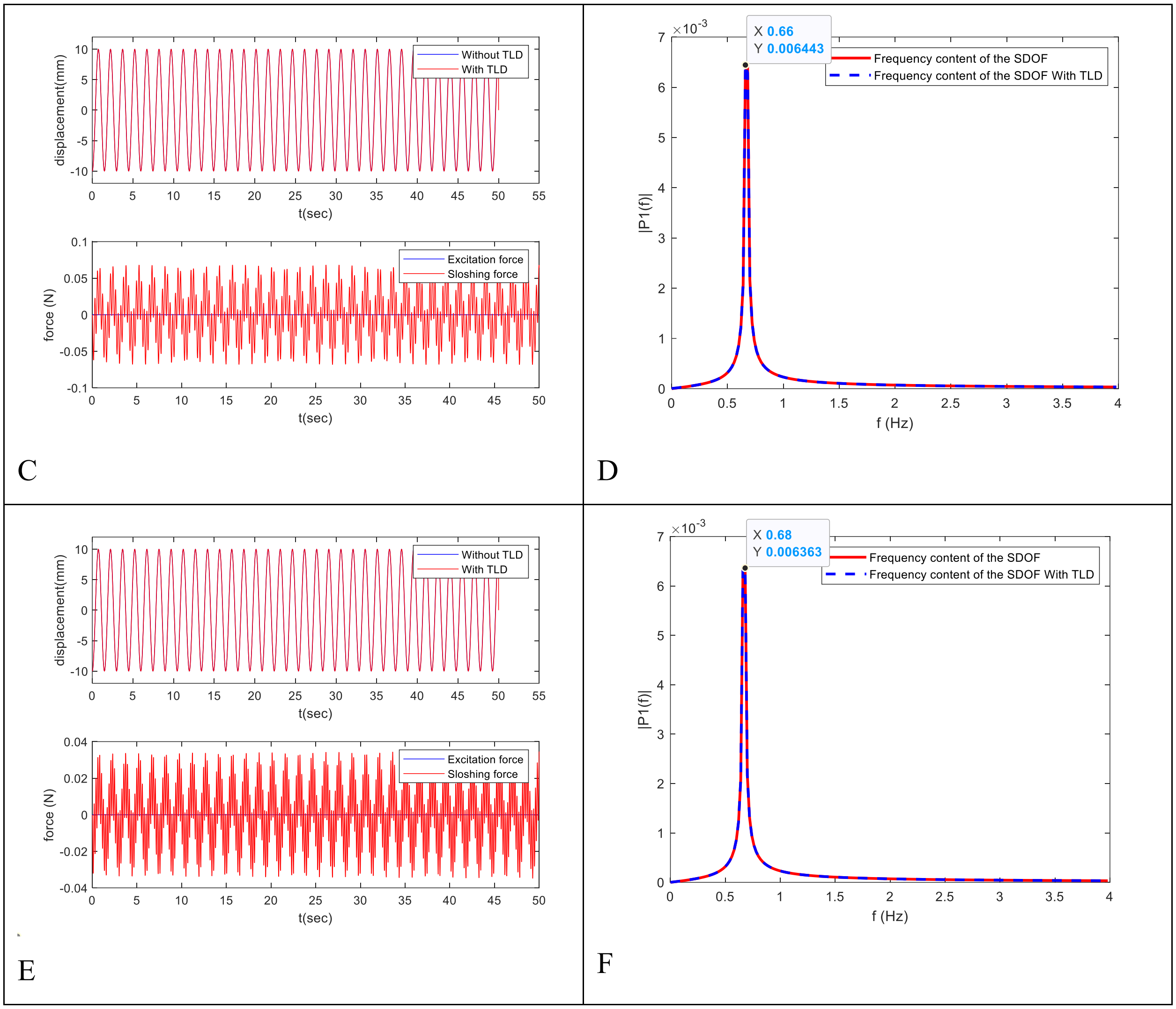

Fig. 4.6. The numerical results for higher modes related to the coupled system subjected to free vibration: a, c, e: time history of displacements and sloshing forces for modes 3, 5, and 7, respectively and b, d, f: FFT transformations of displacements for modes 3, 5, and 7, correspondingly

Remark: Using the current analytical approach demonstrate that in the case of free vibration, a greater natural frequency of higher modes does not contribute to the response of the coupled system, including TLD and SDOF.

Proof: As proved analytically, the response of the coupled system is obtained from the expression $X = A\sin(\omega_1 t) + B\cos(\omega_1 t) + C\sin(\omega_2 t) + D\cos(\omega_2 t) \quad where \quad \omega_2 > \omega_1$, and unknown constants are also determined from matrix equation (4-37) as follows

$$X_{0n} = B + D$$
$$\dot{X}_{0n} = A\omega_1 + C\omega_2$$
$$\ddot{X}_{0n} = -B\omega_1^2 - D\omega_2^2$$
$$\dddot{X}_{0n} = -A\omega_1^3 - C\omega_2^3$$

Elimination B from equations (1) and (3) of the upper system yields $\ddot{X}_{on} + X_{on}\omega_1^2 = D(\omega_1^2 - \omega_2^2)$. Recall Equation (4-39), where $\ddot{X}_{0n} = -(k_{3n}A_{0n} + kX_{on}) / m$. Substituting $\ddot{X}_{0n}$ leads to the following expression:

$$-\frac{k_{3n}A_{0n}}{m} + (\omega_1^2 - \frac{k}{m})X_{0n} = D(\omega_1^2 - \omega_2^2) \tag{4-57}$$

As the initial perturbation for $A_{0n} = 0$, the first term on the left-hand side was zero. Regarding $\frac{k}{m} = \omega_s^2$, the second term on the left-hand side is the $(\omega_1^2 - \omega_s^2)X_{0n}$. As demonstrated earlier, the lower natural frequency of the higher mode, ω_1, is very close to the natural frequency of the SDOF, ω_s. Subsequently, the second term on the left-hand side approaches zero. With this understanding and $\omega_1 \neq \omega_2$, it can be inferred from Equation (4-57) that the constant D is determined to be zero. Similarly, eliminating A from equations (2) and (4) in the upper system of equations and recalling $\dddot{X}_{0n} = [k_{3n}H(\frac{n\pi}{L})B_{0n} - k\dot{X}_{0n}] / m$, the following equation is developed:

$$\frac{k_{3n}H(n\pi / L)B_{0n}}{m} + (\omega_1^2 - \frac{k}{m})\dot{X}_{0n} = C\omega_1(\omega_1^2 - \omega_2^2) \tag{4-58}$$

Because the initial conditions for $B_{0n} = 0$ and ω_1^2 approach $\omega_s^2 = \frac{k}{m}$, the constant C is very close to zero.

In conclusion, because the coefficients of higher frequency are zero, it is proved that higher natural frequency of the higher modes do not participate in the response of the coupled system for the free vibration test.

However, to verify the accuracy of the current analytical approach, a higher frequency should be excited numerically and compared with analytical approaches.

Remark: An initial perturbation is required to stimulate a higher frequency in the response of the coupled system.

Proof: Let us examine Equations (4-57) and (4-58). Employing a rigorous approximation method, it has been demonstrated that the second term on the left-hand side of these equations tends towards zero. Consequently, to establish significant values for *D* and *C*, it is necessary to define the initial values for A_{0n} and B_{0n}, correspondingly. This necessitates the introduction of an initial perturbation linked to either the free surface or the velocity, which consequently leads to the involvement of higher frequencies in each mode.

4.4.2.2. perturbated free vibration

In the following, the numerical model is subjected to both the initial displacement ($X_0 = -0.01m$) and the initial perturbation of the free surface ($A_0 = 1$m). It is worth noting that although the initial perturbation may lack a physical basis, it is utilized in a numerical capacity to assess the accuracy of the present solution.

Figures (4-7a to 4-7f) reveal the results of the numerical model for the coupled model subjected to the aforementioned initial conditions. The figures on the left show the time history of the displacements for modes *n*=3, 5,7 and the figures on the right refer to the frequency content of this data resulting from the FFT application. As proven analytically, the initial perturbation excites two natural frequencies for each mode. The fundamental frequencies observed in these figures closely align with the analytical predictions in Table (4.1), thereby underscoring the precision of the current methodology.

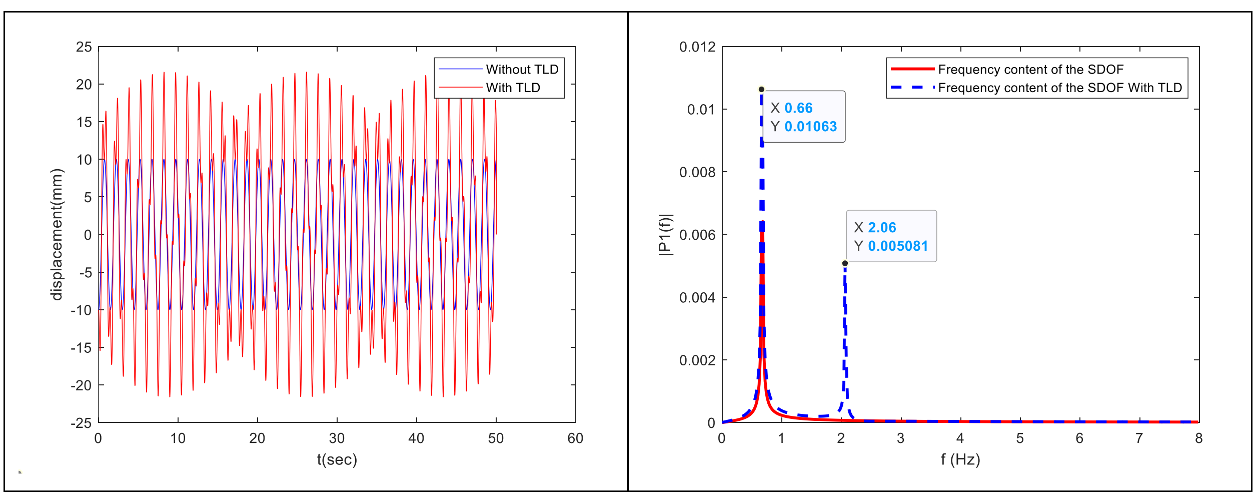

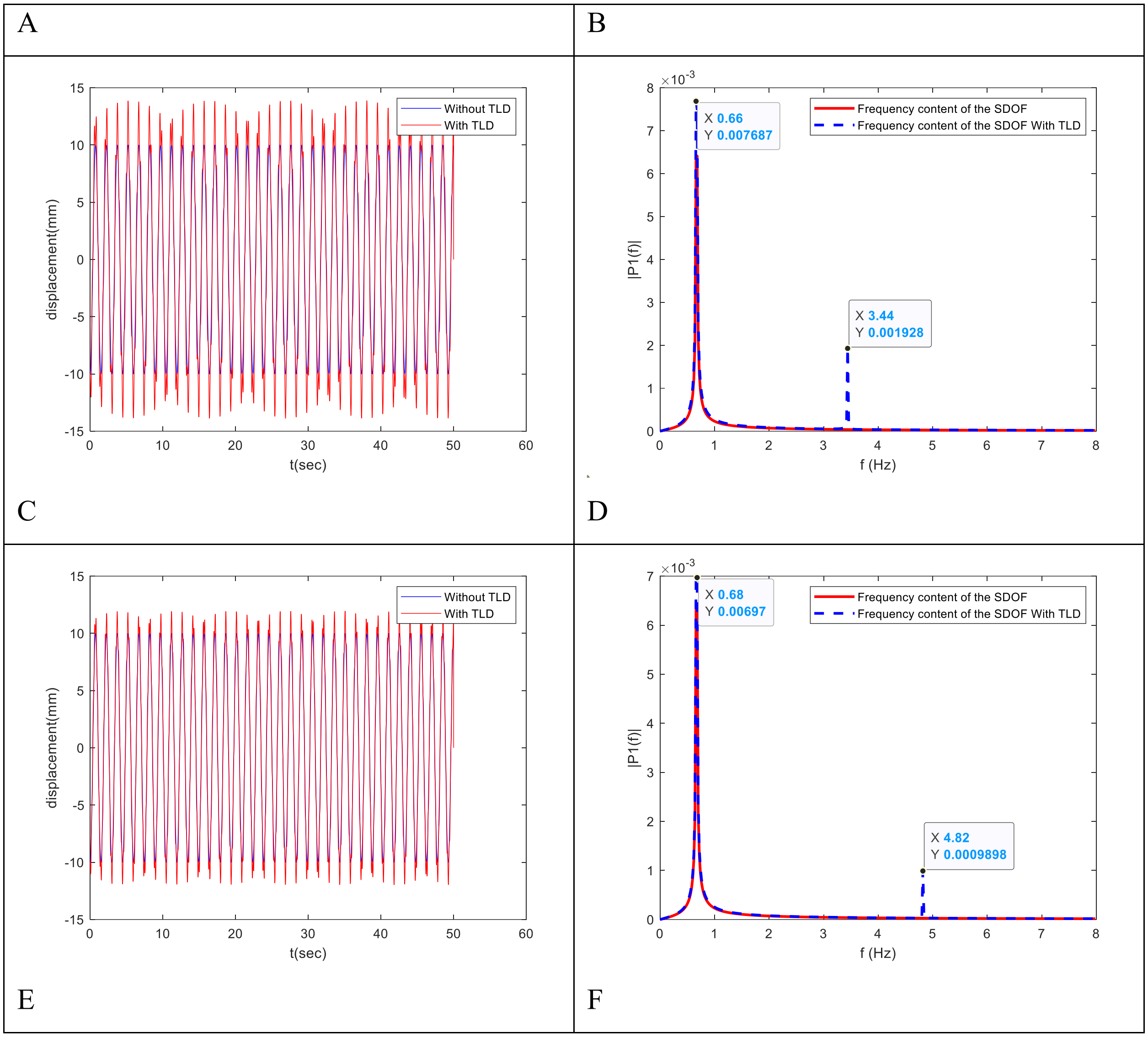

Fig. 4.7. The numerical results for higher modes related to the coupled system subjected to free vibration with initial perturbation: a, c, e: time history of displacements for modes 3, 5, and 7, respectively and b, d, f: FFT transformations of displacements for modes 3, 5, and 7, correspondingly

4.4.3. approximation of the total response with first mode of the fluid

Remark: The response of a coupled system including TLD and SDOF can be approximated simply by the first-mode contribution:

Proof:

The initial displacement of the coupled system was assumed to be X_0. Regarding the modal decomposition (Equation 4-44), the total initial displacement can be transformed into the initial displacement of each mode.

$$X_0 = X_{o1}\sin[\frac{1\pi x}{L}] + X_{o3}\sin[\frac{3\pi x}{L}]... + X_{on}\sin[\frac{n\pi x}{L}] + ...X_{oN}\sin[\frac{N\pi x}{L}] \tag{4-59}$$

Owing to the orthogonality of the modes, as mentioned in Equation (4-45), the initial displacement of each odd mode (e.g., *n*) is:

$$X_{on} = \frac{4}{n\pi}X_o \tag{4-60}$$

Regarding equation (4-35), the response of the system resulting from each mode is:

$$X_i = A_i\sin(\omega_{i,1}t) + B_i\cos(\omega_{i,1}t) + C_i\sin(\omega_{i,2}t) + D_i\cos(\omega_{i,2}t) \tag{4-61}$$

In this equation, $\omega_{i,j}$, *i* refers to the number of modes and *j* denotes the number of fundamental frequencies in each mode. As proved, each mode has brought about two fundamental frequencies which $\omega_{i,1} < \omega_{i,2}$.

Recall that the constant coefficients are determined from the matrix equation (4-43) in which initial displacement of mode *n*, X_{0n}, initial velocity of mode *n*, $\dot{X}_1(0)$, $\ddot{X}_{0n} = -(k_{3n}A_{0n} + kX_{on})/m$, $\dddot{X}_{0n} = [k_{3n}H(\frac{n\pi}{L})B_{0n} - k\dot{X}_{0n}]/m$, are employed to develop the known vector.

First mode: The response from the contribution of the first mode with respect to the initial boundary is:

$$X_1 = A_1\sin(\omega_{1,1}t) + B_1\cos(\omega_{1,1}t) + C_1\sin(\omega_{1,2}t) + D_1\cos(\omega_{1,2}t) \tag{4-62}$$

In this case, associated with the initial displacement, X_0 , the known vector is $X_1(0) = \frac{4}{\pi}X(0)$, $\dot{X}_1(0) = 0$, $\ddot{X}_1(0) = -k\frac{X_1(0)}{m}$, $\dddot{X}_1(0) = 0$). Regarding this initial condition, the constants multiplied by the sinus function in the response of the system are zero.

$$X_1 = B_1 \cos(\omega_{1,1} t) + D_1 \cos(\omega_{1,2} t) \tag{4-63}$$

Higher modes (n>1): According to the previous discussion, two important points were proven for higher modes.

1- For each mode, the lower fundamental frequency is very close to the natural frequency of the SDOF, which means $\omega_{n,1} = \omega_s$

2- The greater fundamental frequency in each mode has no contribution to the response of the system, which implies that $C_n = D_n = 0$. In this case, regarding the prescribed initial condition, the coefficients are $A_n = 0$, $B_n = \frac{4}{n\pi} X_0$. Therefore, the response of the system from the contribution of mode n is:

$$X_n = \frac{4}{n\pi} X_0 \cos(\omega_s t) \tag{4-64}$$

After deriving the contribution of each mode, the modal superposition technique is used to acquire the total response of the coupled system.

$$X = X_1 \sin[\frac{1\pi x}{L}] + X_3 \sin[\frac{3\pi x}{L}] ... + X_n \sin[\frac{n\pi x}{L}] + ... X_N \sin[\frac{N\pi x}{L}] \tag{4-65}$$

Substituting Equations (4-63) and (4-64) into Equation (4-65) yields

$$\begin{aligned} X &= [B_1 \cos(\omega_{1,1} t) + D_1 \cos(\omega_{1,2} t)] \sin(\frac{1\pi x}{L}) + \\ & X_0 \cos(\omega_s t) [\frac{4}{3\pi} \sin(\frac{3\pi x}{L}) ... + \frac{4}{n\pi} \sin(\frac{n\pi x}{L}) + ... \frac{4}{N\pi} \sin(\frac{N\pi x}{L})] \end{aligned} \tag{4-66}$$

The term $X_0 \cos(\omega_s t) \frac{4}{\pi} \sin(\frac{\pi x}{L})$ is added and subtracted from the right-hand side of Equation (4-66) to form Equation (4-67):

$$X = [B_1 \cos(\omega_{1,1} t) + D_1 \cos(\omega_{1,2} t) - \frac{4}{\pi} X_0 \cos(\omega_s t)] \sin(\frac{1\pi x}{L}) +$$
$$X_0 \cos(\omega_s t)[\frac{4}{\pi}\sin(\frac{\pi x}{L}) + \frac{4}{3\pi}\sin(\frac{3\pi x}{L})... + \frac{4}{n\pi}\sin(\frac{n\pi x}{L}) + ... \frac{4}{N\pi}\sin(\frac{N\pi x}{L})] \quad (4\text{-}67)$$

The term $[\frac{4}{\pi}\sin(\frac{\pi x}{L}) + \frac{4}{3\pi}\sin(\frac{3\pi x}{L})... + \frac{4}{n\pi}\sin(\frac{n\pi x}{L}) + ... \frac{4}{N\pi}\sin(\frac{N\pi x}{L})]$ is a Fourier series of 1. Thus, the total response can be written as:

$$X = [B_1 \cos(\omega_{1,1} t) + D_1 \cos(\omega_{1,2} t) - \frac{4}{\pi} X_0 \cos(\omega_s t)] \sin(\frac{1\pi x}{L}) + X_0 \cos(\omega_s t)[1] \quad (4\text{-}68)$$

The term $X_0 \cos(\omega_s t)$, in fact, is the response of the SDOF under the initial displacement (Humar, 2012). Therefore, the total response is

$$X = [B_1 \cos(\omega_{1,1} t) + D_1 \cos(\omega_{1,2} t) - \frac{4}{\pi} X_{SDOF}] \sin(\frac{1\pi x}{L}) + X_{SDOF}$$
$$or \quad (4\text{-}69)$$
$$X = [B_1 \cos(\omega_{1,1} t) + D_1 \cos(\omega_{1,2} t)] \sin(\frac{1\pi x}{L}) + X_{SDOF}[1 - \frac{4}{\pi}\sin(\frac{1\pi x}{L})]$$

In other words, the total response of the system includes the response of the SDOF and participation of only $\sin(\frac{1\pi x}{L})$. To simplify the analytical solution, based on Fourier transformation, it is approximated that $[1 - \frac{4}{\pi}\sin(\frac{1\pi x}{L})] \approx 0$. Therefore, the second term on the right-hand side of Equation (4-69) can be canceled out. As a result, it is analytically proven that the total response of the coupled system relies mainly on the first mode.

To verify the accuracy of this approximation method, the numerical method is manipulated for two scenarios: first, the response of the system is obtained from the contributions of modes 1; and second, the response of the system is derived from the contributions of modes 1, 3, 5, and 7. The outcome of the numerical model in Figure (4.8) demonstrates that the results of both scenarios are approximately the same. This reveals that the coupled system is mainly affected by the first mode.

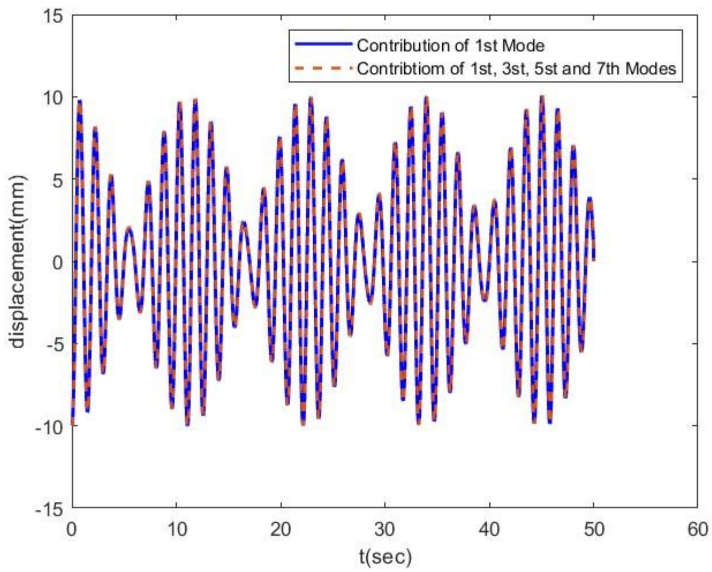

Fig. 4.8. Time history of the numerical displacements of the coupled system for two cases 1- The contribution of the first mode 2- the contribution of the first, third, fifth and seventh modes

An analytical approach relying only on the first mode for the free vibration of the coupled system with initial displacement is expressed in Equation (4-70).

$$X = [B\cos(\omega_1 t) + D\cos(\omega_1 t)] \tag{4-70}$$

where *B, D* are obtained from the initial boundary conditions which $X(0) = -0.01,\ \ddot{X}(0) = -k\dfrac{X(0)}{m}$. The total response derived from Equation (4-70) is presented in Figure (4.9). In addition, the figure (4.9) contains the numerical results, which show great agreement with the analytical solution.

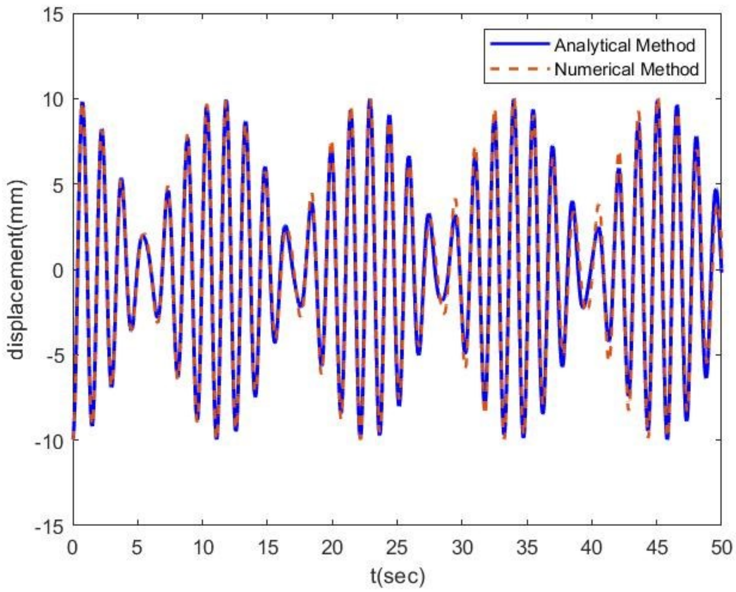

Fig. 4.9. Time history of the analytical and numerical displacements of the coupled system from the contribution of the first mode

4.4.4. Further validation

4.4.4.1 Second-order finite difference scheme

A numerical solution, which is not based on the mode coordinate system, is employed to solve the system of equations (4-71) to validate the accuracy and reliability of the current analytical approach. Specifically, the fluid equations (4-71-1) and (4-71-2) were solved using the semi-implicit Preismann scheme, which is known for its second-order accuracy in both time and space, resulting in a matrix equation (Wang et al. 2019). Meanwhile, the single degree of freedom equation (4-71-3) was addressed using the second-order finite difference method (Humar, 2012), coupled with the fluid governing equation via the partitioned method (Liao and Hu, 2013). Equation (4-71-4), representing the disparity in pressure force between the right wall ($x=L$) and left wall ($x=0$) of the tank, was utilized for calculating the sloshing force. Notably, Figure (4-10) demonstrates good agreement between the current analytical solution and the numerical results.

$$\frac{\partial \eta}{\partial t} + H\frac{\partial u}{\partial x} = 0 \quad (4\text{-}71\text{-}1)$$

$$\frac{\partial u}{\partial t} + g\frac{\partial \eta}{\partial x} = -\ddot{X} \quad (4\text{-}71\text{-}2)$$

$$m\ddot{X} + c\dot{X} + kX = F_{exc} + F_{slo} \tag{4-71-3}$$

$$F_{slo} = F_{RW} - F_{LW} = \frac{1}{2}\rho g[(\mathrm{H}+\eta_{x=L})^2 - (\mathrm{H}+\eta_{x=0})^2] \tag{4-71-4}$$

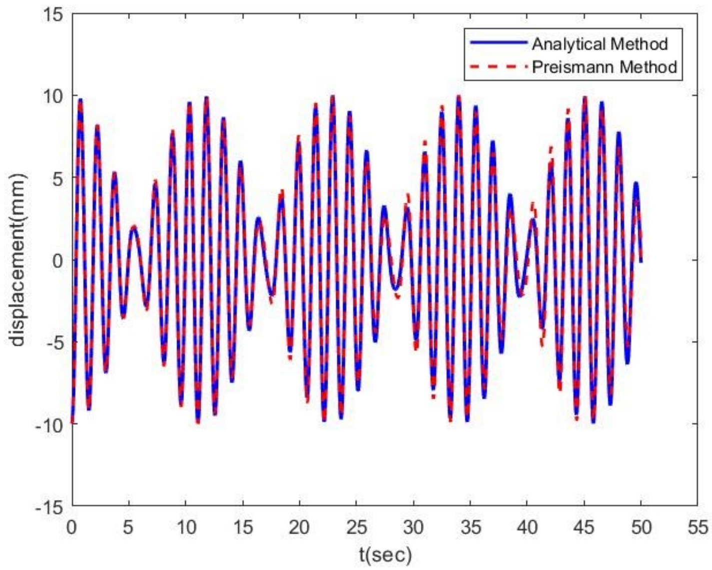

Fig. 4.10. Time history of the coupled system displacement subjected to free vibration

4.4.4.2 The impact of nonlinear terms

In this section, we investigate the significance of other terms, particularly nonlinear terms, because the current analytical coupled system predominantly relies on linear terms. To achieve this goal, a numerical model was devised based on the equations employed by Tait (2005) for a Tuned Liquid Damper simulation, specifically Equation (4-72). In this equation, h is the water depth, which is equivalent to the $H+\eta$ in the current analytical approach. This equation encompasses nonlinear terms, along with the dispersion term treated as a source terms implicitly. Additionally, the model relies on the central upwind scheme (Kurganov et al. 2002) and the minmode function (Mohammadian et al. 2007) for the flux and variables approximation within the control volume cells, respectively. Remarkably, the numerical model demonstrated proficiency in simulating nonlinear and asymmetric sloshing waves, particularly under harmonic excitation, with minimal numerical diffusion errors. For additional details on the numerical schemes and validation of the numerical model, please refer to Khanpour et al. (2024).

$$
\begin{aligned}
&\frac{\partial h}{\partial t}+\frac{\partial (uh)}{\partial x}=0 \\
&\frac{\partial (uh)}{\partial t}+\frac{\partial (u^2h+0.5gh^2)}{\partial x}=-ah-c_d uh+\frac{1}{3}h^3\frac{\partial^3 u}{\partial t\partial^2 x}
\end{aligned}
\tag{4-72}
$$

The fluid model, integrated with a single degree of freedom equation using the partitioned method (Liao and Hu 2013), underwent free vibration analysis with varying initial displacements, resulting in different sloshing wave amplitudes. The Tuned Liquid Damper employed in this study mirrors that utilized in the previous sections. A comparative analysis between the analytical and numerical results has been conducted using nondimensional parameters, as depicted in Figure (4-11). The outcomes reveal that while the analytical model yields precise results for small sloshing waves, its accuracy diminishes for higher sloshing waves. This discrepancy underscores the growing significance of the other terms in the equation, rendering the linear analytical approach less accurate in such scenarios.

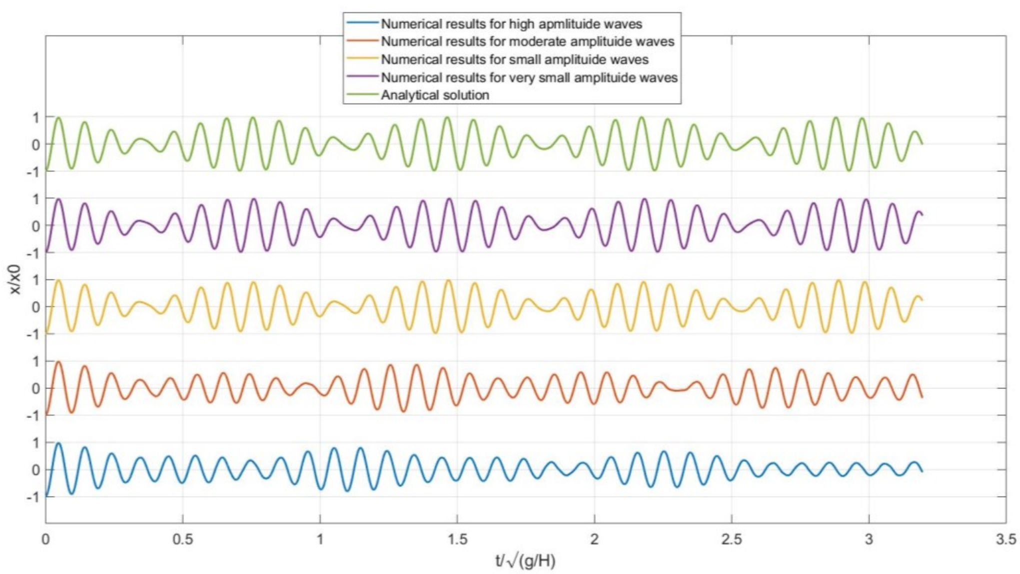

Fig. 4.11. Time history of the coupled system displacement subjected to free vibration with considering nonlinearity

4.5. Conclusion

This study primarily focuses on providing an analytical solution for the free vibration analysis of a coupled system involving a single degree of freedom and a sloshing shallow water tank. The analysis of free vibration is crucial because it yields the natural period of the system, which is a key determinant of its seismic behavior. The governing equations consist of linear shallow water equations for fluid dynamics and a dynamic equation for SDOF. The analytical approach involves transforming the free-surface wave and velocity into modal coordinates, allowing for the derivation of a fourth-order differential equation. This equation encompasses the continuity and momentum of the fluid, as well as the SDOF dynamics, showcasing each mode's contribution to the overall system response. Notably, while odd modes influence the response, even modes do not.

Solving the derived fourth-order differential equation yields a characteristic equation expressed as a fourth polynomial equation. This study delved into two essential conditions necessary for the stability of the system, confirming that the characteristic equation satisfies these conditions, rendering the coupled system unconditionally stable under free vibration. This analytical solution further reveals that the system exhibits two distinct natural periods emanating from the influence of each mode's contribution.

This research introduces four boundary conditions aimed at determining the coefficients of the sine and cosine functions present in the system's response. These conditions encompass not only the initial displacement and velocity but also the initial amplitudes of the fluid wave height and velocity. By leveraging modal decomposition and modal orthogonality principles, the approach extracts the initial displacement and velocity corresponding to each mode. Finally, the modal superposition technique is employed to attain the complete response of the system.

In the subsequent section of the study, the application of the developed analytical model to a single degree of freedom system coupled with a TLD is discussed. By analyzing the properties of the TLD and performing an order of magnitude analysis, it is shown that for modes higher than the first mode, the lower natural frequency closely aligns with the natural frequency of the SDOF. In addition, the higher frequency approximates n times the frequency of the SDOF, where n signifies the mode number. This analysis sheds light on the behavior of a system with TLD in relation to its various modes.

A numerical approach relying upon the separation of variables and modal decomposition was utilized for verification. Concerning the first mode contribution, the numerical model of the system subjected to initial displacement or velocity generated natural frequencies agrees well with the analytical results. Meanwhile, in the higher mode there is no contribution from greater frequency. The analytical model not only explains why in higher modes the response of the system undergoing the initial displacement is composed of only lower natural frequency but also reveals that the initial perturbation in terms of wave height or velocity is necessary to derive both frequencies of each mode. Subsequently, the numerical initial perturbation for the free vibration test generates two natural frequencies for each mode that agree well with the analytical prediction. This close agreement between the numerical findings and analytical approach reinforces the validity and effectiveness of the proposed methodology.

The numerical method demonstrates that the free vibration behavior of a Tuned Liquid Damper is primarily governed by the first mode. Similarly, the analytical approach presented in this study, which utilizes the modal coordinate system, supports the notion that the free vibration response can be effectively approximated using the first mode. Furthermore, the validity and accuracy of the model are confirmed when the second order Preismann method was employed to solve the relevant equations. Lastly, a developed and validated numerical model, incorporating nonlinear and dispersion terms, reveals that the current analytical model is accurate when the sloshing waves are small. However, for high-amplitude waves, the role of nonlinear terms becomes more pronounced, causing the analytical model to lose its accuracy.

References

Abd-Elhamed, A., & Tolan, M. (2022). Tuned liquid damper for vibration mitigation of seismic-excited structures on soft soil. *Alexandria Engineering Journal*, *61*(12), 9583-9599.

Antuono, M., Bouscasse, B., Colagrossi, A., & Lugni, C. (2012). Two-dimensional modal method for shallow-water sloshing in rectangular basins. *Journal of Fluid Mechanics*, *700*, 419-440.

Ardakani, H. A., & Bridges, T. J. (2012). Shallow-water sloshing in vessels undergoing prescribed rigid-body motion in two dimensions. *European Journal of Mechanics-B/Fluids*, *31*, 30-43.

Ashasi-Sorkhabi, A., Malekghasemi, H., Ghaemmaghami, A., & Mercan, O. (2017). Experimental investigations of tuned liquid damper-structure interactions in resonance considering multiple parameters. *Journal of Sound and Vibration*, *388*, 141-153.

Awad, B. N., & Tait, M. J. (2022). Macroscopic modelling for screens inside a tuned liquid damper using incompressible smoothed particle hydrodynamics. *Ocean Engineering*, *263*, 112320.

Baghban, M. H., Razavi Tosee, S. V., Valerievich, K. A., Najafi, L., & Faridmehr, I. (2022). Seismic Analysis of Baffle-Reinforced Elevated Storage Tank Using Finite Element Method. *Buildings*, *12*(5), 549.

Bahreini Toussi, I., Kianoush, R., & Mohammadian, A. (2020). Numerical and Experimental Investigation of Rectangular Liquid-Containing Structures under Seismic Excitation. *Infrastructures*, *6*(1), 1.

Banerji, P., Murudi, M., Shah, A. H., & Popplewell, N. (2000). Tuned liquid dampers for controlling earthquake response of structures. *Earthquake engineering & structural dynamics*, *29*(5), 587-602.

Banerji, P., Samanta, A., & Chavan, S. A. (2010). Earthquake vibration control of structures using tuned liquid dampers: experimental studies. *International Journal of Advanced Structural Engineering*, *2*(2), 133-152.

Bhattacharjee, E., Halder, L., & Sharma, R. P. (2013). An experimental study on tuned liquid damper for mitigation of structural response. *International Journal of Advanced Structural Engineering*, *5*, 1-8.

Cao, X. Y., Ming, F. R., & Zhang, A. M. (2014). Sloshing in a rectangular tank based on SPH simulation. *Applied Ocean Research*, *47*, 241-254.

Chaiviriyawong, P., Webster, W. C., Pinkaew, T., & Lukkunaprasit, P. (2007). Simulation of characteristics of tuned liquid column damper using a potential-flow method. *Engineering Structures*, *29*(1), 132-144.

Crowley, S., & Porter, R. (2012). An analysis of screen arrangements for a tuned liquid damper. *Journal of Fluids and Structures*, *34*, 291-309.

Elkholy, S. A., Elsayed, A. A., El-Ariss, B., & Sadek, S. A. (2014). Optimal finite element modelling for modal analysis of liquid storage circular tanks. *International Journal of Structural Engineering*, *5*(3), 207-241.

Faltinsen, O. M., Rognebakke, O. F., Lukovsky, I. A., & Timokha, A. N. (2000). Multidimensional modal analysis of nonlinear sloshing in a rectangular tank with finite water depth. *Journal of fluid mechanics*, *407*, 201-234.

Fuchs, S. L., Meier, C., Wall, W. A., & Cyron, C. J. (2021). A novel smoothed particle hydrodynamics and finite element coupling scheme for fluid–structure interaction: The sliding boundary particle approach. *Computer methods in applied mechanics and engineering*, *383*, 113922.

Fujino, Y., Sun, L., Pacheco, B. M., & Chaiseri, P. (1992). Tuned liquid damper (TLD) for suppressing horizontal motion of structures. *Journal of engineering mechanics*, *118*(10), 2017-2030.

Ghaemmaghami, A. R., & Kianoush, M. R. (2010). Effect of wall flexibility on dynamic response of concrete rectangular liquid storage tanks under horizontal and vertical ground motions. *Journal of structural engineering*, *136*(4), 441-451.

Housner, G. W. (1963). The dynamic behavior of water tanks. *Bulletin of the seismological society of America*, *53*(2), 381-387.

Humar, J. (2012). *Dynamics of structures*. CRC press.

Kamarroudi, S. H., Hosseini, M., & Hosseini, K. (2021). Influence of earthquake vertical excitations on Sloshing-Created P-Δ effect in elevated water Tanks: Experimental Validation, numerical simulation and proposing a modification for Housner model. *Engineering Structures*, *246*, 112995.

Khanpour, M., Mohammadian, A., Shirkhani, H., & Kianoush, R. (2024). Simulation of sloped bed Tuned Liquid Dampers using nonlinear shallow water model. *Water*, *(under review)*.

Koh, C. G., Mahatma, S., & Wang, C. M. (1994). Theoretical and experimental studies on rectangular liquid dampers under arbitrary excitations. *Earthquake engineering & structural dynamics*, *23*(1), 17-31.

Kurganov, A., & Levy, D. 2002. Central-upwind schemes for the Saint-Venant system. ESAIM: Mathematical Modelling and Numerical Analysis, 36(3), 397-425.

Liao, K., & Hu, C. (2013). A coupled FDM–FEM method for free surface flow interaction with thin elastic plate. *Journal of marine science and technology*, *18*, 1-11.

Liu, D., & Lin, P. (2008). A numerical study of three-dimensional liquid sloshing in tanks. *Journal of Computational physics*, *227*(8), 3921-3939.

Livaoglu, R. A. M. A. Z. A. N., & Dogangun, A. (2007). Effect of foundation embedment on seismic behavior of elevated tanks considering fluid–structure-soil interaction. *Soil Dynamics and Earthquake Engineering*, *27*(9), 855-863

Malekghasemi, H., Ashasi-Sorkhabi, A., Ghaemmaghami, A. R., & Mercan, O. (2015). Experimental and numerical investigations of the dynamic interaction of tuned liquid damper–structure systems. *Journal of Vibration and Control*, *21*(14), 2707-2720.

Marivani, M., & Hamed, M. S. (2009). Numerical simulation of structure response outfitted with a tuned liquid damper. *Computers & structures*, *87*(17-18), 1154-1165.

Mishra, A. (2023). Seismic assessment of different vertical bracing systems in staging of elevated liquid retaining tank. *Materials Today: Proceedings*.

Mohammadian, A., Le Roux, D. Y., & Tajrishi, M. (2007). A conservative extension of the method of characteristics for 1-D shallow flows. *Applied mathematical modelling*, *31*(2), 332-348.

Moslemi, M., & Kianoush, M. R. (2016). Application of seismic isolation technique to partially filled conical elevated tanks. *Engineering Structures*, *127*, 663-675.

Moslemi, M., Farzin, A., & Kianoush, M. R. (2019). Nonlinear sloshing response of liquid-filled rectangular concrete tanks under seismic excitation. *Engineering Structures*, *188*, 564-577.

Moslemi, M., Kianoush, M. R., & Pogorzelski, W. (2011). Seismic response of liquid-filled elevated tanks. *Engineering structures*, *33*(6), 2074-2084.

Murudi, M., & Banerji, P. (2012). Effective control of earthquake response using tuned liquid dampers. *Journal of Earthquake Technology*, *49*(3-4), 53-71.

Ocak, A., Bekdaş, G., Nigdeli, S. M., Kim, S., & Geem, Z. W. (2022). Optimization of tuned liquid damper including different liquids for lateral displacement control of single and multi-story structures. *Buildings*, *12*(3), 377.

Olson, D. E., & Reed, D. A. (2001). A nonlinear numerical model for sloped-bottom tuned liquid dampers. *Earthquake engineering & structural dynamics*, *30*(5), 731-743.

Pandit, A. R., & Biswal, K. C. (2020, June). Seismic control of multi degree of freedom structure outfitted with sloped bottom tuned liquid damper. In *Structures*, (25), 229-240.

Rawat, A., Mittal, V., Chakraborty, T., & Matsagar, V. (2019). Earthquake induced sloshing and hydrodynamic pressures in rigid liquid storage tanks analyzed by coupled acoustic-structural and Euler-Lagrange methods. *Thin-Walled Structures*, *134*, 333-346.

Robinson-Mosher, A., Shinar, T., Gretarsson, J., Su, J., & Fedkiw, R. (2008). Two-way coupling of fluids to rigid and deformable solids and shells. *ACM Transactions on Graphics (TOG)*, *27*(3), 1-9.

Saburin, D. S. (2015). Tank sloshing simulations in shallow-water approximation. In *MARINE VI: proceedings of the VI International Conference on Computational Methods in Marine Engineering* (pp. 1039-1050). CIMNE.

Sun, L. M., & Fujino, Y. (1994). A semi-analytical model for tuned liquid damper (TLD) with wave breaking. *Journal of Fluids and Structures*, *8*(5), 471-488.

Sun, L. M., Fujino, Y., Pacheco, B. M., & Chaiseri, P. (1992). Modelling of tuned liquid damper (TLD). *Journal of Wind Engineering and Industrial Aerodynamics*, *43*(1-3), 1883-1894.

Sun, Y., Xi, G., & Sun, Z. (2021). A generic smoothed wall boundary in multi-resolution particle method for fluid–structure interaction problem. *Computer Methods in Applied Mechanics and Engineering*, *378*, 113726.

Tait, M. J., El Damatty, A. A., Isyumov, N., & Siddique, M. R. (2005). Numerical flow models to simulate tuned liquid dampers (TLD) with slat screens. *Journal of Fluids and Structures*, *20*(8), 1007-1023.

Takahashi, T., & Lin, M. C. (2019, May). A Geometrically Consistent Viscous Fluid Solver with Two-Way Fluid-Solid Coupling. In *Computer Graphics Forum* (Vol. 38, No. 2, pp. 49-58).

Toro, E. F. (2001). *Shock-capturing methods for free-surface shallow flows* (pp. 1-309). Wiley and Sons Ltd..

Veletsos, A. S., Tang, Y., & Tang, H. T. (1992). Dynamic response of flexibly supported liquid-storage tanks. *Journal of Structural Engineering*, *118*(1), 264-283.

Wang, Yanmei & Zhang, Chengcai & Li, Zhansong & Sun, Bin & Zhou, Haolan. (2019). Applicability of Preissmann box scheme for calculation of transcritical flow in pipes. Water Science and Technology: Water Supply. 19 (5): 1429–1437.

Wu, G. X., Ma, Q. W., & Taylor, R. E. (1998). Numerical simulation of sloshing waves in a 3D tank based on a finite element method. *Applied ocean research*, *20*(6), 337-355.

Xie, T., Li, M., Yang, Y., & Jiang, C. (2023). A Contact Proxy Splitting Method for Lagrangian Solid-Fluid Coupling. *ACM Transactions on Graphics (TOG)*, *42*(4), 1-14.

Zhang, Y., Chen, D., Qian, H., Chen, Z., Fan, F., & Khoo, B. C. (2024). An Efficient Partitioned Framework to Couple Arbitrary Lagrangian-Eulerian and Meshless Vector Form Intrinsic Finite Element Methods for Fluid-Structure Interaction Problems with Deformable Structures. *Applied Mathematical Modelling*.

List of Symbols

H	Mean water level
η	Wave height
u	Depth- average velocity
m	Mass of SDOF
k	Stiffness of SDOF
c	Damping coefficient of SDOF
X	Displacement of SDOF
$\dot{X}$	Velocity of SDOF
$\ddot{X}$	Acceleration of SDOF
F_{exc}	Excitation force on SDOF
F_{slo}	Sloshing Force on SDOF
L	Length of the water tank
ρ	Water density
g	Gravity acceleration
b	Width of the water tank
ω_1	Smaller natural frequency of the coupled system
ω_2	greater natural frequency of the coupled system
X_0	Initial displacement of the coupled system

$\dot{X}_0$	Initial velocity of the coupled system
$\ddot{X}_0$	Initial acceleration of the coupled system
A_0	Initial wave height perturbation
B_0	Initial wave velocity perturbation
$\omega_{1,n}$	Smaller natural frequency of the coupled system of the mode n
$\omega_{2,n}$	greater natural frequency of the coupled system of the mode n
$X_{0,n}$	Initial displacement of the coupled system of the mode n
h	Total Water depth

5. Analytical Solution to The Free Vibration of The Shallow Water Elevated Tank with Considering Dissipations- Case Study: Tuned Liquid Dampers[4]

Abstract

The shallow water equations, incorporating appropriate shape functions, undergo transformation into a modal coordinate system. This transformation couples these equations with the dynamics of a single degree of freedom, yielding a fourth-order ordinary differential equation that represents the coupled system's displacement for each mode, accounting for fluid and structural dissipation. The innovative solution generates a comprehensive fourth-order polynomial equation, known as the characteristic equation, encompassing natural frequencies and dissipation rates. Manipulating this equation allowed for in-depth discussions on stability and dynamic properties of a coupled system concerning dissipation. After introduction of a novel solution to derive the response coefficients and modal techniques, the analytical model was implemented on a Tuned Liquid Damper (TLD) for analysis. To assess the accuracy of the assumptions and derived analytical formulas for natural frequencies and dissipation factors, a developed numerical model and Fast Fourier Transform (FFT) were employed. Establishing the primary influence of the first mode on TLDs, the analytical model proposes a novel solution for TLDs equipped with screens. Across all cases, accounting for dissipation in both initial displacement and initial perturbation scenarios, the model consistently produces accurate and closed form solutions, demonstrating the precision and efficiency of the innovative analytical method developed.

Keywords: Free Vibration of Shallow Water Elevated Tanks; Modal Decomposition and Stability Analysis; Tuned Liquid Dampers; Structural, Fluid, and Screen Dissipations; Dissipation of TLD Coupled System Response; First Mode Dominance

---

[4] Mahdiyar Khanpour ," *Analytical Solution to The Free Vibration of The Shallow Water Elevated Tank with Considering Dissipations- Case Study: Tuned Liquid Dampers*", **International Journal of Mechanical Sciences (IJMS)**, Submitted

5.1. Introduction

Liquid storage tanks play a pivotal role in various industries, particularly in engineering disciplines. When these tanks undergo seismic excitation, the resulting sloshing waves exert hydrodynamic pressure, which can potentially jeopardizes their stability. Therefore, researchers have explored the seismic characteristics of tanks by utilizing certain assumptions to simplify the complexities arising from the distinct dynamic properties of fluids and structures, as well as the interaction between the fluid and the structure. They consider a range of factors affecting the tank's dynamic response, including the support structure presence (elevated tank) (Zhou & Zhao, 2021 and Kamarroudi et al. 2021) , tanks' shape impact (Xue et al., 2019), wall flexibility (Ghaemmaghami & Kianoush, 2010 and Strand & Faltinsen, 2017), base connection type (Moslemi & Kianoush 2012) , soil-structure interaction (Hernandez et al., 2021 and Meng et al., 2022), elevated tank's P-delta effect (Kamarroudi et al., 2022), roof presence (Bahreini et al.,2020 and Goudarz et al., 2010) , base isolation presence (Saha, 2014 and Narayanasetti et al., 2022) , screen presence (Panigrahy et al. 2007 and Huang 2023), and water depth (fill level) (Lu et al. 2018 and Aedo et al. 2020). Some studies have specifically examined excitation characteristics and their impact on the response, such as vertical acceleration (Ghaemmaghami & Kianoush 2010 and Martínez & González, 2021), resonance excitation (Frandsen, 2004), bi-directional excitation (Bahreini et al., 2020) and impulse blast excitations (Mittal et al., 2014), sway, heave, roll excitations (Chen & Wu, 2011), and both near- and far-field excitations (Vern et al., 2021)

Various methods have been adopted to incorporate fluid sloshing, the first of which relies on the groundbreaking analytical approach proposed by Housner (1957), in which the fluid is divided into convective and impulsive parts. Subsequently, shallow water models, depth-averaged models (Sun et al., 1992, Antuono et al., 2012 and Saburin 2015) and potential theory (Hu et al., 2018 and Faltinsen et al., 2011) offer a more realistic picture of fluid sloshing yet they are limited to small wave amplitudes. Additionally, the Volume of Fluid (VOF) (Elahi et al., 2015 and Liu & Lin, 2008) and Smoothed Particle Hydrodynamics (SPH) (Pilloton et al., 2022 and Cao et al., 2014) have been proposed to simulate violent sloshing waves.

The Tuned Liquid Damper (TLD), a specific type of sloshing tank installed atop structures, mitigates vibrations during excitation. For optimal performance, the natural frequency of the sloshing tank should align with that of the structure while ensuring that its mass remains significantly smaller than the structure's mass (Sun et al., 1992; Fujino et al., 1992). Following the emergence of TLDs as passive dampers, extensive research has focused on optimizing their performance with respect to various parameters. These include the mass ratio (Sorkhabi et al., 2017), frequency ratio (Sun et al., 1992), tank shape (Gardarsson et al., 2001; Pandit & Biswal, 2020), screen presence and arrangement (Tait et al., 2005; Crowley & Porter, 2012), water fill levels (Bhattacharjee et al., 2013), modified connections between the TLD and structure (Chang et al., 2018), and inclusion of an inerter-based subsystem, TLIS (Zhao et al., 2019).

The methodologies used to simulate fluid sloshing tanks can be adapted for Tuned Liquid Dampers (TLDs). Because TLDs typically operate as shallow water tanks, employing shallow water models appears to be a suitable approach. Additionally, unlike the potential flow and Volume of Fluid (VOF) methods, shallow water models do not require extra equations for tracking free surfaces, making them advantageous for TLD simulations. `

Several studies have explored free vibration analyses of sloshing tanks. Tedesco et al. (1987) conducted numerical investigations on the free vibrational behavior of cylindrical liquid storage tanks. They utilized a shell-fluid system to examine two coupled systems: (1) the shell structure combined with a stationary fluid mass, and (2) the sloshing fluid mass. Cho et al. (2002) utilized a symmetric structural-acoustic finite element formulation to analyze the free vibration characteristics of liquid storage tanks, both with and without baffles. Amabili (1996) proposed an analytical solution for the free vibration of shell elements, albeit without considering the effect of the free surface. Han et al. (2022) subsequently modified this method by incorporating the sloshing effect of the free surface. Biswal (2003) utilized the finite element method to determine the natural frequencies of liquid within a liquid-filled cylindrical rigid tank, examining scenarios with and without baffles. Hu et al. (2018) employed the Boundary Element Method (BEM) to analyze the free vibration of two-dimensional baffled tanks featuring arbitrary geometries. Additionally, Rezaiee et al. (2019) analyzed the free vibration of liquid sloshing within a partially filled two-dimensional flexible rectangular tank.

Although a few numerical rare analytical studies have been conducted based on linear wave theory, this study distinguishes itself by offering a new approach to shallow elevated tanks subjected to free vibration. This study presents a characteristic equation resulting from coupling the linear shallow water equation, expressed in a modal coordinate system, with single degree of freedom motion. The innovative analytical approximation based on the characteristic equation offers novel solutions to important questions regarding the dynamics of the coupled system. For instance, it addresses how fluid and structural dissipation affect the natural frequency of the coupled system and examines the stability of the coupled system in free vibration concerning structural and fluid dissipations. This approach introduces novel analytical relationships for the dissipation of the coupled system's response, explaining which factors influence response dissipation. The current analytical approach introduces a vector initial condition to derive the analytical response of the coupled system, incorporating both structural and fluid dissipation. Then, this original model focuses on the coupled system, including a single degree of freedom and a Tuned Liquid Damper (TLD), referred to as the TLD coupled system. Fast Fourier Transform and a verified numerical model based on linear shallow water equations coupled with single degree of freedom motion were presented to assess the accuracy of the analytical approach. The original analytical method, alongside the numerical model, investigates crucial concepts for the damped TLD coupled system, including the effect of dissipations on natural frequencies, dissipation factors, initial perturbation for the stimulation of higher frequencies, and the domination of the first mode in the total response. It offers an analytical closed-form solution for the displacement of a damped TLD coupled system in both initial displacement and initial perturbation, marking a milestone finding in the literature. Finally, the current analytical model incorporates a linearized mode assumption and is creatively modified for the TLD coupled system outfitted with screens to investigate natural frequencies, dissipation factors, and total response.

5.2. Governing Equations & Methodology

The current research employed an analytical approach to couple a shallow tank with an underlying single degree of freedom system while considering dissipation (Figure5. 1). This analytical method utilizes the linear shallow water equation, incorporating fluid dissipation, to model sloshing waves. In Equations (5-1-1) and (5-1-2), u and h represent the fluid velocity and depth, respectively, both of which are functions of space (x) and time (t). The parameter h denotes the wave height, and H represents the mean water level. All these parameters are depicted in Figure (5.1).

$\ddot{X}$ represents the acceleration of the tank. The term $c_f u$ accounts for fluid dissipation (Sun et al., 1992; Fujino et al., 1992; Tait et al., 2005), and C_f is the fluid dissipation constant. The system comprises the continuity equation (5-1-1) and the momentum equation (5-1-2).

$$\frac{\partial h}{\partial t}+H\frac{\partial u}{\partial x}=0 \tag{5-1-1}$$

$$\frac{\partial u}{\partial t}+g\frac{\partial h}{\partial x}=-\ddot{X}-C_f u \tag{5-1-2}$$

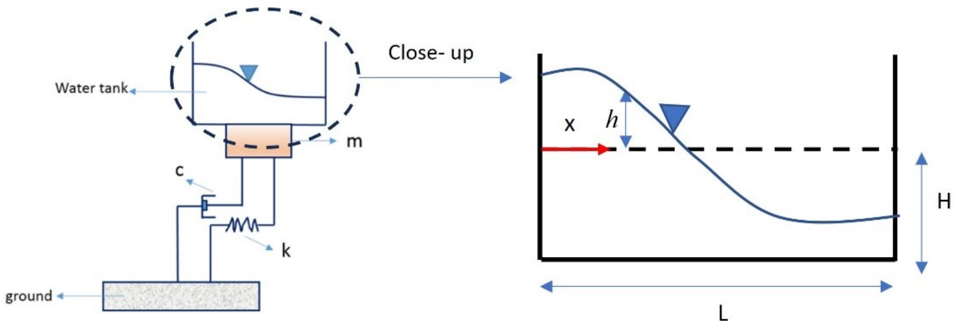

Fig. 5.1. Schematic of a coupled system in the current research

The separation of variables technique is applied to the dependent variables *h* and *u*. In this approach, the parameters *h* and *u* can be expressed as in Equation (5-2), with the corresponding $\cos(\frac{n\pi x}{L})$ and $\sin(\frac{n\pi x}{L})$ as shape functions for each mode, denoted as *n*. These shape functions satisfy the boundary conditions, including the zero gradient height and zero velocity for *h* and *u*, respectively, at the tank's walls ($x=0$ & $x=L$). In this equation, A_n and B_n are the sole functions of time for each mode.

$$h=\sum_{n=1}^{N}A_n\cos(\frac{n\pi x}{L}) \ \& \ u=\sum_{n=1}^{N}B_n\sin(\frac{n\pi x}{L}) \tag{5-1-1}$$

The Fourier transformation of constant 1 can be written as:

$$1=\sum_{n=1}^{N} M_n \sin(\frac{n\pi x}{L})$$
$$where\, M_n = -2\frac{(-1)^n - 1^n}{n\pi} = \begin{bmatrix} \frac{4}{n\pi} \quad for\ n=2k+1 \\ 0 \quad for\ n=2k \end{bmatrix} \tag{5-3}$$

Substituting equations (5-2) and (5-3) into equations (5-2-1) and (5-2-2) yields the following expression: To put it simply, applying the separation of variables technique to the partial differential equations in system (5-1) results in the system of ordinary differential equations (5-4).

$$\dot{A}_n = -B_n H \frac{n\pi}{L} \tag{5-4-1}$$

$$\dot{B}_n - gA_n \frac{n\pi}{L} = -\ddot{X}M_n - C_f B_n \tag{5-4-2}$$

Taking the derivative of the equation (5-4-1) with respect to time and performing some operations leads to Equation (5-5):

$$\dot{B}_n = -\frac{L}{Hn\pi}\ddot{A}_n \tag{5-5}$$

Substituting B_n and $\dot{B}_n$ from equations (5-4-1) and (5-5) into equation (5-4-2) and simplifying, the following expression is developed for each mode. Evidently, using presented scheme, the continuity and momentum equations are combined and transformed from the Cartesian coordinate system to the modal coordinate system.

$$\ddot{A}_n + C_f \dot{A}_n + K_{1n} A_n - K_{2n}\ddot{X} = 0$$
$$where\ K_{1n} = \frac{Hgn^2\pi^2}{L^2} > 0 \ \ \&\ \ K_{2n} = \frac{Hn\pi}{L} M_n = \begin{Bmatrix} 0 \quad for\, n=2k \\ 4\frac{H}{L} \quad for\, n=2k+1 \end{Bmatrix} \tag{5-6}$$

Where K_{1n} and K_{2n} are positive coefficients that depend on mode number, depth, and length of the water tank. According to Equation (5-6), in contrast to odd modes, in even modes, the parameter K_{2n} equals zero, signifying that fluid sloshing is not influenced by tank acceleration.

As depicted in Figure (5.1), the other component of the coupled system in this study is an underlying single degree of freedom (SDOF). This coupling system can represent various structures, such as shallow elevated tanks, tuned liquid dampers, fluid tanks on spring isolators, or rooftop pools. The dynamic equation of the SDOF is characterized by parameters such as mass (*m*), stiffness (*K*), and damping coefficient (*c*), and can be represented as Equation (5-7).

$$m\ddot{X}(t) + c\dot{X}(t) + kX(t) = F_{slo}(t) + G(t) \tag{5-7}$$

In this equation, the variables $\ddot{X}(t)$, $\dot{X}(t)$, and $X(t)$ represent the acceleration, velocity, and displacement of SDOF, respectively. Consequently, $m\ddot{X}(t)$, $c\dot{X}(t)$, and $kX(t)$ correspond to inertia force, damping force, and stiffness forces, respectively. The terms $F_{slo}(t)$ and $G(t)$ denote the excitation force and sloshing forces, respectively. Since the current study focuses on the free vibration of a coupled system, the excitation force is disregarded, with emphasis placed on the role of the sloshing force. The coupling between the fluid equations and the SDOF equation hinges on two key parameters: SDOF acceleration and sloshing force.

In a prior study (Khanpour et al. 2024), expression (5-8) for the sloshing force associated with each mode was developed. In this equation, F_{slo} represents the sloshing force due to the contribution of mode *n* and k_{3n} is a positive coefficient that depends on the water depth *H*, tank width *b*, and water density ρ. As anticipated, based on this equation, the sloshing force affects the response of the SDOF system only for odd modes, and remains inactive for even modes.

$$\begin{aligned} &F_{slo} = -K_{3n} A_n \\ &where \\ &K_{3n} = \left\{ \begin{matrix} 0 & for\ n = 2i \\ 2\rho g H b & for\ n = 2i+1 \end{matrix} \right\} \quad k_{3n} \geq 0 \end{aligned} \tag{5-8}$$

Consequently, the dynamic equation of the single degree of freedom (SDOF) system resulting from the sloshing force of mode *n* can be expressed as follows:

$$m\ddot{X} + c\dot{X} + kX = -K_{3n} A_n \tag{5-9}$$

According to the above equation, parameter A_n can be derived from Equation (5-10).

$$A_n = (-\frac{m}{K_{3n}})\ddot{X} + (-\frac{c}{K_{3n}})\dot{X} + (-\frac{k}{K_{3n}})X \tag{5-10}$$

The first and second derivatives of the above equation with respect to time lead to expressions (5-11) and (5-12), respectively.

$$\dot{A}_n = (-\frac{m}{K_{3n}})\dddot{X} + (-\frac{c}{K_{3n}})\ddot{X} + (-\frac{k}{K_{3n}})\dot{X} \tag{5-11}$$

$$\ddot{A}_n = (-\frac{m}{K_{3n}})\ddddot{X} + (-\frac{c}{K_{3n}})\dddot{X} + (-\frac{k}{K_{3n}})\ddot{X} \tag{5-12}$$

After substituting A_n, $\dot{A}_n$, and $\ddot{A}_n$ from equations (5-10), (5-11), and (5-12), accordingly into equation (5-6) and applying some simplifications, the following relation is derived:

$$m\ddddot{X} + (c + C_f m)\dddot{X} + (k + C_f c + K_{1n}m + K_{2n}K_{3n})\ddot{X} + (kC_f + K_{1n}c)\dot{X} + (K_{1n}k)X = 0 \tag{5-13}$$

Equation (5-13) represents a fourth-order ordinary equation, incorporating the continuity and momentum equations of the fluid, as well as the dynamic equation of the SDOF. This equation describes the response of the SDOF in free vibration when subjected to the sloshing force generated by the contribution of mode *n*, and it accounts for both structural and fluid dissipation.

5.2.1. First scenario: No dissipation in fluid and structure:

This scenario, which neglects dissipation, was investigated thoroughly by Khanpour et al. 2024. In this case, *c* (structure dissipation) and C_f (fluid dissipation) are removed from Equation (5-13) to obtain Equation (5-14).

$$m\ddddot{X} + (k + K_{1n}m + K_{2n}K_{3n})\ddot{X} + (K_{1n}k)X = 0 \tag{5-14}$$

The solution to this equation is in the form of $e^{\lambda t}$. Applying this solution to equation (5-14) leads to the characteristic equation presented in Equation (5-15).

$$(m)\lambda^4 + (k + mK_{1n} + K_{2n}K_{3n})\lambda^2 + (kK_{1n}) = 0 \tag{5-15}$$

The previous work focused on this scenario, discussing its stability requirements and demonstrating that the coupled system meets these conditions, rendering it unconditionally stable.

The roots of the characteristic equation are complex numbers without a real part, taking the forms of $\lambda_1 = i\omega_1$ and $\lambda_2 = i\omega_2$. Hence, the values of ω_1 and ω_2, which represent the natural frequencies of the coupled system for each mode, satisfy Equation (5-16-1) and can be derived using Equation (5-16-2).

$$(m)\omega^4 - (k + mK_{1n} + K_{2n}K_{3n})\omega^2 + (kK_{1n}) = 0 \tag{5-16-1}$$

$$\omega_1 = \sqrt{(\frac{p+\sqrt{\Delta}}{2m})} \quad and \quad \omega_2 = \sqrt{(\frac{p-\sqrt{\Delta}}{2m})} \tag{5-16-2}$$
$$where \;\; p = k + mK_{1n} + K_{2n}K_{3n} \;\; and \;\; q = kK_{1n} \; and \;\; \Delta = p^2 - 4mq$$

It is evident that the natural frequencies are functions of the stiffness and mass of the structure, water depth, length and width of the tank, and mode number.

5.2.2. Second scenario: Structure dissipation and fluid dissipation are active:

The characteristic equation of Equation (5-13) takes the form of expression (5-17). This novel equation plays a significant role in analyzing the dynamics of the damped coupled system, where both structural and fluid dissipation are considered. Clearly, in this scenario, the characteristic equation is a complete fourth-order polynomial in contrast to the previous scenario.

$$m\lambda^4 + (c + C_f m)\lambda^3 + (k + C_f c + K_{1n}m + K_{2n}K_{3n})\lambda^2 + (kC_f + K_{1n}c)\lambda + (K_{1n}k) = 0 \tag{5-17}$$

Remark: the characteristic equation (5-17) has two complex conjugate pair roots:

Proof: Dividing both sides of equation (5-17) by k yields the following expression.

$$\frac{m}{k}\lambda^4 + (\frac{c}{k} + C_f\frac{m}{k})\lambda^3 + (1 + \frac{C_f c}{k} + K_{1n}\frac{m}{k} + \frac{K_{2n}K_{3n}}{k})\lambda^2 + (C_f + K_{1n}\frac{c}{k})\lambda + (K_{1n}) = 0 \tag{5-18}$$

The natural angular frequency of the SDOF, ω_s, and the damping ratio, ξ, are determined from Equations (5-19) and (5-20), respectively. The c_{cr} in equation (5-20) is critical damping. The damping ratio in the regular structure ranges from 0.001 to 0.05.

$$\omega_s = \sqrt{\frac{k}{m}} \tag{5-19}$$

$$\xi = \frac{c}{c_{cr}} \quad where \quad c_{cr} = 2m\omega_s = 2\sqrt{km} \tag{5-20}$$

With respect to the above equations, it can be inferred that $\frac{m}{k} = \frac{1}{{\omega_s}^2}$ and $\frac{c}{k} = \frac{2\xi}{\omega_s}$. Substituting these values into Equation (18) yields Equation (21):

$$\frac{1}{\omega_s^2}\lambda^4 + (\frac{2\xi}{\omega_s} + \frac{C_f}{\omega_s^2})\lambda^3 + (1 + \frac{2\xi C_f}{\omega_s} + \frac{K_{1n}}{\omega_s^2} + \frac{K_{2n}K_{3n}}{k})\lambda^2 + (C_f + K_{1n}\frac{2\xi}{\omega_s})\lambda + (K_{1n}) = 0 \tag{5-21}$$

Consider the complete fourth-order polynomial equation (5-21) in the form of $\hat{a}\lambda^4 + \hat{b}\lambda^3 + \hat{c}\lambda^2 + \hat{d}\lambda + \hat{e} = 0$ where

$\hat{a} = (\frac{1}{\omega^2}),\ \hat{b} = (\frac{2\xi}{\omega_s} + \frac{C_f}{\omega_s^2}),\ \hat{c} = (1 + \frac{2\xi C_f}{\omega_s} + \frac{K_{1n}}{\omega_s^2} + \frac{K_{2n}K_{3n}}{k}),\ \hat{d} = (C_f + k_{1n}\frac{2\xi}{\omega}),\ \hat{e} = (k_{1n})$. In this equation, all constants are constituted from parameters $m, c, C_f, k, k_{1n}, k_{2n}, k_{3n}$ which are positive, so all constants of the fourth-order polynomial are positive $\hat{a},\ \hat{b},\ \hat{c},\ \hat{d}, \hat{e} > 0$. To explore the roots of the characteristic equation let's focus on the discriminant of the polynomial. The discriminant of a fourth-order equation, $\hat{\Delta}$, is defined based on Equation (5-22).

$$\begin{aligned}\hat{\Delta} &= 256\hat{a}^3\hat{e}^3 - 192\hat{a}^2\hat{b}\hat{d}\hat{e}^2 - 128\hat{a}^2\hat{c}^2\hat{e}^2 + 144\hat{a}^2\hat{c}\hat{d}^2\hat{e}^2 - 27\hat{a}^2\hat{d}^4 \\ &+ 144\hat{a}\hat{b}^2\hat{c}\hat{e}^2 - 6\hat{a}\hat{b}^2\hat{d}\hat{e} - 80\hat{a}\hat{b}\hat{c}^2\hat{d}\hat{e} + 18\hat{a}\hat{b}\hat{c}\hat{d}^3 + 16\hat{a}\hat{c}^4\hat{e} - 4\hat{a}\hat{c}^3\hat{d}^2 \\ &- 27\hat{b}^4\hat{e}^2 + 18\hat{b}^3\hat{c}\hat{d}\hat{e} - 4\hat{b}^3\hat{d}^3 - 4\hat{b}^2\hat{c}^3\hat{e} + \hat{b}^2\hat{c}^2\hat{d}^2\end{aligned} \tag{5-22}$$

In typical structures, $\frac{\xi}{\omega_s}$ is significantly smaller than one; therefore, with a high degree of accuracy, the square of $\frac{\xi}{\omega_s}$ approaches zero. Moreover, C_f in water tanks, originating from water viscosity, is generally small, typically on the order of magnitude of 0.01. In essence, both $\frac{\xi}{\omega_s}$ and $\frac{C_f}{\omega_s}$ are considerably small parameters. As a result, the square of $\frac{C_f}{\omega_s}$ can likewise be approximated as approaching zero. Evidently, the product of two small values, $\frac{\xi C_f}{\omega_s}$, is very close to zero.

Based on this discussion, the terms $\widehat{b}^2$, $\widehat{d}^2$ and $\widehat{b}\widehat{d}$ can be neglected. Under this assumption, the discriminant relation, represented by Equation (5-22), simplifies to $\widehat{\Delta} = 256\widehat{a}^3\widehat{e}^3 - 128\widehat{a}^2\widehat{c}^2\widehat{e}^2 + 16\widehat{a}\widehat{c}^4\widehat{e} = 16\widehat{a}\widehat{e}(4\widehat{a}\widehat{e} - \widehat{c}^2)^2 > 0$. In cases where $\widehat{\Delta} > 0$, the characteristic equation exhibits two possible root configurations: 1- Four distinct real roots and 2- Two pairs of complex conjugate roots.

To analyze these conditions further, two parameters, $\widehat{p} = 8\widehat{a}\widehat{c} - 3\widehat{b}^2$, and $\widehat{D} = 64\widehat{a}^3\widehat{e} - 16\widehat{a}^2\widehat{c}^2 + 16\widehat{a}\widehat{b}^2\widehat{c} - 16\widehat{a}^2\widehat{b}\widehat{d} - 3\widehat{b}^4$ are defined based on the references. Using order-of-magnitude approximations discussed above, these parameters reduce to $\widehat{p} = 8\widehat{a}\widehat{c}$ and $\widehat{D} = 64\widehat{a}^3\widehat{e} - 16\widehat{a}^2\widehat{c}^2 = 16\widehat{a}^2(4\widehat{a}\widehat{e} - \widehat{c}^2)$. Given that all constants of the characteristic equation are positive, it follows that $\widehat{p} > 0$.

Furthermore, if the term $\dfrac{2\xi C_f}{\omega_s}$ within $\widehat{c}$ is neglected (due to the multiplication of two small values, ξ and C_f), the equation $\widehat{a}\lambda^4 + \widehat{c}\lambda^2 + \widehat{e} = 0$ represents the characteristic equation for the undamped case, excluding fluid and structural dissipation. As demonstrated by Khanpour et al. (2024b), $\widehat{c}^2 - 4\widehat{a}\widehat{e} > 0$, which implies $\widehat{D} = 16\widehat{a}^2(4\widehat{a}\widehat{e} - \widehat{c}^2) < 0$.

Roots Classification:

If $\widehat{\Delta} > 0 \ and \ (\widehat{P} < 0 \ and \ \widehat{D} < 0)$, the characteristic equation possesses four distinct real roots.

If $\widehat{\Delta} > 0 \ and \ (\widehat{P} > 0 \ or \ \widehat{D} > 0)$, the characteristic equation yields two pairs of complex conjugate roots.

Consequently, in this case, based on the signs of $\widehat{\Delta}, \widehat{P}, and\ \widehat{D}$ the roots of the characteristic equation consist of two pairs of complex conjugate numbers.

In other words, as discussed in Khanpour et al. (2024b), the characteristic equation for the undamped case (excluding dissipation), $\widehat{a}\lambda^4 + \widehat{c}\lambda^2 + \widehat{e} = 0$, possesses two pairs of complex conjugate roots with zero real parts. The introduction of small perturbations $(\widehat{b}, \widehat{d})$ results in the emergence of small real parts in these previously purely imaginary roots.

Remark: the coupled system subjected to free vibration in this scenario is stable

First Proof: Based on previous research (Khanpour et al., 2024), a coupled system without dissipation under free vibration is unconditionally stable. Therefore, in this scenario, where structural dissipation is introduced and the structural response is damped, the coupled system remains stable.

Second proof: In accordance with the previous proof, the fourth-order characteristic polynomial contains two conjugate complex pair roots. Let us consider these roots to be $\lambda_1 = a_1 + \omega_1 i,\ \lambda_2 = a_1 - \omega_1 i,\ \lambda_3 = a_2 + \omega_2 i,\ \lambda_4 = a_2 - \omega_2 i$. As a result, the solution to the characteristic equation takes the form of equation (5-23).

$$X = e^{a_1 t}(\hat{A}e^{iw_1 t} + \hat{B}e^{-iw_1 t}) + e^{a_2 t}(\widehat{C}e^{iw_2 t} + \hat{D}e^{-iw_2 t}) \tag{5-23}$$

Applying some simplification and Moivre’s theorem, the response can be expressed as:

$$X = e^{a_1 t}(\hat{A}\cos(\omega_1 t) + \hat{B}\sin(\omega_1 t)) + e^{a_2 t}(\hat{C}\cos(\omega_2 t) + \hat{D}\sin(\omega_2 t)) \tag{5-24}$$

As per the above expression, the imaginary part of the characteristic roots holds a significant physical concept. These values represent the natural frequencies of the coupled system, which are crucial factors affecting the dynamic response. In addition, the real part of the characteristic equation roots influences the amplitude of the response; it can either amplify or dampen the response.

In light of the previous equation, if $a_1 \,\&\, a_2 < 0$, the coupled system response not only does not grow over time, but also diminishes with the passage of time. Consequently, in this case, the coupled system is unconditionally stable.

Assuming that the roots of the fourth-order polynomial characteristic equation are $(\lambda_1, \lambda_2, \lambda_3, \lambda_4)$, the characteristic equation can be reconstructed as follows:

$$(\lambda - \lambda_1)(\lambda - \lambda_2)(\lambda - \lambda_3)(\lambda - \lambda_4) = 0 \tag{5-25}$$

Substituting the assumed values of $(\lambda_1, \lambda_2, \lambda_3, \lambda_4)$ into Equation (5-25) results in Equation (5-26):

$$(\lambda - a_1 - b_1 i)(\lambda - a_1 + b_1 i)(\lambda - a_2 - b_2 i)(\lambda - a_2 + b_2 i) = 0 \tag{5-26}$$

Through mathematical operations, Equation (5-27) is derived from the preceding equation. Equation (5-27), constructed from the roots of the characteristic equation, is referred to as the reconstructed characteristic equation in this study:

$$
\begin{aligned}
&\lambda^4 + \tilde{A}\lambda^3 + \tilde{B}\lambda^2 + \tilde{C}\lambda + \tilde{D} = 0 \\
&where \\
&\tilde{A} = (-2a_1 - 2a_2) \quad \tilde{B} = (a_1^2 + 4a_1a_2 + a_2^2 + \omega_1^2 + \omega_2^2) \\
&\tilde{C} = (-2a_1^2a_2 - 2a_1a_2^2 - 2a_1\omega_2^2 - 2a_2\omega_1^2) \quad \tilde{D} = a_1^2a_2^2 + a_1^2\omega_2^2 + a_2^2\omega_1^2 + \omega_1^2\omega_2^2
\end{aligned}
\tag{5-27}
$$

Let us compare characteristic equation (5-17) and the reconstructed characteristic equation expression (5-27). In the characteristic equation, all coefficients are unconditionally positive. The reconstructed equation (5-27) features $\tilde{D}$, which remains positive, regardless of the signs of a_1 and a_2. However, if both a_1 and a_2 are negative, all coefficients $\tilde{A}$, $\tilde{B}$, and $\tilde{C}$ are unconditionally positive. Therefore, if both a_1 and a_2 are negative, it leads to both the characteristic equation and the reconstructed one sharing the same positive sign coefficients. As previously discussed, the negative values of a_1 and a_2 guarantee the stability of the coupled system in this scenario. Since e^{a_1t} and e^{a_2t} dissipate the response of the coupled system, a_1 and a_2 are referred to as dissipation factors in the current study.

Remark: Dissipation has a negligible impact on the natural frequency of the coupled system.

Proof: In a typical structure, a_1 and a_2, which are responsible for the response dissipation with factors e^{a_1t} and e^{a_2t}, are very small number compared to one. Hence, with a high degree of accuracy, ${a_1}^2$, ${a_2}^2$, a_1a_2, and their higher-order approach zero. Regarding this approximation, the coefficients $\tilde{B}$ and $\tilde{D}$, the coefficients of λ^2 and λ^0 in the reconstructed characteristic equation (5-27) can be written as $\tilde{B} = \omega_1^2 + \omega_2^2$ and $\tilde{D} = \omega_1^2\omega_2^2$, respectively . on the other side, the coefficients of λ^2 and λ^0 in the characteristic equation, Equation (5-17), are $\dfrac{(k + C_fc + K_{1n}m + K_{2n}K_{3n})}{m}$ and $\dfrac{(kK_{1n})}{m}$ respectively. The term representing (C_fc) in the coefficient of λ^2 is significantly smaller than the other terms, so it can be omitted without loss of accuracy. Equating the corresponding coefficients of λ^2 and λ^0 from both equations, results in the following expression.

$$\frac{(k + C_f c + K_{1n}m + K_{2n}K_{3n})}{m} = \omega_1^2 + \omega_2^2 \tag{5-28}$$

$$\frac{(kK_{1n})}{m} = \omega_1^2 \omega_2^2 \tag{5-29}$$

In relation to Equations (5-28) and (5-29), following a series of mathematical transformations, it can be stated that ω_1 and ω_2 are the roots of the subsequent equation.

$$m\omega^4 - (k + mK_{1n} + K_{2n}K_{3n})\omega^2 + (kK_{1n}) = 0 \tag{5-30}$$

Let us recall equation (5-16-1), which gives the roots as the natural frequencies of the coupled system in the absence of dissipations. A comparison of equations (5-16-1) and (5-30) shows that they are identical, signifying that the influence of structural dissipation on the natural frequencies can be considered negligible.

Remark: Dissipation factors, a_1 and a_2, are functions of the structural damping coefficient, fluid dissipation coefficient, natural frequency of the coupled system, and tank specification.

Proof: Let us recall $\tilde{A}$ and $\tilde{C}$, the coefficient of λ^3 and λ in the reconstructed characteristic expression, Equation (5-27), $\tilde{A} = (-2a_1 - 2a_2)$, and $\tilde{C} = (-2a_1^2 a_2 - 2a_1 a_2^2 - 2a_1\omega_2^2 - 2a_2\omega_1^2)$. Regarding the previous discussion, the terms $a_1{}^2$, $a_2{}^2$, and $a_1 a_2$ are very small and can be treated as approaching zero. Therefore, the coefficient $\tilde{C}$ can be approximated by $\tilde{C} = (-2a_1\omega_2^2 - 2a_2\omega_1^2)$ with a high degree of accuracy. By equating the coefficients of λ^3 and λ in both the characteristic equation and the reconstructed equation and applying $\frac{c}{m} = 2\zeta\omega_s$, the following expressions is developed.

$$a_1 + a_2 = -(\frac{c}{2m} + \frac{C_f}{2}) = -(\xi\omega_s + \frac{C_f}{2}) \tag{5-31}$$

$$a_1\omega_2^2 + a_2\omega_1^2 = -(K_{1n}\frac{c}{2m} + \frac{k}{2m}C_f) = -(K_{1n}\xi\omega_s + \frac{\omega_s^2 C_f}{2}) \tag{5-32}$$

Solving these two equations simultaneously yields the following expression for the dissipation factors a_1 and a_2.

$$a_1 = \frac{-\xi\omega_s(\omega_1^2 - K_{1n})}{\omega_1^2 - \omega_2^2} + \frac{-C_f(\omega_1^2 - \omega_s^2)}{2(\omega_1^2 - \omega_2^2)} \tag{5-33}$$

$$a_2 = \frac{-\xi\omega_s(K_{1n} - \omega_2^2)}{\omega_1^2 - \omega_2^2} + \frac{-C_f(\omega_s^2 - \omega_2^2)}{2(\omega_1^2 - \omega_2^2)} \tag{5-34}$$

Based on the above equations, the dissipation factors depend not only on the structure and fluid dissipation coefficients but also on the natural frequency of the coupled system and mode number. Both dissipation factors, a_1 and a_2, in this scenario consist of two components: first the structural damping second fluid damping. In other words, the part of the response that has ω_1 natural frequency is damped twice with coefficients $e^{\frac{-\xi\omega_s(\omega_1^2 - K_{1n})t}{\omega_1^2-\omega_2^2}}$ and $e^{\frac{-C_f(\omega_1^2-\omega_s^2)t}{2(\omega_1^2-\omega_2^2)}}$ due to structural and fluid dissipation, respectively. The other part of the response, influenced by the natural frequency of ω_2, is dissipated by the product of two factors: $e^{\frac{-\xi\omega_s(K_{1n}-\omega_2^2)t}{\omega_1^2-\omega_2^2}}$ and $e^{\frac{-C_f(\omega_1^2-\omega_s^2)t}{2(\omega_1^2-\omega_2^2)}}$.

When fluid dissipation is absent in the model, $C_f = 0$, the above equations are transformed to:

$$a_1 = -\frac{\xi\omega_s(\omega_1^2 - K_{1n})}{(\omega_1^2 - \omega_2^2)} \tag{5-35}$$

$$a_2 = -\frac{\xi\omega_s(K_{1n} - \omega_2^2)}{(\omega_1^2 - \omega_2^2)} \tag{5-36}$$

When a sole SDOF undergoes free vibration analysis without a sloshing tank, the displacement of the SDOF is dissipated by the coefficient $e^{-\xi\omega_s t}$ i.e., $\zeta\omega_s$ is the dissipation factor. Evidently, the dissipation factor of the coupled system is the SDOF dissipation factor modified with coefficients $(\omega_1^2 - K_{1n})/(\omega_1^2 - \omega_2^2)$ and $(K_{1n} - \omega_2^2)/(\omega_1^2 - \omega_2^2)$ for a_1 and a_2, respectively. These coefficients encompass the natural frequency of the coupled system, tank specifications (*H, L*), and mode number (*n*). It is worth emphasizing that, despite the dissipation factors of a coupled system having small numerical values, their influence on the response of the system is highly significant.

5.2.3. Evaluation of constant coefficient of the couped system response

Recall the displacement of the coupled system from the contribution of mode *n*, $X = e^{a_1 t}(\hat{A}\cos(\omega_1 t) + \hat{B}\sin(\omega_1 t)) + e^{a_2 t}(\hat{C}\cos(\omega_2 t) + \hat{D}\sin(\omega_2 t))$. To capture the response completely, in addition to the natural frequencies and dissipation factors explained in detail, four constant coefficients, $\hat{A}, \widehat{B}, \widehat{C}, \widehat{D}$, should be evaluated. To achieve this, four boundary conditions must be defined. There are two primary physical initial boundary conditions: 1) initial displacement and 2) initial velocity. The initial displacement can be determined from the response (*X*) at *t*=0, resulting in the following relation:

$$X(0) = \hat{A} + \widehat{C} \tag{5-37}$$

The velocity of the coupled system is determined by taking the derivative of the displacement response with respect to time as follows:

$$\begin{aligned}\dot{X}(t) &= e^{a_1 t}(\widehat{B}\omega_1\cos(\omega_1 t) - \widehat{A}\omega_1\sin(\omega_1 t)) + e^{a_2 t}(\widehat{D}\omega_2\cos(\omega_2 t) - \widehat{C}\sin(\omega_2 t)) + \\ &a_1 e^{a_1 t}(\hat{A}\cos(\omega_1 t) + \hat{B}\sin(\omega_1 t)) + a_2 e^{a_2 t}(\hat{C}\cos(\omega_2 t) + \hat{D}\sin(\omega_2 t))\end{aligned} \tag{5-38}$$

So, the initial velocity is derived from the following expression.

$$\dot{X}(0) = B\omega_1 + D\omega_2 + Aa_1 + Ca_2 \tag{5-39}$$

Similarly, the acceleration of the response is obtained by taking the time derivative of the velocity, and the initial acceleration is determined at *t*=0.

$$\ddot{X}(0) = -A\omega_1^2 - C\omega_2^2 + 2Ba_1\omega_1 + 2Da_2\omega_2 + Aa_1^2 + Ca_2^2 \tag{5-40}$$

Likewise, the third-time derivative of the response at the initial time (*t*=0) is

$$\dddot{X}(0) = -B\omega_1^3 - D\omega_2^2 - 3Ca_2\omega_2^2 - 3Aa_1\omega_1^2 + 3Ba_1^2\omega_1 + 3Da_2^2\omega_2 + Aa_1^3 + Ca_2^3 \tag{5-41}$$

Let us examine the initial boundary conditions, $X(0), \dot{X}(0), \ddot{X}(0), \dddot{X}(0)$, while disregarding the values of a_1^2 and a_2^2 that approach zero. Thus, the following matrix equation can be deduced to compute the constant coefficients of the coupled system's response:

$$\begin{Bmatrix} X(0) \\ \dot{X}(0) \\ \ddot{X}(0) \\ \dddot{X}(0) \end{Bmatrix} = \begin{bmatrix} 1 & 0 & 1 & 0 \\ a_1 & \omega_1 & a_2 & \omega_2 \\ -\omega_1^2 & 2a_1\omega_1 & -\omega_2^2 & 2a_2\omega_2 \\ -3a_1\omega_1^2 & -\omega_1^3 & -3a_2\omega_2^2 & -\omega_2^3 \end{bmatrix} \begin{bmatrix} \hat{A} \\ \hat{B} \\ \hat{C} \\ \hat{D} \end{bmatrix} \tag{5-42}$$

Although the terms $X(0)$ and $\dot{X}(0)$, representing initial velocity and initial displacement, respectively, have clear physical interpretations, the question arises as to how to evaluate $\ddot{X}(0)$ and $\dddot{X}(0)$. To achieve this, Equation (5-9), $m\ddot{X} + c\dot{X} + kX = -k_{3n}A_n$, is employed. Using this equation, the following expression is derived to evaluate $\ddot{X}(0)$.

$$\ddot{X}(0) = -\frac{k_{3n}A_n(0) + c\dot{X}(0) + kX(0)}{m} \tag{5-43}$$

To derive $\dddot{X}(0)$, let us consider equation (5-11), $(m)\dddot{X} + (c)\ddot{X} + (k)\dot{X} + k_{3n}\dot{A}_n = 0$, and equation (5-4-1), $\dot{A}_n = -B_n H \frac{n\pi}{L}$. Combining these equations leads to the following equation for the evaluation of $\dddot{X}(0)$.

$$\dddot{X}(0) = -\frac{c\ddot{X}(0) + k\dot{X}(0) - k_{3n}H\frac{n\pi}{L}B_n(0)}{m} \tag{5-44}$$

Regarding equations (5-43) and (5-44), $\ddot{X}(0)$ and $\dddot{X}(0)$ depend not only on the initial velocity and initial displacement, but also on the initial wave height amplitude and velocity, $A_n(0)$ and $B_n(0)$, accordingly. Therefore, the initial boundary vector is developed from the contribution of the four initial values, that is, $X(0), \dot{X}(0), A(0), B(0)$.

5.2.4. Modal decomposition and modal combination:

This section explains how to estimate the contribution of each mode from the initial displacement of the coupled system, and how to determine the total response from the contribution of each mode. Regarding the first issue, the following equation based on the modal decomposition scheme was proposed: In this equation, X_{0i} is the contribution of mode i from the initial displacement of the coupled system, X_0.

$$X(0) = X_{01}\sin(\frac{\pi x}{L}) + X_{03}\sin(\frac{3\pi x}{L}) + \ldots + X_{0i}\sin(\frac{i\pi x}{L}) + \ldots + X_{0n}\sin(\frac{n\pi x}{L}) \tag{5-45}$$

According to the orthogonality relation, the following expression can be expresses.

$$\int_0^L \sin(\frac{i\pi x}{L})\sin(\frac{j\pi x}{L}) = \frac{1}{2}L\delta_{ij}\,. \tag{5-46}$$

where the factor of δ_{ij} is a Kronecker delta that is defined as

$$\delta_{ij} = \begin{Bmatrix} 1 & if\ i = j \\ 0 & if\ i \neq j \end{Bmatrix}$$

Therefore, the term X_{0i}, which is the contribution of mode i from the initial displacement, can be derived from the following formula:

$$X_{o,i} = \frac{\int_{x=0}^{L} \sin(\frac{i\pi x}{L})}{\int_{x=0}^{L} \sin^2(\frac{i\pi x}{L})} X_0 = \frac{4}{n\pi} X_o \tag{5-47}$$

Using the model composition scheme, the following relationship is proposed to extract the total response of the coupled system from the contribution of each mode at each time.

$$X = X_1\sin(\frac{\pi x}{L}) + X_3\sin(\frac{3\pi x}{L}) + \ldots + X_i\sin(\frac{i\pi x}{L}) + \ldots + X_n\sin(\frac{n\pi x}{L}) \tag{5-48}$$

Up to this point, the current research has concentrated on a shallow water tank elevated with a support structure. This support structure can be simplified into a single degree of freedom system and combined with a shallow water tank to form a coupled system. The core assumption of this analytical approach is the utilization of linear shallow-water models. Hence, the present analytical model holds validity for small-amplitude waves in shallow tanks. Yet, with the onset of high-amplitude waves, nonlinear terms gain significance, resulting in decreased accuracy of the current analytical model (Khanpour et al. 2024). Moreover, under such conditions, the possibility of wave breaking arises, requiring the inclusion of supplementary terms to address this occurrence within the model. Nevertheless, in the subsequent section, the research narrows its focus to a specific case of a shallow water elevated tank.

5.3. Tuned liquid dampers (case study)

This section presents a case study concerning a Tuned Liquid Damper (TLD) sourced from Sorkhabi et al. (2017), which is examined using the current analytical approach. To validate the analytical method and analytical approximations, a numerical model is developed. This numerical model utilizes separation of variable techniques to convert partial differential equations with both *x* and *t* as independent variables into ordinary differential equations, with *t* as the sole independent variable for each mode. It encompasses equations such as the continuity equation (5-49-1), momentum equation (5-49-2), modal superposition of wave height (5-49-3), evaluation of interaction forces (5-49-4), and dynamics of SDOF (5-49-5). These equations provide the advantage of deriving not only the total response of the coupled system but also the response resulting from the contribution of each mode.

$$\dot{A}_n = -HB_n\left(\frac{n\pi}{L}\right) \tag{5-49-1}$$

$$\dot{B}_n - gA_n\frac{n\pi}{L} = -\ddot{X}M_n - C_f B_n \tag{5-49-2}$$

$$\eta(x,t)=\sum_{n=1}^{N} A_n(t)\cos\left(\frac{n\pi x}{L}\right) \tag{5-49-3}$$

$$F_{slo}(x,t)=2\rho gH\left[\eta(x=L)-\eta(x=0)\right] \tag{5-49-4}$$

$$m\ddot{X} + c\dot{X} + kX = 0 + F_{slo} \tag{5-49-5}$$

The solution to the shallow water equations is facilitated through a second-order Runge-Kutta scheme, while the coupling process is based on the partitioned method. For a comprehensive understanding of this model, including the numerical scheme and coupling system, please refer to the detailed flowchart provided in a prior study by Khanpour et al. (2024). This case study includes a SDOF system with characteristics $m = 282(Kg)$, $K = 4997.5(\frac{N}{m})$ and $c = 24(\frac{N.s}{m})$ attached with a TLD tank with specifications including length L=0.46m, width b=0.31m and water depth H=0.04m. So, the mass ratio which is SDOF mass/ TLD mass is 2%. The natural frequency of the SDOF derived from equation (5-20) is 4.2 rad/s. On the other side, the natural frequency of the TLD can be determined from Equation (5-50), which is 4.2 rad/s.

$$\omega_L = \sqrt{\frac{\pi g}{L} tanh(\frac{\pi H}{L})} \tag{5-50}$$

The setup of this case study adheres to the criteria for a Tuned Liquid Damper (TLD), which includes the same natural frequency for both the structure and the TLD $\omega_L = \omega_s$ and a small mass ratio of the TLD to the structure $\frac{m_L}{m} \ll 1$.

Furthermore, the critical damping in this case is $c_c = 2m\omega_s = 2374\frac{Ns}{m}$, resulting in a damping ratio of $\xi = \frac{c}{c_c} = 1\%$. Note, however, that in the original test case $c = 5(\frac{N.s}{m})$, this value is higher in this research to obtain a clearer insight into the response considering structure damping. Evidently, the TLD applied here is a shallow water tank in which there is $\frac{h}{L} \ll 1$. In addition, fluid dissipation was introduced into the model with the fluid dissipation coefficient of the $C_f = 0.05$.

Before applying the analytical approach, it is important to consider two points. First, in TLDs, the parameter K_{1n} can be written as $K_{1n} \simeq n^2\omega_s^2$. Second, the product of K_{2n} and K_{3n} can be expressed as $K_{2n}K_{3n} = \frac{8W_L H}{L^2}$ for odd modes and zero for even modes, where W_L is the TLD weight. For a detailed explanation of how these relationships are derived, please refer to the relevant source (Khanpour et al. 2024). In the subsequent sections, for simplicity, the coupled system including a Single Degree of Freedom (SDOF) and Tuned Liquid Damper (TLD) is referred to as the TLD coupled system.

5.3.1. Analytical solution to the case study

This section discusses the application of the detailed analytical approach to the tuned liquid damper with the specifications outlined in the previous section and considers both structural and fluid dissipation.

5.3.1.1. Natural frequencies of the TLD coupled system

The imaginary components of the roots of the characteristic equation, as described in expression (17) and incorporating both structural and fluid dissipation, correspond to two natural frequencies for each mode. These frequencies are denoted by a larger frequency (f_1) and a smaller frequency (f_1). These frequencies were calculated for modes 1, 3, and 5 and are shown in columns 2 and 3 of Table (5.1). In addition, the imaginary parts of the characteristic equation roots when fluid dissipation is absent, $C_f = 0$, were extracted and are presented in columns 4 and 5 of Table (5.1). These natural frequencies, whether considering both structural and fluid dissipation or solely structural damping, closely align with those obtained from Equation (5-16), which neglects both dissipations (as seen in columns 6 and 7 of the table). This numerical test case confirms the prior analytical finding that the structural dissipation has a negligible impact on the natural frequencies.

Additionally, column (8) represents f_s and column (9) refers to nf_s . A comparison of columns (2), (4), (6), and (8) reveals their proximity, whereas columns (3), (5), (7), and (9) exhibit alignment with each other for higher modes, $n > 1$. The previous work in this context (Khanpour et al. 2024), which disregarded dissipations, proved that in the higher modes (n>1), the smaller frequency, ω_2 , approaches the natural frequency of the SDOF, ω_s , and the greater frequency, ω_1, is close to $n\omega_s$. Given that the introduction of dissipation does not alter the natural frequencies of the coupled system, this validation applies to scenarios with integrated dissipations.

Table 5.1. Natural frequencies of the coupled system for different cases regarding dissipation

Column 1	Column 2	Column 3	Column 4	Column 5	Column 6	Column 7	Column 8	Column 9
	Characteristic Equation (17)		Characteristic Equation (17)		Equation (16)			
	$c \neq 0 \,\&\, C_f \neq 0$		$c \neq 0 \,\&\, C_f = 0$		$c = 0 \,\&\, C_f = 0$			
Mode Number	Greater Frequency	Smaller Frequency	Greater Frequency	Smaller Frequency	Greater Frequency	Smaller Frequency	$n.f_S$	f_S
1	0.72091	0.63309	0.72081	0.63320	0.72095	0.63309	0.67	0.67
3	2.04475	0.66962	2.04475	0.66962	2.04475	0.66965	2.01	0.67
5	3.40561	0.67007	3.40561	0.67007	3.40561	0.67011	3.35	0.67

5.3.1.2. Dissipation factors of the TLD coupled system

As discussed, the dissipation factors a_1 and a_2 in each mode are responsible for the reduction of the response by factors of $e^{a_1 t}$ and $e^{a_2 t}$, respectively. The dissipation factors were determined by solving the characteristic equation, wherein they are manifested as the real parts of roots, forming pairs of complex conjugates. Columns 2 and 3 in Table (5.2) display the dissipation factors obtained from the characteristic equation for each mode. Additionally, the dissipation factors can be obtained from analytical approximations (5-33) and (5-34), as presented in columns 4 and 5 in Table (5.2). A comparison between columns (2) and (4) as well as columns (3) and (5) demonstrates that these two approaches yield approximately similar results. The process was repeated with $C_f = 0$ for the scenario where only structural dissipation was active in the model, and the results derived from both methods are presented in Table (5.3).

Table 5.2. Dissipation factors considering both structural and fluid dissipation

Column 1	Column 2	Column 3	Column 4	Column 5
	Characteristic Equation (17)		Analytical Approximations (33, 34)	
	$c \neq 0$ & $C_f \neq 0$		$c \neq 0$ & $C_f \neq 0$	
Mode Number	Greater Frequency Dissipation Factor	Smaller Frequency Dissipation factor	Greater Frequency Dissipation Factor	Smaller Frequency Dissipation factor
1	-3.488E-02	-3.267E-02	-3.504E-02	-3.196E-02
3	-2.509E-02	-4.246E-02	-2.510E-02	-4.190E-02
5	-2.503E-02	-4.252E-02	-2.503E-02	-4.197E-02

Table 5.3. Dissipation factors considering just structural dissipation

Column 1	Column 2	Column 3	Column 4	Column 5
	Characteristic Equation (17)		Analytical Approximations (35, 36)	
	$c \neq 0$ & $C_f = 0$		$c \neq 0$ & $C_f = 0$	
Mode Number	Greater Frequency Dissipation Factor	Smaller Frequency Dissipation factor	Greater Frequency Dissipation Factor	Smaller Frequency Dissipation factor
1	-2.008E-02	-2.248E-02	-1.981E-02	-2.219E-02
3	-9.718E-05	-4.246E-02	-9.593E-05	-4.190E-02
5	-3.021E-05	-4.252E-02	-2.982E-05	-4.197E-02

In this test case, two crucial points are worth noting: First, the small numbers of dissipation factors validate the assumption that a_1^2, a_2^2 and $a_1 a_2$ approach zero, which was employed to develop the analytical approximations. Second, the negative values of both a_1 and a_2, which were proven using an analytical approach, are confirmed by this test case. Consequently, a_1 and a_2 plays a role in the dissipation of the response. Furthermore, as evident in the table for higher modes ($n > 1$), when fluid damping is absent, a_1 tends to be close to zero, while a_2 approaches $-\xi\omega_s$ (see columns 2 and 3 in Table 5.3 for higher modes).

Remark: When examining higher modes with only structural dissipation, the first dissipation factor of the coupled system, a_1, approaches zero, whereas the second dissipation factor, a_2, aligns with the dissipation factor of the sole SDOF.

Proof: As previously mentioned, $K_{1n} = n^2\omega_s^2$ and for higher modes $\omega_1 = n\omega_s$ and $\omega_2 = \omega_s$. So, for higher modes $K_{1n} = \omega_1^2$ and $\omega_s = \omega_2$. Now, recall the analytical equation for the evaluation of a_1 , $a_1 = -\xi\omega_s(\omega_1^2 - K_{1n})/(\omega_1^2 - \omega_2^2)$. Since for higher modes $K_{1n} = \omega_1^2$, the first dissipation factor, a_1, tends to approach zero. To evaluate the other dissipation factor, a_2 , lets consider the analytical equation to estimate a_2, $a_2 = -\xi\omega_s(K_{1n} - \omega_2^2)/(\omega_1^2 - \omega_2^2)$. Because $K_{1n} = \omega_1^2$ for higher modes, the parameter a_2 in this equation equals $-\xi\omega_s$ which is equivalent to the dissipation factor of a Single Degree of Freedom (SDOF) without a Tuned Liquid Damper (TLD).

In higher modes, when both structure and fluid dissipation are incorporated into the model, using a similar approach and Equation (5-33), $a_1 = \frac{-\xi\omega_s(\omega_1^2 - K_{1n})}{\omega_1^2 - \omega_2^2} + \frac{-C_f(\omega_1^2 - \omega_s^2)}{2(\omega_1^2 - \omega_2^2)}$, the first dissipation factor aligns with $\frac{-C_f}{2}$, whereas the second dissipation factor estimated by Equation (5-34), $a_2 = \frac{-\xi\omega_s(K_{1n} - \omega_2^2)}{\omega_1^2 - \omega_2^2} + \frac{-C_f(\omega_s^2 - \omega_2^2)}{2(\omega_1^2 - \omega_2^2)}$, approaches $-\xi\omega_s$ (see columns 2 and 3 in Table 5.2 for higher modes).

5.3.2. Verification of the current analytical approach with numerical model

To verify the current analytical method, this case study is solved using the numerical model explained earlier to derive the time-history response of the TLD coupled system for each mode.

5.3.2.1. Natural frequencies of the TLD coupled system

First, in the numerical model, $X(0) = X_0 = -0.01m$ is implemented as the initial boundary condition. In addition to the developed numerical model, the Fast Fourier Transform (FFT) is used to transform the wave response from the time domain to the frequency domain; thus, it is viable to derive the constitutive frequency of the wave response. Figures (5.2) illustrates both the time history and the frequency domain of the responses for different modes. In the left column of Figure (5.2), the time-domain response during free vibration demonstrates a decrease in the coupled system's response due to both structural and fluid dissipation. Concurrently, the response of the Single Degree of Freedom (SDOF) diminishes over time solely because of structural damping. Figure (5.2b) displays the fundamental frequencies of mode 1, as derived from the numerical model. A comparison of these frequencies with those obtained analytically in Table (5.1) shows a close agreement between the two sets of results. However, the transformation of the numerical response using FFT indicates that for higher modes greater frequencies do not appear in the results (Figures 5.2d and 5.2f). Indeed, the coupled system’s response to free vibration in higher modes only includes a lower frequency, which is roughly equivalent to the natural SDOF frequency. For simplicity, this point is demonstrated in the subsequent section when considering only structural dissipation. The same approach can be used to confirm this proof when both structural and fluid damping are involved, although it requires more complex mathematical operations.

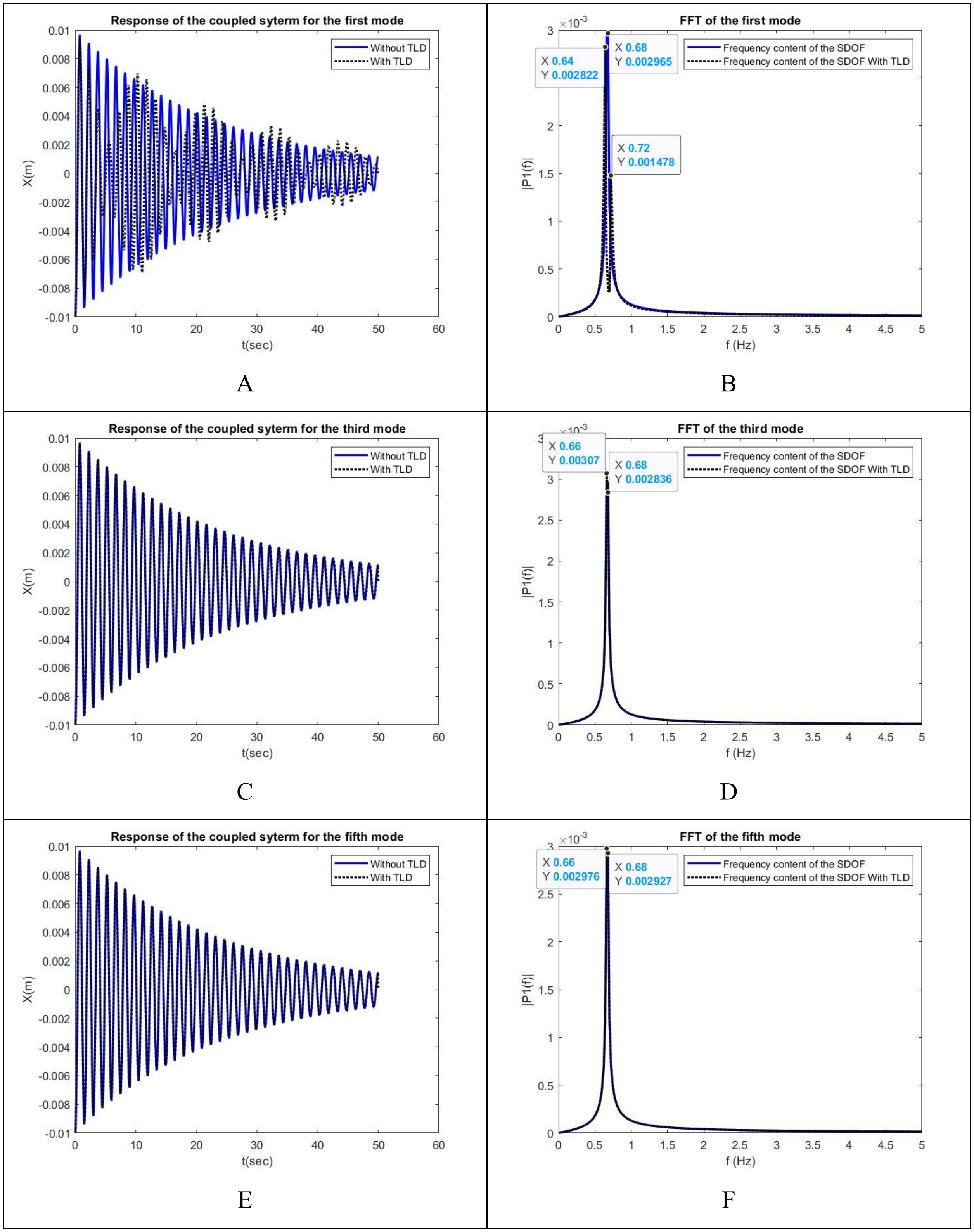

Fig. 5.2. Time domain and frequency domain of the coupled system response excited by initial displacement in different modes with considering structure and fluid dissipations

Remark: In the case of damped free vibration analysis, the response of the coupled system in higher modes does not include a contribution from greater frequencies.

Proof: Recall the system of equation for evaluating the coupled system (Equation 5-42). Let us focus on the left-hand side of this matrix equation, known vector. The initial displacement and initial velocity have physical concepts and are $X(0) = -0.01\,m$ and $\dot{X}(0) = 0$, respectively, for this test case. Meanwhile, as discussed earlier, $\ddot{X}(0)$ and $\dddot{X}(0)$ are derived from Equations (5-43),

$$\ddot{X}(0) = -\frac{k_{3n}A_n(0) + c\dot{X}(0) + kX(0)}{m}, \quad \text{and} \quad (5\text{-}44) \quad \dddot{X}(0) = -\frac{c\ddot{X}(0) + k\dot{X}(0) - k_{3n}H\frac{n\pi}{L}B_n(0)}{m},$$

correspondingly. Because both the initial perturbation for wave height, $A(0)$, and fluid velocity, $B(0)$, are zero, it is determined that $\ddot{X}(0) = -\frac{k}{m}X_0$ and $\dddot{X}(0) = -\frac{c}{m}\ddot{X}_0$. Using $\omega_s = \sqrt{\frac{k}{m}}$ and $\frac{c}{m} = 2\zeta\omega_s$ leads to $\ddot{X}(0) = -\omega_s{}^2 X_0$, and $\dddot{X}(0) = 2\zeta\omega^3{}_s X_0$. Furthermore, in the higher modes $\omega_1 = n\omega_s$, $\omega_2 = \omega_s$, $a_1 = 0$, and $a_2 = -\zeta\omega_s$. Therefore, the following system of equations was derived from Equation (5-42):

$$\begin{Bmatrix} X(0) = X_0 \\ \dot{X}(0) = 0 \\ \ddot{X}(0) = -\omega_s^2 X_0 \\ \dddot{X}(0) = 2\zeta\omega_s^3 X_0 \end{Bmatrix} = \begin{bmatrix} 1 & 0 & 1 & 0 \\ 0 & n\omega_s & -\zeta\omega_s & \omega_s \\ -(n\omega_s)^2 & 0 & -\omega_s^2 & -2\zeta\omega_s{}^2 \\ 0 & -(n\omega_s)^3 & 3\zeta\omega_s^3 & -\omega_s^3 \end{bmatrix} \begin{bmatrix} \hat{A} \\ \hat{B} \\ \hat{C} \\ \hat{D} \end{bmatrix} \tag{5-51}$$

By solving these equations simultaneously, the unknown coefficients $\hat{A}$ and $\hat{B}$ were determined from Equations (5-52) and (5-53).

$$\hat{A} = \frac{-2X_o n^2\zeta^2 + 2X_o\zeta^2}{n^4 - 2n^2\zeta^2 - 2n^2 + 6\zeta^2 + 1} \tag{5-52}$$

$$\hat{B} = \frac{4X_o\zeta^3}{n(n^4 - 2n^2\zeta^2 - 2n^2 + 6\zeta^2 + 1)} \tag{5-53}$$

In the above-mentioned equations, the term included in ζ^2 in the denominator is very small and negligible with respect to the other term. If these small terms are eliminated from the denominator, the following relations for $\hat{A}$ and $\hat{B}$ are established:

$$\hat{A} = \frac{-2X_o\zeta^2(n^2-1)}{(n^2-1)^2} = -2X_o(\frac{\zeta}{n^2-1})^2 \tag{5-54}$$

$$\hat{B} = \frac{4X_o\zeta^3}{n(n^2-1)^2} = 4X_o\frac{\zeta^3}{n(n^2-1)^2} \tag{5-55}$$

The terms $(\frac{\zeta}{n^2-1})^2$ and $\frac{\zeta^3}{n(n^2-1)^2}$ are very small and approach zero for higher modes, causing $\hat{A}$ and $\hat{B}$ to also approach zero. Therefore, $\hat{A}$ and $\hat{B}$, which are coefficients of greater frequency, do not contribute to the response of the coupled system in the higher modes.

Remark: The response of the coupled system for higher modes is very close to the response of the SDOF alone.

Proof: Let us focus on the coefficients of smaller frequency $\hat{C}$ and $\hat{D}$ derived from Equations (5-51), which are expressed as follows:

$$\hat{C} = \frac{X_0n^4 - 2X_0n^2 + 4X_0\zeta^2 + X_0}{n^4 - 2n^2\zeta^2 - 2n^2 + 6\zeta^2 + 1} \tag{5-56}$$

$$\hat{D} = \frac{-[(n^2-1)(-X_0\zeta n^2 + X_0\zeta)}{n^4 - 2n^2\zeta^2 - 2n^2 + 6\zeta^2 + 1} \tag{5-57}$$

If the terms composed of ζ^2, which approaches zero, are removed from the denominator and numerator of $\hat{C}$ and $\hat{D}$, the following expressions are developed:

$$\hat{C} = \frac{X_0n^4 - 2X_0n^2 + 4X_0\zeta^2 + X_0}{n^4 - 2n^2\zeta^2 - 2n^2 + 6\zeta^2 + 1} \simeq \frac{X_0(n^2-1)^2}{(n^2-1)^2} \simeq X_0 \tag{5-58}$$

$$\hat{D} = \frac{-[(n^2-1)(-X_0\zeta n^2 + X_0\zeta)}{n^4 - 2n^2\zeta^2 - 2n^2 + 6\zeta^2 + 1} \simeq \frac{X_0\zeta(n^2-1)^2}{(n^2-1)^2} = X_0\zeta \tag{5-59}$$

Regarding the preceding demonstrations, $\hat{A}$ and $\hat{B}$, the coefficients of the greater frequency, approach zero, and $\omega_2 = \omega_s$, as well as $a_2 = -\zeta\omega_s$. So, the response of the coupled system is transformed from Equation (5.24) to the subsequent equation in higher modes.

$$X = e^{a_2 t}(\hat{C}\cos(\omega_2 t) + \hat{D}\sin(\omega_2 t)) = e^{-\zeta\omega_s t}(X_o \cos(\omega_s t) + X_0\zeta\cos(\omega_s t)) \tag{5-60}$$

The response of an SDOF to a free vibration with an initial displacement is expressed as follows (Humar, 2012):

$$X_{SDOF} = e^{-\zeta\omega_s t}(X_o \cos(\omega_D t) + \frac{X_0\zeta\omega_s}{\omega_D}\cos(\omega_D t)) \tag{5-61}$$

Because in the regular structure the natural damped frequency, ω_D, is very close to the natural frequency of SDOF, $\omega_D \simeq \omega_s$, the response of the SDOF is equivalent to the coupled system response in higher modes.

However, to verify the accuracy of the current analytical approach, greater frequencies should be numerically excited.

Remark: The initial perturbation can excite a higher frequency in the TLD coupled system's response.

Proof: To demonstrate this, along with the initial displacement, X_0, an initial perturbation of the wave height, A_0, was imposed in the analytical model. In this case, regarding Equations (5-43) and (5-44), the following system of equation was developed to evaluate the coefficients.

$$\left\{\begin{aligned} & X(0) = X_0 \\ & \dot{X}(0) = 0 \\ & \ddot{X}(0) = -\omega_s^2 X_0 - \frac{k_{3n}A_n(0)}{m} \\ & \dddot{X}(0) = 2\zeta\omega_s^3 X_0 + 2\zeta\omega_s \frac{k_{3n}A_n(0)}{m} \end{aligned}\right\} = \begin{bmatrix} 1 & 0 & 1 & 0 \\ 0 & n\omega_s & -\zeta\omega_s & \omega_s \\ -(n\omega_s)^2 & 0 & -\omega_s^2 & -2\zeta\omega_s{}^2 \\ 0 & -(n\omega_s)^3 & 3\zeta\omega_s^3 & -\omega_s^3 \end{bmatrix} \begin{bmatrix} \hat{A} \\ \hat{B} \\ \hat{C} \\ \hat{D} \end{bmatrix} \tag{5-62}$$

Solving the above system of equations for $\hat{A}$ and $\hat{B}$, neglecting the term composed of the second-order damping ratio, ζ^2, and making some simplifications, leads to Equations (5-63) and (5-64). In the following equations, both $\hat{A}$ and $\hat{B}$ coefficients are devoid of terms approaching zero, signifying that a higher natural frequency participates in the response of the system in higher modes.

$$\hat{A} = \frac{-k_{3n} A_0}{m\omega_s^2} \frac{1}{(n^2-1)^2} \tag{5-63}$$

$$\hat{B} = \frac{-2k_{3n} A_0 n^2 \zeta}{m\omega_s^2 n(n^2-1)^2} = \frac{-2k_{3n} A_0}{m\omega_s^2} \frac{n\zeta}{(n^2-1)^2} \tag{5-64}$$

Therefore, at this stage, the results of the numerical model with initial perturbation $A(0) = A_0 = 0.5\,m$ and initial displacement $X(0) = X_0 = -0.01\,m$ are presented in the first column of Figures (5.3). These are relevant to Modes 1, 3, and 5. The fundamental frequencies of each mode were derived using the FFT approach, as shown in the second column of Figures (5.3). As evident, this initial perturbation not only excites a smaller frequency, but also stimulates a greater frequency. Therefore, as predicted analytically, the coupled system response constitutes two natural frequencies for each mode, and both agree well with the analytical ones in Table (5.1).

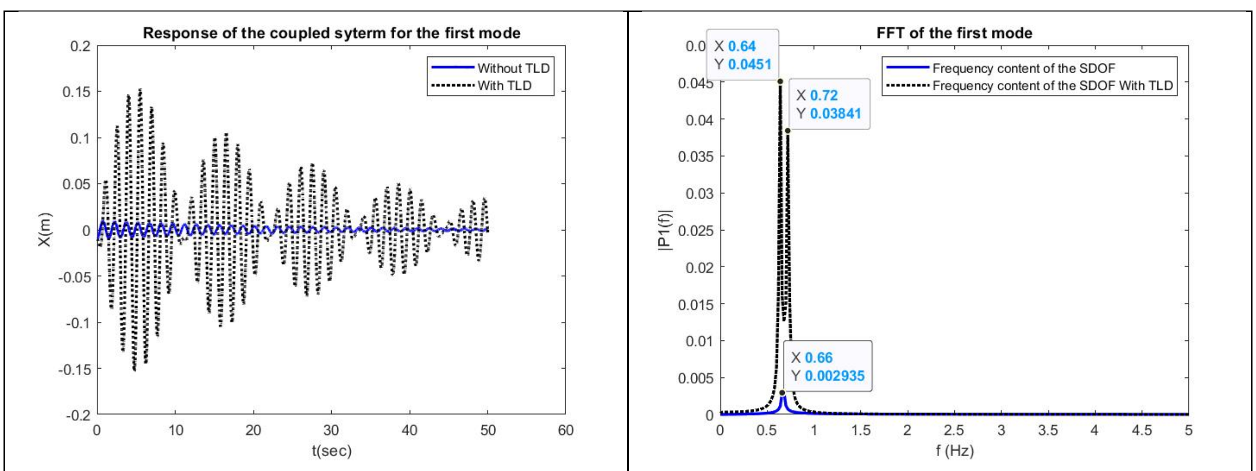

A B

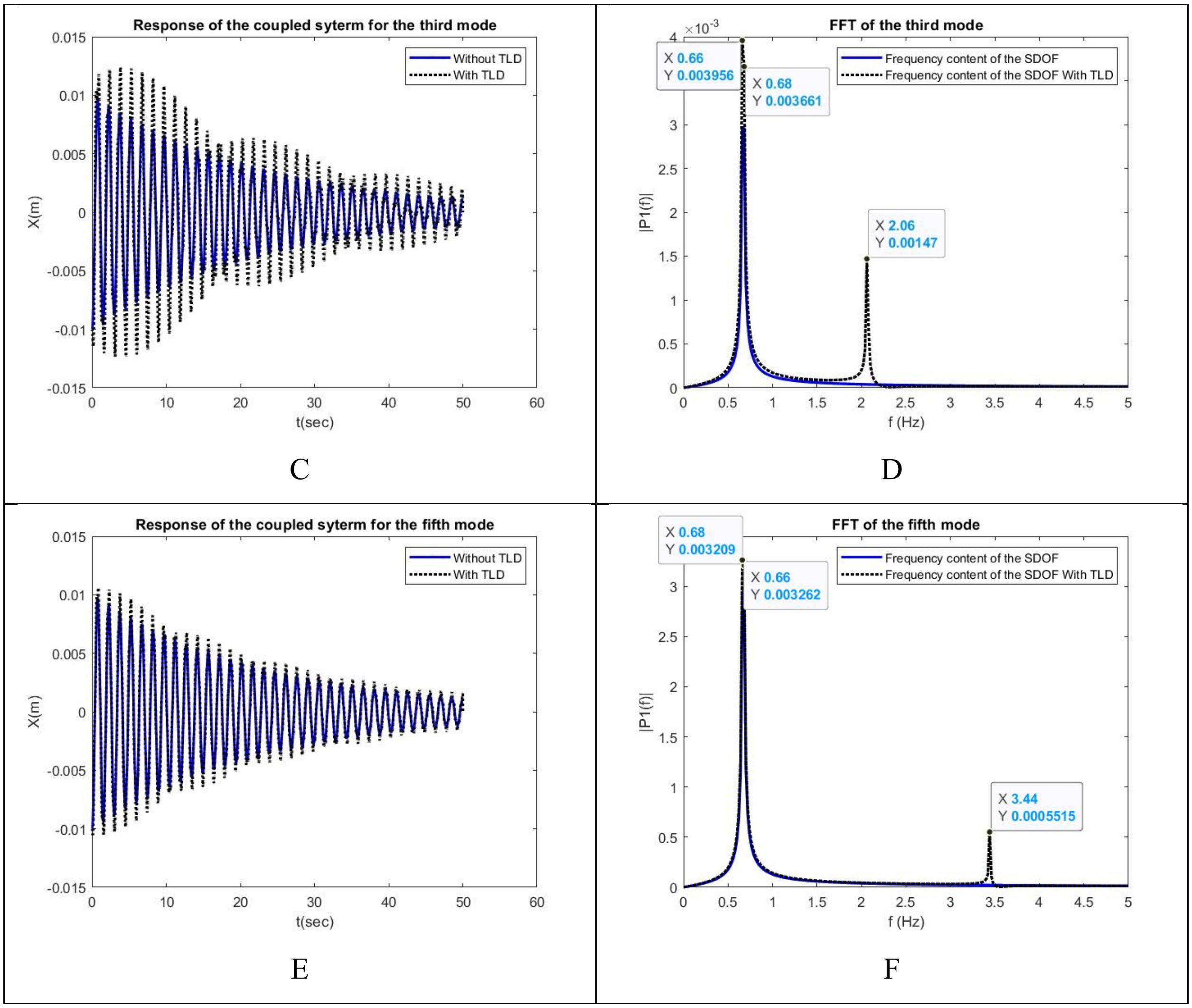

Fig. 5.3. Time domain and frequency domain of the coupled system response excited by both initial displacement and perturbation in different modes with considering structure and fluid dissipation

5.3.2.2. Total response of the TLD coupled system

In the following section, it is demonstrated that the total response of TLD coupled system, when only structural dissipation is integrated, primarily depends on the first method. When both structure and fluid dissipation are incorporated, this point can be confirmed using a similar approach.

Regarding Equation (5-47), which relies on modal decomposition, the contribution of each mode from the initial displacement, that is, $X_{o,i}$, is $X_{o,i} = \dfrac{4}{n\pi} X_o$.

According to Equation (5-65), the response of the coupled system resulting from the contribution of mode *i* is derived from the following equation. In this equation, $\omega_{i,1}$ and $\omega_{i,2}$ are smaller and greater natural frequencies of mode *i,* accordingly. $a_{i,1}$ and $a_{i,2}$ denote dissipation factors corresponding to smaller and greater frequencies, respectively. In addition, $\hat{A}_i$, $\hat{B}_i$, $\hat{C}_i$, and $\hat{D}_i$ are constant coefficients that correspond to mode *i*.

$$X_i = e^{a_{i,1}t}(\hat{A}_i \cos(\omega_{i,1}t) + \hat{B}_i \sin(\omega_{i,1}t)) + e^{a_{i,2}t}(\hat{C}_i \cos(\omega_{i,2}t) + \hat{D}_i \sin(\omega_{i,2}t)) \tag{5-65}$$

For higher modes, n>1, according to Equations (5-54), (5-55), (5-58), and (5-59), $\hat{A}_i \simeq 0$ and $\hat{B}_i \simeq 0$ also $\hat{C}_i \simeq X_{0,i}$ and $\hat{D}_i \simeq X_{0,i}\zeta$. Furthermore, with respect to section (5.3.1.2.), $a_{i,2} \simeq -\zeta\omega$, and $\omega_{i,2} \simeq \omega_s$. Therefore, the response of the coupled system for the higher mode is obtained from the following equation, which equals $\frac{4}{n\pi}X_{SOD}$ with assuming $\omega_D \simeq \omega_s$.

$$X_i = e^{-\zeta\omega t}(X_{0i}\cos(\omega_{i,2}t) + X_{0i}\zeta(\omega_{i,2}t)) = \frac{4}{n\pi}e^{-\zeta\omega t}(X_0\cos(\omega_s t) + X_0\zeta(\omega_s t)) = \frac{4}{n\pi}X_{SOD} \tag{5-66}$$

The response of each mode is composed according to Equation (5-48) to obtain the total response.

$$X_T = X_1\sin(\frac{\pi x}{L}) + X_{SDOF}(\frac{4}{3\pi}\sin(\frac{3\pi x}{L}) + ... + \frac{4}{i\pi}\sin(\frac{i\pi x}{L}) + ... + \frac{4}{n\pi}\sin(\frac{n\pi x}{L})) \tag{5-67}$$

The term $X_{SDOF}\frac{4}{\pi}\sin(\frac{\pi x}{L})$ is added to and subtracted from equation (5-67), leading to expression (5-68).

$$\begin{aligned} X_T &= X_1\sin(\frac{\pi x}{L}) - X_{SDOF}\frac{4}{\pi}\sin(\frac{\pi x}{L}) + \\ &X_{SDOF}(\frac{4}{\pi}\sin(\frac{\pi x}{L}) + \frac{4}{3\pi}\sin(\frac{3\pi x}{L}) + ... + \frac{4}{i\pi}\sin(\frac{i\pi x}{L}) + ... + \frac{4}{n\pi}\sin(\frac{n\pi x}{L})) \end{aligned} \tag{5-68}$$

Regarding the Fourier transformation, the following term is equal to one.

$$\frac{4}{\pi}\sin(\frac{\pi x}{L}) + \frac{4}{3\pi}\sin(\frac{3\pi x}{L}) + ... + \frac{4}{i\pi}\sin(\frac{i\pi x}{L}) + ... + \frac{4}{n\pi}\sin(\frac{n\pi x}{L}) = 1 \tag{5-69}$$

Therefore, a subsequent equation is established for the evaluation of the total response. As seen in the total response, only the responses of the first mode and SDOF response contribute.

$$X_T = X_1 \sin(\frac{\pi x}{L}) - X_{SDOF} \frac{4}{\pi} \sin(\frac{\pi x}{L}) + X_{SDOF}(1) = X_1 \sin(\frac{\pi x}{L}) + X_{SDOF}(1 - \frac{4}{\pi} \sin(\frac{\pi x}{L})) \tag{5-70}$$

The Fourier approximation of 1 with only the first term, $\frac{4}{\pi}\sin(\frac{\pi x}{L})$, results in a zero value for the second term of Equation (5-70). Therefore, the total response depends mainly on the response of the first mode.

5.3.2.3. Dissipation factors of the TLD coupled system

To validate the precision of the analytical approach regarding the initial boundary condition, two cases were considered: 1) the implementation of initial displacement and 2) the introduction of both initial displacement and initial wave height perturbation. The first case of the simulation focuses on the first mode of the coupled system because the higher modes, as demonstrated in the previous section, generate the sole SDOF response. On the other hand, in the second case in which the coupled system subjected to both initial displacement and initial perturbation, first, third, and fifth modes were simulated numerically and compared with analytical solution in Figures (5.4). The analytical solution includes the following steps: 1) The response takes the form of Equation (5-24). 2) The natural frequency of the coupled system, ω_1 & ω_2, the imaginary parts of the roots of the characteristic equation (5-17), are derived. Alternatively, these frequencies can be determined from equation (5-16). All these natural frequencies are presented in Table (5.1). 3) Either the real parts of the characteristic equation's roots (5-17) or equations (5-33) and (5-34) can be introduced as dissipation factors a_1 & a_2. The dissipation factors obtained from the different methods are shown in Table (5.2). 4) The coefficients of the coupled system' response when the coupled system undergoes free vibration are determined from the matrix Equation (5-42) and Equations (5-43,5-44). It is worth noting that the matrix coefficient relies on the natural frequencies and dissipation factors; therefore, it differs when the coupled system incorporates only structural dissipation compared to when both fluid and structural dissipation are considered. Evidently, the known vector in the matrix equation (5-42), which depends on the initial conditions, is different for initial displacement case and initial perturbation case.

As shown in Figures (5.4), although irregular and unsmooth patterns, as well as broken peaks form in the response of the coupled system, the analytical results for the two cases align very well with the numerical results. This alignment is established in terms of both the patterns and the peaks. This agreement indicates two significant points: 1- Alongside the accuracy of the natural frequencies' prediction presented in the previous section, the analytical solution generates precise dissipation factors, and it can dissipate the response in time accurately. Second, the analytical approach appears to be an accurate tool for predicting the response of a coupled system subjected to free vibration, not only for the initial displacement case but also for the initial perturbation.

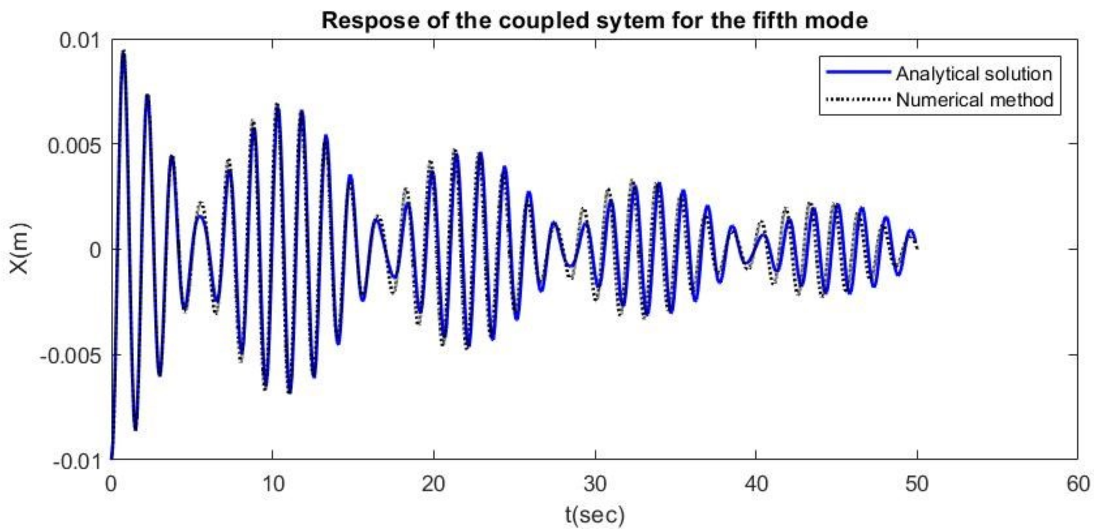

A

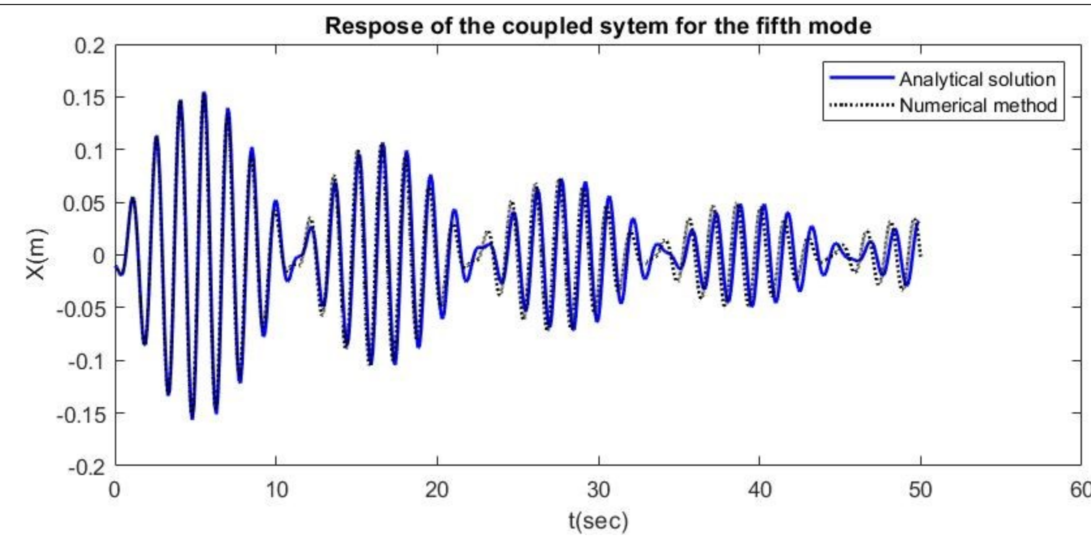

B

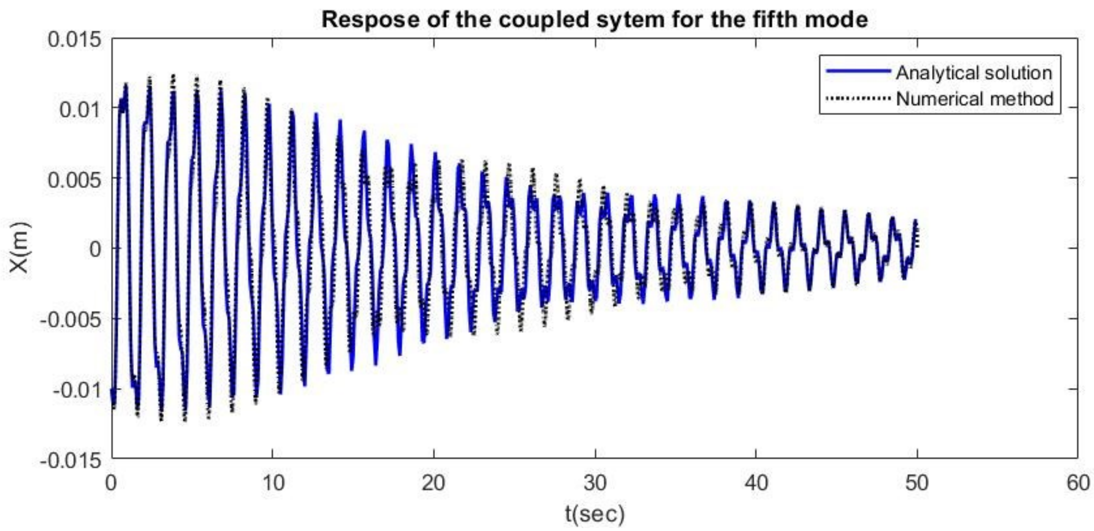

C

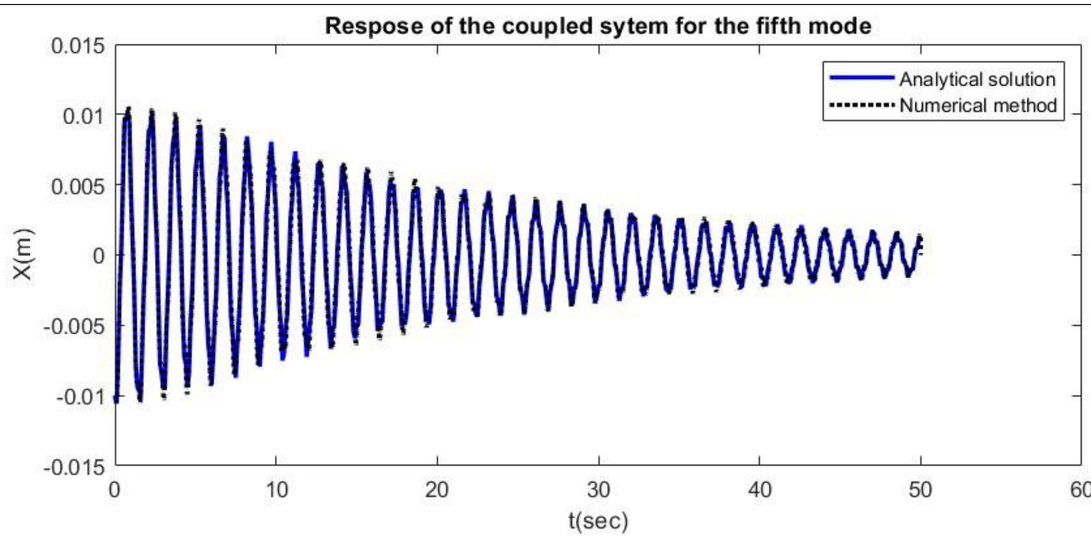

D

Fig. 5.4. Time history of the coupled system response incorporating both structure and fluid dissipations subjected to free vibration with a) initial displacement associated with first mode- b, c, d) initial displacement and perturbation associated with first, third, fifth modes

5.3.3. TLD coupled system response with respect to structure, fluid and screen dissipation (extended case study)

In this case study, local dissipation is introduced into the equation in addition to structural and fluid dissipation. This local dissipation can be attributed to the presence of a screen in the tank, which is used to control the sloshing waves (Cho, 2021 and Yu et al., 2020 and Tait et al., 2005 and Xue and Lin, 2011 and Zang et al., 2019). The formulation for this case incorporates an assumption valid for a special case of shallow elevated tanks, such as Tuned Liquid Dampers (TLDs); therefore, contrary to the previous scenarios, it is presented in the TLD section. The governing equation for fluid sloshing in this scenario accounts for the local head loss and can be expressed as follows:

$$\frac{\partial h}{\partial t} + H\frac{\partial u}{\partial x} = 0 \tag{5-71-1}$$

$$\frac{\partial u}{\partial t} + g\frac{\partial h}{\partial x} = -\ddot{X} - C_f u - ku(x_0) \tag{5-71-2}$$

In this equation, k is the coefficient of the local head loss, and $u(x_0)$ is the velocity at the location of the screen (x_0). The first equation, the continuity equation, does not change, so the transformation of this equation into the modal coordinate is represented by Equation (5-4-1), $\dot{A}_n = -B_n H\frac{n\pi}{L}$. Substituting equations (5-2) and (5-3) into Equation (5-71-2) leads to the following expression:

$$\begin{aligned}&\sum_{n=1}^{N}\dot{B}_n\sin(\frac{n\pi x}{L}) - g\sum_{n=1}^{N}A_n\frac{n\pi}{L}\sin(\frac{n\pi x}{L}) = -\sum_{n=1}^{N}\ddot{X}M_n\sin(\frac{n\pi x}{L}) - \sum_{n=1}^{N}C_f B_n\sin(\frac{n\pi x}{L})\\&-\sum_{n=1}^{N}k_f B_n\sin(\frac{n\pi x_0}{L})\end{aligned} \tag{5-72}$$

The last term on the right-hand side of equation (5-72) was multiplied by the Fourier transformation of 1, $\sum_{n=1}^{N}M_n\sin(\frac{n\pi x}{L})$, leading to the following expression:

$$\begin{aligned}&\sum_{n=1}^{N}\dot{B}_n\sin(\frac{n\pi x}{L}) - g\sum_{n=1}^{N}A_n\frac{n\pi}{L}\sin(\frac{n\pi x}{L}) = -\sum_{n=1}^{N}\ddot{X}M_n\sin(\frac{n\pi x}{L}) - \sum_{n=1}^{N}C_f B_n\sin(\frac{n\pi x}{L})\\&-\sum_{n=1}^{N}k_f B_n\sin(\frac{n\pi x_0}{L})\sum_{n=1}^{N}M_n\sin(\frac{n\pi x}{L})\end{aligned} \tag{5-73}$$

Because this equation should be satisfied for each x, the following equation was developed for each mode:

$$\dot{B}_n - gA_n \frac{n\pi}{L} = -\ddot{X}M_n - C_f B_n - k_f M_n \sum_{n=1}^{n} B_n \sin(\frac{n\pi x_0}{L}) \tag{5-74}$$

Contrary to previous case studies, here, the nonlinear term $M_n \sum_{n=1}^{n} B_n \sin(\frac{n\pi x_0}{L})$ appears, which includes the multiplication of different modes. Here, the product of the different modes was neglected, so it was assumed to be $M_n \sum_{n=1}^{n} B_n \sin(\frac{n\pi x_0}{L}) \simeq M_n B_n \sin(\frac{n\pi x_0}{L})$. Although this assumption may not hold true for modes greater than one, it is valid for *n*=1. According to the previous test case, the total response of TLD coupled system is mainly influenced by the first mode; therefore, incorporating this assumption does not compromise the accuracy. Regarding this assumption, the momentum equation takes the following form:

$$\dot{B}_n - gA_n \frac{n\pi}{L} = -\ddot{X}M_n - C_f B_n - k_f M_n B_n \sin(\frac{n\pi x_0}{L}) \tag{5-75}$$

Or it can be expressed as

$$\dot{B}_n - gA_n \frac{n\pi}{L} = -\ddot{X}M_n - B_n(C_f + k_f M_n \sin(\frac{n\pi x_0}{L})) \tag{5-76}$$

Recall the momentum equation incorporating fluid dissociation, $\dot{B}_n - gA_n \frac{n\pi}{L} = -\ddot{X}M_n - C_f B_n$. Comparing this equation with Equation (5-76) indicates that local dissipation increases the fluid dissipation coefficient from C_f to $C_f + k_f M_n \sin(\frac{n\pi x_0}{L})$. In the smart approach, this particular case study can be addressed in a manner similar to the previous case, with the only difference being the adjusted fluid dissipation coefficient, $\overline{C}_f = C_f + k_f M_n \sin(\frac{n\pi x_0}{L})$. Therefore, as expressed in Equation (5-77), the characteristic equation relevant to this case is Equation (5-17), which replaces C_f with $\overline{C}_f$.

$$m\lambda^4 + (c + \overline{C}_f m)\lambda^3 + (k + \overline{C}_f c + K_{1n} m + K_{2n} K_{3n})\lambda^2 + (k\overline{C}_f + K_{1n} c)\lambda + (K_{1n} k) = 0 \tag{5-77}$$

In addition, analytical formulas (5-33) and (5-34) could be utilized here to evaluate the dissipation factor using $\bar{C}_f$ instead of C.

$$a_1 = \frac{-\xi\omega_s(\omega_1^2 - K_{1n})}{\omega_1^2 - \omega_2^2} + \frac{-\bar{C}_f(\omega_1^2 - \omega_s^2)}{2(\omega_1^2 - \omega_2^2)} \tag{5-78}$$

$$a_2 = \frac{-\xi\omega_s(K_{1n} - \omega_2^2)}{\omega_1^2 - \omega_2^2} + \frac{-\bar{C}_f(\omega_s^2 - \omega_2^2)}{2(\omega_1^2 - \omega_2^2)} \tag{5-79}$$

similar to the previous cases, it can be demonstrated that the introduction of the screen does not have a significant impact on the natural frequencies of the coupled system' response.

5.3.3.1. Analytical solution to the extended case study

In this section, in addition to the structural and fluid dissipation, the local dissipation resulting from the screen is introduced in the model. Therefore, the previous case study was extended to include the local head loss resulting from the screen. In the extended case study, the head loss coefficient, k_f , was assumed to be 0.2, and the screen was located at $x_0 = 0.2L$.

The analytical approach used for this test case was based on the assumption that is accurate and valid for the first mode. Consequently, the analytical solution presented herein is specific to the first mode. The natural frequencies and dissipation factors were derived from the characteristic equation (5-77) and are presented in columns 2 and 3 in Table (5.4). Comparing these natural frequencies to those obtained from the assumption of neglecting dissipations in Table (5.1) indicates the minimal impact of dissipation on the natural frequency. In addition, the dissipation factors derived from equations (5-78) and (5-79) in columns 4 and 5 approximately align well with the real part of the characteristic roots of Equation (5-77), columns 2 and 3.

Table 5.4. Natural frequencies and dissipation factors considering structure, fluid, and screen dissipation

Column 1	Column 2	Column 3	Column 2	Column 3	Column 4	Column 5
	Characteristic Equation (77)		Characteristic Equation (77)		Analytical Approximations (78, 79)	
	$c \neq 0 \,\&\, C_f \neq 0 \,\&\, k_f \neq 0$		$c \neq 0 \,\&\, C_f \neq 0 \,\&\, k_f \neq 0$		$c \neq 0 \,\&\, C_f \neq 0 \,\&\, k_f \neq 0$	
Mode Number	Greater Frequency	Smaller Frequency	Greater Frequency Dissipation Factor	Smaller Frequency Dissipation factor	Greater Frequency Dissipation Factor	Smaller Frequency Dissipation factor
1	0.720607591	0.633211368	-7.918E-02	-6.322E-02	-8.065E-02	-6.119E-02

5.3.3.2. Numerical solution to the extended case study

The coupled system, including structural, fluid, and screen dissipation, underwent free vibration with an initial displacement $X_0 = -0.01m$. The governing equation used in this case is the same as the system of Equation (5-49), except that Equation (5-49-2) is substituted with Equation (5-74). Therefore, unlike the analytical approach, the numerical model incorporates the interaction of different modes.

The time history of the response and the fundamental frequency of the response are presented in Figure (5.5). As shown, the fundamental frequencies align with the analytical frequencies.

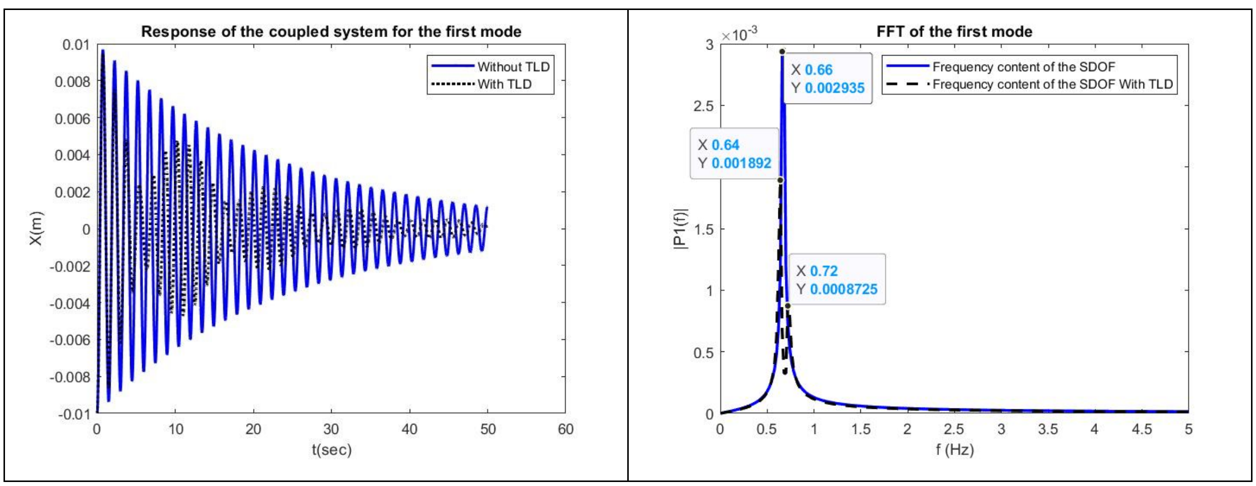

Fig. 5.5. Time domain and frequency domain of the coupled system response excited by initial displacement in different modes with considering structure, fluid, and screen dissipations

The time history of the response is compared with the analytical solution in Figure (5.6) for two cases: 1-free vibration with initial displacement and 2- free vibration with initial displacement and initial perturbation ($X_0 = -0.01m$ & $A_0 = 0.5\,m$). As shown, the analytical solution agrees well with the numerical results in both scenarios. This agreement reflects the high level of accuracy of the analytical model in predicting the frequency, dissipation, and response pattern. Besides, the numerical model is manipulated to simulate this case study for a combination of nine modes, without relying on the assumptions made in the analytical approach. This is, it incorporates the product of different modes in the dissipation term of the momentum equation. It was observed that the response of the coupled system did not change considerably when compared to the case dominated by the first mode, emphasizing the dominance of the first mode in TLD coupled system. Additionally, the results obtained from the numerical model considering all nine modes exhibit strong agreement with the analytical solution in Figure (5.7).

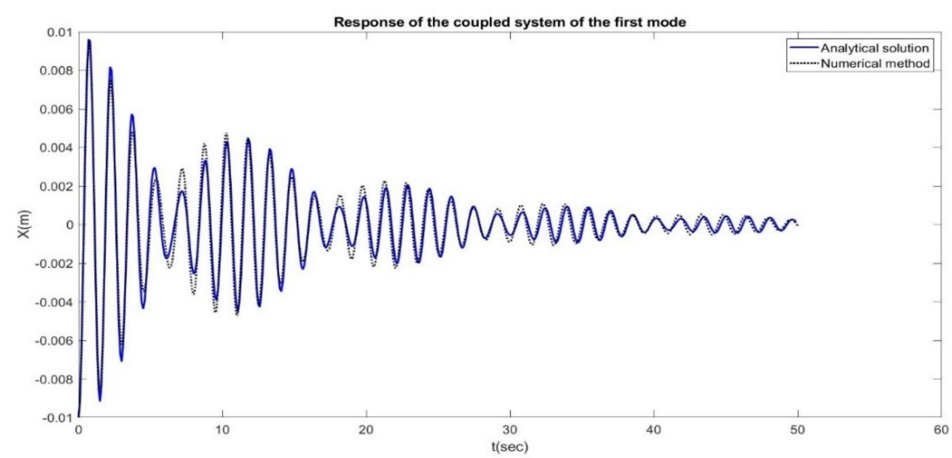

A

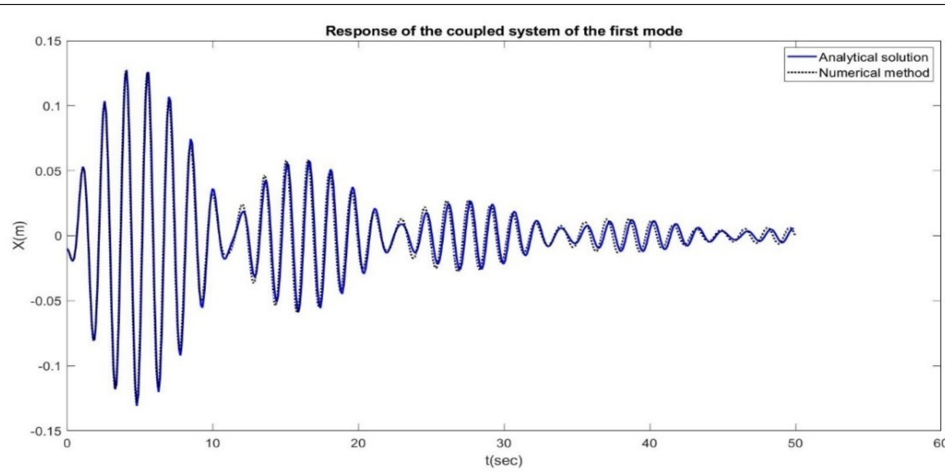

B

Fig. 5.6. Time history of the first mode of the coupled system response incorporating structure, fluid, and screen dissipations subjected to free vibration with A) initial displacement B) initial displacement and perturbation

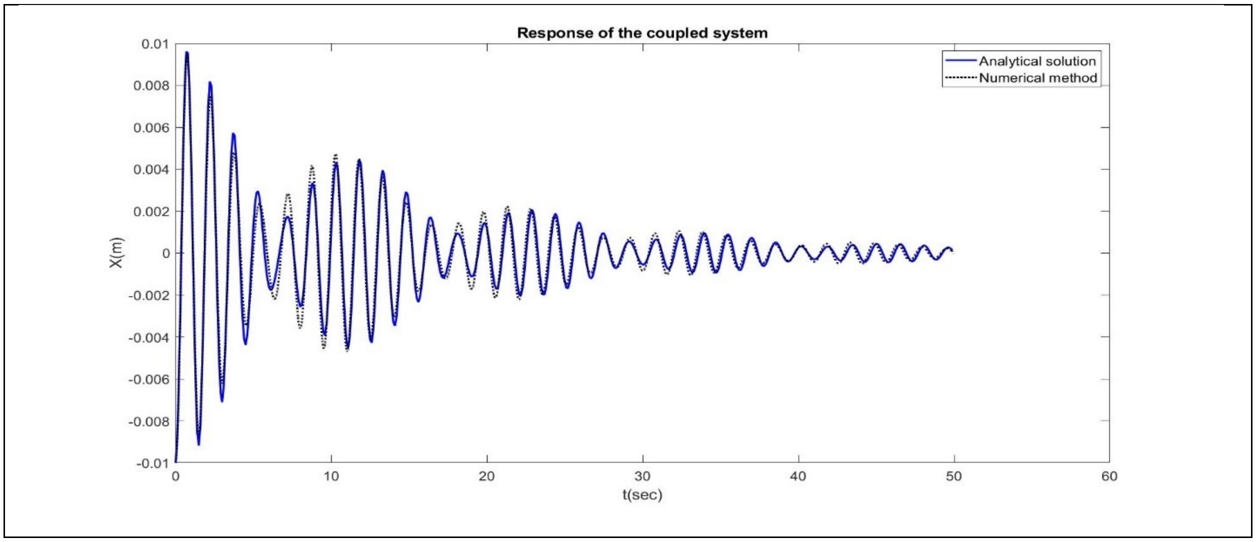

Fig. 5.7. Time history of the first mode of the coupled system response incorporating structure, fluid, and screen dissipations subjected to free vibration with initial displacement A) first mode in analytical solution B) composition of nine modes in the numerical model

At the end of this research, the TLD coupled system was subjected to free vibration with initial displacement, analyzed through both numerical and analytical approaches in four distinct scenarios: 1) without dissipation; 2) with structural dissipation; 3) with structural and fluid dissipation; and 4) with structural, fluid, and screen dissipation. It is evident from Figures (5.8a and 5.8b) that the analytical solution accurately predicts frequencies, dissipations, and the response pattern when compared to numerical results.

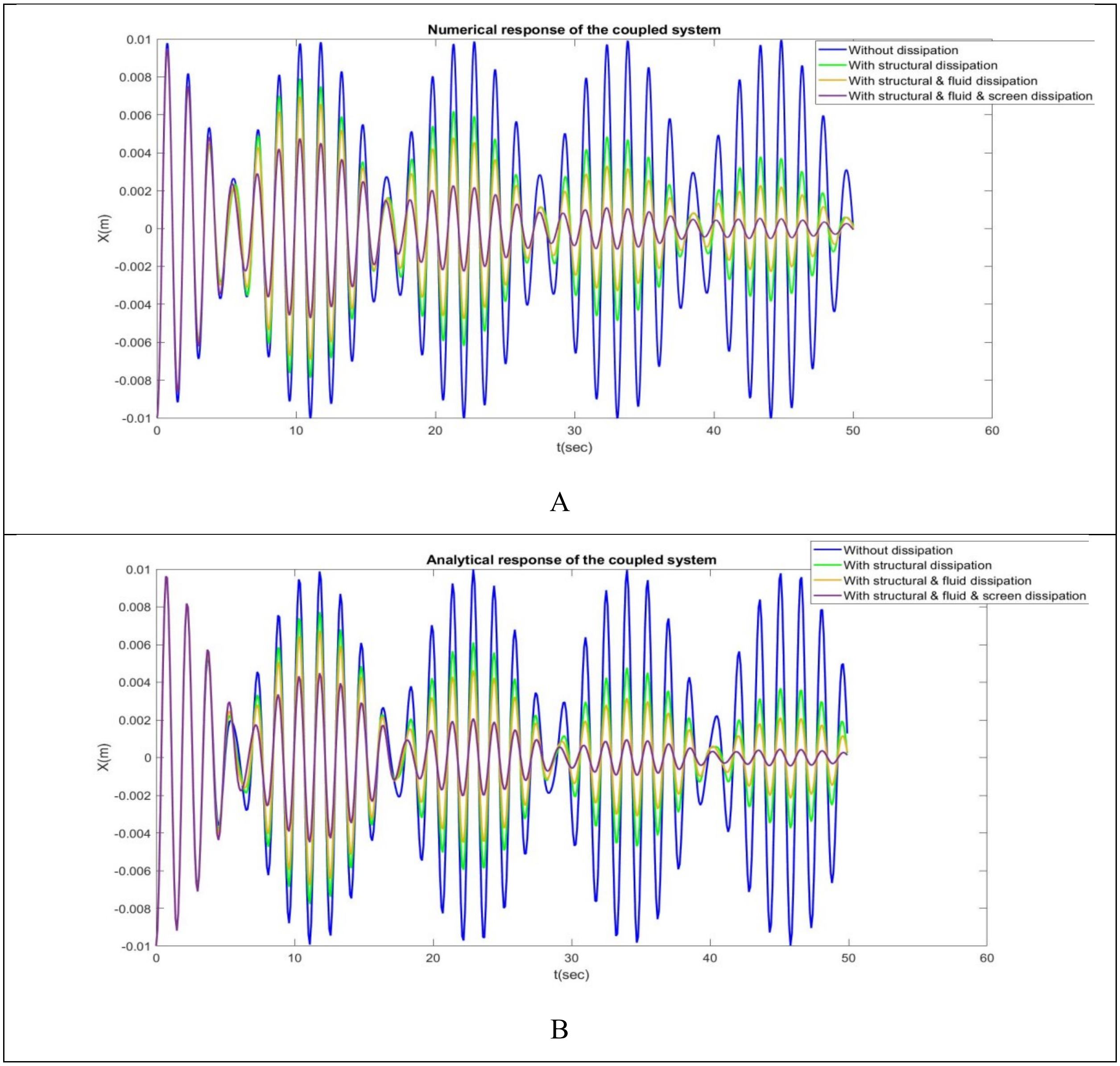

Fig. 5.8. Time history of the coupled system response in different cases of incorporating dissipations obtained from a) Numerical method b) Analytical solution

5.4. Discussion & Conclusion:

This study explored the free vibration of a coupled system involving a Single Degree of Freedom (SDOF) and a shallow water tank, considering the structural and fluid dissipation. By transforming the linear shallow water equations into modal coordinates and coupling them with the SDOF equations, a novel fourth-order ordinary differential equation was obtained. The solution to this equation yielded a characteristic polynomial governing the response of the coupled system for a given mode. Using an innovative approach, it was confirmed that the characteristic equation has two conjugate complex roots with negative real parts, signifying the stability of the coupled system. It was clarified that both parts of the roots of this equation play an important role: the imaginary part represents the natural frequency, whereas the real part indicates dissipation. Furthermore, using a current analytical approach that neglects higher orders of small values, it was demonstrated that dissipation minimally affects the natural frequencies. Furthermore, novel analytical formulas were proposed for the dissipation factors, showing their dependence on the structure, fluid damping, and natural frequencies. The analytical approach introduced new matrix equations based on the initial conditions to evaluate the response coefficients. It also suggested equations for the modal composition and decomposition to derive the total coupled system response.

The remaining portion of the research focused on applying the proposed analytical approach to Tuned Liquid Dampers (TLDs) and verifying it using a developed numerical model. A comparison of the results and the use of Fast Fourier Transform (FFT) analysis demonstrated the accuracy of the analytical solution in predicting natural frequencies. Originally, this approach justified why, in higher modes, not only does a greater natural frequency not contribute significantly to the response, but also an initial perturbation is required to stimulate the higher frequency. This approach clarified why for higher modes the coupled system response approaches a Single Degree of Freedom (SDOF) response with an equivalent dissipation factor. Comparative analyses in different dissipation scenarios and various initial boundary conditions underscored the high-level accuracy of the analytical approach in assessing the natural frequencies, dissipation factors, and response coefficients. Additionally, this illustrated that when a Tuned Liquid Damper (TLD) is coupled with an SDOF, the total response is primarily influenced by the contribution of the first mode.

A similar approach was employed here to develop the current analytical model that incorporates local dissipation, likely due to the presence of screen dissipation, along with structure and fluid dissipation. In contrast to the previous case, this model included a nonlinear term and embraced the assumption of neglecting the product of different modes, which is valid for TLD coupled system that is primarily influenced by the contribution of the first mode. The derived equations in the coordinate system suggested that this case study can be treated similarly to the previous study, with a modified fluid dissipation coefficient. A comparison between the results of the numerical method, which excludes this assumption, and the analytical approach demonstrated an accurate agreement in terms of frequencies, dissipation, and amplitude.

References

1. Amabili, M. (1996). Free vibration of partially filled horizontal cylindrical shells. *Journal of Sound and Vibration*, *191*(5), 757-780.
2. Antuono, M., Bouscasse, B., Colagrossi, A., & Lugni, C. (2012). Two-dimensional modal method for shallow-water sloshing in rectangular basins. *Journal of Fluid Mechanics*, *700*, 419-440.
3. Ashasi-Sorkhabi, A., Malekghasemi, H., Ghaemmaghami, A., & Mercan, O. (2017). Experimental investigations of tuned liquid damper-structure interactions in resonance considering multiple parameters. *Journal of Sound and Vibration*, *388*, 141-153.
4. Bahreini Toussi, I., Kianoush, R., & Mohammadian, A. (2020). Numerical and Experimental Investigation of Rectangular Liquid-Containing Structures under Seismic Excitation. *Infrastructures*, *6*(1), 1.
5. Bhattacharjee, E., Halder, L., & Sharma, R. P. (2013). An experimental study on tuned liquid damper for mitigation of structural response. *International Journal of Advanced Structural Engineering*, *5*, 1-8.
6. Biswal, K. C., Bhattacharyya, S. K., & Sinha, P. K. (2003). Free-vibration analysis of liquid-filled tank with baffles. *Journal of Sound and vibration*, *259*(1), 177-192.
7. Cao, X. Y., Ming, F. R., & Zhang, A. M. (2014). Sloshing in a rectangular tank based on SPH simulation. *Applied Ocean Research*, *47*, 241-254.
8. Chang, Y., Noormohamed, A., & Mercan, O. (2018). Analytical and experimental investigations of modified tuned liquid dampers (MTLDs). *Journal of Sound and Vibration*, *428*, 179-194.
9. Chen, B. F., & Wu, C. H. (2011). Effects of excitation angle and coupled heave–surge–sway motion on fluid sloshing in a three-dimensional tank. *Journal of marine science and technology*, *16*, 22-50.

10. Cho, I. H. (2021). Liquid sloshing in a swaying/rolling rectangular tank with a flexible porous elastic baffle. *Marine Structures*, *75*, 102865.
11. Cho, J. R., Lee, H. W., & Kim, K. W. (2002). Free vibration analysis of baffled liquid-storage tanks by the structural-acoustic finite element formulation. *Journal of Sound and Vibration*, *258*(5), 847-866
12. Crowley, S., & Porter, R. (2012). An analysis of screen arrangements for a tuned liquid damper. *Journal of Fluids and Structures*, *34*, 291-309.
13. Elahi, R., Passandideh-Fard, M., & Javanshir, A. (2015). Simulation of liquid sloshing in 2D containers using the volume of fluid method. *Ocean Engineering*, *96*, 226-244.
14. Faltinsen, O. M., Firoozkoohi, R., & Timokha, A. N. (2011). Analytical modeling of liquid sloshing in a two-dimensional rectangular tank with a slat screen. *Journal of Engineering Mathematics*, *70*, 93-109.
15. Frandsen, J. B. (2004). Sloshing motions in excited tanks. *Journal of computational physics*, *196*(1), 53-87.
16. Fujino, Y., Sun, L., Pacheco, B. M., & Chaiseri, P. (1992). Tuned liquid damper (TLD) for suppressing horizontal motion of structures. *Journal of engineering mechanics*, *118*(10), 2017-2030.
17. Gardarsson, S., Yeh, H., & Reed, D. (2001). Behavior of sloped-bottom tuned liquid dampers. *Journal of engineering mechanics*, *127*(3), 266-271.
18. Ghaemmaghami, A. R., & Kianoush, M. R. (2010). Effect of wall flexibility on dynamic response of concrete rectangular liquid storage tanks under horizontal and vertical ground motions. *Journal of structural engineering*, *136*(4), 441-451.
19. Goudarzi, M. A., Sabbagh-Yazdi, S. R., & Marx, W. (2010). Seismic analysis of hydrodynamic sloshing force on storage tank roofs. *Earthquake Spectra*, *26*(1), 131-152.
20. Han, Y., Zhu, X., Guo, W., Li, T., & Zhang, S. (2022). Coupled vibration analysis of partially liquid-filled cylindrical shell considering free surface sloshing. *Thin-Walled Structures*, *179*, 109555.
21. Hernandez-Hernandez, D., Larkin, T., & Chouw, N. (2021). Shake table investigation of nonlinear soil–structure–fluid interaction of a thin-walled storage tank under earthquake load. *Thin-Walled Structures*, *167*, 108143.

22. Housner, G. W. (1957). Dynamic pressures on accelerated fluid containers. *Bulletin of the seismological society of America*, *47*(1), 15-35.
23. Hu, Z., Zhang, X., Li, X., & Li, Y. (2018). On natural frequencies of liquid sloshing in 2-D tanks using boundary element method. *Ocean Engineering*, *153*, 88-103.
24. Huang, P. (2023). A comprehensive investigation on liquid sloshing of rectangular water tank with vertical baffles. *Ocean Engineering*, *288*, 116126.
25. Humar, J. (2012). *Dynamics of structures*. CRC press.
26. Ikeda, T., Harata, Y., & Osasa, T. (2016). Internal resonance of nonlinear sloshing in rectangular liquid tanks subjected to obliquely horizontal excitation. *Journal of Sound and Vibration*, *361*, 210-225.
27. Kamarroudi, S. H., Hosseini, M., & Hosseini, K. (2021). Influence of earthquake vertical excitations on Sloshing-Created P-Δ effect in elevated water Tanks: Experimental Validation, numerical simulation and proposing a modification for Housner model. *Engineering Structures*, *246*, 112995.
28. Khanpour, M., Mohammadian, A., Shirkhani, H., & Kianoush, R. (2024). Analytical solution to a coupled system including Tuned Liquid Damper and Single Degree of Freedom under free vibration with modal decomposition method. *Journal of Physics of Fluids. 36(5)*
29. Liu, D., & Lin, P. (2008). A numerical study of three-dimensional liquid sloshing in tanks. *Journal of Computational physics*, *227*(8), 3921-3939.
30. Lu, Y., Zhou, T., Cheng, L., Zhao, W., & Jiang, H. (2018). Dependence of critical filling level on excitation amplitude in a rectangular sloshing tank. *Ocean Engineering*, *156*, 500-511.
31. Martínez-Carrascal, J., & González-Gutiérrez, L. M. (2021). Experimental study of the liquid damping effects on a SDOF vertical sloshing tank. *Journal of Fluids and Structures*, *100*, 103172.
32. Meng, X., Zhou, D., Lim, Y. M., Wang, J., & Huo, R. (2023). Seismic Response of Rectangular Liquid Container with Dual Horizontal Baffles on Deformable Soil Foundation. *Journal of Earthquake Engineering*, *27*(7), 1943-1972.

33. Mittal, V., Chakraborty, T., & Matsagar, V. (2014). Dynamic analysis of liquid storage tank under blast using coupled Euler–Lagrange formulation. *Thin-Walled Structures*, *84*, 91-111.
34. Moslemi, M., & Kianoush, M. R. (2012). Parametric study on dynamic behavior of cylindrical ground-supported tanks. *Engineering Structures*, *42*, 214-230.
35. Narayanasetti, M. D., Pandit, A., & Biswal, K. C. (2022). Seismic analysis of base-isolated liquid storage tank with submerged block. *Practice Periodical on Structural Design and Construction*, *27*(1), 04021052.
36. Núñez Aedo, J., Cruchaga, M., & Castillo del Barrio, E. (2020). Study on the dependence with the filling level of the sloshing wave pattern in a rectangular tank. *Physics of Fluids*, *32*(1).
37. Pandit, A. R., & Biswal, K. C. (2020, June). Seismic control of multi degree of freedom structure outfitted with sloped bottom tuned liquid damper. In *Structures* (Vol. 25, pp. 229-240). Elsevier.
38. Panigrahy, P. K., Saha, U. K., & Maity, D. (2009). Experimental studies on sloshing behavior due to horizontal movement of liquids in baffled tanks. *Ocean engineering*, *36*(3-4), 213-222.
39. Pilloton, C., Bardazzi, A., Colagrossi, A., & Marrone, S. (2022). SPH method for long-time simulations of sloshing flows in LNG tanks. *European Journal of Mechanics-B/Fluids*, *93*, 65-92.
40. Rezaiee-Pajand, M., & Kazemiyan, M. S. (2019). A formula for calculating fundamental natural frequency of partially-filled tanks. *Ocean Engineering*, *191*, 106400.
41. Saburin, D. S. (2015). Tank sloshing simulations in shallow-water approximation. In *MARINE VI: proceedings of the VI International Conference on Computational Methods in Marine Engineering* (pp. 1039-1050). CIMNE.
42. Saha, S. K., Matsagar, V. A., & Jain, A. K. (2014). Earthquake response of base-isolated liquid storage tanks for different isolator models. *Journal of Earthquake and Tsunami*, *8*(05), 1450013.
43. Strand, I. M., & Faltinsen, O. M. (2017). Linear sloshing in a 2D rectangular tank with a flexible sidewall. *Journal of Fluids and Structures*, *73*, 70-81.

44. Sun, L. M., Fujino, Y., Pacheco, B. M., & Chaiseri, P. (1992). Modelling of tuned liquid damper (TLD). *Journal of Wind Engineering and Industrial Aerodynamics*, *43*(1-3), 1883-1894.
45. Tait, M. J., El Damatty, A. A., Isyumov, N., & Siddique, M. R. (2005). Numerical flow models to simulate tuned liquid dampers (TLD) with slat screens. *Journal of Fluids and Structures*, *20*(8), 1007-1023.
46. Tedesco, J. W., Kostem, C. N., & Kalnins, A. (1987). Free vibration analysis of cylindrical liquid storage tanks. *Computers & structures*, *26*(6), 957-964.
47. Vern, S., Shrimali, M. K., Bharti, S. D., & Datta, T. K. (2021). Seismic behavior of baffled liquid storage tank under far-field and near-field earthquake. In *Recent Advances in Computational Mechanics and Simulations: Volume-I: Materials to Structures* (pp. 445-456). Springer Singapore.
48. Xue, M. A., & Lin, P. (2011). Numerical study of ring baffle effects on reducing violent liquid sloshing. *Computers & Fluids*, *52*, 116-129.
49. Xue, M. A., Chen, Y., Zheng, J., Qian, L., & Yuan, X. (2019). Fluid dynamics analysis of sloshing pressure distribution in storage vessels of different shapes. *Ocean Engineering*, *192*, 106582.
50. Yu, L., Xue, M. A., & Zhu, A. (2020). Numerical investigation of sloshing in rectangular tank with permeable baffle. *Journal of Marine Science and Engineering*, *8*(9), 671.
51. Zang, Q., Fang, H., Liu, J., & Lin, G. (2019). Boundary element model for investigation of the effects of various porous baffles on liquid sloshing in the two dimensional rectangular tank. *Engineering Analysis with Boundary Elements*, *108*, 484-500.
52. Zhao, Z., Zhang, R., Jiang, Y., & Pan, C. (2019). A tuned liquid inerter system for vibration control. *International Journal of Mechanical Sciences*, *164*, 105171.
53. Zhou, J., & Zhao, M. (2021). Impact of earthquake direction and liquid sloshing on column supported tank. *Engineering Structures*, *247*, 113037.

List of Symbols

H	Mean water level
η	Wave height
U	Depth- average velocity
C_f	Fluid dissipation constant
m	Mass of SDOF
k	Stiffness of SDOF
c	Damping coefficient of SDOF
X	Displacement of SDOF
$\dot{X}$	Velocity of SDOF
$\ddot{X}$	Acceleration of SDOF
F_{exc}	Excitation force on SDOF
F_{slo}	Sloshing Force on SDOF
L	Length of the water tank
ρ	Water density
g	Gravity acceleration
B	Width of the water tank
ω_s	Natural frequency of SDOF
ξ	Damping ratio
c_{cr}	Critical damping
ω_1	Greater natural frequency of the coupled system

ω_2	Smaller natural frequency of the coupled system
a_1	Dissipation factor associated to greater natural frequency
a_2	Dissipation factor associated to greater natural frequency
$X(0)$	Initial displacement of the coupled system
$\dot{X}(0)$	Initial velocity of the coupled system
$\ddot{X}(0)$	Initial acceleration of the coupled system
A_0	Initial wave height perturbation
B_0	Initial wave velocity perturbation
$\omega_{1,n}$	Smaller natural frequency of the coupled system of the mode *n*
$\omega_{2,n}$	greater natural frequency of the coupled system of the mode *n*
$X_{0,n}$	Initial displacement of the coupled system of the mode *n*
W_L	TLD's weight
ω_L	Natural frequency of water tank
k	Coefficient of the head loss

6. A novel analytical solution to a TLD coupled system under harmonic excitation[5]

Abstract:

This paper presents a novel analytical approach that relies on the separation of variables technique to model a system incorporating a Tuned Liquid Damper (TLD) at the top of a Single Degree of Freedom (SDOF) under forced excitation. By coupling the linear wave theory with the dynamic behavior of an SDOF in a modal coordinate system, a fourth-order differential equation was derived. This equation represents the dynamic behavior of a shallow elevated tank under small-amplitude force excitation, and is modified for the TLD-coupled system. The coupled differential equation was examined in three scenarios: undamped, structurally damped, and both fluid and structurally damped. Key concepts such as the dynamic amplification factor, phase difference between the excitation force and system displacement, and their variations with frequency ratio are discussed in different scenarios. Particular and complementary solutions were introduced, and innovative initial boundary conditions were proposed to derive the total response of the TLD-coupled system. Notably, these solutions and concepts are tailored for two specific conditions: when the excitation frequency approaches the TLD tank frequency and the natural frequency of the coupled system. A numerical method based on the partitioned approach was employed to assess the accuracy and validity of the model. The results of this model not only bridge the gap in the literature but also offer significant insights and a profound understanding of the dynamic behavior of the coupled system.

Keywords: Analytical response of a TLD coupled system, Particular and complementary response, Dynamic amplification, Initial value vector, Resonance excitation

[5] Mahdiyar Khanpour, Abdolmajid Mohammadian, Hamidreza Shirkhani, and Reza Kianoush "*A novel analytical solution to a TLD coupled system under harmonic excitation*". ***Physics of Fluids***, *Submitted*.

6.1. Introduction

Due to rapid urbanization and the limited availability of land in urban areas, there is an increasing interest in constructing and living in tall, slender buildings. These buildings are highly susceptible to significant vibrations during earthquakes or strong winds. Damping devices are used to counteract these severe and undesirable vibrations. Among these, tuned liquid dampers (TLDs) offer notable advantages such as easy installation and cost-effectiveness, making them suitable for both new and existing structures. However, the fluid-structure interaction inherent in TLDs poses a substantial challenge to researchers. Typically installed at the top of structures, these dampers are tuned to leverage the sloshing waves induced by external excitations to reduce the vibrations in the underlying structures.

A key aspect of TLD modeling is the accurate simulation of sloshing waves within the tank. Various methodologies have been explored to address this challenge. These approaches can be broadly classified into five categories:

Shallow water model (SWM): These equations are a set of hyperbolic partial differential equations (PDEs) derived by depth-integrating Navier–Stokes equations under the assumption that the horizontal length scale is much greater than the vertical length scale. Given that TLDs are shallow water tanks, shallow water models (SWMs) are particularly suitable for their modeling. These models enforce the no-penetration boundary condition at the tank bottom while directly incorporating atmospheric pressure and the kinematic boundary condition at the free surface into the continuity and momentum equations. Consequently, the free surface location is derived from shallow water equations (SWE), eliminating the need for additional equations and thereby significantly reducing computational costs compared to other CFD models. Sun et al. (1992), Fujino et al. (1992), Banerji et al. (2000), Tait et al. (2005), Khanpour et al. (2024a), and Khanpour et al. (2024b) are examples employed the SWM to model tuned liquid dampers.

Potential flow theory: Potential theory models sloshing waves based on the assumptions of incompressible, inviscid, and irrotational flows. By defining a velocity potential function, the continuity equation is transformed into a Laplace equation, which is a second-order linear PDE. The Laplace equation is a boundary value problem, meaning that to solve for potential flow, the value or its derivatives must be specified at the boundaries. In sloshing problems, the velocity, which is the gradient of potential flow, is known at the walls and bottom of the tank. The dynamic and kinematic boundary conditions at the free surface introduce an additional nonlinear differential equation. To simplify the problem and reduce the computational cost, sloshing models often neglect nonlinear terms, which is valid for sloshing waves with small amplitudes, aligning with the linear potential flow theory. Pandit and Biswal (2020), Zhang (2020), and Su (2021) employed potential flow theory to model sloshing waves in Tuned Liquid Dampers (TLDs).

Volume of Fluid (VOF): The Volume of Fluid (VOF) method is a mesh-based approach for tracking the free surface using a scalar parameter known as the fluid fraction, which represents the ratio of the Volume of Fluid within a cell to the total volume of that cell. The fluid fraction is derived using the advection equation, which must be coupled with the Navier-Stokes equations to accurately model the free surface flow. The choice of numerical scheme for solving the VOF equation is crucial. Low-order numerical schemes can introduce numerical diffusion errors, thereby reducing the accuracy of the solution, while higher-order schemes may generate noisy results. Therefore, the numerical scheme in this method must be capable of modeling sharp and violent free surfaces while maintaining a monotonic profile. To achieve this, various schemes, such as the donor-acceptor scheme, have been proposed. Marivani and Hamed (2009, 2017) utilized this approach to model the free surface of Tuned Liquid Dampers (TLDs).

Smoothed Particle Hydrodynamics (SPH): Smoothed Particle Hydrodynamics (SPH) is a Lagrangian numerical scheme in which the flow domain is represented by particles. In this method, the continuity equation is used to calculate the density of each particle and the movement within the domain is governed by the momentum equation. The scheme relies on a kernel function for integral approximation, which must meet specific conditions. The initial SPH approach, which assumes low compressibility, introduces an equation of state to link the pressure and density, thus coupling the continuity and momentum equations in what is known as Weakly Compressible SPH (WCSPH) (Khanpour et al. 2016a). In contrast, the more recent Incompressible SPH (ISPH) method derives a partial differential equation for pressure (Poisson equation) through the projection method. SPH is a Lagrangian method that benefits from minimal numerical diffusion and can effectively model violent free surfaces without additional equations, thereby making it suitable for sloshing simulations. However, this method also has drawbacks, including void formation, high computational costs, challenges in modeling the inflow and outflow (Khanpour et al. 2016b), noisy pressure fields, and low convergence. McNamara et al. (2022a, 2022b) utilized the SPH method to model violent sloshing waves induced by high-amplitude excitations.

Housner Theory: Housner (1963) made a pivotal contribution to the modeling of sloshing tanks by conceptualizing the fluid dynamics within the tank as a two-degree-of-freedom system. He characterized the lower portion, termed the impulsive component, as moving in unison with the tank and being rigidly connected to the walls, while the upper portion, known as the convective component, corresponded to sloshing waves. Housner introduced the equivalent mass, stiffness, and natural frequencies for each degree of freedom. Upon the introduction of Housner's analytical formulation, it has been refined by various researchers. For instance, Veletsos (1974) posited that the flexibility of the tank influences the dynamic properties of the impulsive component, but does not affect the convective component. In the case of Tuned Liquid Dampers (TLDs), the mass of water in the tank is significantly smaller than that of the underlying structure. Consequently, the impulsive component of the water tank, which moves with the tank structure at a frequency different from the underlying structure, does not substantially affect the structure below. In contrast, the sloshing component, tuned to match the frequency of the underlying structure, has a significant effect on the structural response, despite its relatively small mass. Therefore, some researchers have modeled TLDs using equivalent mass, spring, and damping parameters based on the first mode of sloshing (Abd-Elhamed and Tolan 2022; Konar and Ghosh 2020).

Following the introduction of tuned liquid dampers (TLDs), researchers began to investigate the dynamic behavior of these systems and sought ways to optimize their effectiveness in mitigating structural vibrations. Some research efforts have concentrated on conducting parametric studies on TLDs using experimental methods. For example, Bhattacharjee et al. (2013) investigated the impact of water depth on TLD performance and identified an optimal depth corresponding to minimal vibration levels. Some studies have focused on the TLD/structure mass ratio. For example, Ashasi-Sorkhabi et al. (2018) utilized a real-time hybrid simulation (RTHS) to investigate this parameter. In addition, they compared the performance of coupled TLDs with that of a single TLD. Another critical parameter that has garnered significant attention from researchers is the TLD/structure frequency ratio. For instance, Fujino (1992) and Banerji et al. (2000) examined the effectiveness of TLDs in damping vibrations with respect to this parameter, considering the harmonic excitation and bandwidth of ground motion, respectively.

Sun et al. (1992) investigated the breaking waves in TLDs and introduced two terms to account for the dissipation effects resulting from breaking waves in a shallow water model.

Murudi et al. (2012) examined the impact of ground motion parameters such as frequency content, bandwidth, and intensity on TLD performance. Their study also demonstrated that TLDs are more effective in mitigating vibrations caused by far-field ground motions.

Abd-Elhamed and Tolan (2023) integrated soil-structure interaction (SSI) into their model of tuned liquid dampers (TLDs). Their approach utilized Housner's theory and included screens in the TLD model.

Researchers have sought to enhance the efficiency of tuned liquid dampers (TLDs) by increasing the sloshing force, or counterbalance force. Khanpour et al. (2024a) demonstrated that TLDs with sloped beds produced higher sloshing waves, resulting in a more pronounced damping effect. Pandit and Biswal (2020) investigated the performance of a slope-bottom-tuned liquid damper on a multi-degree-of-freedom system subjected to three types of earthquake excitations. Their model was based on the potential flow theory and utilized the finite element method.

Some research on tuned liquid dampers (TLDs) has focused on the integration of screens or baffles as supplementary damping components within a water tank. For instance, Konar and Ghosh (2020) employed an equivalent spring-mass-damper system derived from the first mode of sloshing to model TLDs and introduced an additional damping ratio to account for these flow-damping devices. Tait et al. (2004) utilized a numerical approach based on the shallow water model to examine TLDs equipped with screens under a wide range of excitation amplitudes. Additionally, Marivani and Hamed (2017) applied the Volume of Fluid (VOF) model to simulate the flow around slot screens and assess the pressure drop, which is a critical factor in the damping effectiveness of TLDs. Their study explored various slot configurations, including slot height and solid projected area, to understand their impact on the damping performance.

Some studies have focused on enhancing the effectiveness of tuned liquid dampers (TLDs) by incorporating or improving additional elements. For example, Chang et al. (2018) developed an advanced TLD that integrates a rational spring at the base. This modification not only augments the sloshing force but also transfers a moment to the underlying structure, thereby increasing the counterbalancing effect. Zhao et al. (2019) introduced a tuned liquid inerter damper (TLID) by combining a TLD with a subsystem that includes the stiffness, damping, and inerter mass. This configuration, modeled using Housner's theory, enhances the efficiency of TLD. Sun et al. (2024) employed a TLID with a damping net (a porous media obstacle) and sloped bottom, referred to as TLID-NS, to amplify the energy dissipation of the underlying structure.

Technically, sloshing waves typically exhibit lower frequencies than short or moderately high structures. Martín Domizio et al. (2024) proposed a system that incorporates a series of springs on a floating roof to increase the restoring force on the free surface, resulting in a higher TLD frequency. Additionally, Pandey et al. (2019) explored a different approach by installing a TLD on an array of compliant elastomeric pads that function as springs. This setup allows adjustment of the pad's vibration frequency to match that of the underlying structure.

Tuned liquid dampers (TLDs) are known for their stabilizing effects on tall structures subjected to wind or seismic forces, but they can also be effective in marine applications that experience wave excitation. Sardar and Chakraborty (2022) evaluated the performance of TLDs in mitigating the vibrations of offshore jacket platforms under wave loading, considering both regular and random wave conditions. Additionally, Saghi et al. (2024) employed the Volume of Fluid (VOF) method to assess the effectiveness of bidirectional tuned liquid dampers in stabilizing floating offshore substructures. Their study focused on how these TLDs reduce the pitch motions induced by wave action.

Most research has focused on single-degree-of-freedom (SDOF) systems as the underlying structure. In contrast, there has been limited investigation into how tuned liquid dampers (TLDs) affect multi-degree-of-freedom (MDOF) systems. Tang et al. (2022) explored the stabilization of MDOF systems using TLDs by introducing a transfer function and employing the Housner theory for TLD modeling. Similarly, Pabarja et al. (2019) conducted experimental studies to evaluate the performance of multiple TLDs in a three-story structure with vertical irregularities, which resulted in more significant contributions from the higher modes.

McNamara et al. (2022) examined the performance of tuned liquid dampers (TLDs) with consideration of limited freeboard. They utilized smoothed particle hydrodynamics (SPH) to model sloshing waves in the tank and introduced additional damping effects resulting from the impact of waves on the ceiling.

In reviewing the existing literature, it is evident that there is a substantial gap in the analytical modeling of TLD coupled systems under forced excitation. The term "TLD coupled system" in this research refers to a Tuned Liquid Damper (TLD) positioned atop an underlying structure. For this study, a single-degree-of-freedom (SDOF) system is used to represent the underlying structure. Technically, the development of an analytical solution is highly valuable and crucial because it elucidates the relationships between key parameters, thereby deepening the understanding of this complex process. In this study, the continuity and momentum equations are transformed into a modal coordinate system and integrated with the dynamic equation of a single-degree-of-freedom (SDOF) system representing the underlying structure. After deriving a novel characteristic equation and applying initial boundary conditions, this study introduces for the first time the general, particular, and total solutions of a TLD-coupled system across different scenarios, including 1) undamped, 2) structurally damped, and 3) fluid and structurally damped systems. Moreover, novel concepts within the coupled system, such as 1) dynamic amplification factors and 2) the phase difference between the excitation force and displacement of the coupled system, are examined, and their relationships are derived. In each scenario, in addition to the general case, the solutions are further refined for two special conditions: 1) the resonance excitation of the TLD coupled system where the excitation force frequency approaches the natural frequencies of the coupled system, and 2) The scenario in which the excitation frequency approaches the natural frequency of the TLD tank. A numerical model has been developed throughout this research to validate and assess the accuracy of the proposed analytical approach.

Two significant points warrant explanation. First, the present analytical approach is based on linear wave theory and assumes a linear behavior of the underlying structure, making it accurate primarily under conditions of small-amplitude excitation and wave sloshing. However, under high excitation conditions, where nonlinear effects become more pronounced, additional terms, particularly nonlinear terms, must be introduced into the equations. In such cases, the analytical approach becomes increasingly complex and may even become infeasible. Additionally, although this research is based on harmonic excitation forces, the developed methodology can be extended to accommodate any arbitrary periodic excitation force. This is possible because any periodic function can be decomposed into harmonic components with fundamental frequencies obtained through a Fourier transformation. The response of the coupled system can be derived for each fundamental frequency by applying the current analytical approach. Given that the model operates within the framework of the linear theory, the responses corresponding to all fundamental frequencies can then be superimposed to obtain the total system response

6.2. Governing Equations and Methodology

As previously mentioned, fluid simulation primarily relies on linear shallow water equations, encompassing both the continuity equation (6-1.1) and momentum equation (6-1.2) (Toro, 2001). In these equations, the parameters η and u represent wave height and velocity, respectively, both of which are functions of space (x) and time (t) (Refer to Figure 6.1). The parameter H denotes the mean water level, g represents gravitational acceleration, and $\ddot{X}$ signifies tank acceleration. The term $C_f u$ represents fluid dissipation, and the coefficients C_f is referred to as fluid damping coefficient.

$$\frac{\partial \eta}{\partial t} + H\frac{\partial u}{\partial x} = 0 \tag{6-1.1}$$

$$\frac{\partial u}{\partial t} + g\frac{\partial \eta}{\partial x} = -\ddot{X} - C_f u \tag{6-1.2}$$

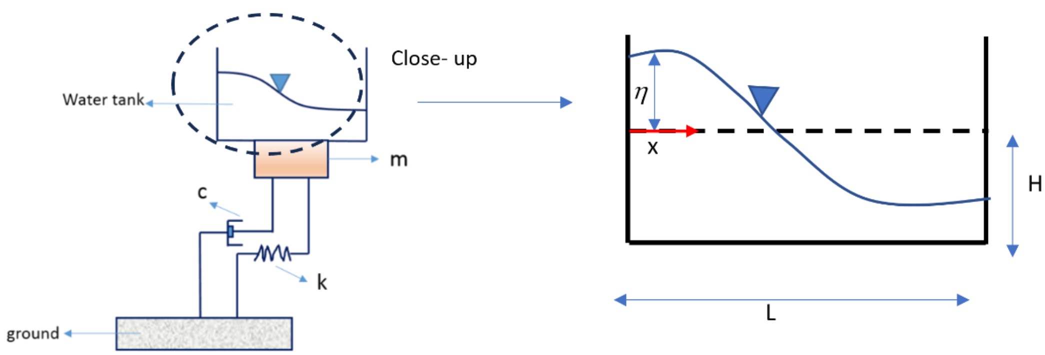

Fig. 6.1. Schematic of a tuned liquid damper at the top of a single degree of freedom

To convert these partial differential equations into ordinary differential equations, the separation of variables approach is used. According to this approach, variables u and η can be expressed as shown in Equations (6-2) and (6-3). In these equations, $cos(\frac{i\pi x}{L})$ and $sin(\frac{i\pi x}{L})$ are the mode shapes that satisfy the boundary conditions of zero-gradient wave height and zero velocities at the walls ($x = 0$ & $x = L$). The parameters A_n and B_n are functions of time (t) only.

$$\eta(x,t)=\sum_{i=1}^{N} A_i(t)cos(\frac{i\pi x}{L})=A_1(t)cos(\frac{i\pi x}{L})+...+A_n(t)cos(\frac{n\pi x}{L})+...A_N(t)cos(\frac{N\pi x}{L}) \tag{6-2}$$

$$u(x,t)=\sum_{i=1}^{N} B_i(t)sin(\frac{i\pi x}{L})=A_1(t)sin(\frac{i\pi x}{L})+...+A_n(t)sin(\frac{n\pi x}{L})+...A_N(t)sin(\frac{N\pi x}{L}) \tag{6-3}$$

Substituting equations (6-2) and (6-3) into equations (6-1.1) and (6-1.2) and applying the Fourier transformation results in equations (6-4) and (6-5). These equations represent the continuity and momentum equations in the modal coordinate system. For further details, please refer to Khanpour et al. (2024b). According to equation (6-5), the acceleration of each mode is $\ddot{X}M_n$, where M_n is derived from equation (6-5). In this context, tank acceleration affects only the odd modes, while the even modes remain inactive.

$$\dot{A}_n = -HB_n(\frac{n\pi}{L}) \tag{6-4}$$

$$\begin{aligned} &\dot{B}_n + gA_n(-\frac{n\pi}{L}) = -\ddot{X}M_n - C_f B_n \\ &where \\ &M_n = -2\left[\frac{(-1)^n - 1^n}{n\pi}\right] \rightarrow \left\{ \begin{aligned} &M_n = 0 \quad for\ n = 2K \\ &M_n = \frac{4}{n\pi} \quad for\ n = 2K+1 \end{aligned} \right\} \end{aligned} \tag{6-5}$$

Taking the derivative of the modal continuity equation, Equation (6-4) with respect to time results in Equation (6-6). Substituting the B_n, $\dot{B}_n$ from Equations (6-4) and (6-6) into the modal momentum equation, Equation (6-5), yields equation (6-7). The latter equation is a second-order ordinary differential equation that includes both the continuity and momentum equations. It introduces two parameters, k_{1n} and k_{2n}, which depend on the mode numbers and specifications of the tanks, such as the water height and tank length.

$$\ddot{A}_n = -\dot{B}_n(\frac{Hn\pi}{L}) \tag{6-6}$$

$$\ddot{A}_n + C_f \dot{A}_n + K_{1n} A_n - K_{2n} \ddot{X} = 0$$

where (6-7)

$$k_{1n} = (\frac{Hgn^2\pi^2}{L^2}) > 0 \quad k_{2n} = (\frac{Hn\pi}{L}) M_n = \begin{Bmatrix} 0 \;\; for\, n = 2K \\ \frac{4H}{L} \; for\, n = 2K+1 \end{Bmatrix} \geq 0$$

Now, let us consider the well-known established expression, Equation (6-8), which describes the natural frequency of the water tank, ω_f.

$$\omega_f = \sqrt{\frac{\pi g}{L} tanh(\frac{\pi H}{L})} \tag{6-8}$$

When the ratio of the water height to the tank length approaches zero, the shallow water tank is $tanh(\frac{\pi H}{L}) \simeq (\frac{\pi H}{L})$. Therefore, the following approximation is established between k_{1n} in equation (6-7) and ω_f in equation (6-8) with a high degree of accuracy.

$$k_{1n} \simeq (n\omega_f)^2 \tag{6-9}$$

As depicted in Figure (6.1), the underlying structure of the shallow water tank is represented by a single degree of freedom (SDOF) system. The acceleration of the SDOF is transferred to the water tank, and the sloshing force of the water tank is conveyed to the SDOF, thereby developing a coupled system. The dynamic equation of a single degree of freedom is expressed as Equation (6-10), where X_n, $\dot{X}_n$, $\ddot{X}_n$ refer to the displacement, velocity, and acceleration of the SDOF resulting from the contribution of each mode, such as mode *n*. The parameters m, c, k denote the mass, damping coefficient, and stiffness of the SDOF, respectively.

With respect to Equation (6-10), the SDOF not only experiences internal forces, namely $m\ddot{X}_n$, $c\dot{X}_n$, kX_n, which represent the inertial force, damping force, and elastic force, but is also subjected to external forces, including the excitation force, F_{exc}, and sloshing force, F_{exc}, for each mode. In this study, the excitation force is considered to be a harmonic function. In this equation, F and $\bar{\omega}$ represent the amplitude and frequency of force excitation, respectively.

$$m\ddot{X}_n + c\dot{X}_n + kX_n = (F_{exc})_n + (F_{slo})_n = F_n \sin(\bar{\omega}t) + (F_{slo})_n \tag{6-10}$$

As demonstrated in a previous study by Khanpour et al. (2024b), the sloshing force resulting from each mode can be derived from Equation (6-11).

$$(F_{slo})_n = -k_{3n} A_n$$
$$where \qquad (6\text{-}11)$$
$$k_{3n} = \begin{cases} 0 & for\ n = 2i \\ 2\rho g H b & for\ n = 2i+1 \end{cases} \quad k_{3n} \geq 0$$

Concerning Equation (6-11), Equation (6-10) can be expressed as:

$$m\ddot{X}_n + c\dot{X}_n + kX_n = (F_{exc})_n + (F_{slo})_n = F_n \sin(\varpi t) - k_{3n} A_n \qquad (6\text{-}12)$$

With respect to Equation (6-12), the parameter A_n and its first- and second-time derivatives are determined using Equations (6-13.1), (6-13.2), and (6-13.3), respectively.

$$A_n = (-\frac{m}{k_{3n}})\ddot{X}_n + (-\frac{c}{k_{3n}})\dot{X}_n + (-\frac{k}{k_{3n}})X_n + (\frac{F_n \sin(\varpi t)}{k_{3n}}) \qquad (6\text{-}13.1)$$

$$\dot{A}_n = (-\frac{m}{k_{3n}})\dddot{X}_n + (-\frac{c}{k_{3n}})\ddot{X}_n + (-\frac{k}{k_{3n}})\dot{X}_n + (\frac{\varpi F_n \cos(\varpi t)}{k_{3n}}) \qquad (6\text{-}13.2)$$

$$\ddot{A}_n = (-\frac{m}{k_{3n}})\ddddot{X}_n + (-\frac{c}{k_{3n}})\dddot{X}_n + (-\frac{k}{k_{3n}})\ddot{X}_n + (\frac{-\varpi^2 F_n \sin(\varpi t)}{k_{3n}}) \qquad (6\text{-}13.c)$$

These values are then substituted into Equation (6-7), and after some mathematical simplification, the subsequent expression is established.

$$\ddddot{X}(m) + \dddot{X}(c + C_f m) + \ddot{X}(k + C_f c + mk_{1n} + k_{2n}k_{3n}) + \dot{X}(k_{1n}c + C_f k) + X(k_{1n}k) =$$
$$F(k_{1n} - \varpi^2)\sin(\varpi t) + C_f \varpi F \cos(\varpi t) \qquad (6\text{-}14)$$

Equation (6-14), which plays a pivotal role in this research, reflects the dynamic equation of the coupled system for each mode, n, under both sloshing and harmonic excitation forces. To avoid repetition, the subscript n is removed from the parameter X. The right-hand side of this fourth-order differential equation is independent of X. Therefore, this ordinary differential equation is inhomogeneous and generates both complementary and particular solutions. To obtain the complementary solution, the right-hand side of the equation is set to zero. For simplicity and clear explanation, the damping term is initially disregarded in the current analytical model, representing an undamped coupled system. Then, in subsequent steps, this parameter is incorporated into the analytical model.

6.2.1. Undamped coupled system

In the undamped case, where $c = 0,\ C_f = 0$, ordinary differential equation (6-14) simplifies to Equation (6-15).

$$\ddot{\ddot{X}}(m) + \ddot{X}(k + mk_{1n} + k_{2n}k_{3n}) + X(kk_{1n}) = F\sin(\varpi t)(k_{1n} - \varpi^2) \tag{6-15}$$

6.2.1.1. Complementary Response

The complementary solution of Equation (6-15) is derived by setting the right-hand side of the equation to zero. Khanpour et al. (2024b) demonstrates that it can be presented as Expression (6-16). This solution represents the response of an undamped coupled system under free vibration analysis.

$$X_C = A\sin(\omega_1 t) + B\cos(\omega_1 t) + C\sin(\omega_2 t) + D\cos(\omega_2 t) \tag{6-16}$$

In equation (6-16), ω_1 and ω_2 represent the natural frequencies of the coupled system, derived from equation (6-17). The analytical work conducted by Khanpour et al. (2024b) provides a detailed explanation on how these relationships are established.

$$\begin{gathered}\omega_1 = \sqrt{\left(\frac{p + \sqrt{\Delta}}{2m}\right)} \quad and \quad \omega_2 = \sqrt{\left(\frac{p - \sqrt{\Delta}}{2m}\right)} \\ where \\ p = k + mk_{1n} + k_{2n}k_{3n} \quad and \quad q = kk_{1n} \ and \quad \Delta = p^2 - 4mq\end{gathered} \tag{6-17}$$

6.2.1.2. Particular Response

In this scenario, considering the right-hand side of equation (6-15) and the order of time derivatives of X in this equation, the particular solution of the coupled system is assumed to follow the form of equation (6-18).

$$X_p = a\sin(\varpi t) \tag{6-18}$$

As the particular response is independent of damping, it is termed as steady response. In a steady response, the frequency of the particular response aligns with that of the excitation force. The first, second, third, and fourth derivatives of this solution are presented in Equations (6-19).

$$X_p = a\sin(\bar{\omega}t),\ \dot{X}_p = a\bar{\omega}\cos(\bar{\omega}t),\ \ddot{X}_p = -a\bar{\omega}^2\sin(\bar{\omega}t),\ \dddot{X}_p = -a\bar{\omega}^3\cos(\bar{\omega}t),\ \ddddot{X} = a\bar{\omega}^4\sin(\bar{\omega}t) \quad (6\text{-}19)$$

To obtain the amplitude of the particular solution, a, the steady response is substituted into the ordinary differential equation (6-15), resulting in (6-20). Thus, the unknown parameter a is determined from Equation (6-21).

$$(m)a\bar{\omega}^4\sin(\bar{\omega}t) - (k + mk_{1n} + k_{2n}k_{3n})a\bar{\omega}^2\sin(\bar{\omega}t) + (kk_{1n})a\sin(\bar{\omega}t) = F\sin(\bar{\omega}t)(k_{1n} - \bar{\omega}^2) \quad (6\text{-}20)$$

$$a = \frac{F(k_{1n} - \bar{\omega}^2)}{(m)\bar{\omega}^4 - (k + mk_{1n} + k_{2n}k_{3n})\bar{\omega}^2 + (kk_{1n})} \quad (6\text{-}21)$$

Special Cases

remark: When the frequency of the excitation force approaches the natural frequencies of the coupled system, $\bar{\omega} \to \omega_1 \ or\ \bar{\omega} \to \omega_2$, the particular response tends towards infinity.

proof: Consider the denominator of Equation (6-21). If it is demonstrated that $\omega_1 \,\&\, \omega_2$, the natural frequencies of the coupled system, are the roots of the denominator, then the particular solution tends to infinity as the excitation frequency approaches the natural frequencies of the coupled system.

By defining $y = \bar{\omega}^2$, the fourth-order polynomial equation is converted to a second-order polynomial equation. The roots of this polynomial $y_1 \,\&\, y_2$ are derived from Equation (6-22).

$$y_1 = \frac{\tilde{C} - \sqrt{\tilde{C}^2 - 4\tilde{A}\tilde{E}}}{2\tilde{A}} \quad y_2 = \frac{\tilde{C} + \sqrt{\tilde{C}^2 - 4\tilde{A}\tilde{E}}}{2\tilde{A}} \quad (6\text{-}22)$$
$$\tilde{A} = m \quad \tilde{C} = k + mk_{1n} + k_{2n}k_{3n} \quad \tilde{E} = kk_{1n}$$

The square roots of $y_1 \,\&\, y_2$ are determined using Equation (6-23). A comparison between Equation (6-23) and Equation (6-17) reveals that $\sqrt{y_1} \,\&\, \sqrt{y_2}$, which represent the positive roots of the denominator, are equal to $\omega_1 \,\&\, \omega_2$, respectively.

$$\sqrt{y_1} = \sqrt{(\frac{\tilde{C} - \sqrt{\tilde{C}^2 - 4\tilde{A}\tilde{E}}}{2\tilde{A}})} \quad and \quad \sqrt{y_2} = \sqrt{(\frac{\tilde{C} + \sqrt{\tilde{C}^2 - 4\tilde{A}\tilde{E}}}{2\tilde{A}})} \tag{6-23}$$

$$\tilde{A} = m \quad \tilde{C} = k + mk_{1n} + k_{2n}k_{3n} \quad \tilde{E} = kk_{1n}$$

Therefore, the natural frequencies of the coupled system coincide with the roots of the denominator. Consequently, as the excitation frequency converges towards the natural frequencies, the particular response tends towards infinity.

Following the last demonstration, the following equation can be established.

$$(m)\bar{\omega}^4 - (k + mk_{1n} + k_{2n}k_{3n})\bar{\omega}^2 + (kk_{1n}) = m(\bar{\omega}^2 - \omega_1^2)(\bar{\omega}^2 - \omega_2^2) \tag{6-24}$$

Hence, the amplitude of the particular response can be determined from equation (6-25).

$$a = \frac{F(k_{1n} - \bar{\omega}^2)}{m(\bar{\omega}^2 - \omega_1^2)(\bar{\omega}^2 - \omega_2^2)} \tag{6-25}$$

Equation (6-26) outlines the relationship between the mass, stiffness, and natural frequency of the SDOF. $\omega = \sqrt{\frac{k}{m}}$ (6-26)

Substituting the mass from the previous equation into Equation (6-25) yields Equation (6-27):

$$a = \frac{F}{k}\frac{(k_{1n} - \bar{\omega}^2)\omega_s^2}{(\bar{\omega}^2 - \omega_1^2)(\bar{\omega}^2 - \omega_2^2)} \tag{6-27}$$

Since the term $\frac{F}{k}$ represents the static displacement, denoted as Δ_{st}, Equation (6-27) can be expressed as:

$$a = \Delta_{st}\delta_d \qquad \delta_d = \frac{(k_{1n} - \bar{\omega}^2)\omega_s^2}{(\bar{\omega}^2 - \omega_1^2)(\bar{\omega}^2 - \omega_2^2)} \tag{6-28}$$

In this equation, δ_d is referred to as the dynamic amplification factor of the coupled system in the undamped case. An insightful observation regarding the dynamic amplification factor indicates that it comprises five frequencies: 1,2) the natural frequencies of the coupled system, $\omega_1 \& \omega_2$, 3) the natural frequency of the SDOF, ω_s , 4) the natural frequency of the water tank, $\sqrt{k_{1n}}$; and 5) the excitation frequency ($\bar{\omega}$).

It is worth noting that in this scenario, which disregards both structural and fluid dissipation, the total response phase aligns with the excitation force phase.

Remark: When the excitation frequency approaches the natural frequency of the water tank ($\sqrt{k_{1n}}$), the steady response of the coupled system is approximately zero.

Proof: Let's consider Equation (6-28). Based on this expression, when the excitation force ($\bar{\omega}$) is identical to the tank frequency ($\sqrt{k_{1n}}$), the numerator of Equation (6-28) becomes zero. Since the natural frequencies of the coupled system, ω_1 & ω_2, are different from the water tank frequency, the steady-state response approaches zero.

Second solution: This solution employs both Equations (6-7) and (6-12) to arrive at the same conclusion. It not only validates the coupling equations, but also provides the time history of the wave amplitude, a crucial parameter in the sloshing process. Consider Equation (6-7), $\ddot{A}_n + A_n k_{1n} - \ddot{X} k_{2n} = 0$. Based on the preceding discussion, the steady-state response is given by $X = a\sin(\bar{\omega}t)$, where a is determined from Equation (6-25). In reference to the differential Equation (6-7) and the function *X*, the response of Equation (6-7) can be expressed as (6-29), with *A* representing the amplitude of the wave height.

$$A_n = A\sin(\bar{\omega}t) \tag{6-29}$$

Substituting X and A_n into ordinary differential equation (6-7) results in the following expression:

$$-\bar{\omega}^2 A\sin(\bar{\omega}t) + k_{1n} A\sin(\bar{\omega}t) - k_{2n}(-\bar{\omega}^2 a\sin(\bar{\omega}t)) = 0 \tag{6-30}$$

Therefore, the amplitude of the wave height is obtained from Equation (6-31). When the parameter a is substituted from Equation (6-25), Equation (6-32) for determining A is established.

$$A = \frac{-k_{2n}\bar{\omega}^2}{(k_{1n} - \bar{\omega}^2)} a \tag{6-31}$$

$$A = \frac{-k_{2n}\bar{\omega}^2}{(k_{1n} - \bar{\omega}^2)} \frac{F(k_{1n} - \bar{\omega}^2)}{(m)\bar{\omega}^4 - (m + mk_{1n} + k_{2n}k_{3n})\bar{\omega}^2 + (kk_{1n})} = \frac{-k_{2n}F\bar{\omega}^2}{(m)\bar{\omega}^4 - (m + mk_{1n} + k_{2n}k_{3n})\bar{\omega}^2 + (kk_{1n})}$$

(6-32)

Now, let's reconstruct the right-hand side of Equation (6-12), $F_n \sin(\bar{\omega}t) - k_{3n}A_n$. Upon replacing the parameter A from Equation (6-32), a subsequent expression is developed.

$$\begin{aligned} &F\sin(\bar{\omega}t) - k_{3n}A_n = F\sin(\bar{\omega}t) + k_{3n}\frac{k_{2n}F\bar{\omega}^2}{(m)\bar{\omega}^4 - (k + mk_{1n} + k_{2n}k_{3n})\bar{\omega}^2 + (kk_{1n})}\sin(\bar{\omega}t) = \\ &F\sin(\bar{\omega}t)[1 + \frac{k_{3n}k_{2n}\bar{\omega}^2}{(m)\bar{\omega}^4 - (m + mk_{1n} + k_{2n}k_{3n})\bar{\omega}^2 + (kk_{1n})}] \end{aligned} \tag{6-33}$$

As shown in Equation (6-34), if the excitation frequency aligns with the natural frequency of the tank ($\bar{\omega} = \sqrt{k_{1n}}$), the expression (6-33), which represents the right-hand side of Equation (6-12), vanishes. Therefore, in this scenario, the steady-state response approaches zero.

$$\begin{aligned} &\bar{\omega} = \sqrt{k_{1n}} \rightarrow F\sin(\bar{\omega}t)[1 + \frac{k_{3n}k_{2n}k_{1n}}{(m)k_{1n}{}^2 - (m + mk_{1n} + k_{2n}k_{3n})k_{1n} + (kk_{1n})}] = \\ &F\sin(\bar{\omega}t)[1 + \frac{k_{3n}k_{2n}}{(m)k_{1n} - (k + mk_{1n} + k_{2n}k_{3n}) + (k)}] = F\sin(\bar{\omega}t)[1 + \frac{k_{3n}k_{2n}}{-k_{3n}k_{2n}}] = 0 \end{aligned} \tag{6-34}$$

Remark: In higher modes of the TLD coupled system, those are greater than one, the forced response or steady response of the TLD coupled system replicated the response of the SDOF alone.

Proof: As previously discussed, the TLD coupled system involves a Tuned Liquid Damper (TLD) positioned atop a Single Degree of Freedom (SDOF) system. In this setup, the characteristics of the water tank are adjusted to synchronize the natural frequency of the water tank with that of the underlying SDOF $(\omega_s = \omega_f)$. As outlined in the study by Khanpour et al. (2024b), a TLD coupled system exhibits two natural frequencies for each mode. In higher modes, the lower frequency tends towards the natural frequency of the SDOF, denoted as $(\omega_1 \simeq \omega_s)$, while the higher frequency converges towards $\omega_2 = n\omega_f$. In addition, as previously mentioned, the parameter k_{1n} is approximately equal to $(n\omega_f)^2$; hence, $k_{1n} \simeq \omega_2{}^2$. Now, let us direct attention to Equation (6-28); substituting the parameters with their corresponding values yields Equation (6-35). If the ratio of the excitation frequency to the SDOF frequency is defined as $\beta = \frac{\bar{\omega}}{\omega_s}$, the equation can be defined as:

$$\delta_d = \frac{(k_{1n} - \bar{\omega}^2)\omega_s^2}{(\bar{\omega}^2 - \omega_1^2)(\bar{\omega}^2 - \omega_2^2)} = \frac{(\omega_2^2 - \bar{\omega}^2)\omega_s^2}{(\bar{\omega}^2 - \omega_1^2)(\bar{\omega}^2 - \omega_2^2)} = \frac{\omega_s^2}{(\omega_f^2 - \bar{\omega}^2)} = \frac{1}{(\frac{\omega_f^2}{\omega_s^2} - \frac{\bar{\omega}^2}{\omega_s^2})} = \frac{1}{(1 - \frac{\bar{\omega}^2}{\omega_s^2})} = \frac{1}{(1-\beta^2)}$$

(6-35)

The dynamic amplification derived from Equation (6-35) corresponds to the amplitude dynamic factors of the SDOF alone under a harmonic excitation force (Humar 2012).

6.2.1.3. Total Response

The total response of the coupled system is the sum of the complementary solution (transient solution) and particular response (steady-state solution), as indicated in Equation (6-36).

$$X_t = X_C + X_p = A\sin(\omega_1 t) + B\cos(\omega_1 t) + C\sin(\omega_2 t) + D\cos(\omega_2 t) + a\sin(\bar{\omega} t)$$
$$where \qquad (6\text{-}36)$$
$$a = \frac{F}{k}\frac{(k_{1n} - \bar{\omega}^2)\omega_s{}^2}{(\bar{\omega}^2 - \omega_1{}^2)(\bar{\omega}^2 - \omega_2{}^2)}$$

To evaluate coefficients *A, B, C,* and *D*, four initial boundary conditions are necessary. The initial displacements and initial velocities serve as the physical boundary conditions. However, as discussed in the work by Khanpour et al. (2024b), the initial acceleration and derivative of acceleration at the initial time are also used to determine these constant coefficients.

The initial acceleration presented in Equation (6-37) is obtained from Equations (6-12) for t=0. To derive the initial value for the time derivative of the acceleration, the time derivative of Equation (6-12) is coupled with the continuity equation presented in Expression (6-4), $\dot{A}_n = -HB_n(\frac{n\pi}{L})$, leading to Equation (6-38). These two latter initial conditions depend not only on the initial displacement and velocity, but also on the initial perturbation in the wave height and velocity. Consequently, to derive these coefficients, all four initial parameters—displacement, velocity, wave height, and wave velocity—are involved.

Let us consider the common scenario where the excitation begins from a stagnant condition, corresponding to zero initial displacement, initial velocity, initial wave height, and initial wave velocity. For this initial boundary conditions, the right-hand side of equation (6-37) is zero. Meanwhile, according to Equation (6-38), the initial value of the third derivative of the displacement is not zero, even though the initial displacement, velocity, wave height, and wave velocity perturbation are all zero.

$$\ddot{X}(0) = -\frac{k_{3n}A_n(0) + c\dot{X}(0) + kX(0)}{m} + \frac{F\sin(\varpi t)}{m} = 0 \tag{6-37}$$

$$\dddot{X}(0) = -\frac{c\ddot{X}(0) + k\dot{X}(0) - k_{3n}H\dfrac{n\pi}{L}B_n(0)}{m} + \frac{\varpi F\cos(\varpi t)}{m} = \frac{\varpi}{m}F \tag{6-38}$$

Based on the total response in Equation (6-36) and the initial conditions provided, the following system of equations is derived.

$$\begin{aligned}
&X(t) = 0 \rightarrow B + D = 0\\
&\dot{X}(t) = 0 \rightarrow A\omega_1 + C\omega_2 + a\varpi = 0\\
&\ddot{X}(t) = 0 \rightarrow -B\omega_1^{\,2} - D\omega_2^{\,2} = 0\\
&\dddot{X}(t) = \frac{\varpi F}{m} \rightarrow -A\omega_1^{\,3} - C\omega_2^{\,3} - a\varpi^3 = (p = \frac{\varpi F}{m})
\end{aligned} \tag{6-39}$$

Solving these four equations simultaneously yields the constant coefficient values of the total response expressed in Equation (6-40). In this instance, the coefficients of the cosine function (*B, D*) are zero, and the response encompasses three frequencies: two natural frequencies of the coupled system and the frequency of the excitation force.

$$\begin{aligned}
&A = \frac{a\omega_2^2\varpi - a\varpi^3 - p}{\omega_1^3 - \omega_1\,\omega_2^2}\\
&B = 0\\
&C = \frac{a\omega_1^2\varpi - a\varpi^3 - p}{\omega_2^3 - \omega_1^2\omega_2}\\
&D = 0
\end{aligned} \tag{6-40}$$

Remark: Total response of TLD coupled system for higher modes replicate the individual SDOF

Proof: Recall that for higher modes, $\omega_1 = \omega_s$ & $\omega_2 = n\omega_s$. Let's focus on the coefficient of higher frequency, *C*. Substituting ω_1 & ω_2 with corresponding values yields the equations (6-41-1). In this equation the ratio of excitation frequency to SDOF frequency is $\beta = \frac{\varpi}{\omega_s}$. Furthermore, the following equation utilizes Equation (6-35), $a = \frac{F}{k}\frac{1}{(1-\beta^2)}$, as well as $p = \frac{\varpi F}{m}$. Regarding the equation (6-41-1) the constant *C* is zeros, referring to the fact that in higher modes the greater frequency ($\omega_2 = n\omega_s$) does not contribute to the response. On the other hand, based on the equation (6-41-2), the lower frequency ($\omega_1 = \omega_s$) participates in the response with coefficient $A = -\frac{F}{k}\frac{\beta}{1-\beta^2}$.

$$
\begin{aligned}
&C = \frac{a\omega_1^2\varpi - a\varpi^3 - p}{\omega_2^3 - \omega_1^2\omega_2} = \underbrace{\frac{a\omega_1^2\varpi - a\varpi^3}{\omega_2^3 - \omega_1^2\omega_2}}_{term1} - \underbrace{\frac{p}{\omega_2^3 - \omega_1^2\omega_2}}_{term2}\\
&term1 = \frac{a\omega_1^2\varpi - a\varpi^3}{\omega_2^3 - \omega_1^2\omega_2} = \frac{a\varpi(\omega_1^2 - \varpi^2)}{\omega_2(\omega_2^2 - \omega_1^2)} = \frac{a\varpi(\omega_1^2 - \varpi^2)}{\mathrm{n}\,\omega_s^3(\mathrm{n}^2-1)} \xrightarrow{\beta=\frac{\varpi}{\omega_s}} = a\frac{\beta(1-\beta^2)}{\mathrm{n}(\mathrm{n}^2-1)}\\
&term1 \xrightarrow{a=\frac{F}{K}\frac{1}{1-\beta^2}} = \frac{F}{k}\frac{1}{1-\beta^2}\frac{\beta(1-\beta^2)}{\mathrm{n}(\mathrm{n}^2-1)} = \frac{F}{k}\frac{1}{1-\beta^2}\frac{\beta(1-\beta^2)}{\mathrm{n}(\mathrm{n}^2-1)} = \frac{F}{k}\frac{\beta}{\mathrm{n}(\mathrm{n}^2-1)}\\
&term2 = \frac{p}{\underbrace{\omega_2^3 - \omega_1^2\omega_2}_{term2}} = \frac{p}{\omega_2(\omega_2^2 - \omega_1^2)} \xrightarrow{p=\frac{\varpi F}{m}} = \frac{\frac{\varpi F}{m}}{\omega_2(\omega_2^2 - \omega_1^2)} = \xrightarrow{m=\frac{k}{\omega_s^2}}\\
&term2 = \frac{\frac{\varpi\omega_s^2 F}{k}}{\omega_2(\omega_2^2 - \omega_1^2)} = \frac{F}{k}\frac{\varpi\omega_s^2}{\omega_2(\omega_2^2 - \omega_1^2)} = \frac{F}{k}\frac{\varpi\omega_s^2}{n\omega_S^3(\mathrm{n}^2-1)} \xrightarrow{\beta=\frac{\varpi}{\omega_s}} = \frac{F}{k}\frac{\beta}{\mathrm{n}(\mathrm{n}^2-1)}\\
&term1 - term2 = 0
\end{aligned}
\tag{6-41-1}
$$

$$A=\frac{a\omega_2^2\bar{\omega}-a\bar{\omega}^3-p}{\omega_1^3-\omega_1\,\omega_2^2}=\underbrace{\frac{a\omega_2^2\bar{\omega}-a\bar{\omega}^3}{\omega_1^3-\omega_2^2\omega_1}}_{term1}-\underbrace{\frac{p}{\omega_1^3-\omega_2^2\omega_1}}_{term2}$$

$$term1=\frac{a\omega_2^2\bar{\omega}-a\bar{\omega}^3}{\omega_1^3-\omega_2^2\omega_1}=\frac{a\bar{\omega}(\omega_2^2-\bar{\omega}^2)}{\omega_1\,(\omega_1^2-\omega_2^2)}=\frac{a\bar{\omega}(n^2\omega_s^2-\bar{\omega}^2)}{\omega_s^3(1-n^2)}\xrightarrow{\beta=\frac{\bar{\omega}}{\omega_s}}=a\,\frac{\beta(n^2-\beta^2)}{(1-n^2)}$$

$$term1\xrightarrow{a=\frac{F}{K}\frac{1}{1-\beta^2}}=\frac{F}{k}\frac{1}{1-\beta^2}\frac{\beta(n^2-\beta^2)}{(1-n^2)}=\frac{F}{k}\frac{\beta}{1-\beta^2}\frac{(n^2-\beta^2)}{(1-n^2)}$$

$$term2=\underbrace{\frac{p}{\omega_1^3-\omega_2^2\omega_1}}_{term2}=\frac{p}{\omega_1\,(\omega_1^2-\omega_2^2)}\xrightarrow{p=\frac{\bar{\omega}F}{m}}=\frac{\frac{\bar{\omega}F}{m}}{\omega_1\,(\omega_1^2-\omega_2^2)}=\xrightarrow{m=\frac{k}{\omega_s^2}}$$

$$term2=\frac{\frac{\bar{\omega}\omega_s^2F}{k}}{\omega_1\,(\omega_1^2-\omega_2^2)}=\frac{F}{k}\frac{\bar{\omega}\omega_s^2}{\omega_1\,(\omega_1^2-\omega_2^2)}=\frac{F}{k}\frac{\bar{\omega}\omega_s^2}{\omega_S^3(1-n^2)}\xrightarrow{\beta=\frac{\bar{\omega}}{\omega_s}}=\frac{F}{k}\frac{\beta}{(1-n^2)}$$

$$term1-term2=\frac{F}{k}\frac{\beta}{(1-n^2)}\left\{\frac{(n^2-\beta^2)}{1-\beta^2}-1\right\}=\frac{F}{k}\frac{\beta}{(1-n^2)}\left(\frac{n^2-\beta^2-1+\beta^2}{1-\beta^2}\right)=-\frac{F}{k}\frac{\beta}{1-\beta^2}\quad(6\text{-}41\text{-}2)$$

Concern to the upper discussion, the total response Equation is transformed to the below expression.

$$X_t=X_C+X_p=A\sin(\omega_1 t)+a\sin(\bar{\omega}t)=\frac{F}{k}\frac{1}{1-\beta^2}(\sin(\bar{\omega}t)-\beta\sin(\omega_s t))$$
$$where \qquad (6\text{-}42)$$
$$a=\frac{F}{k}\frac{1}{1-\beta^2}$$

Let's focus the total response of an individual SDOF subjected to harmonic excitation which is determined from the equation (6-43) (Humar 2014). Since this research consider the common initial conditions, stagnant displacement and velocity $X(0)=0$ & $\dot{X}(0)=0$, both equation (6-42) and (6-43) are identical.

$$X_t=X(0)\cos(\omega_s t)+\frac{\dot{X}(0)\sin(\omega_s t)}{\omega}+\frac{F}{k}\frac{1}{1-\beta^2}(\sin(\bar{\omega}\,\mathrm{t})-\beta\sin(\omega_s t)) \qquad (6\text{-}43)$$

Special Cases:

The excitation frequency is the same as fluid tank frequency ($\varpi \rightarrow \sqrt{k_{1n}}$):

In this scenario, as demonstrated earlier, the particular response of the coupled system is zero, while the complementary response is nonzero. Therefore, as illustrated in equation (6-44), the response of the coupled system is solely dominated by the two natural frequencies of the tank, with no contribution from the excitation frequency.

$$a = 0 \rightarrow X_t = X_C + X_p = A\sin(\omega_1 t) + C\sin(\omega_2 t) = -\frac{F}{k}\varpi\omega_s^2\left(\frac{\sin(\omega_1 t)}{\omega_1^3 - \omega_1\omega_2^2} + \frac{\sin(\omega_2 t)}{\omega_2^3 - \omega_1^2\omega_2}\right) \qquad (6\text{-}44)$$
$$\varpi \rightarrow \sqrt{k_{1n}}$$

The excitation frequency approaches the natural frequency of the TLD coupled system ($\varpi \rightarrow \omega_1$ or $\varpi \rightarrow \omega_2$):

Referring to the total response of the coupled system, equation (6-36), with no contribution from the cosine functions, the total response can be expressed as Equation (6-45).

$$\begin{aligned} &X_t = X_C + X_p = A\sin(\omega_1 t) + C\sin(\omega_2 t) + a\sin(\varpi t) \\ &\varpi \rightarrow \omega_1 \\ &\textit{where} \\ &a = \frac{F}{k}\frac{(k_{1n} - \varpi^2)\omega_s^{\ 2}}{(\varpi^2 - \omega_1^{\ 2})(\varpi^2 - \omega_2^{\ 2})} \end{aligned} \qquad (6\text{-}45)$$

After substituting the coefficients A and C from equation (6-40), the following expression is obtained:

$$\begin{aligned} &X_t = X_C + X_p = \frac{a\omega_2^2\varpi - a\varpi^3 - p}{\omega_1^3 - \omega_1\omega_2^2}\sin(\omega_1 t) + \frac{a\omega_1^2\varpi - a\varpi^3 - p}{\omega_2^3 - \omega_1^2\omega_2}\sin(\omega_2 t) + a\sin(\varpi t) \\ &\textit{where} \\ &a = \frac{F}{k}\frac{(k_{1n} - \varpi^2)\omega_s^{\ 2}}{(\varpi^2 - \omega_1^{\ 2})(\varpi^2 - \omega_2^{\ 2})} \end{aligned} \qquad (6\text{-}46)$$

The total response can be expressed as equation (6-47), which comprises four terms. First, let us focus on the case in where the excitation frequency approaches the lower natural frequency ($\bar{\omega} \to \omega_1$).

$$X_t = X_C + X_p = \underbrace{a(\frac{\omega_2^2\bar{\omega} - a\bar{\omega}^3}{\omega_1^3 - \omega_1\,\omega_2^2}\sin(\omega_1 t) + \sin(\bar{\omega}t))}_{term1} + \underbrace{\frac{-p}{\omega_1^3 - \omega_1\,\omega_2^2}\sin(\omega_1 t)}_{term2} +$$

$$\underbrace{\frac{a\omega_1^2\bar{\omega} - a\bar{\omega}^3}{\omega_2^3 - \omega_1^2\omega_2}\sin(\omega_2 t)}_{term3} + \underbrace{\frac{-p}{\omega_2^3 - \omega_1^2\omega_2}\sin(\omega_2 t)}_{term4} \tag{6-47}$$

$$\bar{\omega} \to \omega_1$$

Let us examine the first term of this equation. After substituting parameter *a* from equation (6-27), the amplitude of the particular response, expression (6-48) is derived.

$$term1 = a(\sin(\bar{\omega}t) + \frac{\omega_2^2\bar{\omega} - a\bar{\omega}^3}{\omega_1^3 - \omega_1\,\omega_2^2}\sin(\omega_1 t)) =$$

$$\frac{F}{k}\frac{(k_{1n} - \bar{\omega}^2)\omega_s^{\,2}}{(\bar{\omega}^2 - \omega_1^{\,2})(\bar{\omega}^2 - \omega_2^{\,2})}\ \ [\sin(\bar{\omega}t) + (\omega_2^2\bar{\omega} - \bar{\omega}^3)/(\omega_1^3 - \omega_1\,\omega_2^2)\sin(\omega_1 t)] = \frac{0}{0} \tag{6-48}$$

$$\bar{\omega} \to \omega_1$$

As demonstrated in expression (6-48), when the excitation frequency nears the coupled system's lower natural frequency ($\bar{\omega} \to \omega_1$), the term1 ratio results in an indeterminate form, $\frac{0}{0}$. To address this ambiguity, L'Hôpital's rule is applied. Let's introduce the parameters $\alpha_1, \alpha_2, \alpha_3, \beta_1, \beta_2$ into Equation (6-48) and rewrite this expression in the form of Equation (6-49) using these parameters.

$$term1 = \frac{F}{k}\frac{(\alpha_2^{\,2} - \beta_1^{\,2})\alpha_1^{\,2}}{(\beta_1^{\,2} - 1)(\beta_1^{\,2} - \alpha_3^{\,2})}\ \ [\sin(\beta_1\omega_1 t) - (\beta_1^{\,3} - \alpha_3^{\,2}\beta_1)/(1 - \alpha_3^{\,2})\sin(\omega_1 t)] = \frac{0}{0}$$

$$\beta_1 = \frac{\bar{\omega}}{\omega_1} \quad \alpha_1 = \frac{\omega_s}{\omega_1} \quad \alpha_2 = \frac{\sqrt{k_{1n}}}{\omega_1} \quad \alpha_3 = \frac{\omega_2}{\omega_1} \quad \beta_2 = \frac{\bar{\omega}}{\omega_2} \qquad \beta_1 \to 1 \tag{6-49}$$

The case $\bar{\omega} \to \omega_1$ is equivalent to $\beta_1 \to 1$. Equation (6-50) demonstrates the application of L'Hôpital's rule to the first term, showing the ratio of the derivative of the numerator to the derivative of the denominator with respect to β_1.

$$Hopital\,(term1) = \frac{F}{k}\frac{(-2\beta_1\ )\alpha_1^{\ 2}\,\overbrace{[\sin(\beta_1\omega_1 t) - (\beta_1^{\ 3} - \alpha_3^{\ 2}\beta_1)/(1-\alpha_3^{\ 2})\sin(\omega_1 t)]}^{term*}}{(2\beta_1)(\beta_1^{\ 2} - \alpha_3^{\ 2}) + (\beta_1^{\ 2} - 1)(2\beta_1)} +$$

$$\frac{F}{k}\frac{(\alpha_2^{\ 2} - \beta_1^{\ 2})\alpha_1^{\ 2}[\omega_1 t\cos(\beta_1\omega_1 t) - (3\beta_1^{\ 2} - \alpha_3^{\ 2})/(1-\alpha_3^{\ 2})\sin(\omega_1 t)]}{(2\beta_1)(\beta_1^{\ 2} - \alpha_3^{\ 2}) + (\beta_1^{\ 2} - 1)(2\beta_1)} \quad (6\text{-}50)$$

$$\beta_1 \to 1$$

As β_1 approaches 1, the first term * in the equation (6-50) approaches zero. Consequently, Equation (6-50) is transformed into Equation (6-51).

$$Hopital\,(term1) = \frac{F}{k}\frac{(\alpha_2^{\ 2} - \beta_1^{\ 2})\alpha_1^{\ 2}[\omega_1 t\cos(\beta_1\omega_1 t) - (3\beta_1^{\ 2} - \alpha_3^{\ 2})/(1-\alpha_3^{\ 2})\sin(\omega_1 t)]}{(2\beta_1)(\beta_1^{\ 2} - \alpha_3^{\ 2})} \quad (6\text{-}51)$$

$$\beta_1 \to 1$$

After setting $\beta_1 \to 1$ and performing some simplifications, Equation (6-52) is obtained.

$$Hopital\,(term1) = \frac{F}{k}\ [\frac{\alpha_1^{\ 2}(\alpha_2^{\ 2} - 1)}{2(1-\alpha_3^{\ 2})}\omega_1 t\cos(\omega_1 t) - \frac{\alpha_1^{\ 2}(\alpha_2^{\ 2} - 1)(3-\alpha_3^{\ 2})}{2(1-\alpha_3^{\ 2})^2}\sin(\omega_1 t)] \quad (6\text{-}52)$$

Replacing $\alpha_1, \alpha_2, \alpha_3$ with corresponding values in Equation (6-52), the expression (6-53) is developed.

$$Hoitla\ term1 = \frac{F}{k}\frac{\omega_s^{\ 2}(k_{1n} - \omega_1^{\ 2})}{2(\omega_2^{\ 2} - \omega_1^{\ 2})\omega_1^{\ 2}}\ [\frac{(\omega_2^{\ 2} - 3\omega_1^{\ 2})}{(\omega_2^{\ 2} - \omega_1^{\ 2})}\sin(\omega_1 t) - \omega_1 t\cos(\omega_1 t)] \quad (6\text{-}53)$$

Upon substituting p with its corresponding value, $p = \frac{\bar{\omega}F}{m}$, and imposing $m = \frac{k}{\omega_s^2}$, term 2 is transformed into Equation (6-54) when the excitation frequency approaches the first natural frequency.

$$term2 = \frac{-p}{(\omega_1^3 - \omega_1\,\omega_2^2)}\sin(\omega_1 t) = -\frac{F}{k}\frac{\bar{\omega}\omega_s^{\ 2}}{\omega_1\,(\omega_1^2 - \omega_2^2)}\sin(\omega_1 t) = -\frac{F}{k}\frac{\omega_s^{\ 2}}{(\omega_1^2 - \omega_2^2)}\sin(\omega_1 t) \quad (6\text{-}54)$$

$$\bar{\omega} \to \omega_1$$

Let's analyze term 3. After replacing a from Equation (6-27), expression (6-55) is developed. When $\bar{\omega}$ approaches ω_1, term 3 results in an indeterminate form of $\frac{0}{0}$.

$$term\,3 = (a\omega_1^2\bar{\omega} - a\bar{\omega}^3)/(\omega_2^3 - \omega_1^2\omega_2)\sin(\omega_2 t) =$$

$$\frac{F}{k}\frac{(k_{1n} - \bar{\omega}^2)\omega_s^{\,2}}{(\bar{\omega}^2 - \omega_1^{\,2})(\bar{\omega}^2 - \omega_2^{\,2})}\frac{\bar{\omega}(\omega_1^2 - \bar{\omega}^2)}{(\omega_2^3 - \omega_1^2\omega_2)}\sin(\omega_2 t) = \frac{0}{0} \tag{6-55}$$

$$\bar{\omega} \to \omega_1$$

Upon removing $(\omega_1^2 - \bar{\omega}^2)$, the ambiguity factor, from both numerator and denominator, Equation (6-56) is developed for determining term 3.

$$term3 = -\frac{F}{k}\frac{(k_{1n} - \bar{\omega}^2)}{(\bar{\omega}^2 - \omega_2^{\,2})}\frac{\bar{\omega}\omega_s^{\,2}}{(\omega_2^3 - \omega_1^2\omega_2)}\sin(\omega_2 t) \tag{6-56}$$

Term 4 can be translated to Equation (6-57) using $p = \frac{\bar{\omega}F}{m}$ and the definition of the SDOF frequency, $m = \frac{k}{\omega_s^2}$.

$$term4 = \frac{-p}{(\omega_2^3 - \omega_1^2\omega_2)}\sin(\omega_2 t) = -\frac{F}{k}\frac{\bar{\omega}\omega_s^{\,2}}{(\omega_2^3 - \omega_1^2\omega_2)}\sin(\omega_2 t) = -\frac{F}{k}\frac{\omega_1\omega_s^{\,2}}{\omega_2(\omega_2^2 - \omega_1^2)}\sin(\omega_2 t) \tag{6-57}$$

$$\bar{\omega} \to \omega_1$$

Therefore, the total response, which is the sum of the four terms, can be expressed as Equation (6-58).

$$X = \frac{F}{k}\frac{\omega_s^{\,2}}{(\omega_2^2 - \omega_1^2)}[(\frac{(\omega_2^{\,2} - 3\omega_1^{\,2})(k_{1n} - \omega_1^{\,2})}{2(\omega_2^{\,2} - \omega_1^{\,2})\omega_1^{\,2}} + 1)\sin(\omega_1 t) + (\frac{\omega_1}{\omega_2}\frac{(k_{1n} - \omega_1^{\,2})}{(\omega_2^{\,2} - \omega_1^{\,2})} - \frac{\omega_1}{\omega_2})\sin(\omega_2 t) - \frac{(k_{1n} - \omega_1^{\,2})}{2\omega_1^{\,2}}\omega_1 t\cos(\omega_1 t)] \tag{6-58}$$

Following some simplification in Equation (6-58), the total response, as the excitation frequency nears the first natural frequency (the smaller natural frequency), can be described by Equation (6-59).

$$X = \frac{F\omega_s^{\,2}}{2k\omega_1^{\,2}\omega_2(\omega_1^{\,2} - \omega_2^{\,2})^2}[(k_{1n}\omega_2^{\,3} + \omega_1^{\,4}\omega_2 + \omega_1^{\,2}\omega_2^{\,3} - 3k_{1n}\omega_1^2\omega_2)\sin(\omega_1 t) + (\omega_1^{\,3}\omega_2^{\,3} - \omega_1^{\,5}\omega_2 - k_{1n}\omega_1\omega_2^3 + k_{1n}\omega_1^3\omega_2)t\cos(\omega_1 t) + (2k_{1n}\omega_1^{\,3} - 2\omega_1^{\,3}\omega_2^{\,2})\sin(\omega_2 t)] \tag{6-59}$$

Regarding Equation (6-59), the coefficients of $\sin(\omega_1 t)$ and $\sin(\omega_2 t)$ are constants. Meanwhile, due to the appearance of the coefficient t in the term $\cos(\omega_1 t)$, not only does the vibration of the structure grow over time, leading to instability of the coupled system, but it also results in a significantly higher contribution of the smaller natural frequency (ω_1) compared to the greater natural frequency (ω_2).

When the excitation frequency approaches the second natural frequency (the greater natural frequency), similar procedures, including the application of L'Hôpital's rule, were implemented. Following this process and significant simplifications, the total response is obtained from Equation (6-60). Using similar explanations, the greater natural frequency participates more considerably in the total response in this case.

$$X = \frac{F\omega_s^2}{2k\omega_1\omega_2^2(\omega_1^2-\omega_2^2)^2}[(2k_{1n}\omega_2^3 - 2\omega_1^2\omega_2^3)\sin(\omega_1 t) + (k_{1n}\omega_1^3 + \omega_1\omega_2^4 + \omega_1^3\omega_2^2 - 3k_{1n}\omega_1\omega_2^2)\sin(\omega_2 t) + (\omega_1^3\omega_2^3 - \omega_1\omega_2^5 - k_{1n}\omega_1^3\omega_2 + k_{1n}\omega_1\omega_2^3)t\cos(\omega_2 t)] \quad (6\text{-}60)$$

6.2.2. Structural damped case

Let us consider Equation (6-14), which describes the coupled system subjected to harmonic excitation for each mode, when structural dissipation is incorporated, and fluid dissipation is absent ($c \neq 0$, $C_f = 0$). This case is referred to as structural damped coupled system. In this scenario, Equation (6-14) is transformed into Equation (6-61).

$$\ddot{\ddot{X}}_n(m) + \dddot{X}_n(c) + \ddot{X}_n(k + mk_{1n} + k_{2n}k_{3n}) + \dot{X}_n(ck_{1n}) + X_n(kk_{1n}) = F_n\sin(\bar{\omega}t)(k_{1n} - \bar{\omega}^2) \quad (6\text{-}61)$$

As previously stated, X in this equation denotes the response of the coupled system resulting from the contribution of mode n of the sloshing waves.

6.2.2.1. Complementary Response

The complementary response of equation (6-61) is derived by setting the right-hand side to zero. Khanpour et al. (2024c) conducted diligent work focusing on this complementary response. According to their study, the complementary solution represents the response of a TLD coupled system under free vibration when structural damping is considered. This study analytically demonstrates that the response of the damped coupled system under free vibration analysis is derived from Equation (6-62). Technically, Equation (6-62) represents the complementary response of Equation (6-61).

$$
\begin{aligned}
&X_t = e^{\alpha_1 t}(A\sin(\omega_1 t) + B\cos(\omega_1 t)) + e^{\alpha_2 t}(C\sin(\omega_2 t) + D\cos(\omega_2 t)) \\
&where \\
&\alpha_1 = -\zeta\omega_s \frac{(k_{1n} - \omega_1{}^2)}{(\omega_2{}^2 - \omega_1{}^2)} \\
&\alpha_2 = -\zeta\omega_s \frac{(\omega_2{}^2 - k_{1n})}{(\omega_2{}^2 - \omega_1{}^2)}
\end{aligned}
\tag{6-62}
$$

In this equation, α_1 and α_2 are dissipation factors, while ω_1 and ω_2 are the natural frequencies of the coupled system in the damped case. Moreover, the analytical study by Khanpour (2024c) demonstrates that the dissipation factors, α_1 and α_2, are negative, indicating that the complementary response diminishes over time. Based on this analytical work, the presence of damping has a negligible effect on the natural frequencies of the coupled system; therefore, they can be derived from the equation of the undamped system, Equat02ion (6-17). Furthermore, in Equation (6-62), the analytical expressions for α_1 and α_2 are introduced to determine the dissipation factors. Equation (6-62) proposes that the dissipation factors depend not only on the structural dissipation, but also on four natural frequencies: 1,2- natural frequencies of the coupled system, 3- natural frequency of the SDOF, and 4- the natural frequency of the water tank.

6.2.2.2. Particular response

For simplicity, the equation (6-61) can be expressed as follows.

$$
\begin{aligned}
&\ddot{\ddot{X}}(\tilde{A}) + \dddot{X}(\tilde{B}) + \ddot{X}(\tilde{C}) + \dot{X}(\tilde{D}) + X(\tilde{E}) = \tilde{F}\sin(\bar{\omega}t) \\
&\tilde{A} = m \quad \tilde{B} = c \quad \tilde{C} = k + mk_{1n} + k_{2n}k_{3n} \quad \tilde{D} = ck_{1n} \quad \tilde{E} = kk_{1n} \quad \tilde{F} = F(k_{1n} - \bar{\omega}^2)
\end{aligned}
\tag{6-63}
$$

Regarding the order of time derivatives in the differential equation and the right-hand side of the equation, the particular solution can be expressed as:

$$
X_p = a\sin(\bar{\omega}t) + b\cos(\bar{\omega}t) \tag{6-64}
$$

To determine the constant coefficients of the particular response (a, b), we computed the first-, second-, and third-time derivatives of the particular response and apply them into the fourth-order differential equation (6-63). To avoid extensive details of the calculation procedures and equations, only the conclusive result of this process is presented herein, as expressed in Equation (6-65).

$$\begin{aligned} a &= \frac{\tilde{F}(\tilde{A}\bar{\varpi}^4 - \tilde{C}\bar{\varpi}^2 + \tilde{E})}{(\tilde{A}\bar{\varpi}^4 - \tilde{C}\bar{\varpi}^2 + \tilde{E})^2 + (\tilde{B}\bar{\varpi}^3 - \tilde{D}\bar{\varpi})^2} \\ b &= \frac{\tilde{F}(\tilde{B}\bar{\varpi}^3 - \tilde{D}\bar{\varpi})}{(\tilde{A}\bar{\varpi}^4 - \tilde{C}\bar{\varpi}^2 + \tilde{E})^2 + (\tilde{B}\bar{\varpi}^3 - \tilde{D}\bar{\varpi})^2} \end{aligned} \tag{6-65}$$

In this scenario, both the sine and cosine functions contribute to the particular response. Therefore, unlike in the undamped case, the phase of the particular response phase is different from the excitation force. Equation (6-64) can be expressed as equation (6-66):

$$X_p = a\sin(\bar{\varpi}t) + b\cos(\bar{\varpi}t) = \sqrt{a^2+b^2}\left(\frac{a}{\sqrt{a^2+b^2}}\sin(\bar{\varpi}t) + \frac{b}{\sqrt{a^2+b^2}}\cos(\bar{\varpi}t)\right) \tag{6-66}$$

Let us define $\cos\varphi = \dfrac{a}{\sqrt{a^2+b^2}}$ and $\sin\phi = \dfrac{b}{\sqrt{a^2+b^2}}$. With this definition, equation (6-66) can be written as Equation (6-67). This equation provides the amplitude response (R) and phase difference between the excitation force and response (ϕ).

$$\begin{aligned} &\cos\phi = \frac{a}{\sqrt{a^2+b^2}} \qquad \sin\phi = \frac{b}{\sqrt{a^2+b^2}} \\ &X_p = R\sin(\bar{\varpi}t + \phi) \quad \left\{ \begin{aligned} &R = \sqrt{a^2+b^2} = \frac{\widehat{F}}{\sqrt{(\tilde{A}\bar{\varpi}^4 - \tilde{C}\bar{\varpi}^2 + \tilde{E})^2 + (\tilde{B}\bar{\varpi}^3 - \tilde{D}\bar{\varpi})^2}} \\ &\tan(\phi) = \frac{b}{a} = \frac{(\tilde{B}\bar{\varpi}^3 - \tilde{D}\bar{\varpi})}{(\tilde{A}\bar{\varpi}^4 - \tilde{C}\bar{\varpi}^2 + \tilde{E})} \end{aligned} \right\} \end{aligned} \tag{6-67}$$

Substituting $(\tilde{A}\bar{\varpi}^4 - \tilde{C}\bar{\varpi}^2 + \tilde{E})$, $(\tilde{B}\bar{\varpi}^3 - \tilde{D}\bar{\varpi})^2$, and $\widehat{F}$ with corresponding values $(m)\bar{\varpi}^4 - (k + mk_{1n} + k_{2n}k_{3n})\bar{\varpi}^2 + (kk_{1n})$, $(c\omega^3 - ck_{1n}\bar{\varpi})$, and $F(k_{1n} - \bar{\varpi}^2)$ in Equation (6-67) results in Equation (6-68) for determining the amplitude of the particular response in this scenario.

$$R = \frac{\widehat{F}}{\sqrt{(\tilde{A}\bar{\varpi}^4 - \tilde{C}\bar{\varpi}^2 + \tilde{E})^2 + (\tilde{B}\bar{\varpi}^3 - \tilde{D}\bar{\varpi})^2}} = \frac{F(k_{1n} - \bar{\varpi}^2)}{\sqrt{[(m)\bar{\varpi}^4 - (k + mk_{1n} + k_{2n}k_{3n})\bar{\varpi}^2 + (kk_{1n})]^2 + \left[c\bar{\varpi}^3 - ck_{1n}\bar{\varpi}\right]^2}} \tag{6-68}$$

Replacing the term $(m)\bar{\varpi}^4 - (k + mk_{1n} + k_{2n}k_{3n})\bar{\varpi}^2 + (kk_{1n})$ with its equivalent value $m(\bar{\varpi}^2 - \omega_1^2)(\bar{\varpi}^2 - \omega_2^2)$, as indicated in Equation (6-24), yields Equation (6-69):

$$R = \frac{F(k_{1n} - \bar{\varpi}^2)}{\sqrt{[m(\bar{\varpi}^2 - \omega_1^2)(\bar{\varpi}^2 - \omega_2^2)]^2 + \left[c\bar{\varpi}^3 - ck_{1n}\bar{\varpi}\right]^2}} = \frac{F(k_{1n} - \bar{\varpi}^2)}{\sqrt{[m(\bar{\varpi}^2 - \omega_1^2)(\bar{\varpi}^2 - \omega_2^2)]^2 + c^2\bar{\varpi}^2\left[k_{1n} - \bar{\varpi}^2\right]^2}} \tag{6-69}$$

At this point, the term damping ratio, ξ, is incorporated into the expressions. According to Equation (6-70), the damping ratio is the damping coefficient divided by the critical damping, c_{cr}. The critical damping is equal to $2m\omega_s$. For more details, please refer to Humar (2014).

$$\xi = \frac{c}{c_{cr} = (2m\omega_s)} \tag{6-70}$$

Replacing c with $\xi(2m\omega_s)$ in Equation (6-69) yields Equation (6-71).

$$c = \xi(2m\omega_s) \rightarrow R = \frac{F(k_{1n} - \bar{\varpi}^2)}{\sqrt{[m(\bar{\varpi}^2 - \omega_1^2)(\bar{\varpi}^2 - \omega_2^2)]^2 + m^2(2\xi\omega_s\bar{\varpi})^2\left[k_{1n} - \bar{\varpi}^2\right]^2}} \tag{6-71}$$

After simplifying and setting $m = \frac{k}{\omega_s^2}$, the expression for calculating the amplitude of the particular response is derived as follows.

$$R = \frac{F(k_{1n} - \bar{\varpi}^2)}{m\sqrt{[(\bar{\varpi}^2 - \omega_1^2)(\bar{\varpi}^2 - \omega_2^2)]^2 + (2\xi\omega_s\bar{\varpi})^2\left[k_{1n} - \bar{\varpi}^2\right]^2}} = \frac{F\omega_s^2(k_{1n} - \bar{\varpi}^2)}{k\sqrt{[(\bar{\varpi}^2 - \omega_1^2)(\bar{\varpi}^2 - \omega_2^2)]^2 + (2\xi\omega_s\bar{\varpi})^2\left[k_{1n} - \bar{\varpi}^2\right]^2}} \tag{6-72}$$

Similar to the previous case, let's consider $\Delta_{st} = \dfrac{F}{k}$. Thus, the dynamic amplification (δ_d) when structural damping is introduced can be derived from Equation (6-73).

$$R = \Delta_{st}\delta_d \quad \delta_d = \frac{\omega_s^2 (k_{1n} - \varpi^2)}{\sqrt{[(\varpi^2 - \omega_1^2)(\varpi^2 - \omega_2^2)]^2 + (2\xi\omega_s\varpi)^2 \left[k_{1n} - \varpi^2\right]^2}} \tag{6-73}$$

In this scenario, similar to the previous case, the dynamic amplification encompasses five frequencies: the natural frequencies of the coupled system, tank frequency, SDOF frequency, and excitation frequency. However, unlike the previous case, it includes an additional term due to the contribution of structural damping, which reduces dynamic amplification. Evidently, if damping is neglected ($\xi = 0$), this additional term becomes zero, and the dynamic amplification equals that of the undamped coupled system.

Let us recall the phase angle difference (ϕ) expressed in equation (6-67), where $\tan(\phi) = \dfrac{b}{a} = \dfrac{(\tilde{B}\varpi^3 - \tilde{D}\varpi)}{(\tilde{A}\varpi^4 - \tilde{C}\varpi^2 + \tilde{E})}$. Similar procedures and simplifications are applied to the phase angle difference expression, leading to Equation (6-74). According to this equation, the phase angle difference is a function of the five frequencies and damping ratio, ξ. Obviously, if damping does not participate in the response, the phase angle difference will be zero.

$$\tan(\phi) = \frac{b}{a} = \frac{(\tilde{B}\varpi^3 - \tilde{D}\varpi)}{(\tilde{A}\varpi^4 - \tilde{C}\varpi^2 + \tilde{E})} = \frac{c\varpi(\varpi^2 - k_{1n})}{m(\varpi^2 - \omega_1^2)(\varpi^2 - \omega_2^2)} = 2\xi \frac{\omega_s\varpi(\varpi^2 - k_{1n})}{(\varpi^2 - \omega_1^2)(\varpi^2 - \omega_2^2)} \tag{6-74}$$

Remark: For a coupled TLD system, in higher modes, the amplitude response and phase angle difference of the coupled system approach those of the SDOF system.

Let's focus on Equation (6-73), which expresses the dynamic amplification of the coupled system with the inclusion of structural damping. As mentioned earlier, in higher modes, the smaller natural frequency (ω_1) and the higher natural frequency (ω_2) approach the SDOF natural frequency (ω_s) and *n* times the fluid tank frequency ($n\omega_f$), respectively. Furthermore, k_{1n} can be approximated by the square of the fluid frequency, $(n\omega_f)^2$. In other words, in higher modes $k_{1n} = \omega_2^2$. By substituting these parameters with their approximations, Equation (6-75) is established. The term $\dfrac{1}{\sqrt{(1-\dfrac{\bar{\omega}^2}{\omega_s^2})^2+(2\xi\dfrac{\bar{\omega}}{\omega_s})^2}}$ represents the dynamic factor of an individual damped SDOF.

$$\delta_d=\frac{\omega_s^2(k_{1n}-\bar{\omega}^2)}{\sqrt{[(\bar{\omega}^2-\omega_1^2)(\bar{\omega}^2-\omega_2^2)]^2+(2\xi\omega_s\bar{\omega})^2\left[k_{1n}-\bar{\omega}^2\right]^2}}=$$

$$\frac{\omega_s^2(\omega_2^2-\bar{\omega}^2)}{\sqrt{[(\bar{\omega}^2-\omega_1^2)(\bar{\omega}^2-\omega_2^2)]^2+(2\xi\omega_s\bar{\omega})^2\left[\omega_2^2-\bar{\omega}^2\right]^2}}= \tag{6-75}$$

$$\frac{\omega_s^2}{\sqrt{(\omega_s^2-\bar{\omega}^2)^2+(2\xi\omega_s\bar{\omega})^2}}=\frac{1}{\sqrt{(1-\dfrac{\bar{\omega}^2}{\omega_s^2})^2+(2\xi\dfrac{\bar{\omega}}{\omega_s})^2}}$$

Upon substituting ω_1,ω_s,k_{1n} with their corresponding values as described, the phase difference expression in Equation (6-74) is transformed into Equation (6-76). The term $2\xi\dfrac{\dfrac{\bar{\omega}}{\omega_s}}{(\dfrac{\bar{\omega}^2}{\omega_s^2}-1)}$ indicates the phase difference of a damped individual single degree of freedom system.

$$\phi=2\xi\frac{\omega_s\bar{\omega}(\bar{\omega}^2-k_{1n})}{(\bar{\omega}^2-\omega_1^2)(\bar{\omega}^2-\omega_2^2)}=2\xi\frac{\omega_s\bar{\omega}(\bar{\omega}^2-\omega_2^2)}{(\bar{\omega}^2-\omega_1^2)(\bar{\omega}^2-\omega_2^2)}=2\xi\frac{\omega_s\bar{\omega}}{(\bar{\omega}^2-\omega_s^2)}=2\xi\frac{\dfrac{\bar{\omega}}{\omega_s}}{(\dfrac{\bar{\omega}^2}{\omega_s^2}-1)} \tag{6-76}$$

Special cases:

1-When the excitation frequency approaches the water tank frequency $(\bar{\omega}\to\sqrt{k_{1n}})$: As previously mentioned, $\sqrt{k_{1n}}$ is the water tank frequency (ω_f). According to Equation (6-73), when the excitation frequency equals $\sqrt{k_{1n}}$, the particular response will be zero. Similar to the previous undamped case, in this scenario, the particular response of the coupled system is not influenced by the particular response or the steady state response here.

2- When the excitation frequency approaches the natural frequencies ($\bar{\omega} \to \omega_1 \quad or \quad \bar{\omega} \to \omega_2$): In this scenario, according to Equation (6-73), unlike in the previous case, the particular response does not become infinite due to the presence of the damping term. In this situation, dynamic amplification is obtained from Equation (6-77) when $\bar{\omega} \to \omega_1$. Hence, contrary to the undamped case, in this scenario, the particular response approaches a finite value ($\dfrac{1}{2\xi \dfrac{\omega_1}{\omega_s}}$). Using a similar method, the dynamic amplification when the frequency excitation approaches the higher natural frequency $\bar{\omega} \to \omega_2$ is obtained using Equation (6-78).

$$R = \Delta_{st}\delta_d \qquad \delta_d = \frac{\omega_s^2 (k_{1n} - \bar{\omega}^2)}{\sqrt{[(\bar{\omega}^2 - \omega_1^2)(\bar{\omega}^2 - \omega_2^2)]^2 + (2\xi\omega_s\bar{\omega})^2 \left[k_{1n} - \bar{\omega}^2\right]^2}} =$$

$$\bar{\omega} \to \omega_1$$

$$\delta_d = \frac{\omega_s^2 (k_{1n} - \bar{\omega}^2)}{\sqrt{(2\xi\omega_s\bar{\omega})^2 \left[k_{1n} - \bar{\omega}^2\right]^2}} = \frac{\omega_s (k_{1n} - \bar{\omega}^2)}{2\xi\bar{\omega}(k_{1n} - \bar{\omega}^2)} = \frac{1}{2\xi \dfrac{\omega_1}{\omega_s}} \tag{6-77}$$

$$\bar{\omega} \to \omega_1$$

$$\delta_d = \frac{1}{2\xi \dfrac{\omega_2}{\omega_s}} \tag{6-78}$$

$$\bar{\omega} \to \omega_2$$

6.2.2.2. Total response

The total response, which is the sum of the complementary response and particular response, is derived from Equation (6-79) in coupled system equipped with structural damping.

$$X_t = e^{\alpha_1 t}(A\sin(\omega_1 t) + B\cos(\omega_1 t)) + e^{\alpha_2 t}(C\sin(\omega_2 t) + D\cos(\omega_2 t)) + a\sin(\overline{\omega} t) + b\cos(\overline{\omega} t)$$

where

$$a = \frac{\tilde{F}(\tilde{A}\overline{\omega}^4 - \tilde{C}\overline{\omega}^2 + \tilde{E})}{(\tilde{A}\overline{\omega}^4 - \tilde{C}\overline{\omega}^2 + \tilde{E})^2 + (\tilde{B}\overline{\omega}^3 - \tilde{D}\overline{\omega})^2}$$
$$b = \frac{\tilde{F}(\tilde{B}\overline{\omega}^3 - \tilde{D}\overline{\omega})}{(\tilde{A}\overline{\omega}^4 - \tilde{C}\overline{\omega}^2 + \tilde{E})^2 + (\tilde{B}\overline{\omega}^3 - \tilde{D}\overline{\omega})^2} \tag{6-79}$$
$$\tilde{A} = m \quad \tilde{B} = c \quad \tilde{C} = k + mk_{1n} + k_{2n}k_{3n} \quad \tilde{D} = ck_{1n} \quad \tilde{E} = kk_{1n} \quad \tilde{F} = F(k_{1n} - \overline{\omega}^2)$$
$$\alpha_1 = -\zeta\omega_s \frac{(k_{1n} - \omega_1{}^2)}{(\omega_2{}^2 - \omega_1{}^2)} \qquad \alpha_2 = -\zeta\omega_s \frac{(\omega_2{}^2 - k_{1n})}{(\omega_2{}^2 - \omega_1{}^2)}$$

If four initial boundary conditions, including displacement, velocity, acceleration, and the time derivative of acceleration $\left\{X_t(0) = 0,\ \dot{X}_t(0) = 0,\ \ddot{X}_t(0) = 0,\ \dddot{X}_t(0) = \frac{\overline{\omega}F}{m} = P\right\}^T$ are applied to the total response, the four constant coefficients are derived as follows:

$$A = -\frac{1}{\omega_1(\omega_1^2 - \omega_2^2)^2}[p(\omega_1^2 - \omega_2^2) + a\overline{\omega}(\omega_2^4 + \omega_1^2\overline{\omega}^2 - \omega_2^2\overline{\omega}^2 - \omega_1^2\omega_2^2) +$$
$$\alpha_1 b(-\omega_2^4 + 3\omega_1^2\omega_2^2 - 3\omega_1^2\overline{\omega}^2 + \omega_2^2\overline{\omega}^2) + \alpha_2 b(-2\omega_1^2\omega_2^2 + 2\omega_2^2\overline{\omega}^2)]$$
$$B = -\frac{1}{(\omega_1^2 - \omega_2^2)^2}[2p(\alpha_1 - \alpha_2) + b(\omega_2^4 - \omega_1^2\omega_2^2 + \omega_1^2\overline{\omega}^2 - \omega_2^2\overline{\omega}^2) +$$
$$2a\alpha_1(\overline{\omega}^3 - \omega_2^2\overline{\omega}) - 2a\alpha_2(\overline{\omega}^3 - \omega_1^2\overline{\omega})] \tag{6-80}$$
$$C = \frac{1}{\omega_2(\omega_1^2 - \omega_2^2)^2}[p(\omega_1^2 - \omega_2^2) + a\overline{\omega}(-\omega_1^4 + \omega_1^2\overline{\omega}^2 - \omega_2^2\overline{\omega}^2 + \omega_1^2\omega_2^2) +$$
$$\alpha_2 b(\omega_1^4 - 3\omega_1^2\omega_2^2 - \omega_1^2\overline{\omega}^2 + 3\omega_2^2\overline{\omega}^2) + \alpha_1 b(2\omega_1^2\omega_2^2 - 2\omega_1^2\overline{\omega}^2)]$$
$$D = \frac{1}{(\omega_1^2 - \omega_2^2)^2}[2p(\alpha_1 - \alpha_2) + b(-\omega_1^4 + \omega_1^2\omega_2^2 + \omega_1^2\overline{\omega}^2 - \omega_2^2\overline{\omega}^2) +$$
$$2a\alpha_1(\overline{\omega}^3 - \omega_2^2\overline{\omega}) - 2a\alpha_2(\overline{\omega}^3 - \omega_1^2\overline{\omega})]$$

As discussed in the previous work by Khanpour et al. (2024c), the dissipation factors α_1 and α_2 have small values. Hence, the terms in the last equation that include these parameters as multiplicative factors can be disregarded with high levels of accuracy. By removing these terms from the last equation, the following simplified equations are established to determine the coefficients:

$$
\begin{aligned}
A &= \frac{a\bar{\omega}\omega_2^2 - a\bar{\omega}^3 - p}{\omega_1^3 - \omega_1\omega_2^2} \\
B &= -\frac{b(\bar{\omega}^2 - \omega_2^2)}{\omega_1^2 - \omega_2^2} \\
C &= \frac{a\bar{\omega}\omega_1^2 - a\bar{\omega}^3 - p}{\omega_2^3 - \omega_1^2\omega_2} \\
D &= \frac{b(\bar{\omega}^2 - \omega_1^2)}{\omega_1^2 - \omega_2^2}
\end{aligned}
\tag{6-81}
$$

A comparison of the last equation with Equation (6-40), which represents the coefficients in the undamped coupled system, reveals that the constants for the sinus functions (*A, C*) remain unchanged. However, unlike the undamped case, the constants for the cosine functions (*B, D*) are nonzero.

Special cases:

When the excitation frequency approaches the water tank frequency ($\bar{\omega} \to \sqrt{k_{1n}}$): In this case, because $\tilde{F} = F(k_{1n} - \bar{\omega}^2) = 0$, according to Equation (6-79), both components of the particular response (*a, b*) vanish, leaving the total response comprised solely of the complementary response. In addition, regarding Equation (6-81), the coefficients of the cosine function in the complementary response (*B, D*) are zero. Equation (6-82) reveals the total response of the TLD coupled system with structural dissipation when the excitation frequency nears the natural tank frequency. In this equation, coefficients *A* and *C* are substituted with their corresponding values from Equation (6-81). Equation (6-82) demonstrates that in this scenario, the total response diminishes over time due to the dissipation factors (α_1, α_2).

$$
\begin{aligned}
&\tilde{F} = 0,\ a = 0,\ \ b = 0 \to X_t = X_C + X_p = e^{-\alpha_1 t} A\sin(\omega_1 t) + e^{-\alpha_2 t} C\sin(\omega_2 t) = \\
&-\frac{F}{k}\bar{\omega}\omega_s^2 \left(\frac{e^{-\alpha_1 t}\sin(\omega_1 t)}{\omega_1^3 - \omega_1\omega_2^2} + \frac{e^{-\alpha_2 t}\sin(\omega_2 t)}{\omega_2^3 - \omega_1^2\omega_2}\right) \\
&\bar{\omega} \to \sqrt{k_{1n}}
\end{aligned}
\tag{6-82}
$$

When the excitation frequency approaches the coupled system frequency ($\bar{\omega} \to \omega_1\ \ or\ \bar{\omega} \to \omega_2$): First, let's assume $\bar{\omega} \to \omega_1$. Since ω_1 and ω_2 are the roots of $\tilde{A}\bar{\omega}^4 - \tilde{C}\bar{\omega}^2 + \tilde{E}$, which is equivalent to, $(m)\varpi^4-(k+mk_{1n}+k_{2n}k_{3n})\varpi^2+(kk_{1n})$, according to Equation (6-79), the coefficient a approaches zero. The other particular response coefficient, b, is determined from Equation (6-83) upon substituting $\tilde{A},\tilde{B},\tilde{C},\tilde{D},\tilde{E},\tilde{F}$ with their corresponding values. Furthermore, the constants that constitute the complementary response (*A, B, C, D*) are manipulated in Equation (6-83). These constants are derived from Equation (6-81) when $\varpi\rightarrow\omega_1$. Lastly, the total response, X_t, is determined from the final relation in Equation (6-83). Evidently, the amplitude response of the coupled system when $t\rightarrow\infty$ approaches $\frac{F}{k}\frac{(\frac{\omega_s}{\omega_1})}{2\xi}$.In this expression, all terms are dissipated exponentially by structural dissipation factors except for $\frac{F}{k}\frac{(\frac{\omega_s}{\omega_1})}{2\xi}\cos(\omega_1 t)$. Therefore, it is expected that the smaller natural frequency (ω_1) has a more pronounced participation in the total response compared to the greater natural frequency (ω_2). Similar approach is employed for the case where $\varpi\rightarrow\omega_2$, leading to Equation (6-84) for the total response when the excitation frequency tends to higher natural frequency. Using a similar demonstration, it is predicted that the total response in this case is more dominated by the greater natural frequency (ω_2).

$$a=0,\quad b=\frac{\tilde{F}(\tilde{B}\varpi^3-\tilde{D}\varpi)}{(\tilde{A}\varpi^4-\tilde{C}\varpi^2+\tilde{E})^2+(\tilde{B}\varpi^3-\tilde{D}\varpi)^2}=\frac{F}{k}\frac{\omega_s^2(k_{1n}-\varpi^2)}{-2\xi\omega_s\varpi(k_{1n}-\varpi^2)}=-\frac{F}{k}\frac{(\frac{\omega_s}{\varpi})}{2\xi}$$

$$A=-\frac{p}{\omega_1^3-\omega_1\omega_2^2}\quad C=-\frac{p}{\omega_2^3-\omega_1^2\omega_2}\quad B=-b\quad D=0$$

$$X_t=X_C+X_p=e^{-\alpha_1 t}A\sin(\omega_1 t)+e^{-\alpha_2 t}C\sin(\omega_2 t)+e^{-\alpha_1 t}B\cos(\omega_1 t)+b\cos(\omega_1 t)=$$

$$e^{-\alpha_1 t}A\sin(\omega_1 t)+e^{-\alpha_2 t}C\sin(\omega_2 t)=-\frac{F}{k}\omega_1\omega_s^2[(\frac{e^{-\alpha_1 t}}{\omega_1^3-\omega_1\omega_2^2}\sin(\omega_1 t))+(\frac{e^{-\alpha_2 t}}{\omega_2^3-\omega_1^2\omega_2}\sin(\omega_2 t)]$$

$$e^{-\alpha_1 t}B\cos(\omega_1 t)+b\cos(\omega_1 t)=b\cos(\omega_1 t)[1-e^{-\alpha_1 t}]=-\frac{F}{k}\frac{(\frac{\omega_s}{\omega_1})}{2\xi}(1-e^{-\alpha_1 t})\cos(\omega_1 t)$$

$$X_t=-\frac{F}{k}\omega_1\omega_s^2[(\frac{e^{-\alpha_1 t}}{\omega_1^3-\omega_1\omega_2^2}\sin(\omega_1 t))+(\frac{e^{-\alpha_2 t}}{\omega_2^3-\omega_1^2\omega_2}\sin(\omega_2 t)]-\frac{F}{k}\frac{(\frac{\omega_s}{\omega_1})}{2\xi}(1-e^{-\alpha_1 t})\cos(\omega_1 t)$$

$$\varpi\rightarrow\omega_1 \tag{6-83}$$

$$X_t = -\frac{F}{k}\omega_2\omega_s^2[(\frac{e^{-\alpha_1 t}}{\omega_1^3-\omega_1\omega_2^2}\sin(\omega_1 t))+(\frac{e^{-\alpha_2 t}}{\omega_2^3-\omega_1^2\omega_2}\sin(\omega_2 t)]-\frac{F}{k}\frac{(\frac{\omega_s}{\omega_2})}{2\xi}(1+e^{-\alpha_2 t})\cos(\omega_2 t) \qquad (6\text{-}84)$$

$\bar{\omega} \to \omega_2$

6.2.3. Fluid and Structural damped case

In this scenario, in addition to structural damping, fluid damping is integrated into the governing equation of the coupled system to determine how the response changes ($c \neq 0,\ C_f \neq 0$). In the current research, this case study is referred to as fluid and structural damped coupled system. Let us recall Equation (6-14).

$$\ddot{\ddot{X}}(m)+\dddot{X}(c+C_f m)+\ddot{X}(k+C_f c+mk_{1n}+k_{2n}k_{3n})+\dot{X}(k_{1n}c+C_f k)+X(k_{1n}k)=$$
$$F(k_{1n}-\bar{\omega}^2)\sin(\bar{\omega}t)+C_f\bar{\omega}F\cos(\bar{\omega}t)$$

which denotes the dynamic equation of the coupled system from the contribution of each mode when both fluid and structure damping are integrated. In this equation, the coupled system experiences a sinusoidal excitation force.

6.2.3.1 Complementary response

When the structural and fluid dissipations are integrated into the governing equation, the complementary response of equation (6-14) can be obtained from Equation (6-85). For more details, please refer to Khanpour et al.(2024c). This equation describes the response of the fluid and structural damped coupled system under free vibration.

$$X_t = e^{\alpha_1 t}(A\sin(\omega_1 t)+B\cos(\omega_1 t))+e^{\alpha_2 t}(C\sin(\omega_2 t)+D\cos(\omega_2 t))$$

where

$$a_1 = \frac{-\xi\omega_s(K_{1n}-\omega_1^2)}{\omega_2^2-\omega_1^2}+\frac{-C_f(\omega_s^2-\omega_1^2)}{2(\omega_2^2-\omega_1^2)} \qquad (6\text{-}85)$$

$$a_2 = \frac{-\xi\omega_s(\omega_2^2-K_{1n})}{\omega_2^2-\omega_1^2}+\frac{-C_f(\omega_2^2-\omega_s^2)}{2(\omega_2^2-\omega_1^2)}$$

The parameters α_1 and α_2 refer to the modified dissipation factors incorporating natural frequencies (ω_1, ω_2), SDOF frequencies (ω_s), structural damping ratio (ξ), and fluid damping coefficient (C_f). Moreover, according to Khanpour (2024), the modified dissipation factors, α_1

and α_2, are negative, indicating that the complementary response diminishes exponentially over time. Based on this analytical work, the presence of damping has a negligible effect on the natural frequencies of the coupled system; therefore, they can be derived from the equation of the undamped system, Equation (6-17)

6.2.3.2. Particular response

For the sake of simplicity, equation (6-14), the fourth order ordinary differential equation, is written in the form of equation (6-86) where the corresponding values for parameter $\tilde{A},\tilde{B},\tilde{C},\tilde{D},\tilde{E},\tilde{F},\tilde{G}$ are introduced.

$$\begin{aligned}
&\ddddot{X}(\tilde{A})+\dddot{X}(\tilde{B})+\ddot{X}(\tilde{C})+\dot{X}(\tilde{D})+X(\tilde{E})=\tilde{F}\sin(\varpi t)+\tilde{G}\cos(\varpi t)\\
&\tilde{A}=m \quad \tilde{B}=c+C_f m \quad \tilde{C}=k+mk_{1n}+k_{2n}k_{3n} \quad \tilde{D}=k_{1n}c+C_f k\\
&\tilde{E}=kk_{1n} \quad \tilde{F}=F(k_{1n}-\varpi^2) \quad \tilde{G}=C_f\varpi F
\end{aligned} \tag{6-86}$$

Owing to the shape of the differential equation, the particular response is assumed to follow equation (6-87).

$$X_p=a\sin(\varpi t)+b\cos(\varpi t) \tag{6-87}$$

If the particular response, X_p, is applied to Equation (6-86), coefficients *a* and *b* are obtained from the following Equation:

$$\begin{aligned}
&a=\frac{\tilde{F}XX-\tilde{G}YY}{XX^2+YY^2} \qquad b=\frac{\tilde{F}YY+\tilde{G}XX}{XX^2+YY^2}\\
&where\\
&\tilde{A}=m \quad \tilde{B}=c+C_f m \quad \tilde{C}=k+mk_{1n}+k_{2n}k_{3n} \quad \tilde{D}=k_{1n}c+C_f k\\
&\tilde{E}=kk_{1n} \quad \tilde{F}=F(k_{1n}-\varpi^2) \quad \tilde{G}=C_f\varpi F\\
&XX=(\tilde{A}\varpi^4-\tilde{C}\varpi^2+\tilde{E})=m(\varpi^2-\omega_1{}^2)(\varpi^2-\omega_2{}^2)\\
&YY=(\tilde{B}\varpi^3-\tilde{D}\varpi)=[(C\varpi^3+C_f m\varpi^3)-(k_{1n}C\varpi+C_f k\varpi)]=-\left[C\varpi(k_{1n}-\varpi^2)+C_f\varpi(k-m\varpi^2)\right]=\\
&-\varpi[2\xi m\omega_s(k_{1n}-\varpi^2)+C_f m(\omega_s^2-\varpi^2)]=-\varpi m[2\xi\omega_s(k_{1n}-\varpi^2)+C_f(\omega_s^2-\varpi^2)]
\end{aligned} \tag{6-88}$$

Using similar procedure, if $\sin(\phi)=\dfrac{b}{\sqrt{a^2+b^2}}$, $\cos(\phi)=\dfrac{a}{\sqrt{a^2+b^2}}$, the particular response can be written as:

$$X_p = a\sin(\bar{\omega}t) + b\cos(\bar{\omega}t) = R\sin(\bar{\omega}t + \phi) \rightarrow \left\{ \begin{array}{l} R = \sqrt{a^2 + b^2} \\ \tan(\phi) = \dfrac{b}{a} \end{array} \right\} \tag{6-89}$$

The following procedure explains how to determine the amplitude of the response in this case study. In this equation, the parameter $\tilde{A}, \tilde{B}, \tilde{C}, \tilde{D}, \tilde{E}, \tilde{F}, \tilde{G}$ are substituted with identical values in Equation (6-86) and the term $(\tilde{A}\bar{\omega}^4 - \tilde{C}\bar{\omega}^2 + \tilde{E})$ is replaced with its equivalent $m(\bar{\omega}^2 - {\omega_1}^2)(\bar{\omega}^2 - {\omega_2}^2)$. Furthermore, in Equation (6-90), the definitions of SDOF's natural frequency and damping ratio, $m = \dfrac{k}{\omega_s^2}$, $c = 2\xi m\omega_s$ are utilized.

$$\begin{gathered} R = \sqrt{a^2 + b^2} = \sqrt{\left(\frac{\tilde{F}XX - \tilde{G}YY}{XX^2 + YY^2}\right)^2 + \left(\frac{\tilde{F}YY + \tilde{G}XX}{XX^2 + YY^2}\right)^2} = \frac{\tilde{F} + \tilde{G}}{\sqrt{XX^2 + YY^2}} \\ \sqrt{XX^2 + YY^2} = m\sqrt{[(\bar{\omega}^2 - {\omega_1}^2)(\bar{\omega}^2 - {\omega_2}^2)]^2 + \bar{\omega}^2[2\xi\omega_s(k_{1n} - \bar{\omega}^2) + C_f(\omega_s^2 - \bar{\omega}^2)]^2} \\ R = \frac{\tilde{F} + \tilde{G}}{\sqrt{XX^2 + YY^2}} = \frac{F}{K}\frac{\omega_s^2[(k_{1n} - \bar{\omega}^2) + C_f\bar{\omega}]}{\sqrt{[(\bar{\omega}^2 - {\omega_1}^2)(\bar{\omega}^2 - {\omega_2}^2)]^2 + \bar{\omega}^2[2\xi\omega_s(k_{1n} - \bar{\omega}^2) + C_f(\omega_s^2 - \bar{\omega}^2)]^2}} \end{gathered} \tag{6-90}$$

Similar to the previous cases, $\dfrac{F}{K} = \Delta_{st}$ is referred to as static displacement; therefore, the dynamic amplification (δ_d) in this case is obtained from Equation (6-91).

$$R = \Delta_{st}\delta_d \qquad \delta_d = \frac{\omega_s^2[(k_{1n} - \bar{\omega}^2) + C_f\bar{\omega}]}{\sqrt{[(\bar{\omega}^2 - {\omega_1}^2)(\bar{\omega}^2 - {\omega_2}^2)]^2 + \bar{\omega}^2[2\xi\omega_s(k_{1n} - \bar{\omega}^2) + C_f(\omega_s^2 - \bar{\omega}^2)]^2}} \tag{6-91}$$

The process below delineates the determination of the phase difference (ϕ) in detail. It manipulates the definition of the natural frequency of the SDOF, damping ratio and utilizes the definitions of *XX* and *YY* parameters in Equation (6-88).

$$\begin{gathered} \tan(\phi) = \frac{b}{a} = \frac{\tilde{F}YY + \tilde{G}XX}{\tilde{F}XX - \tilde{G}YY} = \\ \frac{F\bar{\omega}m[-(2\xi\omega_s(k_{1n} - \bar{\omega}^2) + C_f(\omega_s^2 - \bar{\omega}^2))(k_{1n} - \bar{\omega}^2) + C_f(\bar{\omega}^2 - {\omega_1}^2)(\bar{\omega}^2 - {\omega_2}^2)]}{Fm[(\bar{\omega}^2 - {\omega_1}^2)(\bar{\omega}^2 - {\omega_2}^2)(k_{1n} - \bar{\omega}^2) + C_f\bar{\omega}\bar{\omega}(2\xi\omega_s(k_{1n} - \bar{\omega}^2) + C_f(\omega_s^2 - \bar{\omega}^2))]} = \\ \frac{[-(2\xi\omega_s\bar{\omega}(k_{1n} - \bar{\omega}^2) + C_f\bar{\omega}(\omega_s^2 - \bar{\omega}^2))(k_{1n} - \bar{\omega}^2) + C_f\bar{\omega}(\bar{\omega}^2 - {\omega_1}^2)(\bar{\omega}^2 - {\omega_2}^2)]}{[(\bar{\omega}^2 - {\omega_1}^2)(\bar{\omega}^2 - {\omega_2}^2)(k_{1n} - \bar{\omega}^2) + C_f\bar{\omega}^2(2\xi\omega_s(k_{1n} - \bar{\omega}^2) + C_f(\omega_s^2 - \bar{\omega}^2))]} \end{gathered} \tag{6-92}$$

Special cases:

1-When the excitation frequency approaches $(\varpi \to \sqrt{k_{1n}})$: In this scenario, unlike the two previous cases, the nominator of dynamic amplification is nonzero (Equation 6-91); therefore, the particular response is present in this scenario and derived from equation (6-93).

$$R = \frac{F}{K}\frac{\omega_s^2[(k_{1n}-\varpi^2)+C_f\varpi]}{\sqrt{[(\varpi^2-\omega_1{}^2)(\varpi^2-\omega_2{}^2)]^2+\varpi^2[2\xi\omega_s(k_{1n}-\varpi^2)+C_f(\omega_s^2-\varpi^2)]^2}} = \tag{6-93}$$
$$\varpi \to \sqrt{k_{1n}}$$
$$\frac{F}{K}\frac{C_f\sqrt{k_{1n}}\omega_s^2}{\sqrt{[(k_{1n}-\omega_1{}^2)(k_{1n}-\omega_2{}^2)]^2+[C_f k_{1n}(\omega_s^2-k_{1n})]^2}}$$

When the excitation frequency approaches the coupled system frequency ($\varpi \to \omega_1$ *or* $\varpi \to \omega_2$): In this scenario similar to the structural damped coupled system, due to the presence of the damping, the particular response is not infinitive. As an illustration, Equations (6-94) and (6-95) reveal the particular responses in this case when $\varpi \to \omega_1$ and $\varpi \to \omega_2$, respectively.

$$R = \frac{F}{K}\frac{\omega_s^2[(k_{1n}-\varpi^2)+C_f\varpi]}{\sqrt{[(\varpi^2-\omega_1{}^2)(\varpi^2-\omega_2{}^2)]^2+\varpi^2[2\xi\omega_s(k_{1n}-\varpi^2)+C_f(\omega_s^2-\varpi^2)]^2}} = \tag{6-94}$$
$$\varpi \to \omega_1$$
$$\frac{F}{K}\frac{\omega_s^2[(k_{1n}-\omega_1{}^2)+C_f\omega_1]}{\varpi\sqrt{[2\xi\omega_s(k_{1n}-\omega_1{}^2)+C_f(\omega_s^2-\omega_1{}^2)]^2}}$$

$$R = \frac{F}{K}\frac{\omega_s^2[(k_{1n}-\omega_2{}^2)+C_f\omega_2]}{\varpi\sqrt{[2\xi\omega_s(k_{1n}-\omega_2{}^2)+C_f(\omega_s^2-\omega_2{}^2)]^2}} \tag{6-95}$$

6.2.3.3. Total response

The total response, which is the sum of particular response and complementary response, is determined from Equation (6-96).

$$X_t = e^{\alpha_1 t}(A\sin(\omega_1 t) + B\cos(\omega_1 t)) + e^{\alpha_2 t}(C\sin(\omega_2 t) + D\cos(\omega_2 t)) + a\sin(\varpi t) + b\cos(\varpi t)$$

where

$$a = \frac{\tilde{F}XX - \tilde{G}YY}{XX^2 + YY^2} \qquad b = \frac{\tilde{F}YY + \tilde{G}XX}{XX^2 + YY^2}$$

$$XX = (\tilde{A}\varpi^4 - \tilde{C}\varpi^2 + \tilde{E}) = m(\varpi^2 - \omega_1{}^2)(\varpi^2 - \omega_2{}^2) \qquad YY = (\tilde{B}\varpi^3 - \tilde{D}\varpi)$$

$$\tilde{A} = m \quad \tilde{B} = c + C_f m \quad \tilde{C} = k + mk_{1n} + k_{2n}k_{3n} \quad \tilde{D} = k_{1n}c + C_f k \tag{6-96}$$

$$\tilde{E} = kk_{1n} \quad \tilde{F} = F(k_{1n} - \varpi^2) \quad \tilde{G} = C_f \varpi F$$

$$a_1 = \frac{-\xi\omega_s(K_{1n} - \omega_1^2)}{\omega_2^2 - \omega_1^2} + \frac{-C_f(\omega_s^2 - \omega_1^2)}{2(\omega_2^2 - \omega_1^2)}$$

$$a_2 = \frac{-\xi\omega_s(\omega_2^2 - K_{1n})}{\omega_2^2 - \omega_1^2} + \frac{-C_f(\omega_2^2 - \omega_s^2)}{2(\omega_2^2 - \omega_1^2)}$$

Comparing Equations (6-96) and (6-79) reveals that both damped system, structural damped case, and structural and fluid damped case follow a similar shape of the total response. However, the dissipation factors, particular response coefficients, and complementary response coefficients are different for the two solutions. As both solutions assume the same initial boundary conditions, it can be concluded that the coefficients *A, B, C,* and *D* in Equation (6-96) are determined from Equation (6-81), $A = \frac{a\varpi\omega_2^2 - a\varpi^3 - p}{\omega_1^3 - \omega_1\omega_2^2}$ $B = -\frac{b(\varpi^2 - \omega_2^2)}{\omega_1^2 - \omega_2^2}$ $C = \frac{a\varpi\omega_1^2 - a\varpi^3 - p}{\omega_2^3 - \omega_1^2\omega_2}$ $D = \frac{b(\varpi^2 - \omega_1^2)}{\omega_1^2 - \omega_2^2}$, with the coefficients *a* and *b* corresponding to this scenario presented in Equation (6-96).

Special case:

1-When the excitation frequency approaches the water tank frequency $(\varpi \to \sqrt{k_{1n}})$: In this scenario, regarding equation (6-96) $a = \frac{-\tilde{G}YY}{XX^2 + YY^2}$, and $b = \frac{\tilde{G}XX}{XX^2 + YY^2}$. Therefore, in contrast to the preceding cases, the particular response is a nonzero value. Next, according to the nonzero values for *a,* and *b,* the coefficients *A, B, C,* and *D* are nonzero and are derived based on equation (6-81). Finally, the total response, X_t, is derived using equation (6-96), with the contribution of all terms and coefficients associated with this case.

When the excitation frequency approaches the coupled system frequency ($\bar{\varpi} \to \omega_1 \;\; or \;\; \bar{\varpi} \to \omega_2$):

As an illustration, we focus on the case $\bar{\varpi} \to \omega_1$. The value of $XX = \tilde{A}\bar{\varpi}^4 - \tilde{C}\bar{\varpi}^2 + \tilde{E}$, which is equivalent to $(m)\bar{\varpi}^4 - (k + mk_{1n} + k_{2n}k_{3n})\bar{\varpi}^2 + (kk_{1n})$, is zero when $\bar{\varpi} \to \omega_1$. According to Equation (6-96), coefficients *a, b* are $a = \dfrac{-\tilde{G}}{YY}$, $b = \dfrac{\tilde{F}}{YY}$, respectively. Furthermore, based on equation (6-81), the coefficients of the complementary response are $A = \dfrac{a\omega_1\omega_2^2 - a\omega_1^{\;3} - p}{\omega_1^3 - \omega_1\omega_2^2}$, $B = -b$, $C = \dfrac{-p}{\omega_2^3 - \omega_1^2\omega_2}$, $D = 0$, and the total response can be obtained from Equation (6-96) with coefficients pertaining to this case. Similarly, when the excitation frequency tends toward the greater natural frequency, the total response can be derived.

Modal composition:

The following equation, which relies on modal decomposition, was proposed to determine the mode participation for forced vibration: To this end, the Fourier transformation of *1* is employed.

$$F = F \times 1 = F\sum_{n=1}^{N} M_n \sin(\frac{n\pi}{L}x) = F\begin{Bmatrix} M_1 \sin(\dfrac{\pi}{L}x) + M_3 \sin(\dfrac{3\pi}{L}x) + \ldots M_n \sin(\dfrac{n\pi}{L}x) + \ldots \\ +M_N \sin(\dfrac{N\pi}{L}x) \end{Bmatrix}$$

$$where \qquad (6\text{-}97)$$

$$M_n = (-2)\frac{(-1)^n - 1^n}{n\pi} = \begin{Bmatrix} \dfrac{4}{n\pi} \;\; for\, n = 2k+1 \\ 0 \;\; for\, n = 2k \end{Bmatrix}$$

Therefore, the participation of each mode, that is, *n*, from the excitation force is M_nF_n. Although the odd modes contribute to the response of the coupled system, the even modes do not.

As demonstrated, the total response in higher modes (*n* ≥ 3), both in the damped and undamped cases, replicates the particular response of the individual SDOF. Due to factors including the participation of each mode from the total force being M_nF_n, the total response replicating the SDOF response in higher modes, and the linear response, the total response for each mode is equal to the $X_{t,n} = M_nX_t$.

To derive the total response of the coupled based on modes composition, the following expression is introduced:

$$X_t = X_{t,1}\sin(\frac{\pi x}{l}) + X_{t,3}\sin(\frac{3\pi x}{l}) + ... + X_{t,\mathrm{n}}\sin(\frac{n\pi x}{l}) + ...X_{t,\mathrm{N}}\sin(\frac{N\pi x}{l}) \tag{6-98}$$

Based on the preceding clarification, the following relation can be derived for higher modes:

$$\begin{aligned}
&X_{t,3}\sin(\frac{3\pi x}{l}) + ... + X_{t,\mathrm{n}}\sin(\frac{n\pi x}{l}) + ...X_{t,\mathrm{N}}\sin(\frac{N\pi x}{l}) = \\
&M_3\,\mathrm{X}_{SDOF}\sin(\frac{3\pi x}{l}) + ... + M_{\mathrm{n}}\,\mathrm{X}_{SDOF}\sin(\frac{n\pi x}{l}) + ...\mathrm{M_N X}_{SDOF}\sin(\frac{N\pi x}{l}) = \\
&\mathrm{X}_{SDOF}\left\{M_3\sin(\frac{3\pi x}{l}) + ...M_{\mathrm{n}}\sin(\frac{n\pi x}{l}) + ...M_N\sin(\frac{N\pi x}{l})\right\}
\end{aligned} \tag{6-99}$$

Equation (6-99) is applied to Equation (6-98) for higher modes, and the term $M_1 X_{SDOF}\sin(\frac{\pi x}{l})$ is added to and subtracted from Equation (6-98), leading to the following expression:

$$X_t = M_1\sin(\frac{\pi x}{l})(X_{t,1} - X_{SDOF}) + \mathrm{X}_{SDOF}\underbrace{\left\{\begin{array}{l} M_1\sin(\frac{1\pi x}{l}) + M_3\sin(\frac{3\pi x}{l}) + ...M_{\mathrm{n}}\sin(\frac{n\pi x}{l}) + ... \\ M_N\sin(\frac{N\pi x}{l}) \end{array}\right\}}_{1} \tag{6-100}$$

Because the summation of terms in the bracket is equal to 1, based on the Fourier transformation, the following relation is developed for the estimation of the total response of the TLD coupled system:

$$X_t = \underbrace{M_1\sin(\frac{\pi x}{l})X_{t,1}}_{first\,term} + \underbrace{\mathrm{X}_{SDOF}(1 - M_1\sin(\frac{1\pi x}{l}))}_{second\,term} \tag{6-101}$$

Regarding the upper equation, the frequency of the coupled system is influenced by the frequencies of the first mode and natural frequency of the SDOF. When a coupled system is developed, the frequencies of the coupled system differ from the natural frequencies of the constitutive elements. TLD coupled system consists of two elements: 1- SDOF and TLD. Therefore, the coupled system frequency should differ from the SDOF frequency. To remove the contribution of the SDOF frequency, the second term should be zero, and thus, $\sin(\frac{1\pi x}{l})=\frac{1}{M_1}=\frac{\pi}{4}$. Hence, it can be concluded that $X_t \simeq X_{t,1}$, which means that the TLD coupled system is mainly influenced by the first mode.

6.3. Numerical model

A numerical model was employed to assess the accuracy of the current analytical method. This numerical model is based on the governing equations detailed in equations (6-102.1, 6-102.2, 6-102.3, 6-102.4, 6-102.5, and 6-102.6), which correspond to: 1) the continuity equation, 2) the momentum equation, 3) wave height modal composition, 4) wave velocity modal composition, 5) sloshing force, and 6) the SDOF equation. The sloshing force is calculated by subtracting the hydrostatic force on the left wall from that on the right wall.

In contrast to the analytical approach, this numerical model employs a partitioned method and a weak form to couple the equations. Additionally, it utilizes the separation of variables technique to solve the fluid governing equations. The numerical scheme for solving the fluid motion equations is based on the Second Order Runge-Kutta method, while the SDOF equation is solved using the second order finite difference method. This numerical scheme is advantageous because it provides solutions for each mode as well as a sufficient number of modes to ensure convergence. For further details on the numerical schemes and coupling process algorithm, refer to Khanpour et al. (2024b).

$$\ddot{A}_n = -\dot{B}_n(\frac{Hn\pi}{L}) \tag{6-102.1}$$

$$\begin{gathered}\ddot{A}_n + C_f\dot{A}_n + K_{1n}A_n - K_{2n}\ddot{X} = 0 \\ where \\ k_{1n} = (\frac{Hgn^2\pi^2}{L^2}) > 0 \quad k_{2n} = (\frac{Hn\pi}{L})M_n = \begin{Bmatrix} 0 \ \ for\, n = 2K \\ \frac{4H}{L}\ for\, n = 2K+1 \end{Bmatrix} \geq 0\end{gathered} \tag{6-102.2}$$

$$\eta(x,t)=\sum_{i=1}^{N} A_i(t)cos(\frac{i\pi x}{L})=A_1(t)cos(\frac{i\pi x}{L})+...+A_n(t)cos(\frac{n\pi x}{L})+...A_N(t)cos(\frac{N\pi x}{L}) \tag{6-102.3}$$

$$u(x,t)=\sum_{i=1}^{N} B_i(t)sin(\frac{i\pi x}{L})=A_1(t)sin(\frac{i\pi x}{L})+...+A_n(t)sin(\frac{n\pi x}{L})+...A_N(t)sin(\frac{N\pi x}{L}) \tag{6-102.4}$$

$$F_{slo} = 0.5\rho g b[(H+\eta_R)^2-(H-\eta_R)^2] \tag{6-102.5}$$

$$u(x,t)=\sum_{i=1}^{N} B_i(t)sin(\frac{i\pi x}{L})=A_1(t)sin(\frac{i\pi x}{L})+...+A_n(t)sin(\frac{n\pi x}{L})+...A_N(t)sin(\frac{N\pi x}{L}) \tag{6-102.6}$$

6.4. Results and Discussion:

In this section, a TLD coupled system is modelled using the current analytical approach. The numerical method explained in the previous section is employed to assess the accuracy and validity of the analytical approach. The TLD coupled system includes a water tank at the top with a length (0.46 m), width of (0.31m) and mean water depth (0.04 m). Therefore, the mass of the water in the tank is (5.7 Kg). It also accommodates an SDOF as an underlying structure with characteristics of mass (282 kg), stiffness (4997.5 N/m), and damping coefficient (24 kg/s). The mass ratio, which is defined as the ratio of the water mass to the SDOF mass, is equal to 2 percent. Considering equation (6-8) and equation (6-26), both the natural frequency of the water tank and the SDOF are tie and equals (4.2 rad/s). In fact, the case study adheres to the characteristics of tuned liquid damper system, which has identical frequencies for the water tank and underlying structure, as well as a small mass ratio.

The TLD coupled system undergoes a harmonic excitation force ($F\sin(\bar{\omega}t)$). The amplitude of the harmonic sinus force is (*F*=54.53 N). It is worth noting that the excitation initiates from stagnant condition which is zero initial values for displacement, velocity, wave height, and wave velocity. Similar to the methodology section, this section includes three scenarios: 1) undamped TLD coupled system, 3) structural damped TLD coupled system, and 3) fluid and structural damped TLD coupled system, to obtain a more profound understanding and investigate the accuracy of the current analytical approach in various scenarios. Furthermore, each scenario discusses the particular cases investigated in the methodology section. Along with analytical and numerical approaches, the Fast Forieh Transformation (FFT) is employed here to derive the constitutive frequencies of the numerical responses.

The natural frequencies of the coupled system can be determined from equation (6-17). The lower natural frequency of the coupled system is (3.97 rad/s), while the higher natural frequency is (4.52 rad/s). The analytical study by Khanpour (2024c) indicates that the effect of dissipations on the natural frequency is negligible. Therefore, these natural frequencies are introduced as natural frequencies of the coupled system for all three scenarios 1- undamped 2- structural damped 3- fluid & structural damped

6.4.1. undamped TLD coupled system

This case study excludes both structural and fluid dissipation in the analytical response. To obtain a more comprehensive understanding of the dynamic behavior of the TLD coupled system, the dynamic amplification of the particular response is investigated. Recall the relation for dynamic amplification in this case, equation (6-28), and $\delta_d = \dfrac{(k_{1n} - \bar{\omega}^2)\omega_s^2}{(\bar{\omega}^2 - \omega_1^2)(\bar{\omega}^2 - \omega_2^2)}$. Figure (6.2) shows the dynamic amplification versus the frequency ratio, which is the ratio of the excitation frequency to the TLD frequency $(\dfrac{\bar{\omega}}{\sqrt{k_{1n}}})$. As evident from the dynamic amplification expression, when the excitation frequency approaches the smaller or greater natural frequency of the coupled system, dynamic amplification approaches infinity. Equivalently, the graph of the amplification factor versus the frequency ratio has two vertical asymptotes. This scenario, referred to as resonance excitation of the coupled system, leads to infinite vibration and threatens the stability of the coupled system.

When the TLD is absent and the excitation frequency approaches the TLD frequency ($\sqrt{k_{1n}}$), which is nearly the same as the SDOF frequency, the displacement of the structure increases exponentially over time. However, when the excitation frequency approaches the TLD frequency in a TLD-coupled system, as shown in the figure for the frequency ratio $\dfrac{\bar{\omega}}{\sqrt{k_{1n}}} = 1$, the dynamic amplification drops to zero. This leads to optimal performance of the TLD in controlling the vibrations of the coupled system. In this scenario, the total response consists solely of a complementary response.

When the frequency ratio becomes extremely high and mathematically infinite, the dynamic response approaches zero, where $\delta_d \underset{\bar{\varpi} \to \infty}{\simeq} \frac{-\bar{\varpi}^2}{\bar{\varpi}^4} \simeq 0$. On the other side of the spectrum, if the excitation frequency is close to zero, dynamic amplification approaches $\delta_d \simeq \frac{\omega_s^2 k_{1n}}{\omega_1^2 \omega_2^2}$. Because in the TLD coupled system, the SDOF frequency is very close to the TLD frequency, the dynamic amplification for zero frequency ratio can be expressed as $\delta_d \simeq (\frac{\omega_s^2}{\omega_1 \omega_2})^2$.

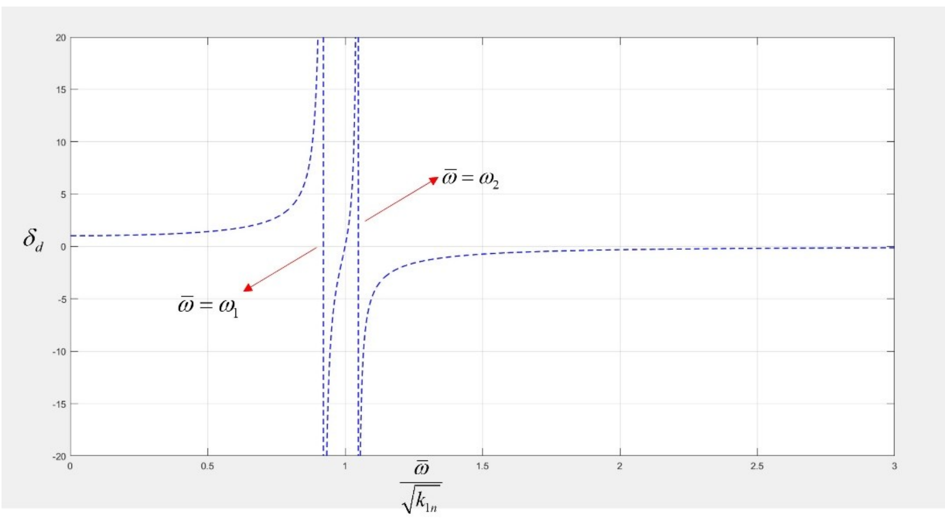

Fig. 6.2. Dynamic amplification factor versus frequencies ratio for the undamped TLD coupled system

General case:

This section focuses on the total response derived using the current analytical approach and its comparison with the numerical method. Additionally, the FFT technique is employed to determine the fundamental frequencies of the numerical response. The FFT technique is utilized here to convert the coupled system displacement from the time domain to the frequency domain. As an illustration, in this section, the natural frequency of the excitation is adjusted to 75 percent of the water tank frequency ($\bar{\varpi} = 0.75\sqrt{k_{1n}}$). The displacement is derived using the numerical method described in Section (6.3). The FFT of the displacement in Figure (6.3) reveals that the numerical response comprises three dominant frequencies. These frequencies are very close to the natural frequencies of the TLD coupled system (ω_1, ω_2) and the force excitation frequency ($\bar{\omega}$).

On the other hand, let us recall Equation (6-36), which provides the analytical solution for the displacement of the coupled system. Based on this equation, the analytical displacement includes three frequencies: the natural frequencies (ω_1, ω_2) and the excitation frequency ($\bar{\omega}$). As shown in Figure (6.3), the constituent frequencies of the analytical response aligned well with the dominant numerical frequencies. In addition to the TLD coupled system, Figure (6.3) also indicates the numerical response of the individual SDOF system. The total response of the individual SDOF takes the form of $X_{SDOF} = A' \sin(\omega_s t) + B' \sin(\bar{\omega} t)$. For more information on how to determine the coefficients (A', B'), please refer to Humar (2014). As expected, the numerical results for the individual SDOF system reflect only two fundamental frequencies: the excitation frequency ($\bar{\omega}$) and SDOF frequency (ω_S).

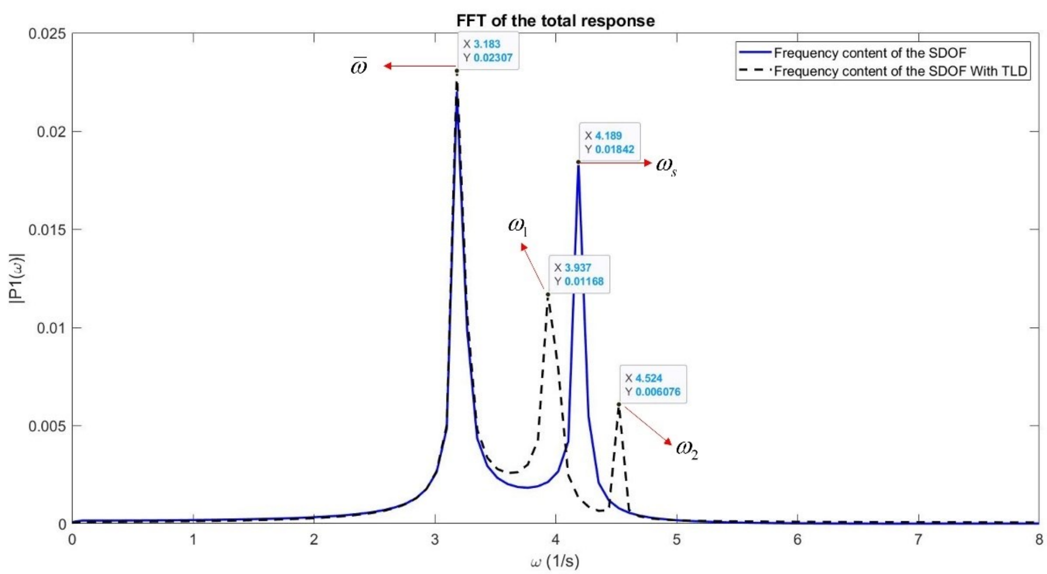

Fig. 6.3. Fundamental frequencies of the undamped TLD coupled system and the individual SDOF where $\bar{\omega} = 0.75\sqrt{k_{1n}}$

To derive the analytical response, the total response is expressed using Equation (6-36), with the coefficients determined through the system of Equations (6-40). The analytical response is then compared with the numerical response shown in Figure (6.4). This comparison shows that the analytical approach accurately predicts the dynamic behavior of the TLD coupled system. Furthermore, the accuracy of the model is assessed when the excitation frequency is equal to half of the tank frequency ($\bar{\omega} = 0.5\sqrt{k_{1n}}$). The comparison in Figure (6.5) demonstrates the excellent agreement between the analytical approach and numerical model, proving the high precision of the current analytical solution. Subsequently, the validity of the analytical approach for special cases of an undamped system are investigated.

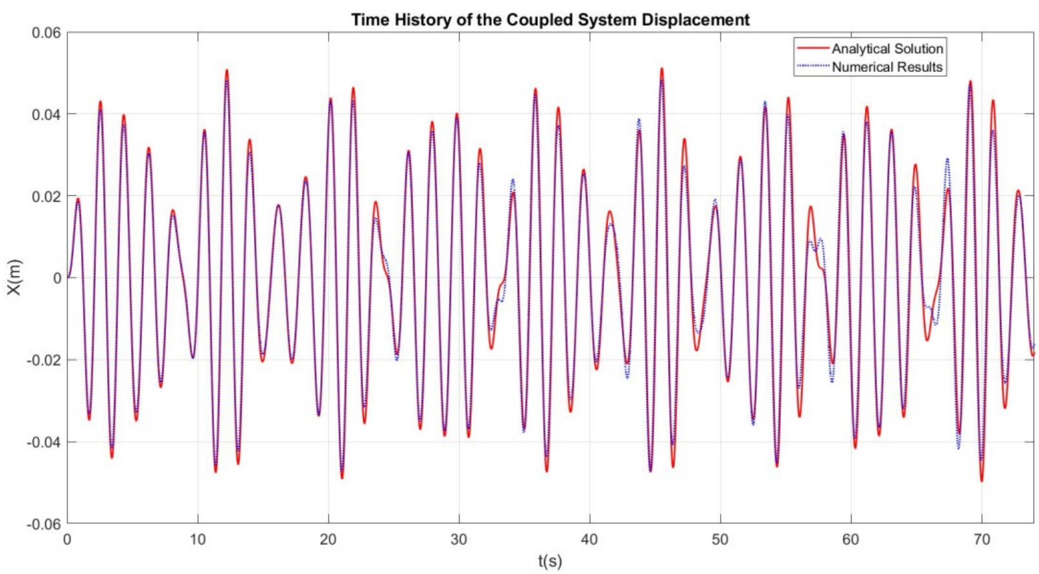

Fig. 6.4. Time history displacements of the undamped TLD coupled system where $\bar{\omega} = 0.75\sqrt{k_{1n}}$

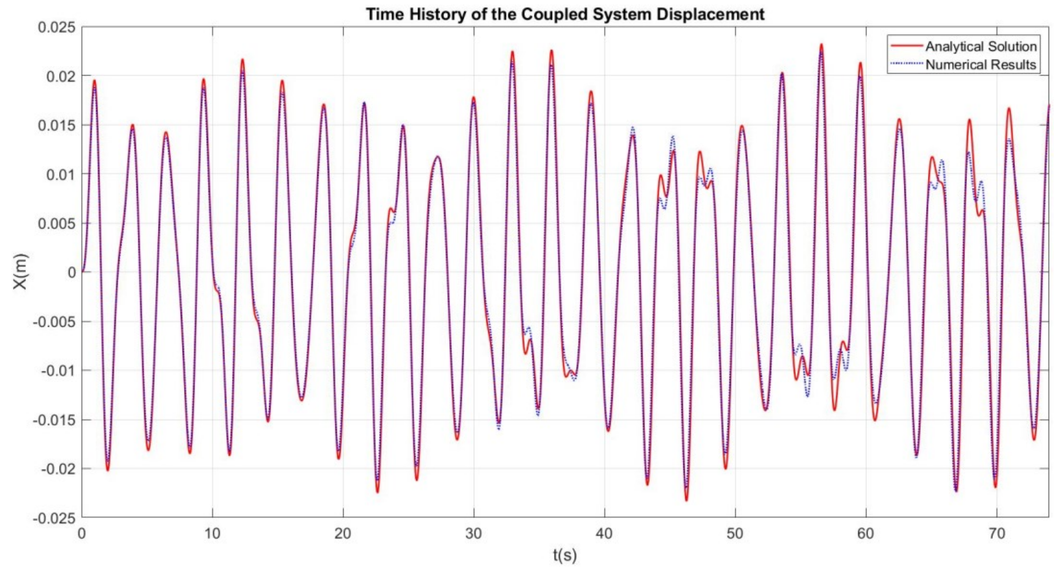

Fig. 6.5. Time history displacements of the undamped TLD coupled system where $\bar{\omega} = 0.5\sqrt{k_{1n}}$

Particular case

When the excitation frequency approaches the TLD frequency ($\bar{\omega} = \sqrt{k_{1n}}$):

The analytical solution in this case, Equation. (6-44), reveals that the particular response does not contribute to the total response. Consequently, the analytical total response includes only the natural frequencies of the coupled system and excludes the excitation frequency. The FFT of the numerical response depicted in Figure (6.6), indicates that the dominant frequencies are close to the natural frequencies of the coupled system, and the excitation frequency is absent in the response. As expected, in this scenario, the FFT of the individual SDOF response shows a significant contribution to the natural SDOF frequency. However, the presence of TLD significantly mitigates the coupled system response, leading to a much smaller contribution of the fundamental frequencies.

In this scenario, the displacement function of the TLD coupled system, referred to as the TLD coupled system response, is derived from Equation (6-44). The analytical total response in this case is compared with the numerical results in Figure (6.7), indicating a close agreement.

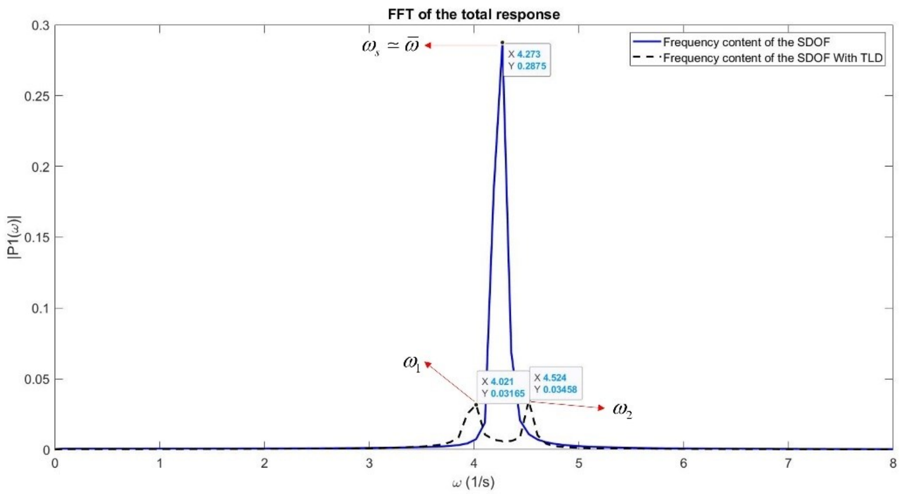

Fig. 6.6. Fundamental frequencies of the undamped TLD coupled system and the individual SDOF where $\bar{\omega} = \sqrt{k_{1n}}$

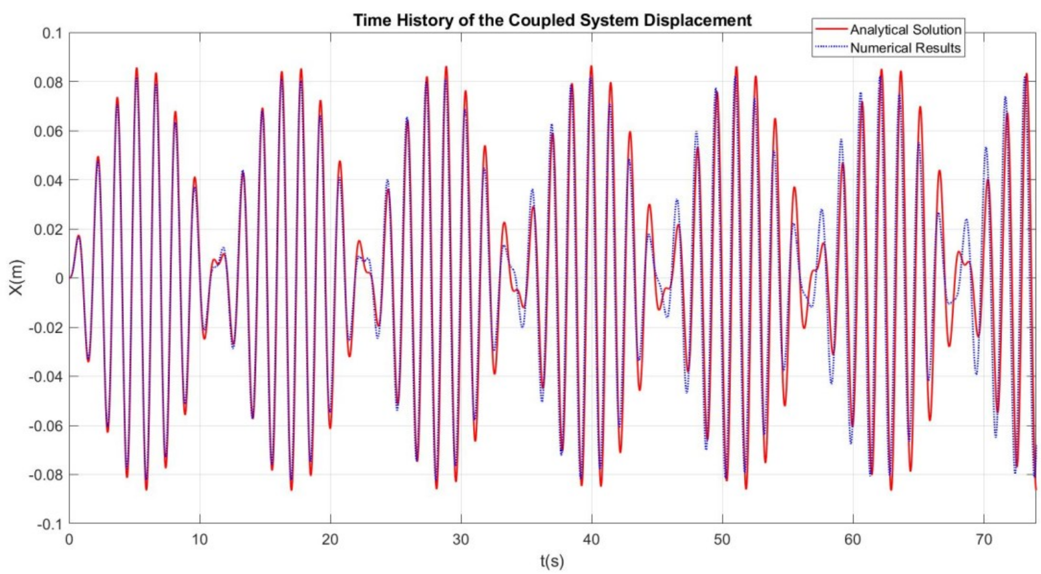

Fig. 6.7. Time history displacements of the undamped TLD coupled system where $\bar{\omega} = \sqrt{k_{1n}}$

When the excitation frequency approaches the coupled system natural frequency ($\bar{\omega} = \omega_1 \; or \; \bar{\omega} = \omega_2$):

Let us consider the case where the excitation frequency approaches the lower natural frequency ($\bar{\omega} = \omega_1$). As mentioned earlier, this scenario is associated with the first resonance excitation case of the TLD coupled system, where the particular response approaches infinity. After extensive calculations and applying L'Hôpital's rule, the total response is derived from Equation (6-59), showing the participation of two frequencies in the response, which are the natural frequencies of the coupled system. Similarly, the numerical results in Figure (6.8) indicate that these two natural frequencies significantly contribute to the TLD coupled system response, and as predicted analytically with a notably higher contribution from the lower frequency. As expected, the individual SDOF exhibits two fundamental frequencies: the excitation frequency (the lower natural frequency of the coupled system) and the natural frequency of the SDOF.

Figure (6.9) presents the analytical response of the TLD coupled system derived from Equation (6-59) along with the numerical results for this scenario. As shown, both methods indicate that the coupled system is unstable in this case, with the system vibrations growing exponentially over time. This scenario, referred to as the first resonance excitation case of the TLD coupled system, shows excellent agreement between the numerical and analytical approaches in both patterns and peaks.

Next, the second resonance excitation case, where the excitation frequency approaches the higher natural frequency of the coupled system, is modeled. The analytical solution in this case is obtained from equation (6-60). The FFT of the numerical response, as predicted by the analytical approach, is shown in Figure (6.10) the participation of the two natural frequencies of the coupled system, with a considerably higher contribution from the higher frequency. Although the comparison in Figure (6.11) shows good alignment, the analytical response predicts a slightly smaller amplitude response.

Overall, the agreement between the numerical and analytical results demonstrates the precision of the analytical approach in predicting the behavior of the undamped coupled TLD system under both resonant excitation cases.

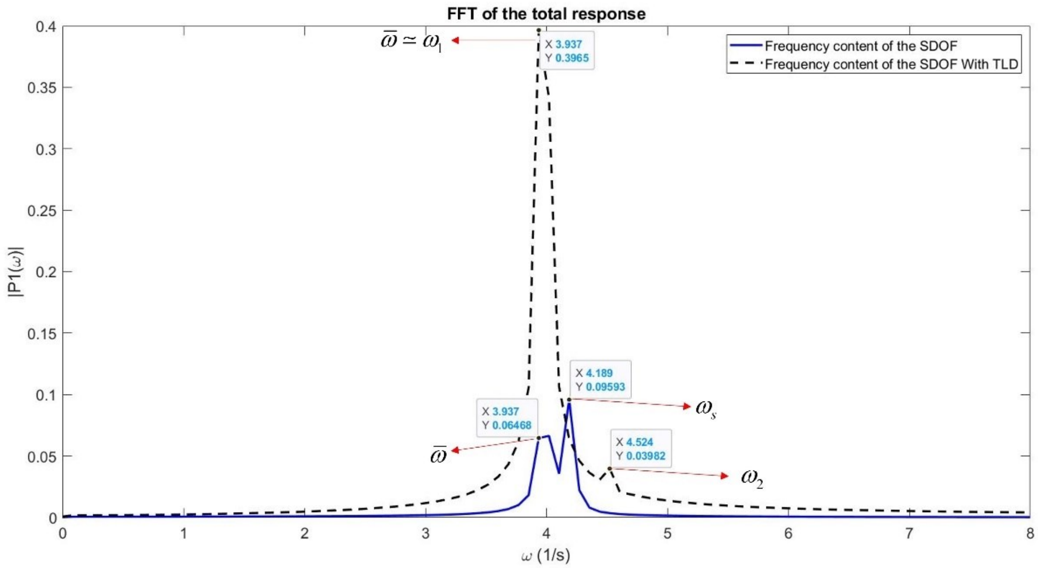

Fig. 6.8. Fundamental frequencies of the undamped TLD coupled system and individual SDOF where $\bar{\omega} = \omega_1$

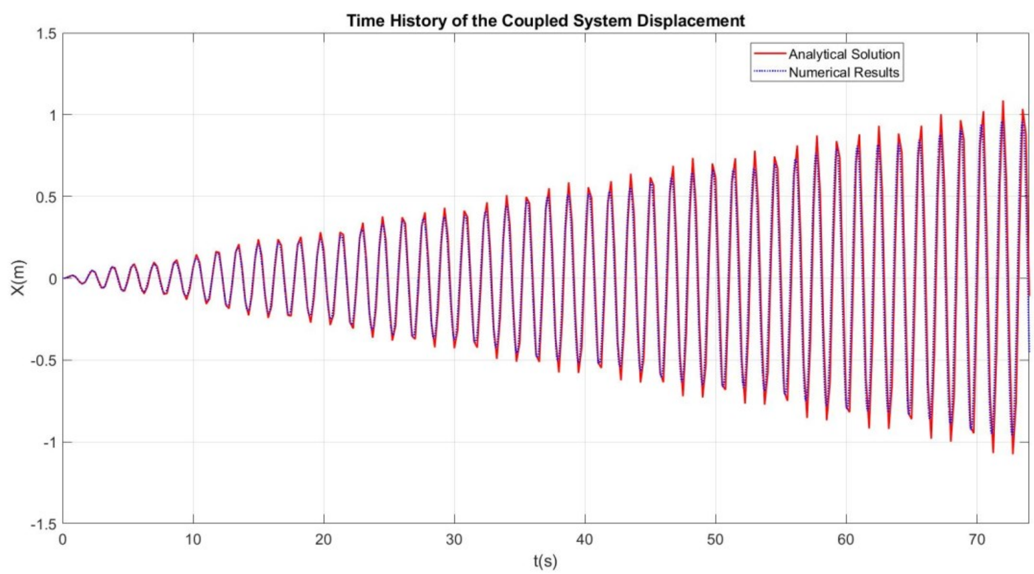

Fig. 6.9. Time history displacements of the undamped TLD coupled system where $\bar{\omega} = \omega_1$

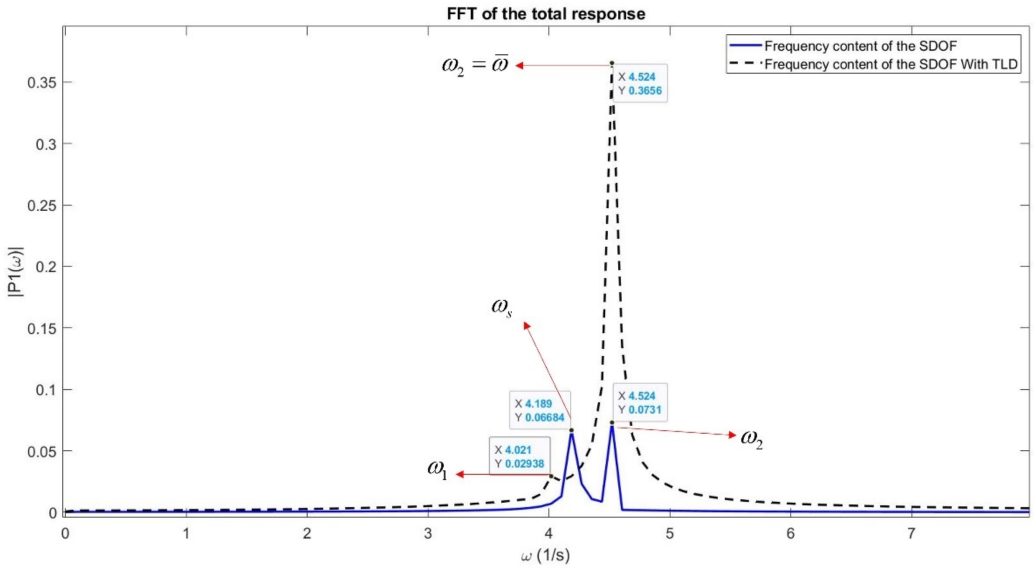

Fig. 6.10. Fundamental frequencies of the undamped TLD coupled system and individual SDOF where $\bar{\omega} = \omega_2$

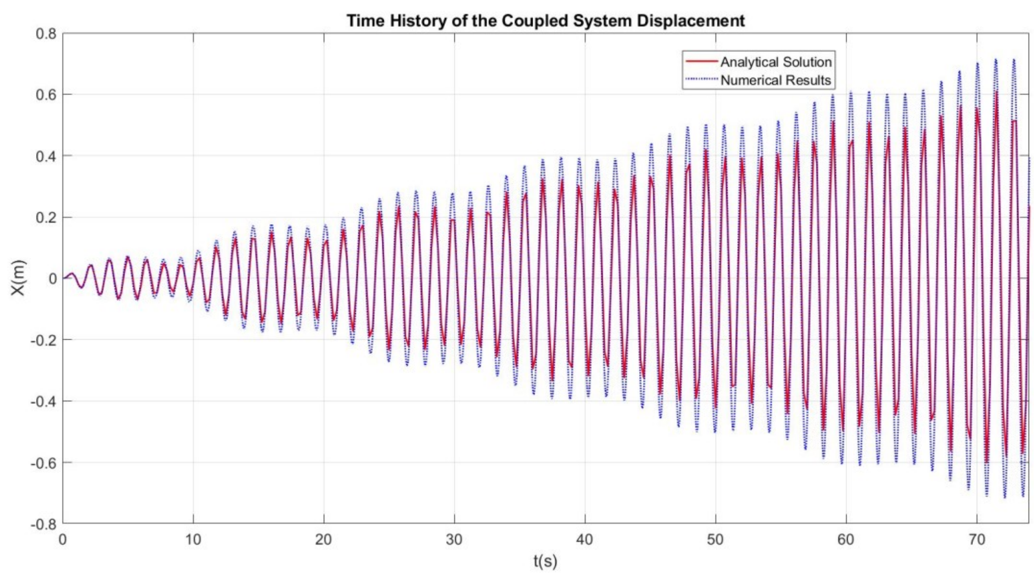

Fig. 6.11. Time history displacements of the undamped TLD coupled system where $\bar{\omega} = \omega_2$

6.4.2. Structural damped TLD coupled system

This scenario incorporates structural damping ($c \neq 0$) and disregards fluid damping ($C_f = 0$). In this case study, referred to as the structurally damped coupled system, the dynamic amplification is determined from Equation (6-73), ($\delta_d = \dfrac{\omega_s^2(k_{1n} - \bar{\varpi}^2)}{\sqrt{[(\bar{\varpi}^2 - \omega_1^2)(\bar{\varpi}^2 - \omega_2^2)]^2 + (2\xi\omega_s\bar{\varpi})^2\left[k_{1n} - \bar{\varpi}^2\right]^2}}$). The dynamic amplification versus the frequency ratio is shown in Figure (6.12). Contrary to the preceding case, according to Equation (6-73), when the excitation frequency approaches the natural frequencies of the coupled system ($\bar{\varpi} \to \omega_1$ and $\bar{\varpi} \to \omega_2$), the amplification factors are not infinite, but close to ($\delta_d = \dfrac{1}{2\xi \dfrac{\omega_1}{\omega_s}}$) and ($\delta_d = \dfrac{1}{2\xi \dfrac{\omega_2}{\omega_s}}$), respectively. Because the first natural frequency is smaller than the greater frequency ($\omega_1 < \omega_2$), the vibration amplitude of the coupled system is higher when $\bar{\varpi} \to \omega_1$. Similar to the preceding case, as shown in Figure (6.12), when the excitation force approaches the tank frequency ($\bar{\varpi} \to \sqrt{k_{1n}}$), the particular response diminishes. This scenario reflects the most advantageous use of TLD in mitigating structural vibrations. As in the previous case, if the excitation frequency approaches zero and infinity, dynamic amplification is approximated by ($\underset{\bar{\varpi} \to 0}{\delta_d} \simeq \dfrac{\omega_s^2 k_{1n}}{\omega_1^2\omega_2^2}$) and ($\underset{\bar{\varpi} \to \infty}{\delta_d} \simeq \dfrac{-\bar{\varpi}^2}{\bar{\varpi}^4} \simeq 0$), respectively.

It is worth noting that, according to Figure (6.12), as structural damping increases, the response of the coupled system decreases, particularly during the resonance excitation of the coupled system, that is, ($\bar{\varpi} \to \omega_1 \; or \; \bar{\varpi} \to \omega_2$). Furthermore, based on Figure (6.12), it appears that structural damping affects only a narrow range of frequency ratios. When the frequency ratio is smaller than 0.7 or greater than 1.3, structural damping has a negligible impact on the vibration of the coupled system.

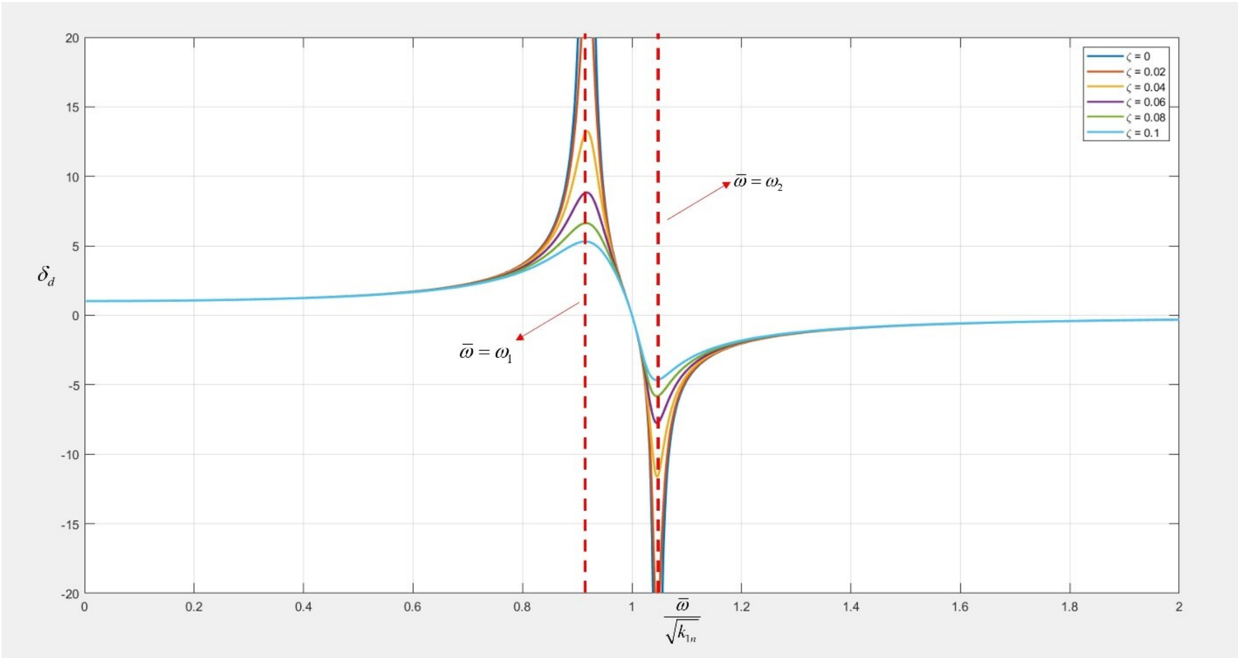

Fig. 6.12. Dynamic amplification factor versus frequencies ratio for the structural damped TLD coupled system

Phase difference:

Recall the phase difference expression (6-74), $\tan(\phi) = 2\xi \frac{\omega_s \bar{\omega}(\bar{\omega}^2 - k_{1n})}{(\bar{\omega}^2 - \omega_1^2)(\bar{\omega}^2 - \omega_2^2)}$. As shown in Figure (6.13), when the excitation frequency approaches the TLD frequency ($\bar{\omega} \to \sqrt{k_{1n}}$), the phase difference approaches zero, indicating that the displacement of the coupled system is in phase with force excitation. Additionally, based on the equation and Figure (6.13), if the excitation frequency approaches zero ($\bar{\omega} \to 0$) or infinity ($\bar{\omega} \to \infty$), the phase difference also approaches zero in both cases. Regarding the smaller natural frequency, if the excitation frequency approaches the smaller frequency ($\bar{\omega} \to \omega_1^-$, $\bar{\omega} \to \omega_1^+$), then the phase difference approaches ($\phi \to -\frac{\pi}{2}$, $\phi \to +\frac{\pi}{2}$). Similarly, if the excitation frequency is close to the higher natural frequency ($\bar{\omega} \to \omega_2^-$, $\bar{\omega} \to \omega_2^+$), then the phase difference approaches ($\phi \to -\frac{\pi}{2}$, $\phi \to +\frac{\pi}{2}$), accordingly. As shown, the phase difference increases with increasing structural damping.

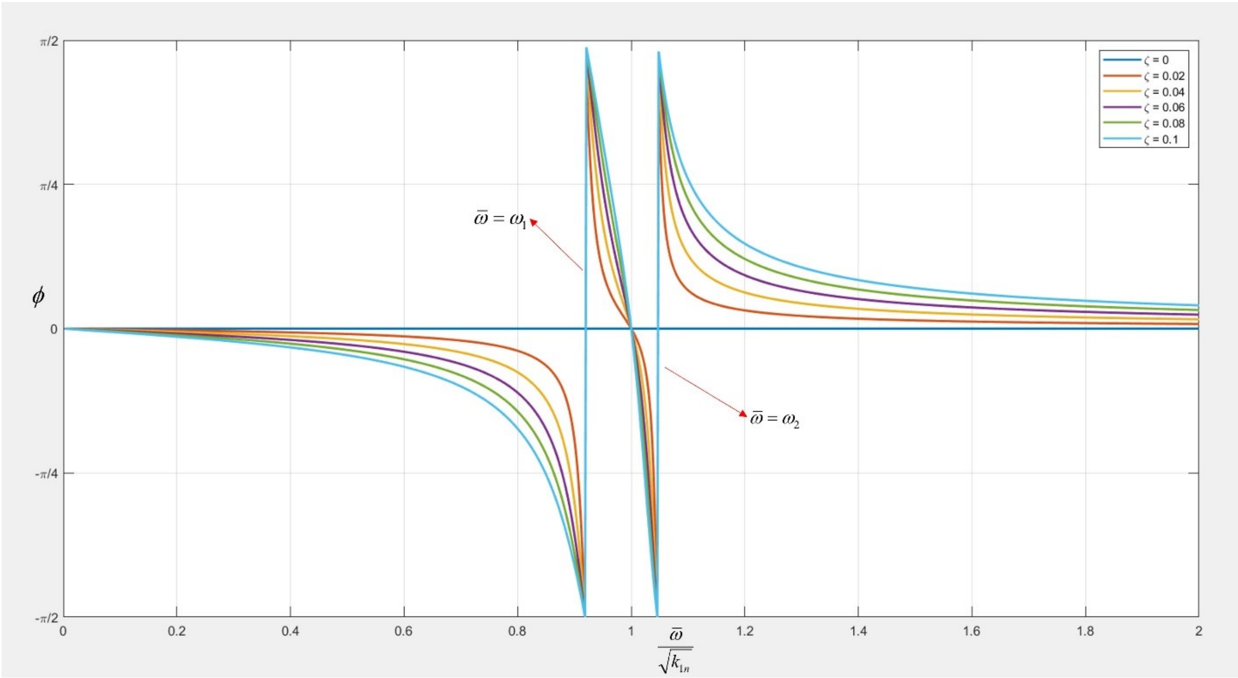

Fig. 6.13. Phase difference versus frequency ratio for the structural damped TLD coupled system

General case:

The TLD coupled system with structural dissipation is subjected to an excitation force where the excitation frequency is 75 percent of the TLD frequency. Similar to the damped case, as presented in Figure (6.14), the numerical response comprises three frequencies: the two natural frequencies of the coupled system and the excitation frequency. Figures (15) illustrates the numerical response along with the analytical solution. The analytical solution for the total response follows equation (6-79). In figure (6.15a) the analytical approach uses Equation (6-80) to derive the response coefficients, incorporating the first power of the dissipation factors coefficients and excluding the second and higher order dissipation factors as coefficients. In contrast, the second analytical approach in the figure (6.15b) ignores both the first and higher order dissipation factors coefficients, using Equation (6-81) to determine the response. Both analytical approaches closely match the numerical results, demonstrating that the assumptions used to derive the simplified equation, Equation (6-81), for calculating the coefficients are valid.

This process is repeated where the excitation frequency approaches half the tank frequency. Figure (6.16) reveals the time history of the TLD coupled system displacements along with the numerical results in this scenario.

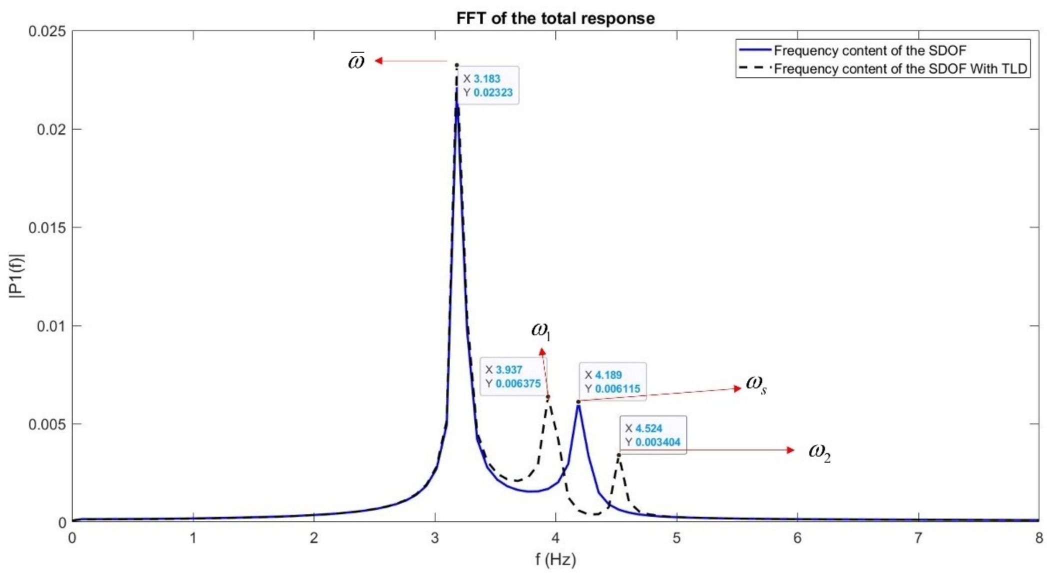

Fig. 6.14. Fundamental frequencies of the structural damped TLD coupled system and individual SDOF where $\bar{\omega} = 0.75\sqrt{k_{1n}}$

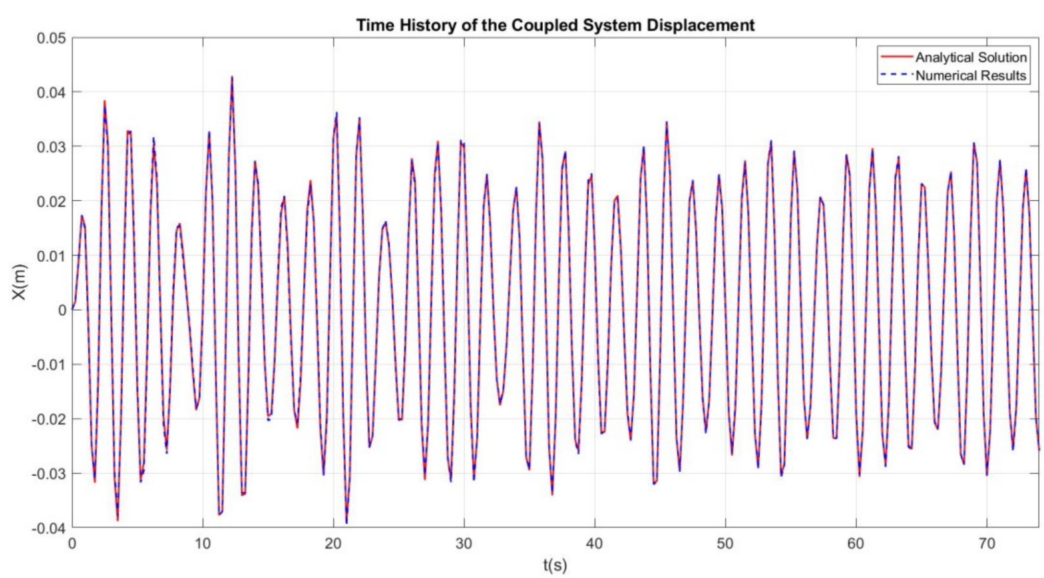

a

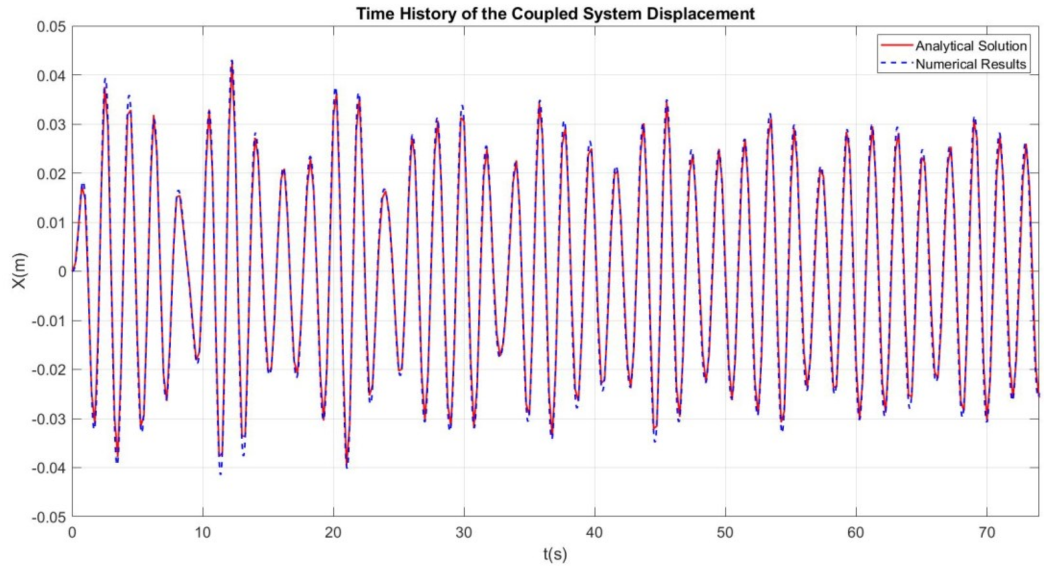

b

Fig. 6.15. Time history displacements of the structural damped TLD coupled system where $\bar{\omega} = 0.75\sqrt{k_{1n}}$

a: considering dissipation factors as coefficient b: disregarding dissipation factors as coefficient

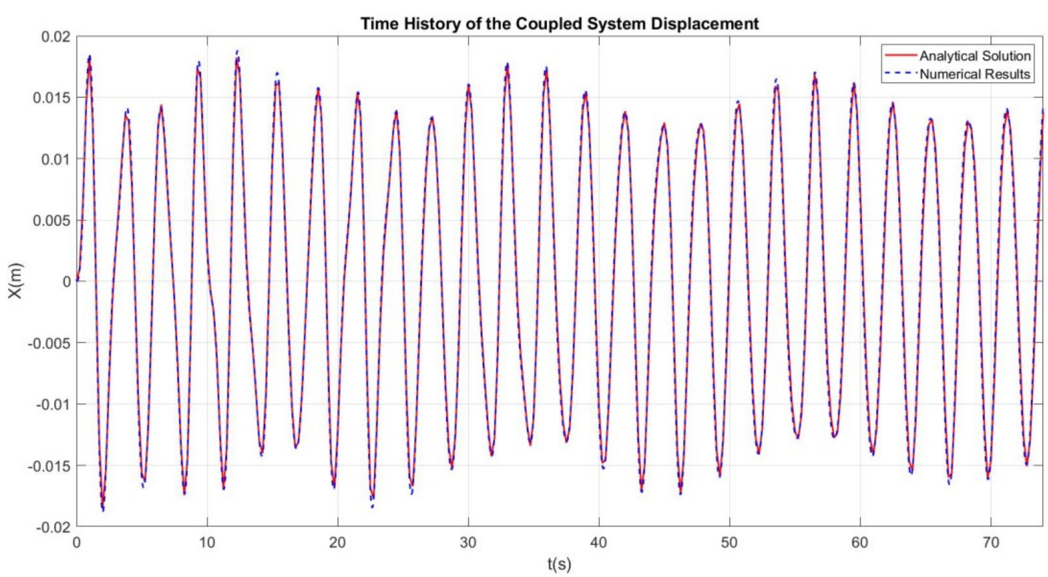

Fig. 6.16. Time history displacements of the structural damped TLD coupled system where $\bar{\omega} = 0.5\sqrt{k_{1n}}$

Particular case

When the excitation frequency approaches the TLD frequency ($\bar{\omega} = \sqrt{k_{1n}}$):

As discussed in the methodology section, similar to the undamped coupled system, the particular response does not contribute, and only the complementary response incorporating natural frequencies is involved (refer to equation 6-82). Correspondingly, as shown in Figure (6.17), the total numerical response includes only the two natural frequencies of the coupled system as fundamental frequencies. The natural frequencies can be determined from Equation (6-17). As presented in the figure, in this scenario, the presence of TLD significantly diminishes the SDOF vibration.

As reflected in Figure (6.18), unlike the undamped case, the presence of structural damping causes the total response to dissipate over time. In this figure, the analytical response is determined from equation (6-82). The excellent alignment between the numerical and analytical results confirms the validity of the current model in this case.

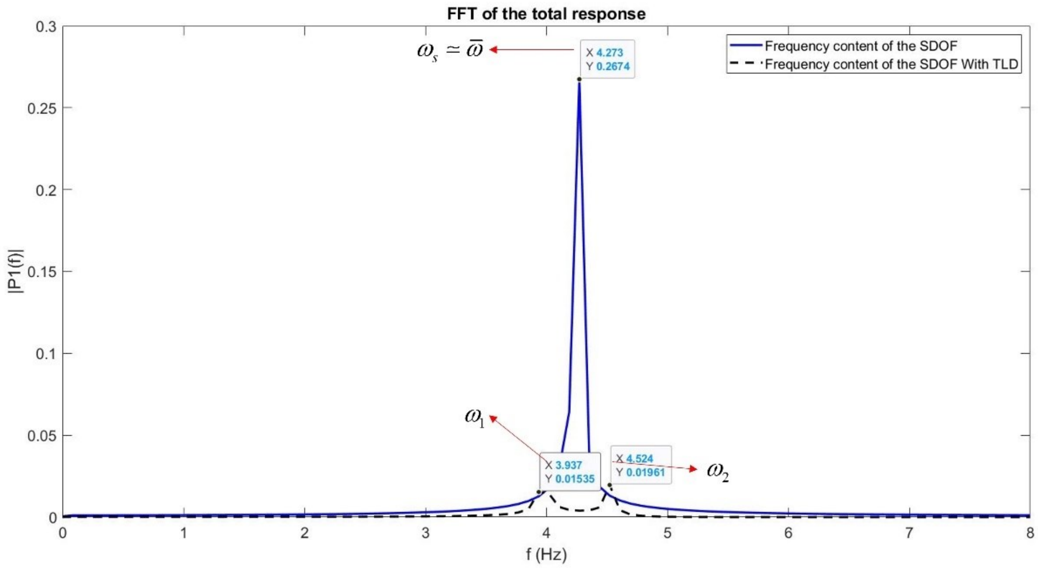

Fig. 6.17. Fundamental frequencies of the structural damped TLD coupled system and individual SDOF where $\bar{\varpi} = \sqrt{k_{1n}}$

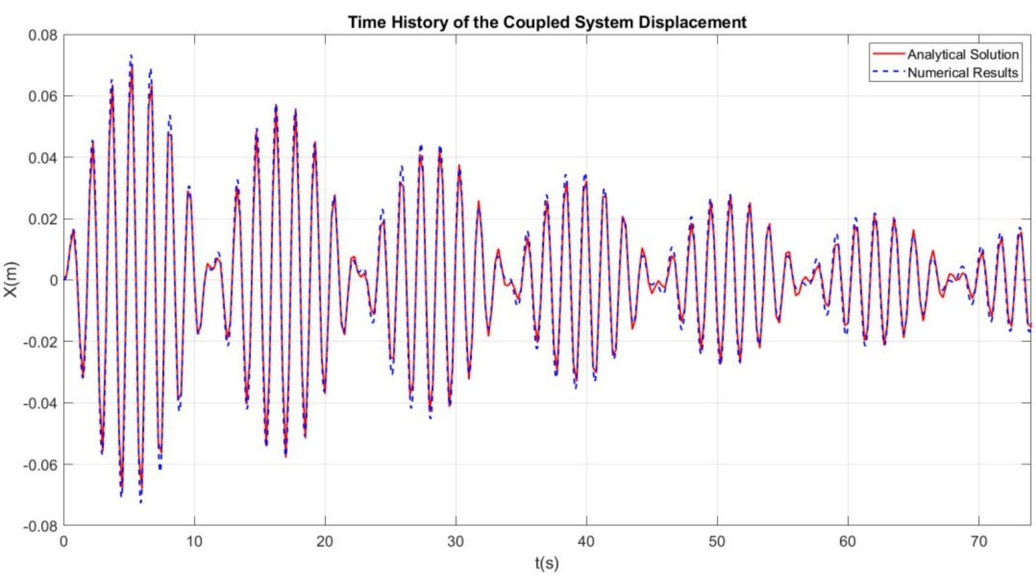

Fig. 6.18. Time history displacements of the structural damped TLD coupled system where $\bar{\varpi} = \sqrt{k_{1n}}$

When the excitation frequency approaches the coupled system natural frequency ($\bar{\varpi} \to \omega_1 \, or \, \bar{\varpi} \to \omega_2$):

Equation (6-83) is used in this section to derive the analytical response when the excitation frequency approaches the smaller frequency ($\bar{\varpi} \rightarrow \omega_1$). As expected from the analytical approach, the numerical response in Figure (6.19) includes two fundamental frequencies, with the smaller frequency having significantly higher participation. This case, associated with the resonance excitation of the coupled system, shows the growth of the vibration over time in Figure (6.20). However, comparing Figures (6.20) and (6.9) reveals that the increase in the vibration of the coupled system is not as high as that in the undamped case. The excellent agreement between the numerical results and current analytical approach is evident in Figure (6.20). A similar process occurs when the excitation frequency is close to the greater natural frequency of the coupled system ($\bar{\varpi} \rightarrow \omega_2$). Figure (6.21) shows the FFT of the numerical response, and Figure (6.22) indicates the displacement of the coupled system obtained from the numerical method and equation (6-84).

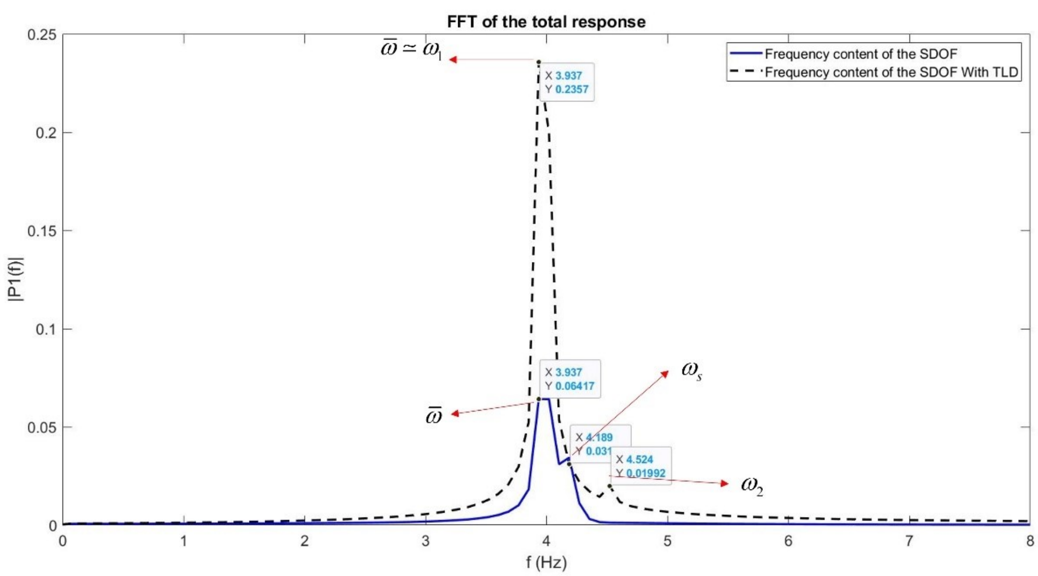

Fig. 6.19. Fundamental frequencies of the structural damped TLD coupled system and individual SDOF where $\bar{\varpi} = \omega_1$

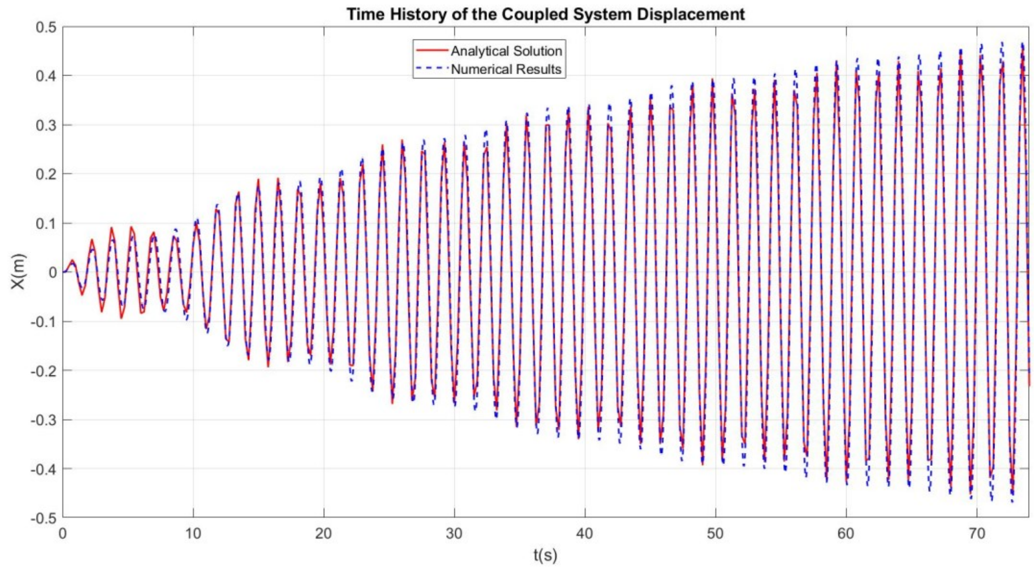

Fig. 6.20. Time history displacements of the structural damped TLD coupled system where $\bar{\varpi} = \omega_1$

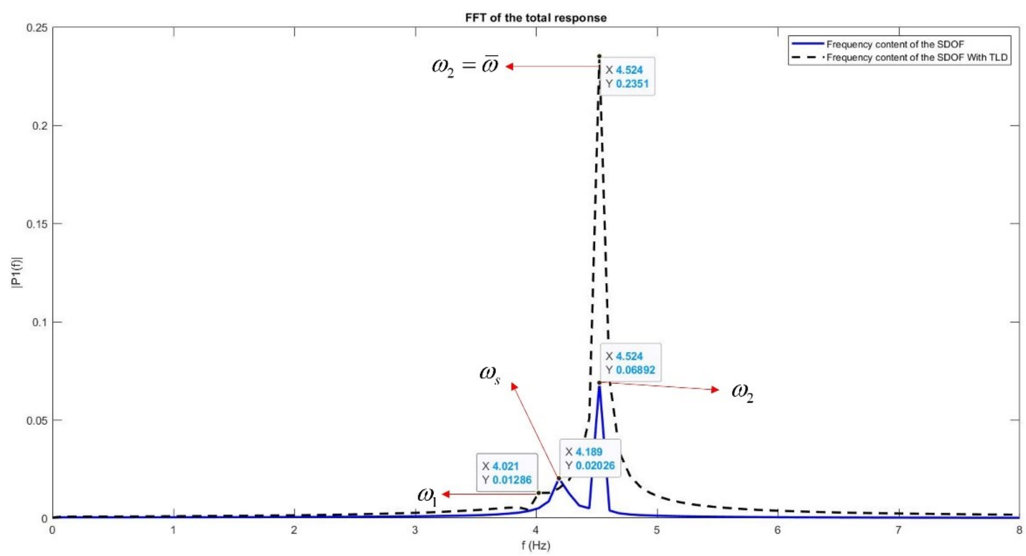

Fig. 6.21. Fundamental frequencies of the structural damped TLD coupled system and individual SDOF where $\bar{\varpi} = \omega_2$

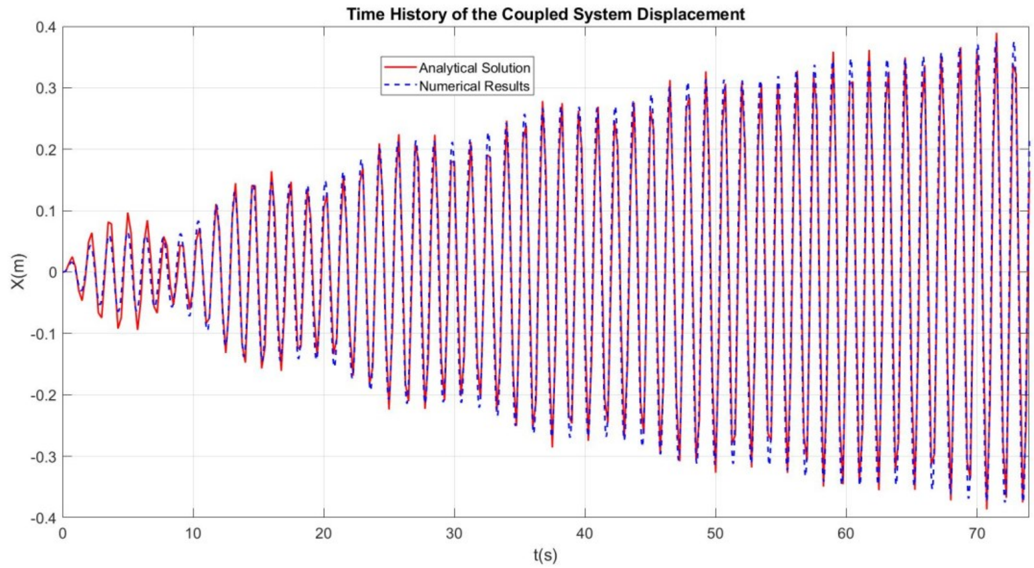

Fig. 6.22. Time history displacements of the structural damped TLD coupled system where $\bar{\omega} = \omega_2$

6.4.3. Structural and fluid damped TLD coupled system

The last part of the discussion revolves around the scenario where both structural and fluid dissipations are considered ($c \neq 0, C_f \neq 0$). As in the preceding cases, we first consider the particular response. Let us recall the dynamic amplification factor in this scenario represented by Equation (6-91), $\delta_d = \dfrac{\omega_s^2[(k_{1n} - \bar{\omega}^2) + C_f \bar{\omega}]}{\sqrt{[(\bar{\omega}^2 - \omega_1{}^2)(\bar{\omega}^2 - \omega_2{}^2)]^2 + \bar{\omega}^2[2\xi\omega_s(k_{1n} - \bar{\omega}^2) + C_f(\omega_s^2 - \bar{\omega}^2)]^2}}$. This parameter versus the frequency ratio is presented for two different fluid damping coefficients, $C_f = 0.05$ and $C_f = 0.25$, as shown in Figures (6.23a) and (6.23b), respectively. The dynamic amplifications for special cases are discussed using Equations (6-93), (6-94), and (6-95).

In the analysis for each fluid damping, various structural damping ratios are incorporated. The response pattern in this scenario is similar to that in the previous case; however, this case dissipates the response more considerably. The higher the fluid dissipation, the greater is the reduction in the total response. Unlike the previous cases, when the excitation frequency matches the TLD frequency, the total response is nonzero. The particular response becomes zero for an excitation frequency between the TLD natural frequency and the greater natural frequency of the coupled system (Figure 6.23b). Notably, the presence of fluid dissipation has a more pronounced impact on the greater natural frequency, leading to a greater reduction in the resonance excitation of the coupled system.

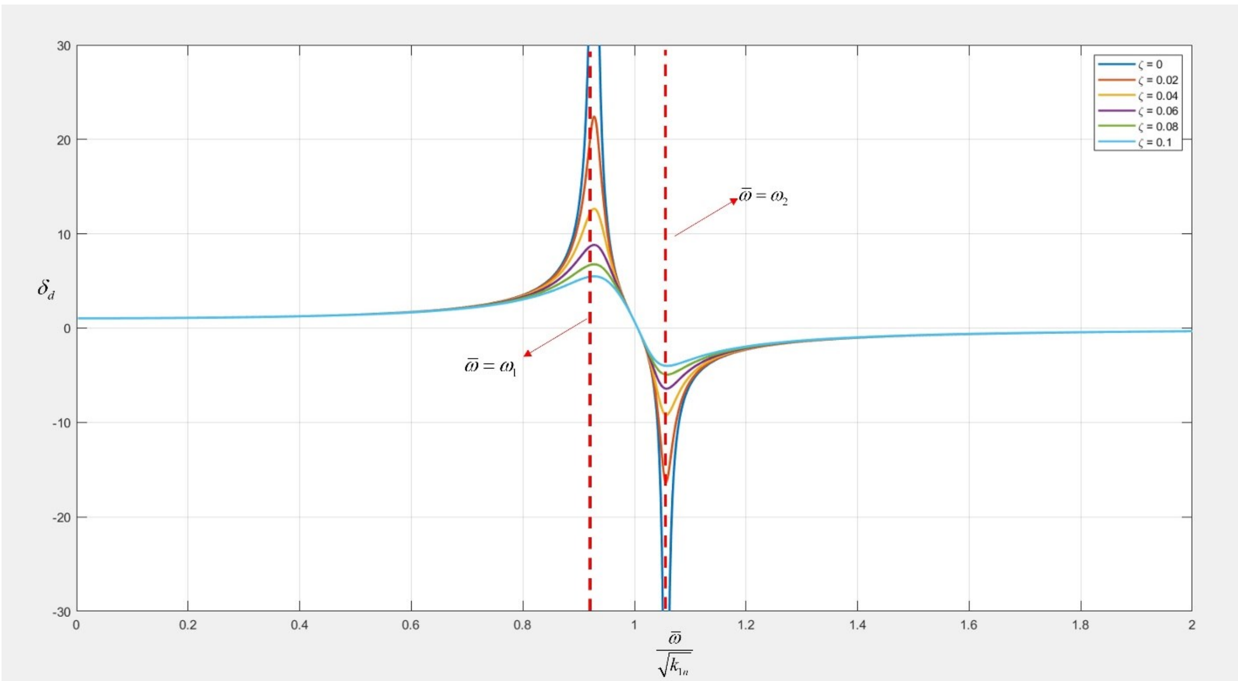

a

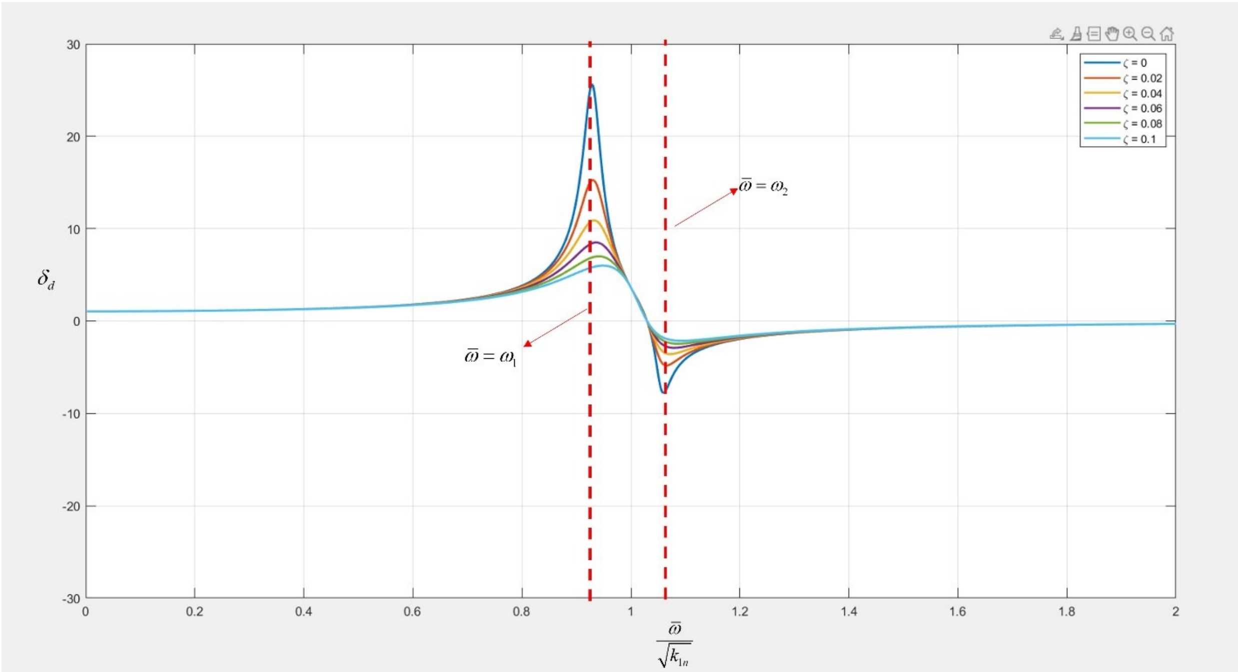

b

Fig. 6.23. Dynamic amplification factor versus frequencies ratio for the fluid and structural damped TLD coupled system. a) $C_f = 0.05$, b) $C_f = 0.25$

Phase difference:

Lets recall the phase difference equation in this scenario, equation (6-92)

$$\tan(\phi) = \frac{[-(2\xi\omega_s\bar{\omega}(k_{1n}-\bar{\omega}^2)+C_f\bar{\omega}(\omega_s^2-\bar{\omega}^2))(k_{1n}-\bar{\omega}^2)+C_f\bar{\omega}(\bar{\omega}^2-\omega_1^{\,2})(\bar{\omega}^2-\omega_2^{\,2})]}{[\underbrace{(\bar{\omega}^2-\omega_1^{\,2})(\bar{\omega}^2-\omega_2^{\,2})(k_{1n}-\bar{\omega}^2)}_{first\,term}+\underbrace{C_f\bar{\omega}^2(2\xi\omega_s(k_{1n}-\bar{\omega}^2)+C_f(\omega_s^2-\bar{\omega}^2))}_{second\,term}]}$$

The second term in the denominator includes high-order small coefficients $2C_f\xi$, $C_f^{\,2}$. Therefore, it can be neglected compared to the first term. Next, the expression can be transformed into two ratios as follows: The first ratio denominator includes $(\bar{\omega}^2-\omega_1^{\,2})(\bar{\omega}^2-\omega_2^{\,2})$. The second ratio incorporates $(k_{1n}-\bar{\omega}^2)$ into the denominator. Therefore, when the excitation frequency approaches (ω_1 or ω_2 or $\sqrt{k_{1n}}$), the value of $\tan(\phi)$ increases substantially, so the phase difference approaches (

$\phi \to \frac{\pi}{2}$ *or* $\phi \to -\frac{\pi}{2}$). Hence, in addition to the two preceding vertical asymptotes ($\bar{\omega} = \omega_1$, $\bar{\omega} = \omega_2$), $\bar{\omega} = \sqrt{k_{1n}}$ acts as another asymptote (see Figure 6.24). Furthermore, in both cases, where $\bar{\omega} \to 0$ or $\bar{\omega} \to \infty$, the phase difference approaches zero. Regarding the vertical asymptote lines, when the excitation frequency tends to smaller or greater natural frequencies ($\begin{Bmatrix} \omega = \omega_1^- \\ \omega = \omega_1^+ \end{Bmatrix}, \begin{Bmatrix} \omega = \omega_2^- \\ \omega = \omega_2^+ \end{Bmatrix}$), the phase difference approaches $\begin{Bmatrix} \phi = -\frac{\pi}{2} \\ \phi = +\frac{\pi}{2} \end{Bmatrix}$, and when the excitation frequency is close to the water tank frequency ($\begin{Bmatrix} \bar{\omega} \to \sqrt{k_{1n}}^- \\ \bar{\omega} \to \sqrt{k_{1n}}^+ \end{Bmatrix}$), the phase differences tends to $\begin{Bmatrix} \phi = +\frac{\pi}{2} \\ \phi = -\frac{\pi}{2} \end{Bmatrix}$.

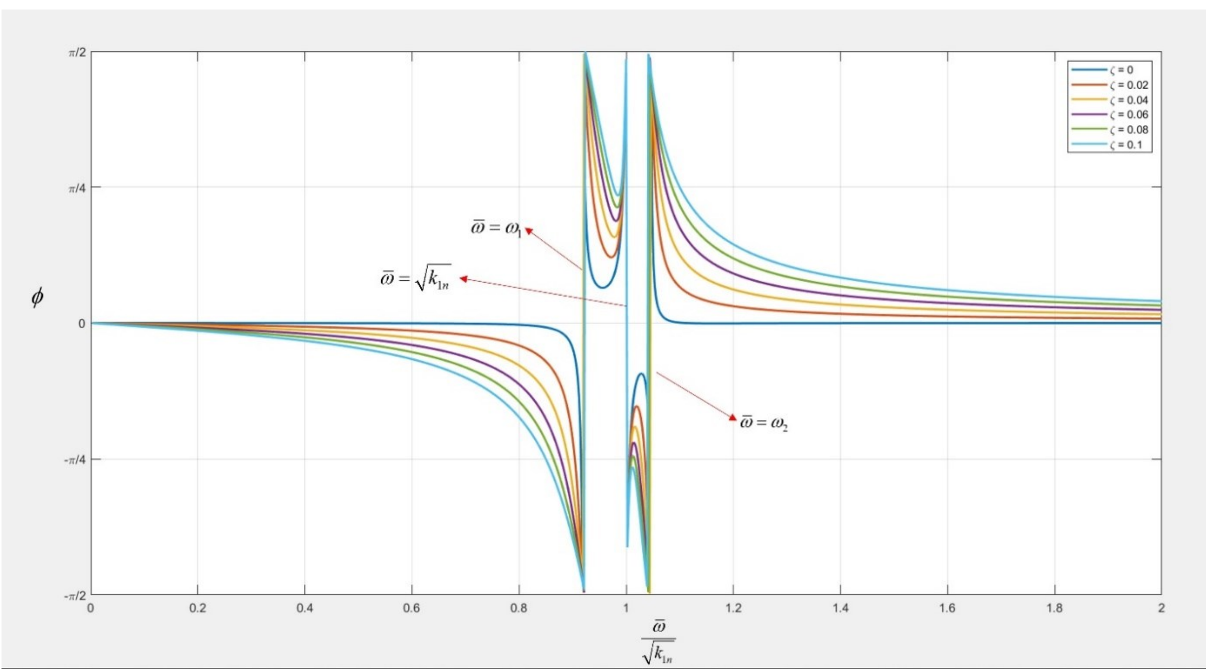

Fig. 6.24. Phase difference versus frequency ratio for the fluid and structural damped TLD coupled system

General case:

In this step, the TLD coupled system incorporating both fluid and structural damping is modeled when the excitation force is equal to 75 percent of the SDOF frequency. Since fluid dissipation is also considered at this stage, as demonstrated in equation (6-85), the dissipation factors (α_1, α_2) are modified. They intensify and include new terms to integrate the fluid dissipation. According to equation (6-96), the complementary response, which includes the natural frequencies of the coupled system, is damped with modified dissipation factors. Unlike the complementary response, the particular response, which includes both sine and cosine functions with the excitation frequency, is not affected by dissipation (refer to equation 6-96). As a result, the particular response, which includes the excitation frequency, contributes more than the complementary response, which integrates the natural frequencies. As predicted by the analytical approach, the FFT of the numerical response indicates the contribution of the three fundamental frequencies in Figures (6.25): the natural frequencies of the coupled system and excitation frequency. In addition, the excitation frequency contributes more significantly than the natural frequencies.

As explained earlier, the total response is the sum of the particular and complementary responses. In this case, the total response is derived from expressions (6-96), and the coefficient of the total response is derived using equation (6-81) with corresponding *a, b*. Notably, terms including the first- and higher-order dissipation factors as coefficients are neglected to reach a simplified equation presented as expression (6-81). The total response is compared with the numerical response for this scenario, as shown in Figure (6.26), reflecting excellent agreement. The same procedure is employed for the case when the excitation frequency is half the TLD frequency. Similarly, as indicated in Figure (6.27), this case study also demonstrates a high level of agreement with the numerical results.

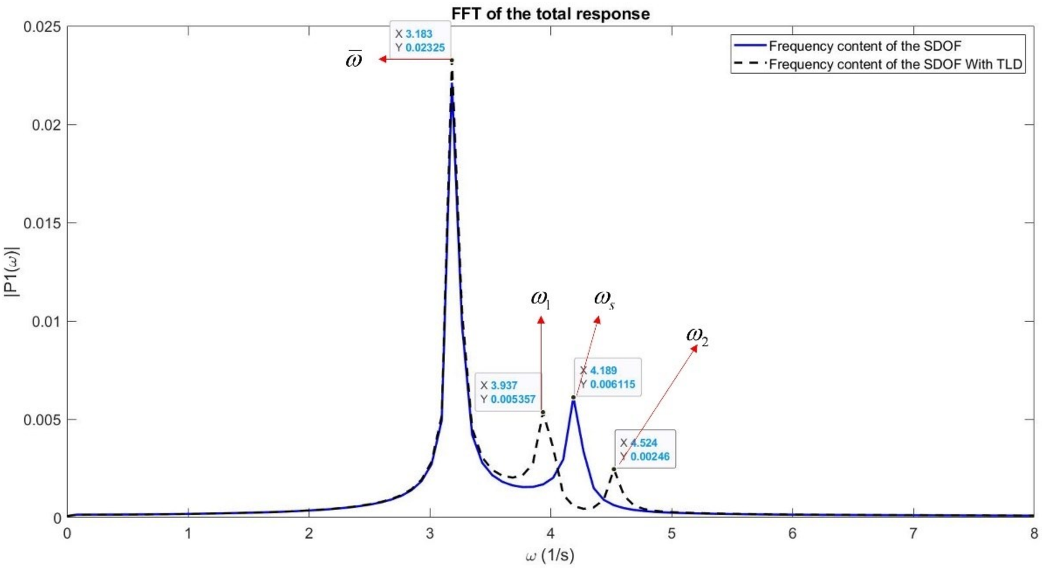

Fig. 6.25. The fundamental frequencies of the fluid and structural damped TLD coupled system and individual SDOF where $\bar{\omega} = 0.75\sqrt{k_{1n}}$

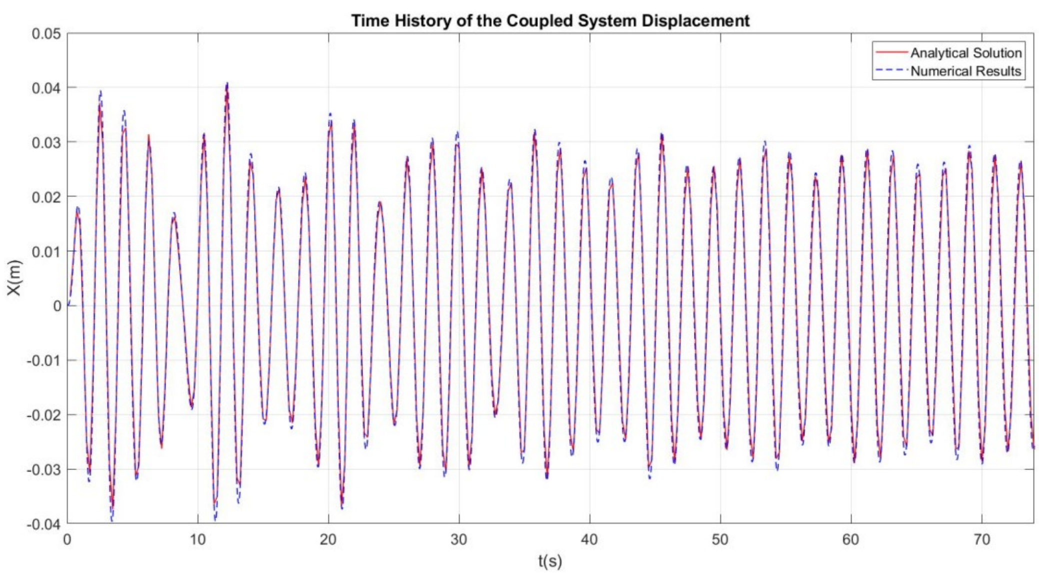

Fig. 6.26. Time history displacements of the fluid and structural damped TLD coupled system where $\bar{\omega} = 0.75\sqrt{k_{1n}}$

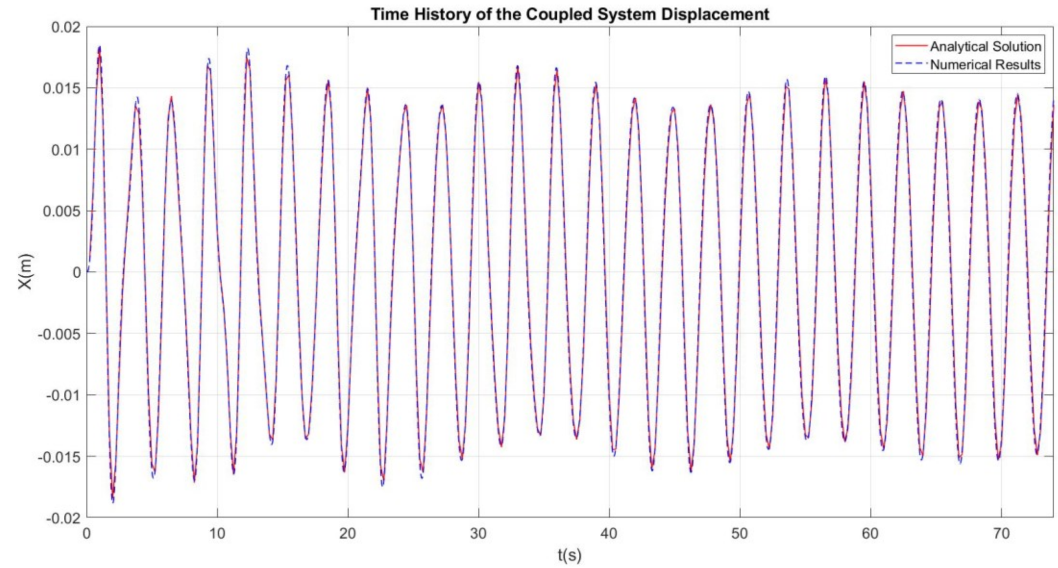

Fig. 6.27. Time history displacements of the fluid and structural damped TLD coupled system where $\bar{\omega} = 0.5\sqrt{k_{1n}}$

When the excitation frequency approaches the TLD frequency ($\bar{\omega} = \sqrt{k_{1n}}$):

Recall the dynamic amplification associated with this scenario, equation (6-93)

$$R = \frac{F}{K} \frac{C_f \sqrt{k_{1n}} \omega_s^2}{\sqrt{[(k_{1n} - \omega_1{}^2)(k_{1n} - \omega_2{}^2)]^2 + [C_f k_{1n} (\omega_s^2 - k_{1n})]^2}}$$

Due to the term $C_f \bar{\omega}$ in the numerator of the ratio, the particular response, unlike in other scenarios, does not disappear entirely (refer to equation 6-93). To verify this point numerically, the response of the coupled system is transformed into the frequency domain using the FFT. As shown in Figure (6.28), apart from the natural frequencies of the coupled system, the excitation frequency has a small contribution. As demonstrated in Figure (6.28), the application of TLD significantly mitigates the response of the coupled system, resulting in a substantially reduced contribution of the fundamental frequencies.

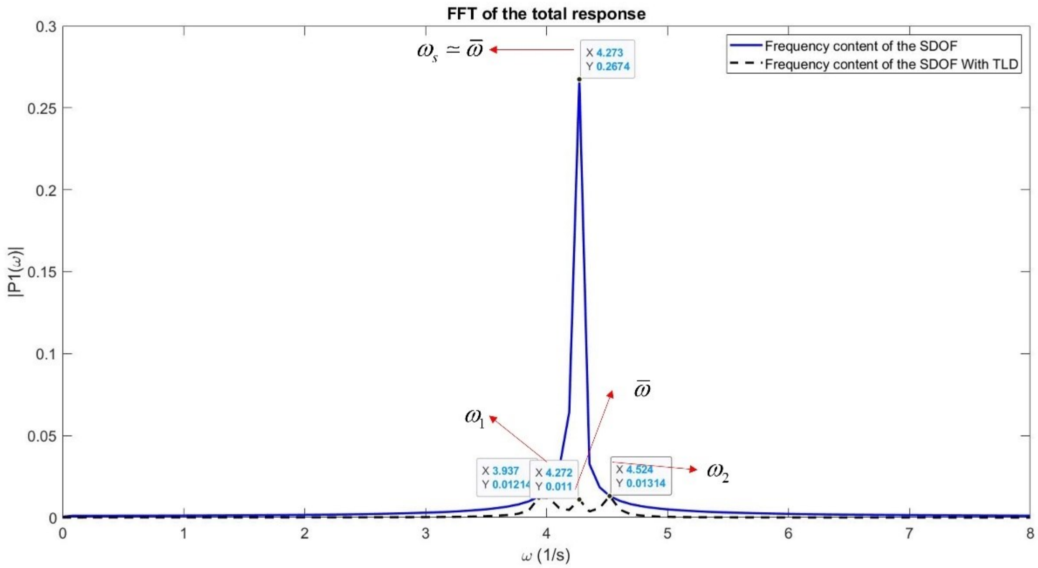

Fig. 6.28. The fundamental frequencies of the fluid and structural damped TLD coupled system and individual SDOF where $\bar{\omega} = \sqrt{k_{1n}}$

The total response in this scenario, resulting from a slight contribution from the particular response and a high contribution from the complementary response, is described in Section (6.2.2.3). The total analytical response in this case study, referred to as the most efficient use of TLD, is depicted in Figure (6.29). Additionally,, the figure integrates the numerical results associated with this case. The comparison demonstrates that the analytical approach maintains high accuracy even when both fluid and structural damping are incorporated.

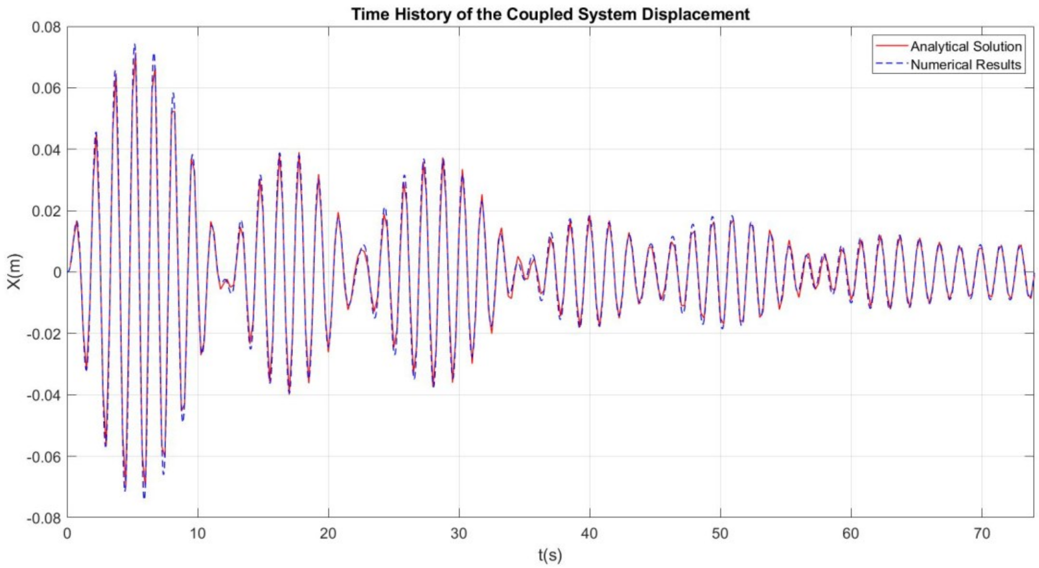

Fig. 6.29. Time history displacements of the fluid and structural damped TLD coupled system where $\bar{\omega} = \sqrt{k_{1n}}$

When the excitation frequency approaches the natural frequencies of the coupled system ($\bar{\omega} \to \omega_1 \; or \; \bar{\omega} \to \omega_2$):

The FFT of the numerical response when the excitation approaches the smaller natural frequency of the coupled system is presented in Figure (6.30). The results reflect the contribution of the two natural frequencies, with a substantially higher participation of the smaller frequency. Meanwhile, the individual SDOF encompasses the excitation frequency (the smaller natural frequency of the coupled system in this case) and the natural frequency of the SDOF. The analytical response described in section (6.2.2.3) is shown in Figure (6.31). As depicted in the Figure, in this resonance excitation scenario for the smaller natural frequency, the vibration of the coupled system grows over time, but this growth is smaller compared to the previous scenarios, undamped case and structural damped case. Similarly, the fundamental frequencies of the particular response when the excitation frequency approaches the greater natural frequency are derived and presented in Figure (6.32). Similar to the previous case (resonance for smaller frequency), it shows that the coupled system includes two natural frequencies as fundamental frequencies; however, in contrast to the previous case, there is a higher contribution from the higher frequency.

The comparison between the numerical and analytical responses in Figure (6.33) reflects a high level of accuracy and validity of the current analytical approach during resonance excitation, where the excitation frequency approaches the greater natural frequency. Notably, when resonance excitation occurs at the greater natural frequency, the coupled system undergoes slightly smaller vibrations compared with resonance excitation at the smaller natural frequency.

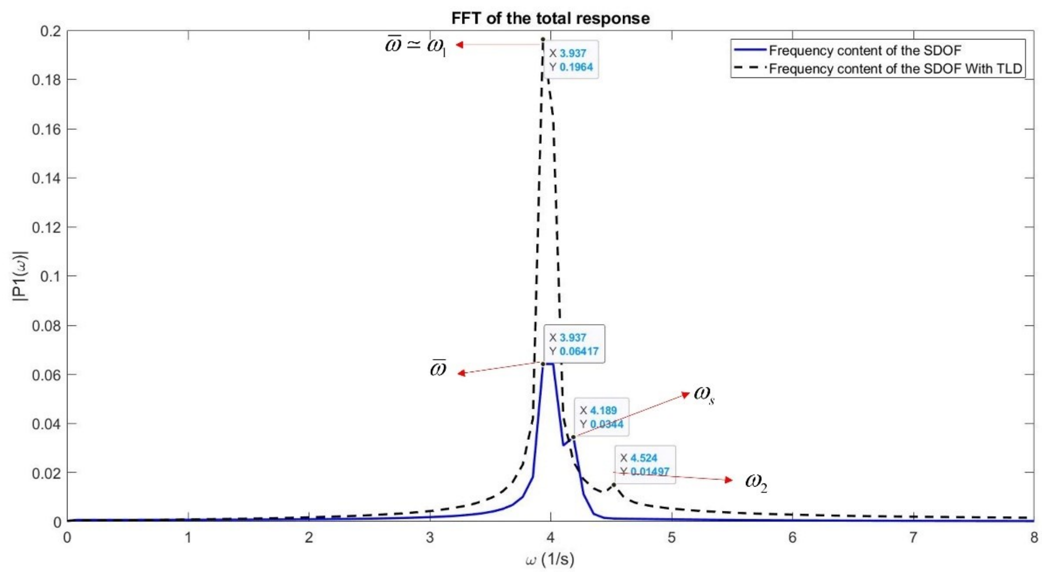

Fig. 6.30. Fundamental frequencies of the fluid and structural damped TLD coupled system and individual SDOF where $\bar{\omega} = \omega_1$

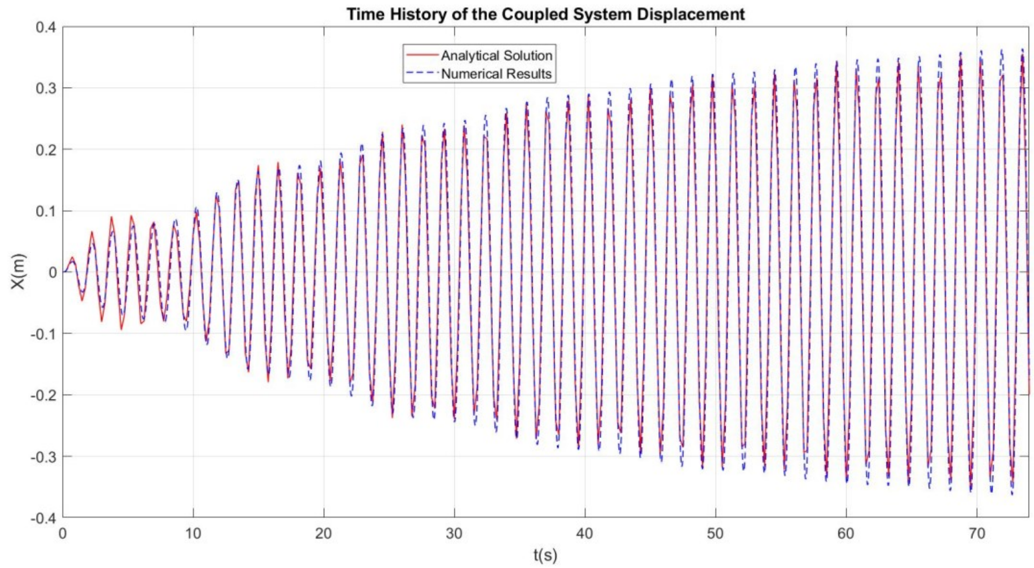

Fig. 6.31. Time history displacements of the fluid and structural damped TLD coupled system where $\bar{\varpi} = \omega_1$

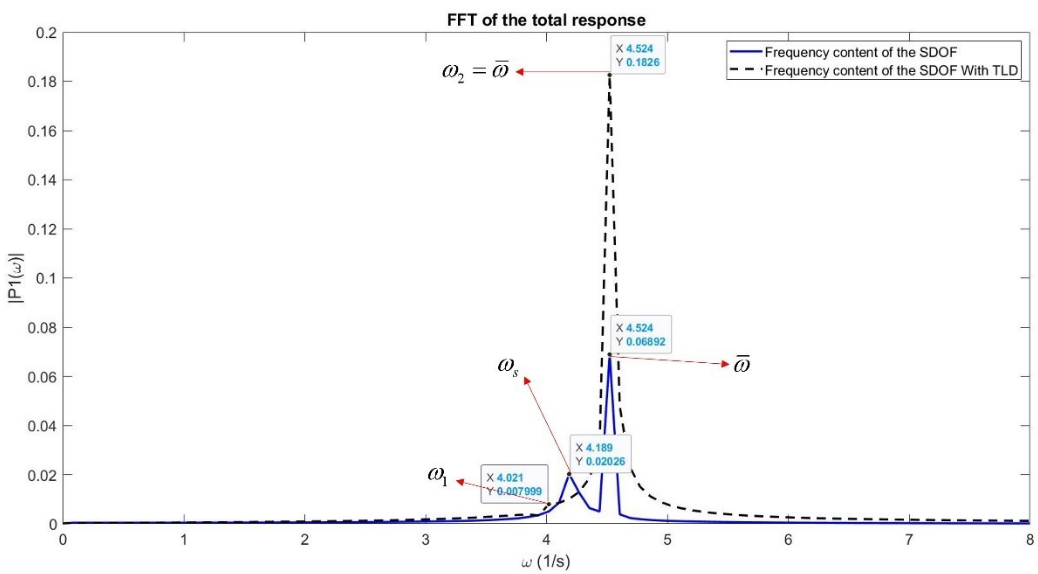

Fig. 6.32. Fundamental frequencies of the fluid and structural damped TLD coupled system and individual SDOF where $\bar{\varpi} = \omega_2$

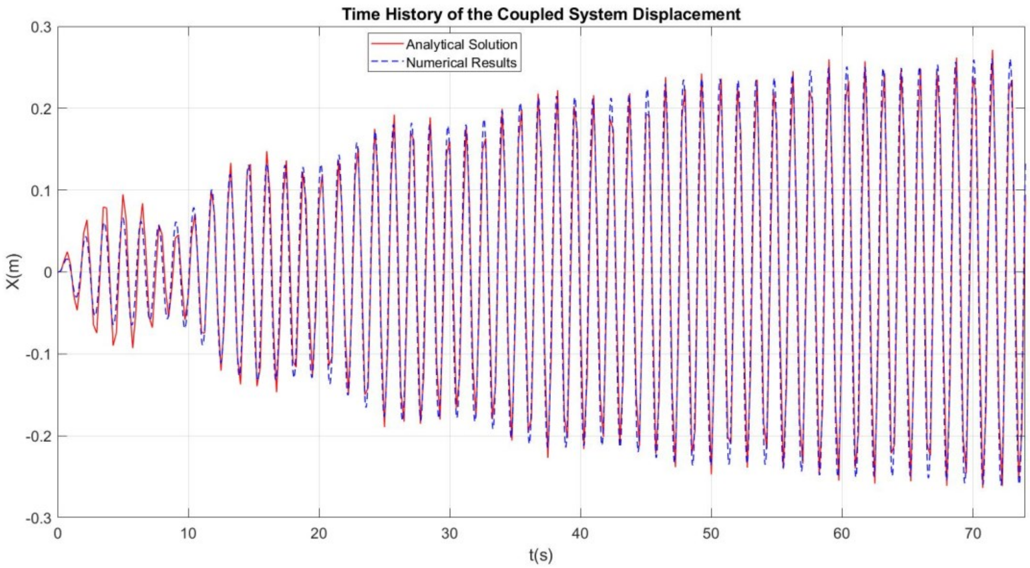

Fig. 6.33. Time history displacements of the fluid and structural damped TLD coupled system where $\bar{\varpi} = \omega_2$

6.5. Conclusion

The separation of variables technique is employed to transform the linear wave theory into modal coordinate system equations. Next, they are coupled with the dynamic equation of a single degree of freedom strongly. This approach leads to a fourth-order ordinary differential equation that integrates the continuity and momentum equations from the fluid with the dynamic equation from the SDOF, thereby representing a coupled system of TLD and SDOF under an excitation force. The solutions to this equation are examined under three scenarios: undamped, structurally damped, and fluid-structural damped systems. In addition, a numerical model is developed to verify the accuracy and validity of the analytical model.

This study introduces a particular solution for the undamped case and proposes the concept of a dynamic amplification factor. It finds that when the excitation frequency approaches the water tank frequency, the dynamic amplification vanishes; therefore, the particular response does not contribute to the total response. Conversely, when the excitation frequency approaches the natural frequencies of the coupled system, the dynamic amplification tends to infinity. By introducing both particular and complementary solutions along with innovative initial boundary conditions, this paper presents a closed-form analytical solution for the response of the coupled system. This response incorporates three frequencies: the excitation frequency and natural frequencies of the coupled system. The total response is then adjusted to address ambiguities using L'Hôpital's rule, particularly when the excitation frequency approaches the natural frequencies. In resonance excitation scenarios, the total response, which grows over time, includes two natural frequencies as fundamental frequencies with a higher contribution from the excitation frequency. When the excitation frequency matches the water tank frequency, the particular response is absent, leaving only the natural frequencies in the response. The accuracy and validity of these innovative findings are confirmed using a numerical model.

A similar approach is used for the structural damping scenario. Here, the particular response involves both sine and cosine functions. As the excitation frequency approaches the natural frequencies, the dynamic amplification increases to a finite value, unlike in the previous case. Additionally, the particular response disappears as the excitation frequency nears the water tank frequency. Unlike the previous case, the displacement is not in phase with the excitation force. The phase difference between them is determined, reaching 90 °as the excitation frequency approaches the natural frequency of the coupled system. In contrast to the previous case, the complementary response, which includes the natural frequencies, is exponentially attenuated by the dissipation factors, leading to a reduced impact of these natural frequencies on the total response. Upon implementing the initial conditions and neglecting the terms involving the dissipation factors as coefficients, simplified equations for determining the total response coefficients are derived. The total response in this scenario is computed for the general case and adjusted for the two additional special cases. The pattern of the total response and its fundamental frequencies are verified against the numerical results for all the cases.

Along with structural dissipation, fluid dissipation is incorporated into the current analytical model. Subsequently, the dynamic amplification and phase difference are derived for this scenario. In this case, the particular response does not completely vanish and retains a small contribution as the excitation frequency approaches the water tank frequency. Additionally, the phase difference function shows a 90-degree shift when the excitation frequency approaches the water tank frequency, along with the natural frequencies. In this case, the complementary response is dissipated using a modified dissipation factor. The total response, including its fundamental frequencies, is analyzed for both the general case and specifically when the excitation frequency approaches the natural frequencies and water tank frequency

References

1. Sun, L. M., Fujino, Y., Pacheco, B. M., & Chaiseri, P. 1992. Modelling of tuned liquid damper (TLD). Journal of Wind Engineering and Industrial Aerodynamics, 43(1-3), 1883-1894.
2. Fujino, Y., Sun, L., Pacheco, B. M., & Chaiseri, P. 1992. Tuned liquid damper (TLD) for suppressing horizontal motion of structures. Journal of Engineering Mechanics, 118(10), 2017-2030.
3. Tait, M., El Damatty, A., Isyumov, N., & Siddique, R. 2005. Numerical flow models to simulate tuned liquid dampers (TLD) with slat screens. Journal of Fluids and Structures, 20, 1007-1023.
4. Khanpour, M., Mohammadian, A., Shirkhani, H., & Kianoush, R. (2024). Simulation of Sloped-Bed Tuned Liquid Dampers Using a Nonlinear Shallow Water Model. *Water*, *16*(10), 1394.
5. Khanpour, M., Mohammadian, A., Shirkhani, H., & Kianoush, R. (2024). Analytical solution to a coupled system including tuned liquid damper and single degree of freedom under free vibration with modal decomposition method. *Physics of Fluids*, *36*(5).
6. Pandit, A. R., & Biswal, K. C. 2020. Seismic control of multi degree of freedom structure outfitted with sloped bottom tuned liquid damper. *Structures*, 25. 229-240.
7. Zhang, Z. (2020). Numerical and experimental investigations of the sloshing modal properties of sloped-bottom tuned liquid dampers for structural vibration control. *Engineering Structures*, *204*, 110042.
8. Su, Y. (2021). Numerical model of energy dissipation and shallow-water sloshing motions in tank under different coupled excitations. *Journal of Marine Science and Technology*, *26*(4), 1038-1050.
9. Marivani, M., & Hamed, M. S. (2009). Numerical simulation of structure response outfitted with a tuned liquid damper. *Computers & structures*, *87*(17-18), 1154-1165.
10. Marivani, M., & Hamed, M. S. 2017. Evaluate pressure drop of slat screen in an oscillating fluid in a tuned liquid damper. Computers & Fluids, 156, 384-401.
11. Khanpour, M., Zarrati, A. R., Kolahdoozan, M., Shakibaeinia, A., & Amirshahi, S. M. (2016b). Mesh-free SPH modeling of sediment scouring and flushing. *Computers & Fluids*, *129*, 67-78.
12. Khanpour, M., Zarrati, A. R., Kolahdoozan, M., Shakibaeinia, A., & Jafarinik, S. (2016b). Numerical modeling of free surface flow in hydraulic structures using Smoothed Particle Hydrodynamics. *Applied Mathematical Modelling*, *40*(23-24), 9821-9834.
13. McNamara, K. P., Love, J. S., & Tait, M. J. (2022a). Numerical investigation of the response of structures equipped with a limited freeboard tuned liquid damper. *Journal of Fluids and Structures*, *108*, 103426.

14. McNamara, K. P., & Tait, M. J. (2022b). Modeling the Response of Structure–Tuned Liquid Damper Systems Under Large Amplitude Excitation Using Smoothed Particle Hydrodynamics. *Journal of Vibration and Acoustics*, *144*(1), 011008.
15. Housner, G. W. (1963). The dynamic behavior of water tanks. *Bulletin of the seismological society of America*, *53*(2), 381-387.
16. Abd-Elhamed, A., & Tolan, M. (2022). Tuned liquid damper for vibration mitigation of seismic-excited structures on soft soil. *Alexandria Engineering Journal*, *61*(12), 9583-9599.
17. Konar, T., & Ghosh, A. D. (2021). Flow damping devices in tuned liquid damper for structural vibration control: a review. *Archives of Computational Methods in Engineering*, *28*, 2195-2207.
18. Bhattacharjee, E., Halder, L., & Sharma, R. P. (2013). An experimental study on tuned liquid damper for mitigation of structural response. *International Journal of Advanced Structural Engineering*, *5*, 1-8.
19. Ashasi-Sorkhabi, A., Malekghasemi, H., Ghaemmaghami, A., & Mercan, O. (2017). Experimental investigations of tuned liquid damper-structure interactions in resonance considering multiple parameters. *Journal of Sound and Vibration*, *388*, 141-153.
20. Banerji, P., Murudi, M., Shah, A. H., & Popplewell, N. (2000). Tuned liquid dampers for controlling earthquake response of structures. *Earthquake engineering & structural dynamics*, *29*(5), 587-602.
21. Murudi, M., & Banerji, P. (2012). Effective control of earthquake response using tuned liquid dampers. *J. Earthq. Technol*, *49*(3-4), 53-71.
22. Chang, Yongjian, Ali Noormohamed, and Oya Mercan. "Analytical and experimental investigations of modified tuned liquid dampers (MTLDs)." *Journal of Sound and Vibration* 428 (2018): 179-194.
23. Zhao, Z., Zhang, R., Jiang, Y., & Pan, C. 2019. A tuned liquid inerter system for vibration control. International Journal of Mechanical Sciences, 164, 105171.
24. Sun, H. D., He, H. X., Cheng, Y., & Gao, X. J. (2024). Theoretical and experimental study on vibration control of a tuned liquid inerter damper with additional damping net and sloped-bottom. *Mechanical Systems and Signal Processing*, *213*, 111356.
25. Domizio, M., Ambrosini, D., & Campi, A. (2024). A novel tuned liquid damper for vibration control in high-frequency structures. *Engineering Structures*, *301*, 117350.
26. Pandey, D. K., Sharma, M. K., & Mishra, S. K. (2019). A compliant tuned liquid damper for controlling seismic vibration of short period structures. *Mechanical Systems and Signal Processing*, *132*, 405-428.
27. Sardar, R., & Chakraborty, S. (2022). Wave vibration control of jacket platform by tuned liquid dampers. *Ocean Engineering*, *247*, 110721.
28. Saghi, H., Ma, C., & Zi, G. (2024). Bidirectional tuned liquid dampers for stabilizing floating offshore wind turbine substructures. *Ocean Engineering*, *309*, 118553.
29. Pabarja, A., Vafaei, M., Alih, S. C., Yatim, M. Y. M., & Osman, S. A. (2019). Experimental study on the efficiency of tuned liquid dampers for vibration mitigation of a vertically irregular structure. *Mechanical Systems and Signal Processing*, *114*, 84-105.
30. Toro, E. F. (2001). *Shock-capturing methods for free-surface shallow flows* (pp. 1-309). Wiley and Sons Ltd.
31. Humar, J. (2012). *Dynamics of structures*. CRC press.

List of Symbols

H	Mean water level
η	Wave height
U	Depth- average velocity
C_f	Fluid damping coefficient
ω_f	Natural frequency of water tank
ϖ	Force excitation frequency
m	Mass of SDOF
k	Stiffness of SDOF
c	Damping coefficient of SDOF
X	Displacement of SDOF
$\dot{X}$	Velocity of SDOF
$\ddot{X}$	Acceleration of SDOF
F	Excitation force on SDOF
F_{slo}	Sloshing Force on SDOF
X_n	Displacement of SDOF form the contribution of mode *n*
$\dot{X}_n$	Velocity of SDOF form the contribution of mode *n*
$\ddot{X}_n$	Acceleration of SDOF form the contribution of mode *n*
F_n	Excitation force on SDOF form the contribution of mode *n*
$(F_{slo})_n$	Sloshing Force on SDOF form the contribution of mode *n*

L	Length of the water tank
b	Width of the water tank
ρ	Water density
g	Gravity acceleration
ω_s	Natural frequency of SDOF
ξ	Damping ratio
c_{cr}	Critical damping
ω_1	Smaller natural frequency of the coupled system
ω_2	Greater natural frequency of the coupled system
a_1	Dissipation factor associated to greater natural frequency
a_2	Dissipation factor associated to greater natural frequency
X_p	Particular response
X_c	Complementary response
X_t	Total response
δ_d	Dynamic amplification factor
ϕ	phase difference between the excitation force and the response
$X(0)$	Initial displacement of the coupled system
$\dot{X}(0)$	Initial velocity of the coupled system
A_0	Initial wave height perturbation
B_0	Initial wave velocity perturbation
$\omega_{1,n}$	Smaller natural frequency of the coupled system of the mode n

$\omega_{2,n}$ greater natural frequency of the coupled system of the mode n

$X_{0,n}$ Initial displacement of the coupled system of the mode n

W_L TLD's weight

7. Summary, Concluding Remarks, and Recommendations

7.1. Summary and Concluding Remarks

This thesis is structured into two main parts to explore the behavior of a tuned liquid damper. The first part, comprising Chapters 2 and 3, is dedicated to developing an accurate, reliable, and stable numerical model for simulating the coupled structure -TLD system. Given the existing gap in the literature and the critical importance of analytical models for achieving a deeper understanding, the second part, which includes Chapters 4, 5, and 6, focuses on analytical modeling of the coupled system. The outcomes from the first part serve as a benchmark for evaluating the accuracy of the analytical approach employed in the second part. Chapter 1 introduces this thesis and outlines key innovations. The concluding remarks of the subsequent chapters are as follows.

Chapter 2.

- ***Evaluating Numerical Methods for Sloshing Problems Using Linear Shallow Water Equations***

This research fills a gap in the literature by applying various widely used numerical models to sloshing problems with linear shallow water equations. Two case studies were modeled: one with an initial perturbation in the free surface and another with forced excitation. The study examined several numerical methods, including upwind methods, McCormack, Central, Preissmann, staggered, and separation of variables techniques. The analysis reveals that first-order upwind methods suffer from significant numerical diffusion, while higher-order schemes equipped with ghost nodes offer more accuracy. McCormack provides precise results, but the central method leads to instability. Semi-implicit Preissmann and staggered methods improve accuracy, and the separation of variables technique also yields reliable results. The research emphasizes the importance of choosing appropriate numerical methods, as incorrect application can cause substantial numerical diffusion errors.

- ***Validation of Natural Frequency Derivation for Shallow Water Tanks***

The analytically derived natural frequency of a shallow water tank aligns with the natural frequency relationship found in the broader literature, confirming its applicability to shallow water tank dynamics.

- ***Development and Validation of an Efficient Numerical Model for TLDs***

To create an accurate and computationally efficient numerical model for TLDs, a linear shallow water equation was combined with a low-cost numerical method that minimizes numerical diffusion. A physical diffusion term was added, and the model was coupled with a single degree of freedom (SDOF) equation, discretized using a second-order finite difference method. The partitioned method was used for coupling, with the sloshing force as an iterative parameter to ensure convergence, as explained in Chapter 2. The model's accuracy was validated by comparing it with experimental data for TLD systems, confirming its reliability.

- ***Parametric Analysis of Frequency and Damping Effects on Structure-TLD Performance***

A parametric study was conducted on a structure-TLD model developed using linear wave theory with minimal numerical diffusion error, focusing on two key parameters: (1) frequency ratio (excitation frequency to natural frequency of the SDOF) and (2) damping ratio (damping coefficient to critical damping). The study shows that TLD significantly reduces structural displacement within a narrow range near a frequency ratio of one, with diminishing effectiveness outside this range.

Chapter 3.

- ***Accurate and Stable Nonlinear Shallow Water Model for High-Gradient Free Surfaces and Sloped Bed Topography***

Then the research develops a stable, accurate, and cost-effective nonlinear computational model for simulating TLDs on sloped beds. The model captures complex phenomena like high-gradient free surfaces, bed topography, and asymmetric wave patterns. Using nonlinear shallow water equations, the central upwind method, and Minmod slope limiter, the model accurately evaluates flux and variables. Applied to a dam break scenario, it demonstrates minimal numerical diffusion. The model is further validated through two case studies: a dam break on a sloped bed and wave run-up/down in a tank with a parabolic bed, confirming its stability and accuracy in handling complex dynamics.

- ***Enhancing Nonlinear Shallow Water Equations for Sloshing Dynamics in Tanks with Sloped Beds***

The classical nonlinear shallow water equation is enhanced by adding dispersion and dissipation terms to capture asymmetric wave patterns and ensure stability. The dispersion term is treated implicitly, leading to a matrix equation solved at each time step. The Fourth Order Runge-Kutta method is used for time discretization. Model verification against experimental data confirms its accuracy and stability. A comparison between a sloshing box tank and an equivalent tank with a sloped bed reveals that the sloped bed generates higher sloshing waves, indicating improved damping performance for TLDs with sloped beds.

Chapter 4.

- ***Coupling a Sloshing Fluid Model with a Single Degree of Freedom System for Enhanced Vibration Mitigation Using Sloped Bed Tuned Liquid Dampers***

The sloshing fluid model is then coupled with a single degree of freedom (SDOF) model using a partitioned method with a second-order accurate scheme, creating a structure-TLD model. The results demonstrate that the TLD equipped with a sloped bed mitigates vibrations in the underlying structure more effectively than the conventional box TLD.

Most research on Tuned Liquid Dampers (TLDs) has focused on experimental and numerical studies, leaving a significant gap in analytical investigations. This study aims to fill that gap by analyzing a coupled system of a sloshing tank and structure, particularly the structure-TLD interaction. By providing analytical solutions to key questions in the literature, this research enhances understanding of TLD systems' dynamic performance. The findings contribute to the development of more efficient vibration mitigation strategies, offering valuable insights that complement existing experimental and numerical studies.

- ***Derivation of the Coupled Free Vibration Equation for an SDOF-TLD System Without Dissipation***

This section focuses on a coupled system undergoing free vibration, with no consideration of dissipation or damping effects. Initially, wave height and velocity were expressed using the separation of variables across different modes. These expressions were then integrated into the linear shallow water equations, incorporating the acceleration of the underlying single degree of freedom (SDOF) system. This led to the formulation of continuity and momentum equations for each mode. The interaction force between the sloshing fluid and SDOF system was rewritten in a modal coordinate framework, facilitating the coupling of the fluid and structural models. This approach resulted in a fourth-order ordinary differential equation for each mode, describing the displacement of the coupled system due to the contributions of each mode. Solving this equation led to the derivation of a characteristic equation.

- ***Stability Analysis of the Undamped Coupled System in Free Vibration***

The roots of the characteristic equation were used to derive the form of the solution, thereby providing insight into the dynamic behavior of the coupled system. The conditions necessary for the stability of the system were thoroughly discussed, and it was demonstrated that the coupled system meets these conditions, confirming its stability.

- ***Discovery of Dual Natural Frequencies in Each Mode of the undamped Coupled System***

In addition, with respect to the solution form, it was shown that each mode of the coupled system possesses two natural frequencies. Analytical expressions were developed to determine these natural frequencies, further contributing to the understanding of the behavior of the system. This finding represents a breakthrough in the body of TLDs' literature

- ***Formulation of a Novel Initial Value Vector for the undamped coupled System Response***

A novel initial value vector was formulated to determine the constants of the response of the system, incorporating key factors such as the initial displacement, initial velocity, initial wave height, and initial wave velocity. To derive the initial displacement from the contribution of each mode, the modal decomposition and orthogonality principles were applied.

- ***Validation of Analytical Findings and Insights into Higher Modes Using Numerical Modeling and FFT***

A numerical model and Fast Fourier Transform (FFT) were used to assess the accuracy of the analytical findings. The results confirmed two natural frequencies in the first mode, consistent with the analytical formula, but only a smaller natural frequency was observed in higher modes. The analytical approach clarified why a greater natural frequency is absent in these modes, explaining that initial perturbations can excite higher frequencies. Additionally, it showed that in higher modes, the smaller natural frequency aligns with either the SDOF or TLD natural frequency, while the larger frequency is a multiple of the smaller one, scaled by the mode number.

- ***First Mode Dominance and Validation of Analytical Accuracy Through Nonlinear Numerical Modeling:***

The analytical approach demonstrated that in higher modes, the coupled system exhibits response characteristics similar to an SDOF system. It also confirmed that the dynamic response of the coupled system is primarily influenced by the first mode, a finding supported by numerical analysis. Moreover, when using a nonlinear numerical method that incorporates dispersion and dissipation effects, it was shown that the linear wave theory-based analytical approach remains accurate for small-amplitude waves. This further validates the robustness and reliability of the analytical model under these conditions.

Chapter 5.

- ***Derivation of the Coupled Equation for Free Vibration of the Coupled System with Structural and Fluid Dissipation***

The research then shifts focus to the role of dissipations from both the fluid and structure on the dynamic behavior of the coupled system. By applying the separation of variables technique to the linear shallow water equation and coupling it with the sloshing force and SDOF equations, a fourth-order ordinary differential equation is derived. Solving this equation leads to a characteristic equation, which, unlike the previous case, is now a complete fourth-order polynomial due to the inclusion of both structural and fluid dissipation. This modification significantly changes the dynamic behavior of the coupled system by introducing damping effects.

- ***Discriminant Analysis of the Characteristic Equation Revealing Unconditional Stability of the Coupled System with Dissipation***

Analyzing the discriminant of the characteristic equation reveals that the roots consist of two pairs of conjugate complex numbers. The real parts of these complex numbers were shown to be negative, indicating that the coupled system is unconditionally stable under the influence of dissipation.

- ***Proof of Negligible Impact of Dissipation on the Natural Frequencies of the Coupled System***

The analytical approach further provided proof that the impact of dissipation on the natural frequencies of the coupled system is negligible.

- ***Analytical Derivation of Exponential Decay Rate and Damping Effect in the Coupled System response***

In addition, the analytical solution reveals that the response of the system decays exponentially over time. The rate of this exponential decay, which represents the damping effect on the coupled system, was derived analytically. This decay rate was found to be a function of the system's natural frequencies as well as the dissipation parameters associated with both the fluid and the structure.

- ***Innovation of Initial Value Vector and Behavior of Higher Modes in the damped Coupled System***

An innovative initial value vector was presented to derive the constants of the system's total response. The analytical model then focused on the behavior of the higher modes. This successfully demonstrates why numerical models for higher modes predict only a smaller natural frequency, excluding the larger one.

- ***Impact of Initial Perturbation and Dissipation Scenarios on Higher Modes and System Response***

The analytical approach further revealed that an initial perturbation is necessary to excite a larger frequency in these higher modes. Additionally, the analytical results for various dissipation scenarios—1) structural dissipation and 2) combined structural and fluid dissipation—and different initial conditions, including 1) initial displacement and 2) both initial displacement and initial wave height, showed strong agreement with the numerical model.

- ***Influence of Dissipation on Higher Modes and Dominance of the First Mode in Coupled System Response***

The analytical model demonstrated that, even when dissipation is incorporated, the response of the higher modes closely replicates that of the SDOF system. Moreover, it was shown that the overall response of the coupled system is predominantly governed by the first mode, emphasizing its significance in the dynamic behavior.

- ***Impact of Screen-Induced Local Dissipation on Coupled System Dynamics- Analytical Solution and Validation***

The final section of this chapter addressed the local dissipation introduced by screens. Although the formulation for this scenario includes nonlinear terms, an analytical solution based on the dominance of the first mode was proposed based on previous experience. This solution utilized the undamped natural frequency (under non-dissipative conditions) and incorporated enhanced dissipation factors that account for the dissipation caused by the screens. Verification of the proposed analytical solution using numerical data that does not assume first-mode dominance confirmed the accuracy and validity of the current analytical approach.

Chapter 6.

The previous two chapters primarily focused on analyzing the free vibration response to provide a deeper understanding of the intrinsic characteristics of the structure–TLD-coupled system. In this chapter, attention shifts to examining how the coupled system responds to forced excitation.

Additionally, this chapter explores the effects of structural and fluid dissipation on the coupled system response under forced excitation, offering key insights into the behavior of the system under these conditions.

- ***Derivation of the Non-Homogeneous Coupled Equation for Displacement in a Coupled System Under Forced Excitation with Three Dissipation Scenarios***

Similar to the previous chapters, the continuity and momentum equations from the fluid and SDOF equation from the underlying structure are coupled and converted to a fourth order ordinary differential equation using the separation of variables technique. The main difference in this equation is that it includes the excitation force, and it is assumed to be a harmonic function in this study. Because the damping term, whether from the structure or fluid, alters the particular response, this coupled equation is studied in three categories: 1) undamped coupled system, 2) structural damped coupled system, and 3) structural and fluid damped coupled system.

- ***Complementary Solution of the Non-Homogeneous Coupled Differential Equation***

The coupled differential equation is non-homogeneous; therefore, the solution includes both complementary and particular solutions. The complementary response obtained for the homogeneous form of the coupled equation describes the response of the coupled system to free vibration. Therefore, the complementary responses are known from the preceding two chapters for all the scenarios.

- ***Derivation of Particular Solutions and Introduction of Dynamic Parameters for Three Dissipation Scenarios***

The particular solutions were derived analytically for these three scenarios. Furthermore, for three different scenarios two important dynamic parameters are introduced: 1-dynamic amplification reflect the dynamic displacement to static displacement and 2-phase difference denote the phase difference between the coupled system displacement and excitation force.

- ***Derivation of Total Response Shape and Coefficients for Different Dissipation Scenarios***

Then, the shape of the total response, that is, the sum of the particular response and complementary response, was derived for each scenario. Upon the introduction of the initial value vector, not the zero vector, the coefficient of the total response is derived

- ***Frequency Contributions and Amplification Factors in the Undamped Coupled System***

In the undamped coupled system, the total solution includes three frequency contributions: the two natural frequencies of the coupled system and the excitation frequency. Amplification factors are influenced by five frequencies: the two natural frequencies of the coupled system, the excitation frequency, the SDOF frequency, and the TLD frequency. When the excitation frequency approaches the coupled system's natural frequencies, the amplification factor becomes infinite, leading to resonance. Conversely, when the excitation frequency aligns with the TLD frequency, the particular response diminishes, leaving only the complementary response in the total displacement. Additionally, in this undamped case, the system's displacement remains in phase with the excitation force.

- ***Resolving Ambiguities in Total Response Near Natural Frequencies and System Instability***

As the excitation frequency nears the system's natural frequencies, the total response becomes ambiguous, often forming indeterminate expressions like 0/0. Applying L'Hospital's rule resolves this ambiguity, revealing that the total response grows over time, ultimately causing system instability. Here, the total response is primarily dominated by the natural frequency matching the excitation frequency. For higher modes, the particular and total responses of the coupled system resemble those of the SDOF system. Validation through a numerical model and FFT analysis confirms the accuracy of the analytical approach under these conditions.

- ***Analysis of Total Response and Dynamic Amplification in the Damped Coupled System***

Similarly, regarding the damped case, the total response comprises three dominant frequencies. However, because the complementary response decays exponentially, the force excitation frequency contribution is more highlighted. In this scenario, the amplification factor is a function of five distinct frequencies as well as the damping characteristics of both the fluid and structure. In this case, when the excitation frequency approaches the natural frequencies (resonance excitation), the dynamic amplification is significantly intensified, but it does not reach infinity.

Structural and fluid damping significantly mitigate structural displacement in this scenario. The phase difference during the resonance excitation tends to 90 degree.

7.2. Recommendations for Future Studies

As elaborated in detail throughout the chapters of this thesis, two models have been developed for simulating the coupled system (structure-TLD): 1) a numerical model and 2) an analytical model. Two models were constructed for the numerical simulation. The first model is based on the linear shallow water equation, while the second employs the nonlinear shallow water equation, incorporating some novel terms.

The analytical approach is grounded in linear wave theory and linear structural response by utilizing a strong coupling procedure. This innovative model was initially introduced to analyze the free vibration of an undamped coupled system and was subsequently extended to include structured, fluid, and screen dissipation in damped systems. Ultimately, the analytical model was further developed to account for harmonic forced excitation in both the damped and undamped scenarios.

Given the characteristics of these models and a meticulous review of the literature, the following topics are proposed for future investigation in this field.

1. **Flow Damping Devices such as Screens:**

Although a novel analytical approach has been introduced to incorporate local dissipation effects due to screens in the context of free vibration analysis, this method can also be extended to develop analytical solutions for scenarios involving harmonic excitation forces. Such an extension would provide a comprehensive understanding of the behavior of coupled systems equipped with screens under dynamic loading conditions.

2. **Sloped Bottom Tuned Liquid Dampers (TLDs):**

In Chapter Three, a precise numerical model is presented to assess the impact of a sloped bed on the effectiveness of TLDs in mitigating structural vibrations. To complement this, an analytical model can be adapted to incorporate a sloped bed. Such an extension would provide valuable insights into the relationship between the bed slope and response of the coupled system, offering a deeper understanding of how variations in the sloped bed influence the performance of TLDs.

3. **Modification for Low-Frequency Structures**

Tuned Liquid Dampers (TLDs) are generally designed for tall buildings with low natural frequencies. However, the literature has introduced a variant of TLD, specifically for high-frequency structures, incorporating a series of spring cables that exert forces on the liquid's free surface through a floating roof. To address this, both the numerical model and the analytical approach can be adapted to include the dynamics of the floating surface and springs. Although the current model couples the TLD directly with the underlying structure, modeling this variant requires a distinct coupling procedure that integrates the floating surface and springs with the free surface of the liquid. This modification poses a challenging yet compelling opportunity, particularly for enhancing the current analytical approach.

4. **Multi-Degree of Freedom Systems**

Most experimental and analytical models in the literature utilize a single degree of freedom (SDOF) representation for the underlying structure. However, only a limited number of experimental studies incorporate multi-degree of freedom (MDOF) systems into their analyses. This represents a significant gap in literature. To address this, an analytical model capable of predicting the displacement and shear at various points along an MDOF structure would be highly valuable. One feasible approach involves using the separation of variables technique to derive the total displacement of the underlying structure. In this method, a shape function is assumed for the structure based on its dominant mode contributions. The amplitude of this shape function, which depends solely on time, is derived from the dynamic equations of the coupled system. By applying this approach, an MDOF system can effectively be reduced to an SDOF system, for which the current analytical model is applicable. Once the vibration amplitude is determined analytically, it can be multiplied by the shape function to obtain the displacement along the structure at any given time. Following the displacement calculations, other structural parameters, such as shear, moment, and drift, can also be computed analytically.

Using this method, the dynamic response of tall structures equipped with TLDs can be derived analytically, representing a highly valuable contribution to the field. This approach provides a comprehensive understanding of how the structure interacts with the TLD, offering insights into the dynamic behavior of the system that can be applied in practical engineering designs.

4. **TLD with Improved Connection**

Recent literature suggests an enhancement in the connection of Tuned Liquid Dampers (TLDs), where the TLD is attached to the underlying structure using a rotational spring. Experimental studies have shown that this connection, which allows for both horizontal and rotational motion of the tank, significantly enhances the damping effectiveness of the TLDs. Integrating this improved connection into the current numerical model, by including new terms appears feasible. However, extending the analytical approach to effectively model this enhanced TLD configuration presents a challenging and valuable area for future research. 4o mini

5. **Analytical Solution to a Coupled System Subjected to Periodic Excitation Force**

The current research provides an analytical solution for a coupled system under free vibration and harmonic excitation. However, this approach can also be extended to accommodate periodic dynamic loads. By decomposing the dynamic load into harmonic components using a Fourier series, the response of the coupled system to each harmonic function can be derived based on the current analytical method. The total response of the system can then be obtained by summing the responses to each harmonic component, assuming that the system's linearity allows for the application of the superposition principle. This extension for handling periodic dynamic loads represents a significant and valuable contribution to the literature.

6. **Analytical Solution to a Coupled System Subjected to Arbitrary Excitation Force**

Chapters four and five provide analytical solutions for the response of the coupled system under free vibration, encompassing both the undamped and damped scenarios. These solutions allow for the derivation of the system response to impulsive forces, which involve free vibration with an initial velocity. The cumulative response of the system under an arbitrary dynamic load function can be determined by summing the responses to each impulsive force applied at any given time. This method integrates the responses over time, facilitating the analytical evaluation of the system response to any arbitrary dynamic load, including ramp and step functions. This approach offers a flexible and comprehensive framework for assessing the dynamic behavior of a system under diverse loading conditions.

7. Analytical Solution to Blast Load

Explosions are characterized as dynamic shock loads that induce an initial shock followed by subsequent free vibrations. The response to such shock loads can be derived using the methodology outlined for arbitrary dynamic loads, whereas the free vibration response is detailed in Chapters four and five. Consequently, it is feasible to analyze the total response of the coupled system subjected to various blast or explosion loading scenarios by combining the response to the initial shock with the free vibration response. This approach provides a comprehensive framework for evaluating the behavior of a system under explosive conditions.

8. Coupled System Subjected to Vertical Excitation

Vertical excitation, often generated alongside horizontal motion during earthquakes, can significantly influence the dynamic behavior of structures. However, the impact of vertical excitation has been insufficiently explored in the context of structure–TLD coupled systems. The literature primarily focuses on horizontal excitations, with limited consideration of the role that vertical motion plays in affecting the sloshing dynamics and overall system response. Future research that delves into how vertical excitation alters the interaction between the structure and TLD and how TLDs might mitigate vibrations when subjected to both horizontal and vertical forces would fill this important gap.

9. Coupled system subjected to torsion

Due to the discrepancy between the mass center and stiffness center, a structure may experience torsional motion during an earthquake. Additionally, wind and tornado forces can induce torsional movements in the structure. There is a notable gap in the literature concerning the influence of TLDs on the structural response under these conditions, and whether the inclusion of TLDs can effectively mitigate torsional effects. To address this, the current numerical model should be expanded to incorporate both the horizontal directions.

10. Coupled System Subjected to Bi-Directional Excitation

Earthquakes and wind events can exert bi-directional effects involving simultaneous forces in two horizontal directions, typically aligned with the principal axes of a structure. Analyzing the structural response to such bi-directional excitations is crucial for accurate seismic design. A literature review indicates a gap in investigating the efficiency of Tuned Liquid Dampers (TLDs) under these conditions. Therefore, future research in this area would contribute significantly to the existing body of knowledge.

11. Comparison Between Boxed TLD and Cylindrical TLD

A literature review indicates that most TLDs are designed in a box shape. This raises an important question regarding how alternative tank shapes, such as cylindrical tanks, might influence the dynamics of the underlying structure when used as TLDs. This inquiry can be extended to various scenarios, including those in which a structure experiences torsional or bidirectional excitation. It is worth investigating whether cylindrical TLDs offer superior performance in mitigating structural vibrations under these conditions.

12. Enhancement of TLD with Liquid or Liquids

The literature review highlights extensive research on the physical properties of tanks used in Tuned Liquid Dampers (TLDs), including tank depth. However, there is a noticeable gap in our understanding of the impact of altering the physical properties of the liquid itself, such as density and viscosity, on the effectiveness of TLDs. This raises important questions about whether variations in these liquid properties influence the performance of TLDs. Furthermore, it is worth exploring whether specific liquids, whether natural or artificial, offer superior characteristics for optimizing the TLD performance. Another intriguing area of research is the use of TLDs comprising two different fluids. Investigating the performance of such multi liquid TLD systems could provide valuable insights and represent a novel contribution to the field.

13. Breaking Waves in TLDs

A literature review indicates a significant gap in recent studies concerning the impact of breaking waves on the performance of Tuned Liquid Dampers (TLDs). Most research in this area dates back approximately thirty years, and advancements in laboratory technology and measurement techniques have suggested a need for updated investigations. Given the importance of breaking waves in high-excitation scenarios, these studies can be opportunity to revisit and refine these studies. Exploring how breaking waves and the resultant energy dissipation influence TLD performance using modern tools and methods could provide valuable insights, thereby enhancing the understanding of TLD dynamics and their effectiveness in vibration control.

14. Efficiency of TLDs in Nonlinear Zones and the Role of Ductility

Although structures are generally designed to exhibit nonlinearity and dissipate energy through hysteresis loops during strong earthquakes, the literature review indicates that there is a notable lack of research on the performance of Tuned Liquid Dampers (TLDs) in this context. Specifically, structural elements are often designed to be ductile, which is crucial for the dynamic behavior of structures within nonlinear zones. However, the impact of TLDs on structural vibrations and the hysteresis behavior of structural elements remains underexplored. It is important to investigate whether TLDs have positive, negative, or neutral effects on the structural response and hysteresis loops in these nonlinear zones. Addressing this gap can provide valuable insights into the effectiveness of TLDs in enhancing the resilience of structures subjected to severe seismic conditions.

15. Extension of the Current Model for Water Storage Tanks

The current model justified that, at higher modes, the smaller natural frequencies converge to a Single Degree of Freedom (SDOF) frequency, whereas higher natural frequencies are absent in the response. This characteristic indicates that the coupled system of the Tuned Liquid Damper (TLD) and the structure is predominantly influenced by the first mode. This conclusion is supported by the assumption that the depth-to-length ratio is relatively small, and that the mass of the water tank is significantly smaller than that of the underlying structure, both of which are valid for TLDs. However, these assumptions may not hold true for storage tanks, where the influence of higher modes on the response of the coupled system, including both the structure and elevated storage tank, becomes more significant. Addressing this issue by extending the current model to accommodate higher modes presents a challenging but invaluable research opportunity. Such an extension could also integrate P–Δ effects to achieve a more realistic response for elevated water tanks.

Additionally, the current numerical model, which accurately predicts sloshing waves, can be adapted for use in storage tanks. This adaptation would enable investigations into phenomena such as local buckling, rupture, and large displacements of tank shells under high-amplitude excitations. Exploring these aspects would enhance the applicability of the model and provide deeper insights into the dynamic behavior of storage tanks.

16. The Combination of TLDs with Other Types of Dampers

In addition to Tuned Liquid Dampers (TLDs), structures also benefit from various other types of dampers that operate on different mechanisms. For instance, Tuned Mass Dampers (TMDs) reduce structural vibrations by moving out of phase with building motion, thereby dissipating energy. Viscous dampers convert motion into heat through fluid resistance, whereas frictional damping dissipates energy through frictional forces between surfaces in contact, converting kinetic energy into heat to reduce vibrations. Base isolators reduce seismic forces on a structure by allowing the building to move independently of ground motion, thereby minimizing vibrations.

The combination of TLDs with these different damping mechanisms presents an intriguing area of study. A key question is whether the integration of TLDs with other damping devices leads to conflicting or synergistic effects in the vibration control. Understanding whether this configuration results in a superior damping effect or whether it potentially deteriorates vibration damping could offer novel insights into the dynamics of tall buildings.

17. Efficiency of TLDs as Active Dampers

Since their inception, Tuned Liquid Dampers (TLDs) have been employed as passive damping devices, with their frequency typically tuned to match the natural frequency of the underlying structure. In the structural response, both the excitation frequency, such as that of an earthquake, and the structure's natural frequency play crucial roles. Consequently, TLDs are the most effective in mitigating vibrations within a narrow range of excitation frequencies centered around the natural frequency of the structure. However, with advancements in technology, there is potential for developing TLDs as active dampers. Such dampers can dynamically adjust their frequency to match the varying frequency of an earthquake in real time, possibly through mechanisms such as rapidly altering the water depth. Investigating the efficiency of these active TLDs in mitigating structural vibrations represents a significant advancement in this field.